BIOPHYSICAL INSIGHT INTO INTERACTION OF LIGANDS TO MONOMERIC PROTEINS AND ASSOCIATED CONFORMATIONAL ALTERATIONS

ABSTRACT

OF THE

THESIS

SUBMITTED FOR THE AWARD OF THE DEGREE OF

Doctor of Philosophy

IN

BIOTECHNOLOGY

BY

NIDA ZAIDI

INTERDISCIPLINARY BIOTECHNOLOGY UNIT
ALIGARH MUSLIM UNIVERSITY
ALIGARH (INDIA)

2013

Protein–ligand interaction is one of process that plays key role in all biological processes that occur in body and thus it underpins the whole biological science. Thus the detailed knowledge of such interactions is of immense importance to understand the physiology and helpful in the discovery of new medicines to benefit human health. To understand the protein-ligand interactions, an-depth knowledge of biophysical behavior of protein and ligand that includes degree of complementarity of the binding site of the protein and the ligand, binding site location, affinity, binding energies, and entropy and enthalpy changes accompanied is pre-requirement There are various examples of biologically relevant protein ligand interaction, where studying binding mechanism, forces involved, and thermodynamics is helpful either in understanding physiology or in designing new medicines. Examples which immediately stand out from the many includes interaction of exogenous and endogenous compounds with carrier protein, human serum albumin (HSA), interaction of detergent, sodium dodecyl sulphate, which mimics membrane, with glycoprotein and interaction of small molecules with amyloidogenic proteins. Keeping in mind the significance of these protein ligand interactions, in this thesis following important protein ligand systems have been investigated with the help of various biophysical techniques:

1. Interaction of hippuric acid (HA), a uremic toxin, with carrier protein, human serum albumin (HSA) to determine plausible reason behind its impaired elimination.

2. Interaction of furosemide (FUR), a diuretic drug, with human serum albumin (HSA) to know FUR binding mechanism and its binding sites on HSA. Binding mechanism obtained help in determination of the reason of FUR impaired binding to HSA in uremia.

3. Interaction of sodium dodecyl sulphate (SDS) that mimics membrane, to bovine serum fetuin (BSF) (a model glycoprotein) at pH 2 and 7.4 to know modes of SDS interaction with BSF under different solution condition.

4. The effect of n-acetylneuraminic acid (Neu5Ac), a monosaccharide that occur naturally at the end of sugar chains attached to the surfaces of cells and soluble proteins, on the amyloid fibrillization of hen egg white lysozyme (HEWL), a model protein, to determine potency of Neu5Ac as inhibitor of amyloid fibrillization.

Chapter 1

As the introduction part of the thesis, overview of basic models of protein ligand interaction, forces involved, changes in thermodynamic parameters and techniques to study protein ligand interaction has been reviewed. Physiologically significant examples of protein ligand interaction related to the work carried out in this thesis were also discussed.

Chapter 2

Binding of hippuric acid (HA), a uremic toxin, with human serum albumin (HSA) has been examined by isothermal titration calorimetry (ITC), differential scanning calorimetry (DSC), molecular docking, circular dichroism (CD) and fluorescence spectroscopy to understand the reason that govern its impaired elimination from biological system. ITC results shows that the HA binds with HSA at high ($K_b \sim 10^4$) and low affinity ($K_b \sim 10^3$) sites whereas spectroscopic results predict binding at a single site ($K_b \sim 10^3$). The HA form complex with HSA that involves electrostatic, hydrogen and hydrophobic binding forces as illustrated by calculated thermodynamic parameters. Molecular docking and displacement studies collectively revealed that HA bound to both site I and site II; however, relatively strongly to the later. Esterase-like activity of HSA confirms the involvement of Arg410 and Tyr411 of Sudlow site II in binding of HA. CD results show slight conformational changes occurs in the protein upon ligation that may be responsible for the discrepancy in van't Hoff and calorimetric enthalpy change. Furthermore, an increase in T_m^1 and T_m^2 is observed from DSC results that indicate increase in stability of HSA upon binding to HA. The combined results provide that HA binds to HSA at both of its binding site with different affinity and thus its elimination is hindered.

Chapter 3

Exogenous substances like drugs, when absorbed, enter into the circulatory system and bind reversibly and extensively to human serum albumin (HSA). But transport of various drugs like a diuretic, furosemide (FUR), via albumin in uremia is seriously compromised due to accumulation of uremic toxins. The reason behind it is explored

by investigating the binding mechanism of FUR to HSA. Isothermal titration calorimetry results show that FUR binds with HSA at high (K_b~10^4) and low affinity (K_b~10^3) sites while spectroscopic results predicts binding at single site (K_b~10^5). Thermodynamic analysis shows that the HSA-FUR complex formation occurs via hydrogen bonds, hydrophobic interactions and undergoes slight structural changes as evident by FTIR, far-UV CD. Further, the fluorescence lifetime of HSA decreases only marginally and thus magnitude of energy transfer efficiency is small as obtained by time resolved measurements. Displacement experiment predicts that the FUR binds mainly to site I but a new site having lower affinity was also observed which shares some residues with site II which is supported by molecular docking results. Results revealed that in uremia, FUR indirectly competes for Arg410, Lys414 and Ser489 with site II bound uremic toxins while directly compete for site I with site I bound uremic toxins.

Chapter 4

Protein-sodium dodecyl sulphate (SDS) interaction has wide range of applications from food industry to cosmetics and the drug industry. Moreover, SDS mimics the native hydrophobic milieu of the phospholipids bilayer in vivo and thus study of protein surfactant interaction serves as model for membrane proteins and lipids interaction. Thus the mode of interaction of SDS with a glycoprotein, bovine serum fetuin (BSF) is studied in sub- critical micellar concentration at pH above (pH 7.4) and below (pH 2) pI to know the effect of solution condition on mode of interaction of SDS to glycoprotein. It has been observed that at pH 2, SDS interacts with BSF through its negatively charged head groups and thus the hydrophobic tails of SDS on protein-SDS complex become free, that increases surface hydrophobicity of protein-SDS complex. As a result, the protein-SDS complex interacts with each other, not the water, and cause protein to undergo aggregation. The nature of aggregates is amyloid due to enhance ThT binding and β-sheet formation. The formation of amyloid fibrils, however, decreases in presence of SDS above 0.75 mM due to repulsion between the protein-SDS complexes. However, at pH 7.4, SDS interacts with BSF at two sites, high affinity (K_1~ 10^5) and low affinity (K_1~ 10^3). Binding of SDS to BSF occurs with the positive entropy change that is originating from the hydrophobic interaction that results in disruption of highly dynamic hydrogen bonds between molecules of water

by the SDS molecules. Moreover, due to hydrophobic environment generated by alkyl chain of SDS molecules around tryptophan, induction of α-helical structure in BSF occurs. This increase in α-helical content on increasing SDS concentrations constrain environment around tryptophan. As a consequence, the interconversion of conformers decreases and resulted in decrement of fluorescence ifetime for BSF. These findings demonstrate that the mode of interaction of SDS to protein is different under different solution condition.

Chapter 5

There is a great interest in developing small inhibitors of amyloid aggregation of proteins which is related to growing pathologic states known as neurodegenerative disorders. In the present study, the effect of n-acetylneuraminic acid (Neu5Ac), a non reducing, monosaccharide that occur naturally at the end of sugar chains attached to the surfaces of cells and soluble proteins, on the amyloid fibrillization of hen egg white lysozyme (HEWL) are reported. When HEWL incubated at 65°C for 168 hours then the amyloid formation occurs as evident from the increase in ThT binding, increased hydrophobicity of solvent-exposed surfaces, transition of α-helix to β-sheet. These amyloid fibrils of HEWL generated under studied condition are cytotoxic to the human *neuronal* glioblastoma. However this fibrillization process is inhibited by Neu5Ac as it decrease ThT binding, hydrophobicity of solvent-exposed surfaces, and transition of α-helical structure to β-sheet. Furthermore, Neu5Ac also protect cells against cytotoxic nature of HEWL amyloid fibrils. The Neu5Ac attenuates the heat induced amyloid formation in HEWL by the stabilization of the native state of HEWL according to the effect of preferential hydration rather than direct interaction with protein. In preferential hydration mechanism, a Neu5Ac molecule get excluded from the environment around the protein and are replaced by water and thus nonspecifically inhibits the heat induced amyloid formation in HEWL. Thus Neu5Ac may be a potential therapeutic candidate for inhibition of amyloid fibril formation.

The present work is the first report on the above mentioned protein ligand interactions with the above illustrated objectives. Thus this work may enable researcher's to understand the physiology and may helpful in the discovery of new medicines to benefit human health.

BIOPHYSICAL INSIGHT INTO INTERACTION OF LIGANDS TO MONOMERIC PROTEINS AND ASSOCIATED CONFORMATIONAL ALTERATIONS

THESIS

SUBMITTED FOR THE AWARD OF THE DEGREE OF

Doctor of Philosophy

IN

BIOTECHNOLOGY

BY

NIDA ZAIDI

INTERDISCIPLINARY BIOTECHNOLOGY UNIT
ALIGARH MUSLIM UNIVERSITY
ALIGARH (INDIA)

2013

Biophysical insight into Interaction of Ligands to Monomeric Proteins and Associated Conformational Alterations

Dated:.....

Approved:.....

***Rizwan Hasan Khan**, Supervisor*

Nida Zaidi

A THESIS SUBMITTED FOR THE AWARD OF DEGREE OF DOCTOR OF PHILOSOPHY IN BIOTECHNOLOGY AT ALIGARH MUSLIM UNIVERSITY, ALIGARH (INDIA)

2013

INTERDISCIPLINARY BIOTECHNOLOGY UNIT
ALIGARH MUSLIM UNIVERSITY, ALIGARH-202 002 (INDIA)

Ph. : 0091-571-2720388
Fax: 0091-571-2721776
E-mail: btisamu@gmail.com

Certificate

This is to certify that the thesis entitled "**Biophysical insight into Interaction of Ligands to Monomeric Proteins and Associated Conformational Alterations**" herewith submitted by **Ms. Nida Zaidi** in the fulfillment of the requirement for the degree of **Doctor of Philosophy in Biotechnology** at the Aligarh Muslim University, Aligarh. It is authentic record of work carried by her under my supervision and is suitable for the award of Ph.D degree in biotechnology at the Aligarh Muslim University, Aligarh.

8/11/13

Dr. Rizwan Hasan Khan
Supervisor

Declaration

I hereby declare that the thesis entitled **"Biophysical insight into Interaction of Ligands to Monomeric Proteins and Associated Conformational Alterations"** embodies the work carried out by me.

Nida Zaidi

Senior Research Fellow

(Council of Scientific and Industrial Research),

Interdisciplinary Biotechnology Unit,

Aligarh Muslim University,

Aligarh 202002 India

Dedicated

To

My Parents

TABLE OF CONTENTS

Chapter 3

Chapter 4

Chapter 5

ACKNOWLEDGEMENTS

First and foremost I express my profound sense of honour and gratitude to the almighty Allah for His great mercy and choicest blessing generously bestowed upon me, without which I could have never seen the completion of my thesis work.

My profound sense of gratitude to Dr. Rizwan Hasan Khan, Interdisciplinary Biotechnology Unit, Aligarh Muslim University, Aligarh, under whose able guidance I had the privilege to undertake and complete my thesis work. His knowledge and experience has benefited me and I have no hesitation to place on records that it is his inspiration and encouragement due to which I could pass through many odds. My association with him also taught me to appreciate the value of patience, sustained efforts and humility in the development of healthy scientific temperament.

I shall always remain beholden to Dr Asadullah Khan, Coordinator, Interdisciplinary Biotechnology Unit, Aligarh Muslim University, Aligarh, for providing all facilities required for work on time. I also thank Prof. Saleemuddin, Dr. M. Owais and Dr. Hina Younus, Dr. Subbarao Naidu who have been a constant source of inspiration to me during the entire course of hard work.

No words are enough to thank my dearest colleague, Ms. Atiyatul Qadeer with whom I cherished every moment. She is my best buddy and shared sisterly attitude in my tough time. I equally thankful to Mr. Sumit Kumar Chaturvedi, who is always generous and helpful to me in every situation from experimental hurdle to common issues. He has a quality of keeping lab environment humors that helps me lot while working. I cannot put in words the contribution of my junior, Mr. Rehan Ajmal who always lends a hand whether it's an experimental work or a day to day problem. He especially deserves biggest thank. Special thanks should also be given to Mr. Parvez Alam, who always selflessly helps me.

It would not be fair, if I will not owe thanks to the most generous people I come across in my Ph.D tenure, Mr. Adeel Husain Zaidi, Mr. Abdullah Sultan, and who help me selflessly inspite of their busy working schedules for carrying out experimental work successfully.

Certainly, my past and present labmates especially Dr. Ejaz Ahmad, Dr. Ankita Varshney, Mr.Iftikhar, Mr. Masihuszaman and Mr.Mohsin Vahid Khan at one time or another have been extremely generous and helpful to me.

The unfathomable blessings of my ammi and papa are the spiritual strength with which I have persuaded this thesis. I owe my deepest thanks to the most precious gift of God, my loving parents for being a source of unseen strength that installed courage in me. I am short of words to thank my sister, Ms. Yusra Zaidi, who is always my best guide in every situation. She is with me in bearing the brunt of the frustrations, and sharing in the joy of the successes. The moral support from my brothers, Mr. Anas Zaidi and Mr. Bilal Zaidi is also acknowledged.

I am thankful to Zahid abba and badi amma who are my first teachers, mentor. I also acknowledge all my maternal and paternal uncles who always believe in me. I specially thank Mrs. Saba Hasan Khan who always bestowed me with blessings.

The acknowledgement will remain incomplete without expressing heartiest thanks to all my friends Ms. Anubha Sagar, Ms. Shafquat Azeem, Ms. Farzana Khatoon, Ms. Saman Ahmad, Mr. Yasir Arfat, Mr. Haseeb Zubair, Mr. Shakir Khan, Mr. Husain Yar Khan, Mr.Mohammad Rehan, Ms. Rumana Khalique, Ms. Nayla Saboor, Ms. Tabeer Nasih for brunting of the frustrations and providing me motivation encouragement and moral support in completing this work.

I also owe thanks to Mr. Faisal Maqbool and Mr. Iqtedar Ahmad who always ready to help me with the computer system problems I come across. Special mention must be made of Mr. Amir and Mr. Nasir who help me in placing orders, claiming scholarships and other office works.

I feel extremely proud to acknowledge contribution of Mr. Lal Mohd Khan, Mr. Ashraf, Mr. Ramesh Chandra, Mr. Chandra Pal, Mr. Mushkoor and Mr. Rajendar for their co-operative behavior.

Council of scientific and industrial research (CSIR) is greatly acknowledged for providing financial support in the form of junior and senior research fellowship.

Nida Zaidi

ABSTRACT

ABSTRACT

Protein–ligand interaction is one of process that plays key role in all biological processes that occur in body and thus it underpins the whole biological science. Thus the detailed knowledge of such interactions is of immense importance to understand the physiology and helpful in the discovery of new medicines to benefit human health. To understand the protein-ligand interactions, an-depth knowledge of biophysical behavior of protein and ligand that includes degree of complementarity of the binding site of the protein and the ligand, binding site location, affinity, binding energies, and entropy and enthalpy changes accompanied is pre-requirement There are various examples of biologically relevant protein ligand interaction, where studying binding mechanism, forces involved, and thermodynamics is helpful either in understanding physiology or in designing new medicines. Examples which immediately stand out from the many includes interaction of exogenous and endogenous compounds with carrier protein, human serum albumin (HSA), interaction of detergent, sodium dodecyl sulphate, which mimics membrane, with glycoprotein and interaction of small molecules with amyloidogenic proteins. Keeping in mind the significance of these protein ligand interactions, in this thesis following important protein ligand systems have been investigated with the help of various biophysical techniques:

1. Interaction of hippuric acid (HA), a uremic toxin, with carrier protein, human serum albumin (HSA) to determine plausible reason behind its impaired elimination.

2. Interaction of furosemide (FUR), a diuretic drug, with human serum albumin (HSA) to know FUR binding mechanism and its binding sites on HSA. Binding mechanism obtained help in determination of the reason of FUR impaired binding to HSA in uremia.

3. Interaction of sodium dodecyl sulphate (SDS) that mimics membrane, to bovine serum fetuin (BSF) (a model glycoprotein) at pH 2 and 7.4 to know modes of SDS interaction with BSF under different solution condition.

4. The effect of n-acetylneuraminic acid (Neu5Ac), a monosaccharide that occur naturally at the end of sugar chains attached to the surfaces of cells and soluble proteins, on the amyloid fibrillization of hen egg white lysozyme (HEWL), a model protein, to determine potency of Neu5Ac as inhibitor of amyloid fibrillization.

Chapter 1

As the introduction part of the thesis, overview of basic models of protein ligand interaction, forces involved, changes in thermodynamic parameters and techniques to study protein ligand interaction has been reviewed. Physiologically significant examples of protein ligand interaction related to the work carried out in this thesis were also discussed.

Chapter 2

Binding of hippuric acid (HA), a uremic toxin, with human serum albumin (HSA) has been examined by isothermal titration calorimetry (ITC), differential scanning calorimetry (DSC), molecular docking, circular dichroism (CD) and fluorescence spectroscopy to understand the reason that govern its impaired elimination from biological system. ITC results shows that the HA binds with HSA at high ($K_b \sim 10^4$) and low affinity ($K_b \sim 10^3$) sites whereas spectroscopic results predict binding at a single site ($K_b \sim 10^3$). The HA form complex with HSA that involves electrostatic, hydrogen and hydrophobic binding forces as illustrated by calculated thermodynamic parameters. Molecular docking and displacement studies collectively revealed that HA bound to both site I and site II; however, relatively strongly to the later. Esterase-like activity of HSA confirms the involvement of Arg410 and Tyr411 of Sudlow site II in binding of HA. CD results show slight conformational changes occurs in the protein upon ligation that may be responsible for the discrepancy in van't Hoff and calorimetric enthalpy change. Furthermore, an increase in T_m^1 and T_m^2 is observed from DSC results that indicate increase in stability of HSA upon binding to HA. The combined results provide that HA binds to HSA at both of its binding site with different affinity and thus its elimination is hindered.

Chapter 3

Exogenous substances like drugs, when absorbed, enter into the circulatory system and bind reversibly and extensively to human serum albumin (HSA). But transport of various drugs like a diuretic, furosemide (FUR), via albumin in uremia is seriously compromised due to accumulation of uremic toxins. The reason behind it is explored by investigating the binding mechanism of FUR to HSA. Isothermal titration

calorimetry results show that FUR binds with HSA at high (K_b~10^4) and low affinity (K_b~10^3) sites while spectroscopic results predicts binding at single site (K_b~10^5). Thermodynamic analysis shows that the HSA-FUR complex formation occurs via hydrogen bonds, hydrophobic interactions and undergoes slight structural changes as evident by FTIR, far-UV CD. Further, the fluorescence lifetime of HSA decreases only marginally and thus magnitude of energy transfer efficiency is small as obtained by time resolved measurements. Displacement experiment predicts that the FUR binds mainly to site I but a new site having lower affinity was also observed which shares some residues with site II which is supported by molecular docking results. Results revealed that in uremia, FUR indirectly competes for Arg410, Lys414 and Ser489 with site II bound uremic toxins while directly compete for site I with site I bound uremic toxins.

Chapter 4

Protein-sodium dodecyl sulphate (SDS) interaction has wide range of applications from food industry to cosmetics and the drug industry. Moreover, SDS mimics the native hydrophobic milieu of the phospholipids bilayer in vivo and thus study of protein surfactant interaction serves as model for membrane proteins and lipids interaction. Thus the mode of interaction of SDS with a glycoprotein, bovine serum fetuin (BSF) is studied in sub- critical micellar concentration at pH above (pH 7.4) and below (pH 2) pI to know the effect of solution condition on mode of interaction of SDS to glycoprotein. It has been observed that at pH 2, SDS interacts with BSF through its negatively charged head groups and thus the hydrophobic tails of SDS on protein-SDS complex become free, that increases surface hydrophobicity of protein-SDS complex. As a result, the protein-SDS complex interacts with each other, not the water, and cause protein to undergo aggregation. The nature of aggregates is amyloid due to enhance ThT binding and β-sheet formation. The formation of amyloid fibrils, however, decreases in presence of SDS above 0.75 mM due to repulsion between the protein-SDS complexes. However, at pH 7.4, SDS interacts with BSF at two sites, high affinity (K_1~ 10^5) and low affinity (K_1~ 10^3). Binding of SDS to BSF occurs with the positive entropy change that is originating from the hydrophobic interaction that results in disruption of highly dynamic hydrogen bonds between molecules of water by the SDS molecules. Moreover, due to hydrophobic environment generated by alkyl

chain of SDS molecules around tryptophan, induction of α-helical structure in BSF occurs. This increase in α-helical content on increasing SDS concentrations constrain environment around tryptophan. As a consequence, the interconversion of conformers decreases and resulted in decrement of fluorescence ifetime for BSF. These findings demonstrate that the mode of interaction of SDS to protein is different under different solution condition.

Chapter 5

There is a great interest in developing small inhibitors of amyloid aggregation of proteins which is related to growing pathologic states known as neurodegenerative disorders. In the present study, the effect of n-acetylneuraminic acid (Neu5Ac), a non reducing, monosaccharide that occur naturally at the end of sugar chains attached to the surfaces of cells and soluble proteins, on the amyloid fibrillization of hen egg white lysozyme (HEWL) are reported. When HEWL incubated at 65°C for 168 hours then the amyloid formation occurs as evident from the increase in ThT binding, increased hydrophobicity of solvent-exposed surfaces, transition of α-helix to β-sheet. These amyloid fibrils of HEWL generated under studied condition are cytotoxic to the human neuronal glioblastoma. However this fibrillization process is inhibited by Neu5Ac as it decrease ThT binding, hydrophobicity of solvent-exposed surfaces, and transition of α-helical structure to β-sheet. Furthermore, Neu5Ac also protect cells against cytotoxic nature of HEWL amyloid fibrils. The Neu5Ac attenuates the heat induced amyloid formation in HEWL by the stabilization of the native state of HEWL according to the effect of preferential hydration rather than direct interaction with protein. In preferential hydration mechanism, a Neu5Ac molecule get excluded from the environment around the protein and are replaced by water and thus nonspecifically inhibits the heat induced amyloid formation in HEWL. Thus Neu5Ac may be a potential therapeutic candidate for inhibition of amyloid fibril formation.

The present work is the first report on the above mentioned protein ligand interactions with the above illustrated objectives. Thus this work may enable researcher's to understand the physiology and may helpful in the discovery of new medicines to benefit human health.

ABBREVIATIONS AND SYMBOLS

$\triangle G$	Gibb's free energy change
$\triangle H$	enthalpy change
$\triangle S_{tot}$	total entropy change
$\triangle S_{sol}$	solvent entropy change
$\triangle S_{conf}$	configurationally entropy change
$\triangle S_{r/t}$	rotation and translation entropy change
λ_{max}	wavelength maxima
θ_{obs}	observe ellipticity
ANS	1-anilino-8-naphthalene sulfonic acid
Arg	arginine
Asp	aspartic acid
a.u.	arbitrary units
BSF	bovine serum fetuin
CD	circular dichroism
CMC	critical micellar concentration
CMPF	3-carboxy-4-methyl-5-propyl-2-furanpropionic acid
Cp	molar fraction
ΔC_P	Heat capacity change
DSC	differential scanning calorimetry
$E^{1\%}_{1cm}$	specific extinction coefficient
FTIR	fourier transform infrared spectroscopy
FUR	furosemide
Glu	glutamic acid
HA	hippuric acid
HEWL	hen egg white lysozyme
HSA	human serum albumin
ITC	isothermal titration calorimetry
IAA	indole 3 acetic acid
IS	Indoxyl sulphate
kcal	kilocalorie
kDa	kilodalton
K_{sv}	stern-Volmer constant
K_b	binding constant

l	path length of the cell
Lys	lysine
M	molar
MTT	3-(4,5-dimethlthiazolyl-2)-2,3-diphenyltetrazolium bromide
MRE	mean residue ellipticity
NeuAc	n-acetyl neuraminic acid
NaCl	sodium chloride
NaOH	sodium hydroxide
NMR	nuclear magnetic resonance
Phe	phenylalanine
Pi	inorganic phosphate
O.D	optical density
SDS	sodium dodecyl sulphate
SPR	surface plasmon resonance
T_m	midpoint of thermal transition
TEM	transmission electron microscopy
ThT	thioflavin-T
Trp	tryptophan
Tyr	tyrosine
UV	ultra violet
w/v	weight by volume
WAR	warfarin

LIST OF FIGURES

LIST OF TABLES

CHAPTER 1

1.1. Protein-ligand interaction and associated conformational changes-an overview

1.1.1. Introduction

All biological processes that occur in body are directly or indirectly based on the fundamental principle of highly regulated intermolecular interaction and recognition. Amongst many types of such interaction, process-one is protein–ligand interactions [Perozzo et al., 2004]. In particular, proteins perform their function through interaction with molecules of low molecular weight called as ligands [Ahmad et al., 2012]. However, in biological systems, the term 'ligand' has many different meanings. In broadest sense, it is used to mean any molecule which interacts with a given macromolecule. The term ligand, thus includes other macromolecules (peptides/proteins/nucleic acids/lipids/carbohydrates or mixed molecular species) as well as, molecules of small molecular mass (arbitrary < ~ 1-2 kDa). So it can be said that, ligand therefore cover a very large and structurally diverse group of molecules which, unsurprisingly also display a wide variety of physico-chemical characteristics. According to Harding and Chowdhry [Harding and Chowdhry, 2001], ligands are those molecules which interact in (potentially) reversible, non-covalent manner with a given molecule and thereby moderate biological role in a controllable manner. Consequently, protein ligand interaction can be described as interaction of ligand to a protein molecule in reversible, non-covalent manner without the requirement to make or break covalent bonds. In light of this scenario, different aspects related to protein ligand interaction, ranging from, the mechanism of interaction, the conformational changes associated, forces involved, thermodynamics, techniques available for their study to importance of physiological significant protein ligand interactions are discussed.

1.1.2. Mechanism involve in protein-ligand interaction

The protein-ligand binding mechanisms have evolved from the early "lock-and-key" [Fischer, 1894] to the "induced fit" [Koshland, 1958] and to the now popular "conformational selection" models [Frauenfelder et al., 1991; Ma et al., 1999; Tsai et al., 1999].

1.1.2.1. Lock and key model. The lock-and-key model was first proposed by Fischer, 1894 [Fischer, 1894] to explain binding of a single substrate (ligand) to the enzyme (protein). According to this model, an analogy that explains enzyme as the lock and substrate as the key was given. The prerequisite of this model is that the enzyme and substrate are both rigid and their surfaces should be complementary, and therefore only the correctly sized key (substrate) fits into the key hole (active site) of the lock (enzyme). Besides, the keys with incorrectly positioned teeth (incorrectly shaped or sized substrate molecules) do not fit into the lock (enzyme) because both the key and the lock cannot change their shape and size as shown in Figure 1.1.1A. However, at that time nothing was known about the active site and thus in 1958, a biochemist, Daniel Koshland, [Koshland, 1958] thought that the 'lock and key' model required some modifications as the existed did not explain discrepancies such as the lack of hydrolytic activity of kinases, noncompetitive inhibition. Therefore, a modification called the 'induced fit' model was proposed to compensate for the rigid, structurally invariable protein and ligand.

1.1.2.2. Induced fit model. In 1958, a biochemist, Daniel Koshland, proposed the induced fit model (Figure 1.1.1B) in the following terms "a) the precise orientation of catalytic groups is required for enzyme action, b) the substrate causes an appreciable change in the three-dimensional relationship of the amino acids at the active site, and c) the changes in the protein structure caused by the substrate will bring the catalytic groups into the proper alignment, whereas a non-substrate will not." Briefly, according to it, the ligand binding induces a conformational change in the protein. However, it seems that this model holds for the proteins showing minor or moderate conformational change after the ligand binding. Bosshard [Bosshard, 2001] suggested that "induced fit is possible only if the match between the interacting sites is strong enough to provide the initial complex enough strength and longevity so that induced fit takes place within a reasonable time". Therefore, the induced fit mechanism alone cannot explain well the association between ligand and proteins undergoing large conformational changes after ligand binding [Tobi and Bahar, 2005]. Thus, the concept of conformational selection model has emerged as an alternative for induced fit and is becoming prevalent.

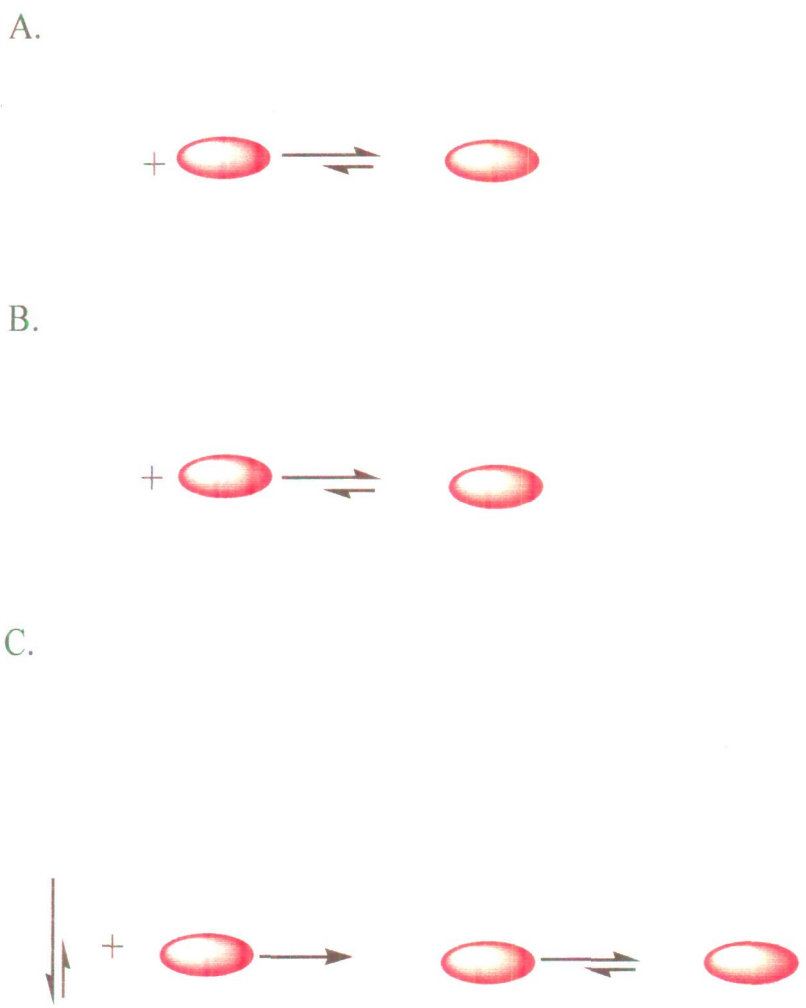

Figure 1.1.1. Different models for mechanism of protein ligand binding. (A) lock and key (B) induced fit (C) conformational selection model.

1.1.2.3. Conformational selection model. Recently, an alternative model, conformational selection (also termed as preexisting equilibrium, population selection, fluctuation fit, or selected fit), for induced fit has emerged and becoming established. Fundamentally, it is extension of folding funnel model, postulated that, among the conformations of the dynamically fluctuating protein the ligand selects the one that is compatible with binding, and shifts the conformational ensemble towards the most compatible state as shown in Figure 1.1.1C. Generally, the conformational changes in this model are beyond local side chains rearrangements near the binding site, but rather display large concerted motions or entire domain movements. Straub and Szabolcsi [Straub and Szabolcsi, 1964], was first to suggest the selective binding

of ligand to a single protein conformation in the ensemble, initial experimental evidence for the hypothesis came from Zavodszky et al in 1966 [Závodszky et al., 1966]. However, later, Frauenfelder, et al described the energy landscape of proteins [Frauenfelder et al., 1991], which in 1999 led to the generalized concept of 'conformational selection and population shift' [Ma et al., 1999; Tsai et al., 1999].

1.1.3. Conformational changes on interaction of ligand to protein

Protein conformation is of principal importance in understanding bimolecular interactions. In the simplest scenario, two molecules may interact with no change in their conformation, as in the key-and-lock model. Molecular interactions that involve conformational changes in the interacting molecules are more versatile and best explained by conformational selection model as explained earlier. Conformational changes may also take place away from the binding interface. This is often the prerequisite for functional activity. Binding of ligand in membrane receptor protein occurs at the extracellular region but causes changes at the cytoplasmic region, so that an extracellular signal is allowed to alter intracellular activity e.g. norepinephrine-induced helical rotational orientation changes in the transmembrane helices of ß2 adrenergic receptor, a G-protein coupled receptors and induced conformational changes that alter intracellular activity. Conformational changes in proteins are made possible by their intrinsic flexibility. These changes may occur with only relatively small expenditure of energy [Bhattacharya et al., 2008]. At the molecular structural level, conformational changes in single polypeptides are the result of changes in main chain torsional angles and side chain orientations. The overall effect of such changes may be localised with reorientations of a few residues and small torsional changes in the regional main chain. On the other hand torsional changes localised at very few critically placed residues may lead to large changes in tertiary structure. The later type of conformational changes is described as domain motions.

1.1.3.1. Domain motions. Domain motions have two basic components. Hinge motions may occur within strands, beta-sheets and alpha-helices not constrained by tertiary packing forces. On hinge-opening the motion is perpendicular to the plane of the interface, which is lost after opening as shown in Figure 1.1.2A.

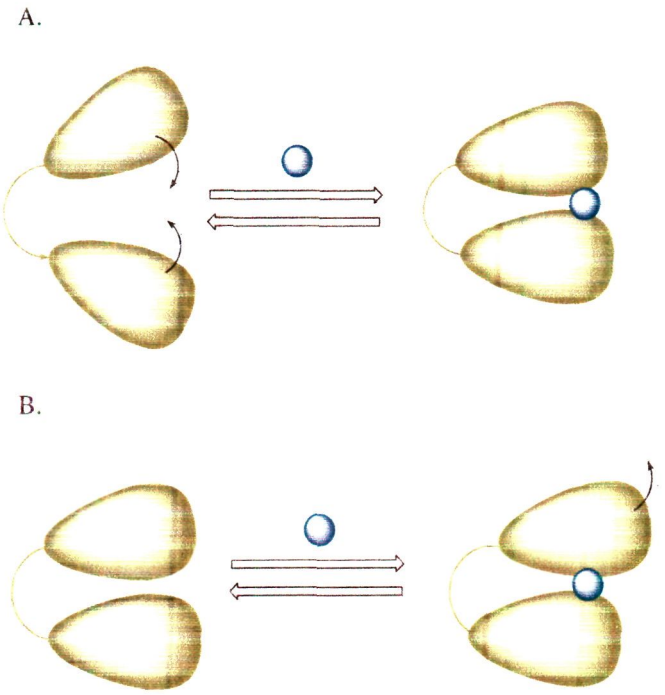

Figure 1.1.2. Mechanism of domain movement. (A) Ligand-induced hinge motion (B) Ligand-induced shear motion.

The closed conformation is usually stabilised by a bound ligand. It occurs in the context of secondary structure interactions. Hinge motion at extended strand involves a few large changes in main chain torsion angles at the hinge connecting two domains, constrained only by the Ramachandran allowance of torsional angles. Shear motions occur parallel to the interface between closely packed segments of polypeptides as shown in Figure 1.1.2B. This type of motion is more severely constrained with additional packing contacts due to interdigitating side chains. It occurs in the context of tertiary structure interactions. Large shear movement that makes the interdigitating lock from one state to another is not observed in domain motions, as in subunit interface of allosteric proteins [Gerstein et al., 1994].

1.1.3.2. Allosteric transitions. Multimeric proteins have an extra dimensionality to conformational transitions due to their quarternary structure. Conformational changes due to allosteric transitions are found in all G-protein binding receptors [Wang and Lewis, 2013], haemoglobin etc [Edelstein, 2013; Kukic and Nielsen, 2010]. Since, haemoglobin is the classic prototype of allosteric proteins with cooperative behaviour, thus the binding of small molecules (oxygen) at a region of the protein affects its binding affinity with other molecules at a distant region as shown in Figure1.1.3.

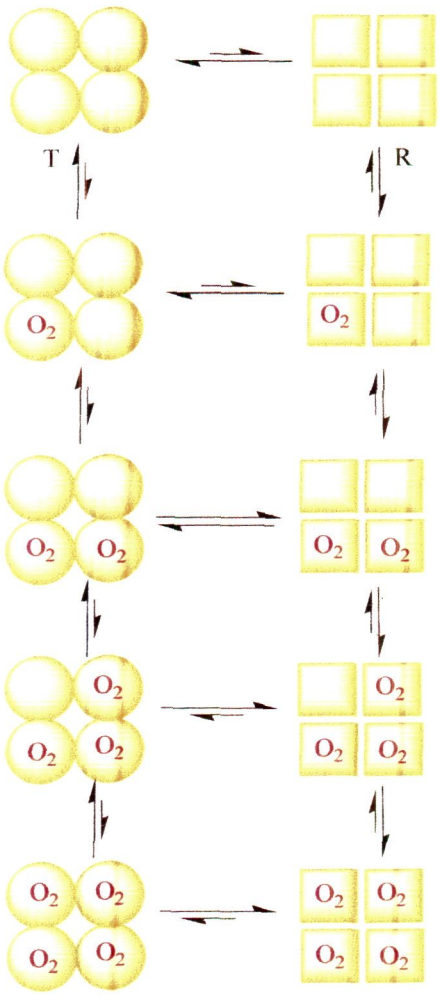

Figure 1.1.3.Allosteric behavior of hemoglobin on oxygen binding.

1.1.4. Forces involved in protein-ligand interaction

Protein ligand interaction can be described as interaction of ligand to a protein molecule in reversible, non-covalent manner without the requirement to make or break covalent bonds. The interacting molecules in each type of forces that held protein and ligand together are shown in Figure 1.1.4.

The main forces are discussed below:

1.1.4.1. Electrostatic interactions. These interactions play a prominent role in steering charged ligands into the protein binding site and thus are among the most important forces to be considered when analyzing the protein ligand binding interaction [Kukic and Nielsen, 2010]. The strength of these bonds may vary from 30-120 kcal/mol. The bond length is around 0.25 nm. There are three types of electrostatic interaction found:

1.1.4.1.1. Charge-charge interactions. These are found between oppositely charged atoms, ligand functional groups, or protein side chains, such as positively charged (amine or imine groups, lysine, arginine, histidine) and negatively charged (carboxyl group, phosphate groups, glutamate side chain). This type of electrostatic interaction has been observed in number of protein ligand systems in biological and non-biological systems [Sharp and Honig, 1990]. Since many drugs like virstatin, lomefloxacin etc contain acid or amine functional groups which gets ionized and thus interacts via ionic bonds formation with the positively charged carrier protein, human serum albumin at physiological pH [Chamani et al., 2011; Chatterjee et al., 2012]. Another protein ligand system where these forces predominate is interaction of sodium dodecyl sulphte (SDS) with protein at acidic pH. The headgroups of the surfactants bind to groups of opposite charge on the protein. A change in pH will cause a change in the net-charge of the protein and consequently in the binding as observed in soybean peroxidase [Zhang et al., 2009].

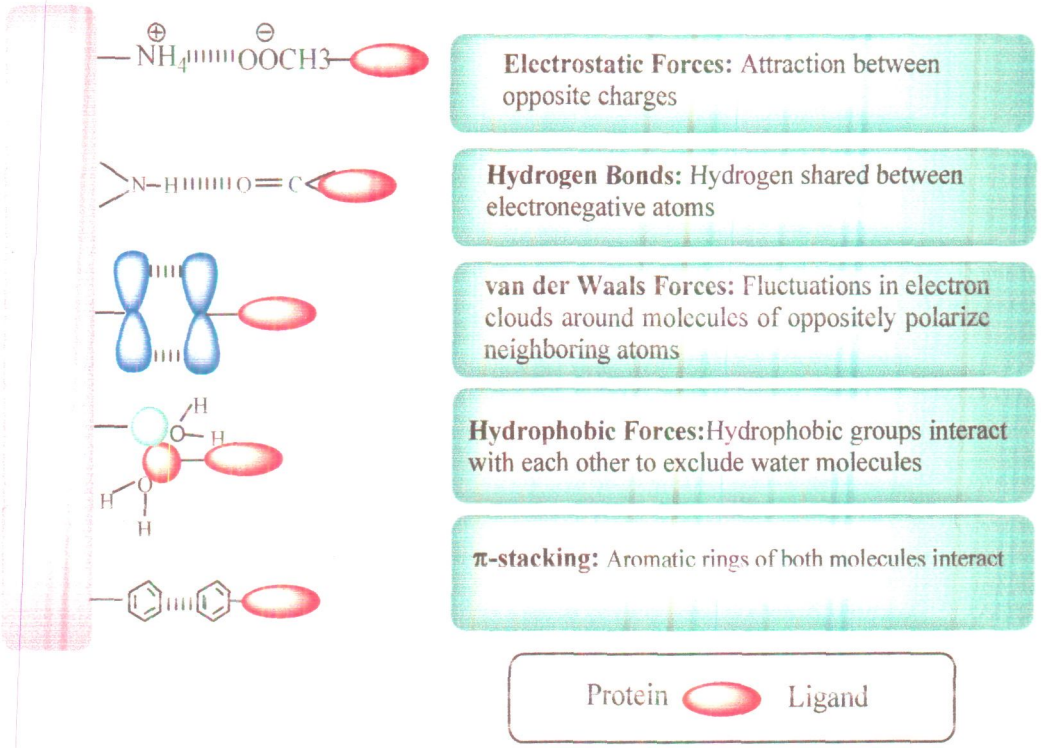

Figure 1.1.4. Diagrammatic representation of forces involved in protein ligand interaction.

Furthermore the characterstic features like bond length, bond strength along with the examples of each type of force are summarized in Table 1.11.

Table 1.1.1. Characteristics and examples of forces involved in protein ligand interaction.

Type of interaction	Bond length (nm)	Bond strength (kcal/mol)	Examples
Electrostatic interaction	0.25	30-120	Interaction of sodium dodecyl sulphate (SDS) and protein in low pH [Naidu and Prabhu, 2011]
Hydrogen bonding	0.30	0.4-35	Interaction of protein kinases and inhibitors [Katayama et al., 2008], tetracyclin interaction with human serum albumin (HSA) [Chi and Liu, 2011].
van der Waal forces	0.35	0.1-4	2-methoxy-3-isobutylpyrazine to the mouse major urinary protein[Barratt et al., 2005]
Hydrophobic interaction	-	-	Human serum albumin (HSA) interaction to halothane, furosemide [Zaidi et al., 2013a]
Aromatic rings interaction	-	-	Interaction of polyphenols with ß-amyloid [Porat et al., 2006], interaction of glycoacridines with ß-amyloid [Seedher and Bhatia, 2006]

1.1.4.1.2. Charge-dipole interactions. These are found between ionized amino acid side chains and the dipole of the ligand moiety or water molecule. An important contribution to the enthalpy change associated with a binding event arises from it. The dipole moments of the polar side chains of amino acid also affect their interaction with ligands [Sharp and Honig, 1990].

Factors. The electrostatic interaction depends upon the many factors:

• **Dielectric constant of the medium**. The strength of electrostatic interaction is inversely propotional to the dielectric constant of the medium. For water, that has highest dielectric constant, have lowest value of binding strength whereas in vacuum, the binding strength is maximum as shown in Table 1.1.1.

• **pH**. Change in pH majorly affects the electrostatic interaction between protein and ligands. As the pH drops, H^+ bind to the carboxyl groups (COO^-) of aspartic acid (Asp) and glutamic acid (Glu), neutralizing their negative charge, and H^+ bind to the unoccupied pair of electrons on the N atom of the amino (NH_2) groups of lysine (Lys) and arginine (Arg) giving them a positive charge. It change the net charge on the molecule (becomes more positive) and thus affects electrostatic interaction. However, with increase in the pH, H^+ are removed from the COOH groups of Asp and Glu, giving them a negative charge (COO^-), and from the NH_3^+ groups of Lys and Arg removing their positive charge. It changes the net charge on the molecule (becomes more negative) and thus affects electrostatic interaction.

• **Ionic strength.** Increasing salt concentration reduces the strength of ionic binding by providing competing ions for the charged residues.

1.1.4.2. Hydrogen bonding. These bonds are formed between hydrogen covalently bonded to some electronegative group ("donor"), and another electronegative atom, such as oxygen or nitrogen ("acceptor"). The hydrogen bond is specific, directional due to their orientations, lengths, and angular preferences. Proteins contain abundant hydrogen bond donors and acceptors in their backbone as well as in the side chains. These hydrogen bond donors and acceptors present in proteins interact with proton donors and acceptors (water molecule or any other ligand) present in the environment. Hydrogen bonding, therefore, occurs not only between ligand and protein and within

the protein itself, but also with the surrounding medium. These bonds are fairly weaker than ionic bond but are stronger than other non covalent bonds with strength between m 0.4-35 kcal/mol [Emsley, 1980]. As these bonds are weak, so can be formed and broken rapidly during binding event, conformational changes, or protein folding. It has been observed in certain cases even simple thermal fluctuations in biological systems may switched on or off hydrogen bonding [Tuckerman et al., 2002]. Due to these properties, the role of hydrogen bonds in governing specific interactions in biological recognition processes is absolutely crucial. Based on the location of donor/acceptor, hydrogen bonding is of two types, intra-and inter-molecular.

1.1.4.2.1. Intramolecular interaction involves the formation of non covalent bond between hydrogen (covalently bonded to electronegative group) with the electronegative atom of same molecule. The formation of a-helical structure secondary of protein is a typical example where intramolecular hydrogen bonding exists.

1.1.4.2.2. Intermolecular interaction involves the formation of non covalent bond between hydrogen (covalently bonded to electronegative group) with the electronegative atom of other molecule. There are ample of examples where intermolecular hydrogen bonding is found, for instance, interaction of human serum albumin (HSA) with drugs like tamoxifen, furosemide and many more [Bourassa et al., 2011; Zaidi et al., 2013a].

Both types of hydrogen bonding are partly responsible for the secondary, tertiary, and quaternary structures of proteins. They play a pivotal role in molecular recognition events, and thus influence the binding specificity of protein towards ligand. These interactions, despite of their weakness, play an important role in stabilising appropriate conformations of ligand-protein complexes, for instance among the complexes between protein kinases and their inhibitors [Bissantz et al., 2010], HSA and drug [Bourassa et al., 2011].

Factors. There are some factors which affects hydrogen bonding, including the

• **Nature of hydrogen donors and acceptors.** Particularly, in the nature of hydrogen-bond donors and acceptors, the resonance of electrons between donors and acceptors plays an important role in affecting the strength of hydrogen bonding. This resonance effect can redistribute the electron density on the hydrogen donors and acceptors by the driving force that having the conformation of structure to reach a most stable state. In addition, it can affect the basicity of the acceptors that further influence the strength of hydrogen bonding.

• **Solvent.** The type of solvent also affects the hydrogen bonding extent because of different level of intermolecular attractions. Some solvents involve in hydrogen bonding and thus interfere with the non covalent bonding of protein and ligand. Water is a very common example of interacting solvent and thus the binding strength of ligand to protein is found to be low in water as compare to vacuum as shown in Table 1.1.1.

1.1.4.3. van der Waals. These interactions are very important for the structure and interactions of biological molecules. There are both attractive and repulsive van der Waals interactions that control the binding events. Attractive van der Waals interactions involve two induced dipoles that arise from fluctuations in the charge densities that occur between adjacent uncharged atoms, which are not covalently bound. The attraction between molecules is greatest at a distance called the van der Waals radius. If molecules approach each other more closely repulsive forces develops. Repulsive van der Waals interactions occur when the distance between two involved atoms becomes very small, but no dipoles are induced. In the latter case, the repulsion is a result of the electron-electron repulsion that occurs in two partly-overlapping electron clouds [Ninham and Parsegian, 1970].

van der Waals interactions are very weak (0.1-4 kcal/mol) compared to other non covalent bonds. The magnitude of these forces depends on how easily an atom is polarized. There are three types of van der Waals forces

1.1.4.3.1. Dipole-dipole interaction. These forces, which occur between molecules containing electronegative atoms cause molecules to orient themselves so that the positive end of one molecule is directed toward the negative end of another.

1.1.4.3.2. Dipole-induced dipole interaction. A permanent dipole induces a transient dipole in an nearby molecule by distorting its electron distribution.

1.1.4.3.3. Induced dipole-induced dipole interaction. The motion of electrons in nearby nonpolar molecules results in transient charge imbalance in adjacent molecules. A transient dipole in one molecule results polarizes the electron in neighbouring molecule. This attractive interaction, often called London dispersion forces, is extremely weak.

Other than hydrogen-bond and disulfide bonds, van der Waals interaction is the another important bonding type that helps stabilizing the protein structure. In the coiled-coil protein and leucine zipper, there are heptad repeat which form by the side chain interaction between each alpha helix; heptad-repeat is repeated at every seventh residues [Landschulz et al., 1988]. If these repeating residues are hydrophobic, such as leucine, van der Waals interaction will be formed to stabilize this protein structure. These interactions were also observed in the binding of 2-methoxy-3-isobutylpyrazine to the mouse major urinary protein [Barratt et al., 2005].

1.1.4.4. Hydrophobic interaction. Hydrophobic interactions, believed to be important determinants of the stability of many protein structures, multisubunit protein complexes, and protein/ligand complexes, may be considered to be the result of two component interaction processes: the removal of nonpolar groups from water (hydration) and the packing of these groups within proteins or protein complexes. The interactions between ligands and the hydrophobic side chains of proteins contribute significantly to the binding free energy. When a ligand interacts with the protein hydrophobically, the first thing come in mind is that the clustering of their hydrophobic groups occurs. But it results in a negative contribution to the change in entropy of the system because the clustering corresponds to a decrease in the disorder of the system. Further, the role of the solvent should not be ignored which should be considered whenever a tendency for an event to occur is calculated. Thus, nonpolar ligand molecules/groups do dissolve slightly in water, but strong interactions of these molecules with water is not possible. Thus, introduction of such a non-hydrogen bonding surface into water causes disruption of the hydrogen bonding network between water molecules. The hydrogen bonds are reoriented tangentially to such

surface to minimize disruption of the hydrogen bonded 3D network of water molecules and thus leads to a structured water "cage" around the nonpolar surface. Thus, the hydrophobic interaction is mostly an entropic effect originating from the disruption of highly dynamic hydrogen bonds between molecules of liquid water by the nonpolar solute [Scatena et al., 2001]. Hydrophobic interaction involves in binding of most of the drugs like etoricoxib [Seedher and Bhatia, 2006], zonisamide [Shahabadi et al., 2013], due to hydrophobic nature of binding pockets of HSA. It also play role in inhibition of human protein kinase CK2a by tetrabromobenzotriazole and some C5-substituted analogues [Wasik et al., 2010].

Factors. The hydrophobic interactions are influenced by many factors, including

• **Temperature.** With increase in temperature, hydrophobic interaction increases. However at very high temperature, denaturation of protein occurs.

• **Carbon chain length**. With increase in length of carbon chain in ligand, generally hydrophobic interaction increases as observed in binding of butyl and octyl group containing ligand to trypsinogen [Lina et al., 2000].

• **Shape of hydrophobes**. Ligands having aliphatic groups, without branches on carbon chain have more chances of interaction via hydrophobic interaction than of aromatic groups and branched molecules because of steric hinderance in interacting with the other molecule.

1.1.4.5. Interactions mediated by aromatic rings. Noncovalent interactions involving aromatic rings such as p-stacking and cation/p are central in understanding many protein ligand complexes. It involves interaction between ligands and rings of aromatic amino acid (Phe, Trp, and Tyr) side chains in protein. The unique steric and electronic properties of these side chains give rise to large polarizabilities and quadrupole moments that result in interaction of aromatic rings of ligand and protein with preferred geometries. These interactions can be considered under electrostatic interaction [Salonen et al., 2011]. For interactions between two aromatic systems, there are two predominant geometries: parallel (two aromatic rings are parallel to each other) and perpendicular (two aromatic rings are perpendicular i.e. edge-to-face arrangement). The preference to perpendicular interactions increases when the acidity

of the interacting "side" atoms increases; this happens upon introduction of a strongly electron-withdrawing substituent in either ortho- or para-position.There are three types of interactions involving aromatic rings:

1.1.4.5.1. Cation-π interaction. This is a strong non-covalent force where the side chains (π components of aromatic amino acids) provide a surface of the negative electrostatic potential to bind with a range of cations and cationic amino acids through electrostatic interaction up to an average interatomic distance of 3.6 Å. In a protein, over 25% of all Trp are involved in cation–π interactions as Trp265-Lys248 in aldehyde oxidoreductase (-8.8 kcal/mol); Trp58-Lys76 in transaldolase B (-4.4 kcal/mol); Trp211-Arg77 in oligopeptide-binding protein (OppA) (-8.4 kcal/mol); Trp1175-Arg1136 in the tyrosine kinase domain of the insulin receptor (-6.8 kcal/mol) [Gallivan and Dougherty, 1999]. Protein–ligand or receptor–drug interactions such as binding of epinephrine, dopamine to G protein coupled receptors [Torrice et al., 2009], Cys-loop receptors (ligand-gated ion channels) with acetylcholine [Nys et al., 2013], tetrodotoxin to Na^+ channels [Santarelli et al., 2007] etc are remarkable examples having cation–π interaction.

1.1.4.5.2. π-stacking. This class of interaction involves direct attraction between arene rings. The π electrons in the aromatic rings of aromatic amino acids residues are localized above and below the face of the ring. This excess of electrons gives the face of the ring a small net negative charge, whereas the hydrogen atoms on its edge have a corresponding positive net charge. The electrostatic interaction between these partial charges dominates the interactions between aromatic rings. Such rings preferentially interact with the positively charged edge of one ring pointing at the negatively charged face of another, or with their rings parallel but offset so that the edge of one ring is interacting with the face of the other. The commonly held impression that aromatic rings interact favorably by stacking their rings one above the other is incorrect. This type of interaction is responsible for the self-assembly mechanism of amyloid formation and thus a lot of inhibitors having chances of π-stacking due to aromatic rings are proposed e.g. polyphenols [Hudson et al., 2009; Porat et al., 2006].

1.1.5. Thermodynamics of protein-ligand interaction

Determination of thermodynamic parameters is necessary for complete understanding of protein ligand interaction. Three important thermodynamic parameters are crucial to consider, change in Gibbs free energy (ΔG), enthalpy (ΔH), entropy (ΔS). These thermodynamic data contain information crucial not only for elucidating the binding mechanism but also for rational drug design through relating the thermodynamic data to the structural data, which alone cannot fully describe the driving forces for binding or predict accurately the binding affinity. The three fundamental parameters ΔG, ΔH, ΔS are discussed further in details.

1.1.5.1. Gibbs free energy (ΔG). It is the most important thermodynamic parameter because it determines the direction of the bimolecular equilibrium. The negative sign means that the binding reaction or conformational transition will proceed spontaneously to an extent governed by the magnitude of ΔG; the positive sign means that the energy is needed to drive the reaction to form a product, with the magnitude of ΔG specifying the amount of the required energy. Free energy changes are a function of states, i.e., their values are defined merely by the initial and final thermodynamic states, regardless of the pathway connecting them. Furthermore, it is a balance between enthalpy and entropy, e.g., the observed ΔG can be the same with completely opposing contribution by enthalpy and entropy (equation 1.1.1):

$$\Delta G^{\circ} = \Delta H^{\circ} - T\Delta S^{\circ} \qquad (1.1.1)$$

A protein ligand interaction with positive ΔH and ΔS (binding dominated by hydrophobic effect) can give the same value of ΔG as a interaction of another set of protein ligand with negative ΔH and ΔS (when specific interactions dominate). This is due to a common phenomenon observed in protein ligand interaction. This makes the binding free energy relatively insensitive to change in molecular details of the interaction process, and thus the consideration of the ΔH and ΔS are crucial for a detailed understanding of the free energy of binding [Perozzo et al., 2004].

Enthalpy-entropy compensation. If ligand interacts with protein by forces other than hydrophobic interaction than the ΔH is negative due to bonding but it occur at the expense of increased order, leading to more negative ΔS. However, if a ligand

interacts hydrophobically, the hydrophobic effect could become much more significant than the loss of entropy (conformational entropy, rotational and translational entropy) or decrease in order. The consequences of the enthalpy-entropy compensation are i) that it does not bring out dramatic change in the binding free energy and as such leads to only small changes in binding affinity over a range of temperatures; ii) that it makes it difficult to distinguish between the entropy-driven or enthalpy-driven binding processes and, therefore, cautions are required to explain the experimental data, design drug, or plan engineering experiments. This phenomenon of enthalpy-entropy compensation has been widely observed in biological systems by using the thermodynamic methods [Chodera and Mobley, 2013; Eftink et al., 1983; Perozzo et al., 2004].

1.1.5.2. Enthalpy (ΔH). It is a measure of the total energy of a thermodynamic system. It includes the internal energy, energy required to make room for it by displacing its environment and establishing its volume and pressure. The total enthalpy, H, of a system cannot be measured directly and, as such, the change in enthalpy, ΔH, is a more useful quantity than its absolute value, which is equal to the sum of non-mechanical work done on it and the heat supplied to it. The ΔH is positive or negative in endothermic or exothermic process, respectively. In the protein-solvent system, the enthalpy change reflects the amount of heat energy required to achieve a particular state. For binding reactions, negative enthalpy values are common (but not omnipresent), reflecting a tendency for the system to fall to lower energy levels by bond formation. The binding enthalpy in its strict sense is considered as the noncovalent bond formation at binding interface. However, the heat effect of a binding reaction is a global property of the entire system, including contribution from solvent and protons [Cooper and Johnson, 1994]. Therefore, the change in enthalpy of binding must be the result of the formation and breaking of many individual bonds, including the loss of protein-solvent and ligand-solvent hydrogen bonds, electrostatic and van der Waals interactions, the formation of noncovalent bonds between the protein and ligand, and the solvent reorganization near the protein surfaces. These individual components may make either favorable or unfavorable contributions, and the result is a combination of these contributions, with specific interactions dominating the binding enthalpy.

1.1.5.3. Entropy (ΔS). It is a measure of the tendency of a process, such as a chemical reaction, to be entropically favored, or to proceed in a particular direction. Further the entropy can be seen as an expression of the disorder or randomness. The total entropy change (ΔS_{tot}) of protein-ligand binding can be expressed as the sum of the three entropic terms: the solvent entropy (ΔS_{solv}), conformational entropy (ΔS_{conf}) and the rotation and translation entropy ($\Delta S_{r/t}$) as shown in equation:

$$\Delta S_{tot} = \Delta S_{solv} + \Delta S_{conf} + \Delta S_{r/t} \quad (1.1.2)$$

where the ΔS_{solv} describes the change in entropy resulting from solvent release upon binding; the ΔS_{conf} is a configurationally term reflecting the reduction in rotational degrees of freedom around torsion angles of protein and ligand; and the $\Delta S_{r/t}$ represents the loss in translational and rotational degrees of freedom of the acceptor and ligand upon complex formation. The most important contribution to the ΔS_{tot} arises from the solvation term ΔS_{solv}, primarily due to the release of well-bound water molecules on the surfaces of the protein and ligand, and the accompanying burial of the hydrophobic surface area. Since the entropy of hydration of polar and apolar groups is large, the burial of solvent accessible surface area and the solvent release upon binding often make a large, favorable contribution to the entropy increase. The ΔS_{conf} and $\Delta S_{r/t}$ make unfavorable contributions to total entropy, i.e., causing entropy reduction. Although the positive entropy changes resulting from a natural tendency for disruption of order and exclusion of water molecules are common for binding reactions [Chodera and Mobley, 2013], all binding reactions would have to overcome the inescapable entropic penalties [Amzel, 2000] (i.e., the negative $\Delta S_{r/t}$ and ΔS_{conf} upon complex formation) through large solvent entropy gain (positive ΔS_{solv}) or favorable protein-ligand interactions (negative ΔH) if binding is to occur. Based on the above details, [Ross and Subramanian, 1981] predicted the forces involved in the binding of protein to ligand by the sign and magnitude of thermodynamic parameters ΔH and ΔS are summarized in Table 1.1.2.

1.1.5.4. Heat capacity (ΔC_P). It characterizes the amount of heat required to change a substance's temperature by a given amount. In protein ligand interaction, when ligand binds to protein, there occurs removal of water molecules from protein surface area

that often results in a large negative ΔC_P. Therefore, the heat capacity provides a link between thermodynamic data and structural information of macromolecules through the correlation of ΔCp and burial of surface area [Rajarathnam and Rosgen, 2013]. It is determine from the value of ΔH by following equation:

$$\Delta C_p^{exp} = \frac{d\Delta H^\circ}{dT} \qquad (1.1.3)$$

Table 1.1.2. Expected signs of thermodynamic parameters (ΔH and ΔS) in different types of interaction as adapted from [Ross and Subramanian, 1981].

Types of interaction	Enthalpy change (ΔH)	Entropy change (ΔS)
Electrostatic	Slight positive/negative	positive
Hydrogen bonding (at low dielectric medium)	negative	negative
van der Waal	negative	negative
Hydrophobic	positive	positive

1.1.6. Techniques used to study protein-ligand interaction

Figure 1.1.5 enlists all techniques that give information directly or indirectly about the binding of ligand to protein. The basis of detection, information obtained, concentration of protein used and limitations of the following discussed techniques are presented in Table1.1.3.

1.1.6.1. Spectroscopic techniques

1.1.6.1.1. Fluorescence spectroscopy. It is widely used method for studying protein conformational changes and protein ligand interaction. This is because of the presence of intrinsic fluorophores (tryptophan, tyrosine and phenylalanine) in almost all proteins. In addition, certain extrinsic fluorophores (like 1-anilino,8-naphthalene sulphate, Thioflavin T) have been developed that can be used for specific probing of the function and structure of proteins [Biancalana and Koide, 2010; Gasymov and Glasgow, 2007]. To study ligand binding to protein, change in quantum yield of ligand fluorescence, intrinsic protein fluorescence, or fluorescence of a covalently or noncovalently bound fluorescent probe whichever is sensitive is determined. It can be

used indirectly to calculate the binding constants and stoichiometry of particular protein-ligand interactions from the dependence of the observed fluorescence of a protein ligand mixture upon total ligand concentration. The relevant theory, approach, and possible pitfalls associated with the fluorescent measurement of interactions is presented with respect to both perturbation of ligand fluorescence on binding, along with the perturbation of the intrinsic fluorescence of acceptor on interacting with ligand. Furthermore, fluorescence spectroscopy can also be used to trace the formation of amyloid by using external fluorophore which specifically binds to amyloid fibrils. It is very sensitive techniques (picogram quantities of protein can be detected). However, it reported the microenvironment of the fluorophores and its data analysis is also not easy. Fluorescence measurements can be broadly classified into two types of measurements:

- **Steady-state measurements.** The most common type, are those performed with constant illumination and observation. The sample is illuminated with a continuous beam of light, and the intensity or emission spectrum is recorded. Because of the nanosecond timescale of fluorescence, most measurements are steady-state measurements. When the sample is first exposed to light, steady state is reached almost immediately.

- **Time-resolved measurements**. It is used for measuring intensity decays or anisotropy decays. For these measurements the sample is exposed to a pulse of light, where the pulse width is typically shorter than the decay time of the sample. This intensity decay is recorded with a high-speed detection system that permits the intensity or anisotropy to be measured on the nanosecond timescale. It provides information not available from the steady-state data. It is important to understand the relationship between steady-state and time-resolved measurements. One can distinguish static and dynamic quenching using lifetime measurements in protein ligand interaction studies. Formation of static ground-state complexes do not decrease the decay time of the uncomplexed fluorophores because only the unquenched fluorophores are observed. Dynamic quenching is a rate process acting on the entire excited-state population, and thus decreases the mean decay time of the entire excited-state population. Resonance energy transfer is also best studied using time-resolved measurements [Alcala et al., 1987; Lakowicz, 2006].

1.1.6.1.2. Circular dichroism spectroscopy (CD). It is used to study structural changes of proteins. Changes in conformation upon changing pH, temperature, presence and absence of ligand can be studied by CD measurements. For determination of structure of protein by CD, it is not necessary to know the amino acids sequence. Further it also take small amount of sample (0.1-1 mg/ml) and consume less time as compare to NMR and X-ray. For protein ligand interaction study, stop flow mode is particularly useful. However, certain compounds have low signal to noise ratio and thus samples should be UV transparent that limits the use of certain buffers, salts and solvents [Kelly and Price, 2000].

1.1.6.1.3. Fourier transform infrared spectroscopy (FTIR). FTIR spectroscopy provides information about the secondary structure content of proteins, like CD and unlike X-ray crystallography and NMR spectroscopy which provide information about the tertiary structure [Barth, 2007]. Characteristic bands found in the infrared spectra region of proteins and polypeptides include the Amide I (1700-1600 cm^{-1}) and Amide II (1600-1500 cm^{-1}). These arise from the amide bonds that link the amino acids. The absorption associated with the Amide I band leads to stretching vibrations of the C=O bond of the amide, absorption associated with the Amide II band leads primarily to bending vibrations of the N—H bond . Because both the C=O and the N—H bonds are involved in the hydrogen bonding that takes place between the different elements of secondary structure, the locations of both the Amide I and Amide II bands are sensitive to the secondary structure content of a protein. It can also be used in amyloid protein and/or peptide studies. The multiple advantages provided by it allow an almost continuous structural view of protein/peptide conversion during the aggregation process. Moreover, it is now well-established that infrared can differentiate oligomers from fibrils simply on their spectral features. Thus it is certainly the fastest and easiest method to obtain this information. It has limitation that it requires higher protein concentration thus there are possible chances of aggregation in the samples [Sarroukh et al., 2013].

1.1.6.2. Calorimetric methods.

1.1.6.2.1. Isothermal titration calorimetry (ITC). ITC measures the heat evolved during macromolecular association events. In an ITC experiment, one binding partner

(ligand) is titrated into a solution containing another binding partner (protein), and the extent of binding is determined by direct measurement of heat exchange (whether heat is being generated or absorbed upon the binding. It helps in understanding the binding mode, binding affinity, stoichiometry, ΔH, ΔS and ΔG. This is the direct method for determination of thermodynamic parameters of protein ligand interaction and the experiments can be performed in a physiologically relevant buffer, no surface effects have to be taken into account, and the interacting species do not require immobilisation or labelling. But the use of higher concentration of protein is the limitation. It is a major limitation as in the case of relatively weak energetic of protein–ligand interactions [Falconer and Collins, 2011] where solubility of protein and ligand is a major issue. Further at higher concentration, molecular crowding, where molecular interactions were also involved, is not ignorable [Ward and Holdgate, 2001]. Besides, the obtained binding constant should be in narrow range (10^4–10^9 M^{-1}).

1.1.6.2.2. Differential scanning calorimetry (DSC). It measures the heat capacity of the system as a function of temperature under isobaric condition. It has become a popular method in biophysical chemistry for evaluating protein conformational stability as well as protein–ligand and protein–protein interactions. As it involves model-based assumptions. More recently, the application of theory to DSC has been proved to be useful for estimating very high binding constants, as well as for characterizing the energetics of binding and unfolding. In this context, it is useful to simulate the signal obtained by DSC in order to:

• Understand the thermodynamic basis underlying the observed changes in protein stability when the macromolecule binds to a specific ligand,

• Identify the chemical equilibria and modifications that give rise to the observed output signal from the calorimeter, and

• Interpret the experimental data by comparing the real and theoretical process, thus confirming or eliminating the assumed model. It also helps to elucidate the redistribution among the different species (native, unfolded, and liganded protein) involved in the global unfolding process by using the species distribution profile. However, like ITC it also requires the higher concentration of protein. But, in DSC,

the temperature range under which thermal denaturation can be studied has a limit due to generation of vapour pressure in sealed chambers as a consequence of gas evolution on the denaturation of proteins that may lead to over pressurization and rupture which limits the effective temperature range of experimentations. Furthermore the dimensional changes in the protein should be measured over any time but the heat exchange during a process from DSC cannot be determined over long times or at slow heating or cooling rates since the finite quantity of heat exchanges will be dispersed over too long a time to be detected. Baseline curvature limits the sensitivity of DSC for detecting weak transitions. As other sensitive instruments, the purity of the sample is a prerequisite to the DSC. For DSC measurements of heteromeric proteins (multimeric), the subunits seem to be polymorphic species which are sensed as an impure sample. The major issue is that DSC can measure heat capacity for reversible process. Further, thermal aggregation of proteins may cause severe harm to the instrument as well as the quality of data because heterogeneous (solid and liquid) systems are difficult to examine [Johnson, 2013].

1.1.6.3. X-ray crystallography. It is well established technique that gives comprehensive atomic level information. It determines the structures of large molecules and assemblies along with the proper surface water molecules positions. It produces a single structural model that is easy to visualize and interpret. However, a crystal is a stationary assemblage procured from an extremely non physiological-concentrated solution. This intense environment may itself cause conformational alterations in the protein molecule to induce an altered mode of ligand interaction which ultimately results in erratic interaction induced conformational changes from its original one. Moreover, the crystal structures of protein bound with the ligand are generally acquired by co-crystallization but the milieu of crystallization conditions for apo-protein are not essentially identical for this co-crystallization [Brylinski and Skolnick, 2008]. Hence, ligand-induced conformational transitions in a protein–ligand complex offer a dispute for the accurate structural determinations. In some cases, even crystal production can be difficult and often impossible. When the protein is large and flexible, then crystals structure formation is problematic and the final structural model represents a time averaged structure, where details of molecular mobility remain unresolved.

1.1.6.4. Nuclear magnetic resonance (NMR). It gives comprehensive atomic level information of proteins or protein ligand complex under solution conditions which are closer to biological condition and also free from artifacts resulting from crystallization as that of X-ray crystallography. It also provides about the information on dynamics and thus increasingly used to monitor conformational changes on ligand binding to proteins/ fragments [Stark and Powers, 2012]. However, it requires concentrated solution and thus presents chances of aggregation. Further it is limited to determination of structure of small proteins (< 20 kDa).

1.1.6.5. Surface plasmon resonance (SPR). It is a rapidly developing technique for the study of ligand binding interactions with membrane proteins, which are the major molecular targets for validated drugs and for current and foreseeable drug discovery. SPR is label-free and capable of measuring real-time quantitative binding affinities and kinetics for membrane proteins interacting with ligand molecules using relatively small quantities of materials and has potential to be medium-throughput. However this is insensitive to the contaminants problem from surface coupling [Patching, 2013].

1.1.6.6. Molecular docking. These methods are used for determination of ligand binding sites on the protein along with binding energies. However, docking is still constrained by their restricted consideration of protein flexibility issues. The degree of flexibility is limited to either side chain motions or small variations of the backbone. However, certain degree of flexibility is allowed by modeling side-chain variations in Autodock4, Gold, FlexX, Rosetta Ligand and small variations of the backbone in Glide, Rosetta Ligand [Ahmad et al., 2012]

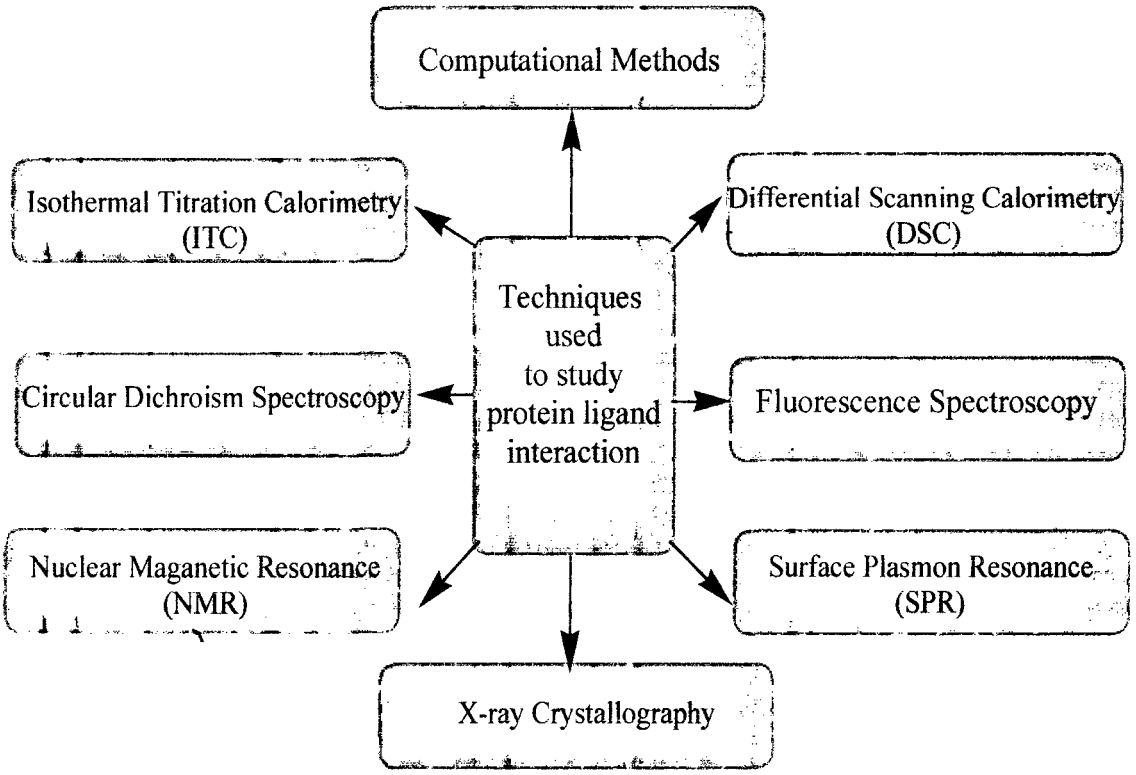

Figure 1.1.5. Overview of techniques used to study protein ligand interaction and associated conformational changes.

Table 1.1.3. Overview of techniques for characterizing protein-ligand interaction [Harding and Chowdhry, 2001].

Techniques	Basis of detection	Information obtained	concentration	Limitation
Fluorescence spectroscopy	rotational diffusion, change in fluorescence property	Binding affinity, Binding energy, change in conformation in the solution	0.1-0.2 mg/mL	Difficulty in distinguishing between ligand induced conformational changes or quenching by ligand.
Circular dichroism spectroscopy	Change in optical rotation	Secondary and teritiary structure changes	0.2-1 mg/mL	Unable to demarcate local changes in the protein molecule
Fourier transform infrared spectroscopy	Change in Amide I band	Secondary structure change	5-10 mg/mL (10 μL-1ml)	High protein concentration is required
Isothermal titration calorimetry	Heat change on ligand binding	Stoichiometry, ΔH, ΔS, ΔG	0.1-1mg/mL (0.5-2 ml)	Higher concentration is required due to which molecular crowding occurs.
Differential scanning calorimetry	Heat change on thermal transition	ΔH, ΔC_P, T_m	0.1-1mg/mL (0.5-2 ml)	for heteromeric proteins (multimeric), the subunits seem to be polymorphic species and are sensed as an impure sample.
X-ray crystallography	Structure change	Conformation of protein, protein ligand complex	100 mg	For large and flexible protein formation of crystals is problematic, chances of artifacts
Nuclear magnetic resonance	Change in chemical shift, diffusion rate (rotational and translation relaxation)	Change in structure dynamics, equilibrium constant ($K_d > 10^{-3}$-10^{-9} M)	50-100 μM for 1D, 3 mM for 2D (0.5 mL)	Requires concentrated solution and thus presents chances of aggregation.
Surface Plasmon resonance	Change in mass bound to surface	Stoichiometry, binding affinity (K_d~10^{-3}-10^{-9} M)	0.01 μg, 100 μL	insensitive to contaminants problem from surface coupling
Docking	-	Binding energy, binding site determination	-	protein flexibility issues
Homology modeling	Homology	protein structure	-	Problematic for proteins having low homology with template

1.1.7. Examples of protein-ligand interaction

1.1.7.1. Ligands interaction to human serum albumin (HSA). The HSA is the most abundant serum protein that serves as a transporter for several endogenous and exogenous compounds [Varshney et al., 2010]. It binds ligands generally on two sites which are present in subdomain II A and subdomain III A [Sudlow et al., 1975]. It transports biologically active ligands like fatty acids, hemin, bilirubin as well as drugs in the body to their target sites. Binding of drugs to HSA plays a major role in drug therapy as it affects pharmacokinetics and pharmacodynamics of drugs. Among pharmacokinetic parameters, distribution plays a key role in determining the ability of drug effectiveness. The unbound or free drug fraction determines the actual volume of distribution and the drug concentration at the target site. However, the free fraction of a drug is significantly reduced when the drug affinity to the HSA is high. Thus, high affinity for HSA may consequently be a benefit or a drawback for efficacy depending on the drug and the target. For instance, HSA binding is particularly useful for lipophilic drugs (β-blockers) and metabolites, because this binding improves their solubility and sometimes decreases their toxicity. Significant changes of the free drug concentration can occur because of the interaction of the administered drug with other therapeutics or endogenous compounds for their binding to the carrier. Illness status can also determine a changing of the unbound drug fraction because of significant alterations of the serum carrier concentration [Lin and Lu, 1997]. For instance, HSA interacts with certain harmful compounds which are synthesized inside the body or accumulated in diseased condition e.g. uremic toxins. It includes variety of compounds including hippuric acid (HA), indoxyl sulfate (IS), and 3-carboxy-4-methyl-5-propyl-2-furanpropionic acid (CMPF), indole-3-acetic acid (IAA), creatinine, p-cresol [Duranton et al., 2012]. These compounds retained in the blood during kidney related diseases and interact negatively with the normal biological functions of the body. These uremic toxins interfere with the binding of drugs to HSA and thus disturb the drug disposition and pharmacological actions. One of the examples is of furosemide, one of the most potent diuretic drugs commercially available. The changes in its pharmacokinetics and pharmacodynamics are frequently seen in patients of renal problem. Even when concentration of HSA is within the reference range, a decrease in serum binding of furosemide is frequently observed

[Takamura et al., 1997]. It is believed to be due to the competition between uremic toxins and drug for the binding site on HSA as shown in Figure 1.1.6. Another example is the concurrent administration of warfarin, anticoagulant drug, with phenylbutazone, which is known to bind to the same high-affinity binding site on HSA, results in an enhanced risk of hemorrhage in patients because of the higher concentration of the free anticoagulant drug being displaced from the shared binding site on the carrier. Thus it is necessary to understand the binding mechanism, location of binding sites, binding energetics to HSA as well as pharmacokinetics and pharmacodynamics of drug in the body.

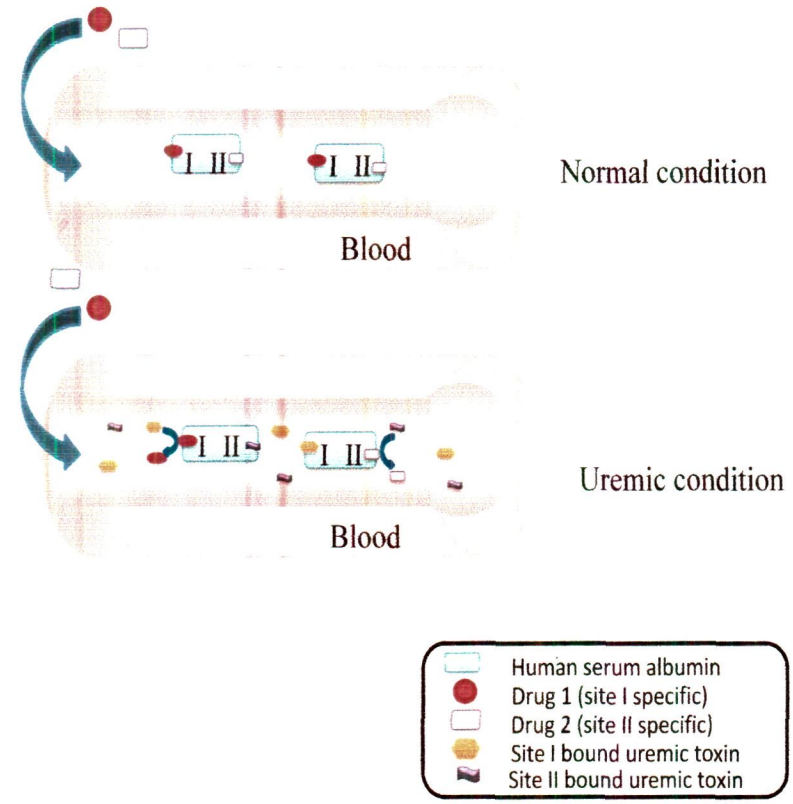

Figure 1.1.6. Schematic representation of mechanism of drug interaction in uremic condition.

1.1. 7.2. SDS-protein interaction. Sodium dodecyl sulphate (SDS) is amphiphilic molecule that preferentially absorbed at interfaces [Tanford, 1973]. It is an anionic surfactant with a 12-carbon hydrophobic tail and a negatively charged sulfate hydrophilic head group. It is known to interact with globular proteins, and in general, causes denaturation almost 1000 times lower concentration that is generally needed for other chemical denaturants such as urea [Chamani et al., 2006; Lee et al., 2011; Moosavi-Movahedi et al., 2005; Nielsen et al., 2007; Tanford, 1968]. However, it also cause refolding of proteins like DNA binding protein having leucine zipper [Lanckriet

and Middelberg, 2004; Moriyama et al., 2003]. The mode of SDS binding to proteins distinguished according to the concentration. At the sub-critical micellar concentrations (sub-CMC), SDS monomers bind to proteins by predominantly hydrophobic interactions causing unfolding of the tertiary structure, and at concentrations higher than CMC, the micelles nucleate on the hydrophobic patches of the protein chain driving it to expand [Bhuyan, 2010]. However, the mode of interaction changes with the change in pH as in the case of soyabean peroxidase [Zhang et al., 2009]. Protein-SDS interaction has wide range of applications from food industry to cosmetics and the drug industry [Li et al., 1995; Moore et al., 2003; Murray et al., 1969; Rangel-Yagui et al., 2005; Wang, 1999]. SDS mimics the native hydrophobic milieu of the phospholipids bilayer in vivo and thus study of protein surfactant interaction serves as model for membrane proteins and lipids interaction [Gangabadage et al., 2008; Ulmer and Bax, 2005]. It is observed that in sub-CMC of SDS the peptide from human complement receptor 1 is initially alpha-helical but converts rapidly to a beta-sheet structure and large quantities of fibrils forms. However, above the CMC, peptide adopts a stable alpha-helical structure and no fibrils are observed. These findings demonstrate the sensitivity of fibril formation to solution conditions and suggest a possible role for membrane components in amyloid fibril formation in living systems [Pertinhez et al., 2002]. Thus increased knowledge in this area may also play role in understanding the membrane protein-lipid interaction under neurodegenerative disorders.

1.1.7.3. Small molecules interact with proteins and inhibit/induce aggregation. Proteins have native functional states but can form amyloid fibrils under certain diseased condition. In the amyloid state, proteins aggregated with β-sheet-rich structures. Accumulation of amyloids can result in protein amyloidosis, which has attracted much attention. Amyloidosis is associated with many serious neurodegenerative diseases, such as Alzheimer's disease [Sipe, 1992], prion disease, [Safar and Prusiner, 1998]. Consequently, it is important to clarify the mechanism of amyloidosis, so that it can be inhibited or controlled. There has been much interest in the past decade in explaining and characterizing small molecules that interacts with amyloids and can either act as labels and allow imaging techniques to detect deposited amyloid structures (e.g. thioflavin T and congo red dye etc) or may have potential to act as future de novo inhibitors' (therapeutic agents) for the treatment of amyloid-

associated diseases (e.g. polyphenols, acridines, osmolytes etc). However, the mode of interaction is different for different type of molecules as shown in Figure 1.1.7.

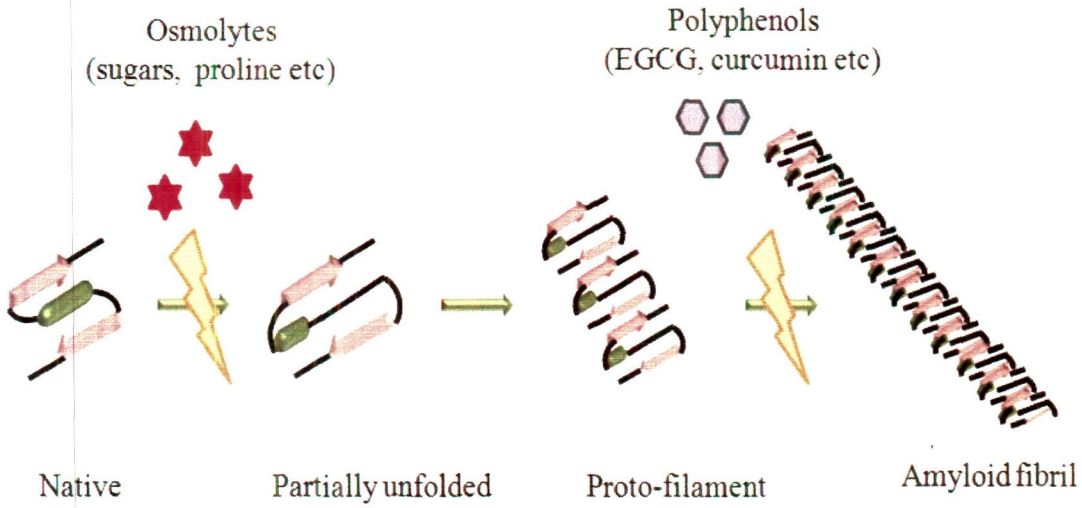

Figure 1.1.7. Schematic representation of mechanism of interaction of small molecules (osmolytes, polyphenols) with the protein amyloids.

For instance it is believed that, polyphenols inhibits amyloid formation by weak forces between inhibitor and peptide chains, including hydrogen bonding, hydrophobic and aromatic interactions have been suggested to be the driving forces in the anti-amyloidogenic role of polyphenols [Porat et al., 2006]. Furthermore, antioxidant capacities are also thought to be involved in the anti-amyloidogenic activity of polyphenols [Conte et al., 2003]. Studies on inhibition of the amyloid formation in lysozyme by glycoacridines suggest that planarity of the acridine core ring is important but not the sole parameter affecting the inhibitory activity of the compounds [Seedher and Bhatia, 2006]. Another group of inhibitor is osmolytes which inhibits amyloid formation of lysozyme also induce refolding of misfolded proteins and stabilizing proteins [Kar and Kishore, 2007]. Mechanisms of protein osmolyte interactions, the effect of osmolytes on protein stability, and how osmolytes correct protein misfolding defects and remove protein aggregation have been widely investigated. It has been demonstrated that the unfavourable interaction between the peptide backbone and the osmolytes leading to the preferential hydration of the protein domain is the driving force of protein stabilization or folding. It was also observed that certain molecules like inorganic phosphate (Pi) that is also a part of normal metabolism binds specifically to the active site of acylphosphatases from Sulfolobus solfataricus and Drosophila melanogaster and inhibits the formation of

amyloid-like aggregates [Soldi et al., 2006]. Furthermore, amyloidosis occurs at the cell surface, the interaction between the protein and cell interface is also important. Thus the molecules on the cell surfaces are of interest as additives to control amyloidosis. Glycosaminoglycans (heparin sulpate) interacts with Amyloid beta (Aβ) (Alzheimer's disease) [Leveugle et al., 1994], β2-microglobulin (dialysis related amyloidosis) [Corlin et al., 2010], and prion protein [Gonzalez-Iglesias et al., 2002], human muscle acylphosphatase [Motamedi-Shad et al., 2012] and induce protein amyloidosis. Thus the interaction between protein amyloids and small molecules are of immense importance for discovery of future de novo therapeutic agents against amyloid-associated diseases.

1.2. Introduction of proteins used in study

Below, a brief introduction of proteins structure and function is given that are used in this thesis.

1.2.1. Human serum albumin (HSA)

It is a multifunctional and non-glycosylated, single-chain protein synthesized in liver cells. It has 585 amino acids and a molecular weight of 66.5 kDa [Varshney et al., 2010]. Due to a large number of acidic (98 Glu + Asp) and basic (83 Lys + Arg) residues, the protein are highly soluble in aqueous media (>20% w/w). The three-dimensional structure has been determined crystallographically in several laboratories, and now the structure is known at a resolution of 2.3 Å [He and Carter, 1992; Sugio et al., 1999]. The protein has 67% α-helix but no β-sheet, and it contains three homologous domains that assemble to form a heart-shaped molecule as shown in Figure 1.2.1 The protein has three homologous domains (I–III), each domain comprises two subdomains (A and B) that possess common structural elements. The A and B subdomains have six and four α-helices, respectively, connected by flexible loops. Except one (Cys34), all 34 cysteine residues are involved in the formation of stabilizing disulfide bonds. The protein has single tryptophan residue present at position 214 of amino acid sequence in drug binding site I. [Peters, 1996] (Table 1.2.1). Small-angle X-ray scattering studies and combined phosphorescence depolarization-hydrodynamic modeling study has suggested that the overall conformation of HSA at neutral pH is very similar to that observed in crystal structures [Ferrer et al., 2001; Olivieri and Craievich, 1995]. In a healthy individual, the daily turnover of HSA is about 14 g, which amounts to about 25% of the protein synthesis activity of the liver. About 120 g is found in the circulation resulting in a plasma concentration of about 0.6 mM, the highest concentration of any protein in plasma. However, an even larger pool of HSA is found in the extra vascular spaces (about 240 g) although at lower concentrations. This fact implies that the functions of HSA are not restricted to the blood [Peters, 1996]. Furthermore, the high plasma concentration and half-life of about 19 days also implies that the protein have a significant role in the metabolism. Among many roles of HSA in the body, the

detoxification, maintenance of osmolarity in plasma and transportation of variety of endogenous and exogenous substances in the body are the most important functions [Kragh-Hansen, 2013]. As of its transporting role, it binds substances at two major binding region, namely Sudlow's site I and II, which are located within cavities in subdomains IIA and IIIA, respectively [Sudlow et al., 1975] (Figure 1.2.1). Thus the remarkable properties of HSA account for the central role in both the efficacy and rate of delivery of drugs, so detailed knowledge of the binding interaction of a drug with HSA becomes an important research field in clinical medicine. So, an extensive investigation of the interaction between HSA and many endogenous and exogenous compounds is always the topic of utmost investigation as it enucleates the transportation and distribution of drug in the body.

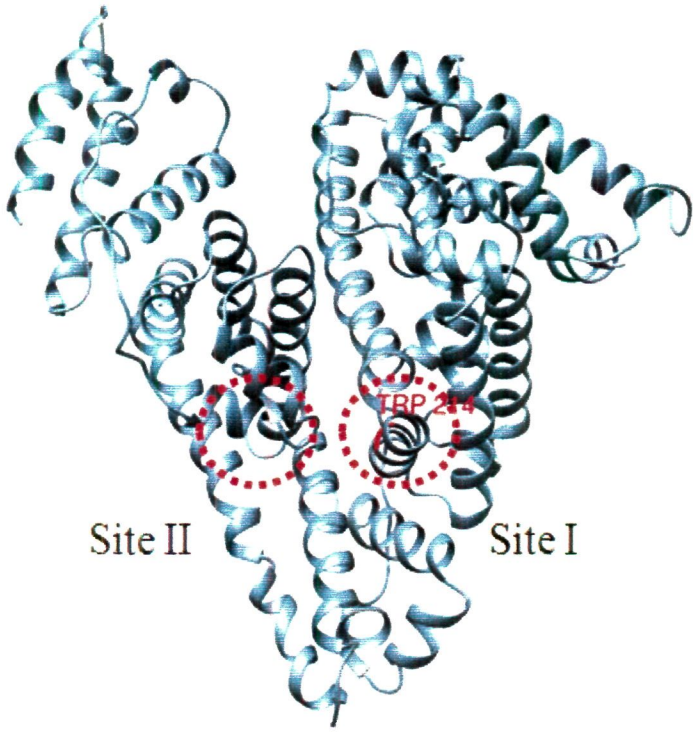

Figure 1.2.1. Crystal structure of human serum albumin (HSA) as obtained from PDB having PDB Id 1AO6.

Furthermore, HSA also possess pseudo esterase like activity that makes it potentially useful for therapeutic purposes. For example, it is capable of hydrolyzing ester prodrugs to their pharmacologically active forms. Drug olmesartan, a novel angiotensin II receptor antagonist used in the treatment of hypertension is converted from olmesartan medoxomil by HSA [Ma et al., 2005]. This esterase activity is due to

the Arg 410 and Tyr 411 which are also important amino acid residues in forming Sudlow's binding site II [Watanabe et al., 2000]. This implies that ligand binding to that site can inhibit the esterase activity in a competitive manner.

1.2.2. Bovine serum fetuin (BSF)

It is glycosylated, single-chain protein having six carbohydrate chains, three N-linked glycosylation sites and three O-linked glycosylation sites, which comprise 24% of its total molecular weight (48.5 kD) along with 8% sialic acid [Green et al., 1988] (Table 1.2.1). It contains 341 amino acids and their sequence shows over 70% similarities to human α_2-HS glycoprotein [Dziegielewska et al., 1990]. It is a member of the cystatin superfamily of cysteine protease inhibitor [Binkert et al., 1999; Galembeck and Cann, 1974].

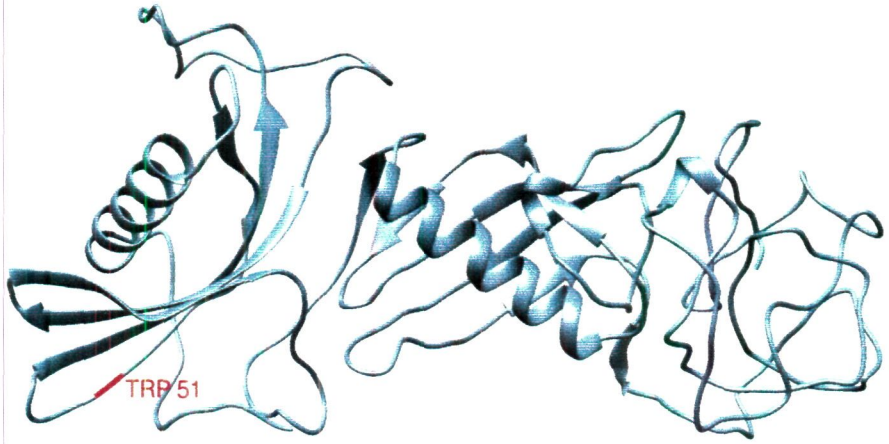

Figure 1.2.2. Structure of fetuin from fetal calf serum (BSF) modeled using Phyre 2 modeling software using sequence from protein database with accession number CAA34596.1 [Kelley and Sternberg, 2009].

Due to a large number of acidic (41 Glu + Asp) and basic (27 Lys + Arg) residues, the protein are highly soluble in aqueous media. Bovine serum fetuin (BSF) has frequently been used as model glycoprotein [Hermentin et al., 1996; Kennedy et al., 1993; Wang et al., 1998a; Wang et al., 1996] because of its easy availability, single chain and less complex glycosylation. Although it is used as a model glycoprotein [Hermentin et al., 1996; Kennedy et al., 1993; Wang et al., 1998b], but its crystal structure is not yet explored. Thus, to get an idea about the molecular structure and location of tryptophan (Trp), BSF is modeled by the Protein Homology/analogY Recognition Engine (Phyre2) in our study reported as a part of chapter 4 and structure

is visualized by Chimera1.7 as shown in Figure 1.2.2. As shown in this figure the tryptophan (Trp 51) is located on outer region.

1.2.3. Hen egg white lysozyme (HEWL)

Lysozyme is an enzyme that act certain bacterial cell wall by cleaving the 1,4-beta-linkages between N-acetylmuramic acid and N-acetyl-D glucosamine residues in a peptidoglycan and between N-acetyl-D-glucosamine residues in chitodextrins. It is abundant in a number of secretions, such as tears, saliva, human milk, mucus and cytoplasmic granules of the polymorphonuclear neutrophils. Large amounts of lysozyme can be found in egg white and are related to alpha-lactalbumin in sequence and structure, making it part of the same family. HEWL is readily available and represents an excellent experimental system to study the determinants of protein aggregation because of high homology to human lysozyme in structure which is one of the proteins that cause an amyloid disease upon mutation [Booth et al., 1997; Uversky and Fink, 2007] and for which aggregation is also observed in vitro [Morshedi et al., 2007; Sasahara et al., 2007].

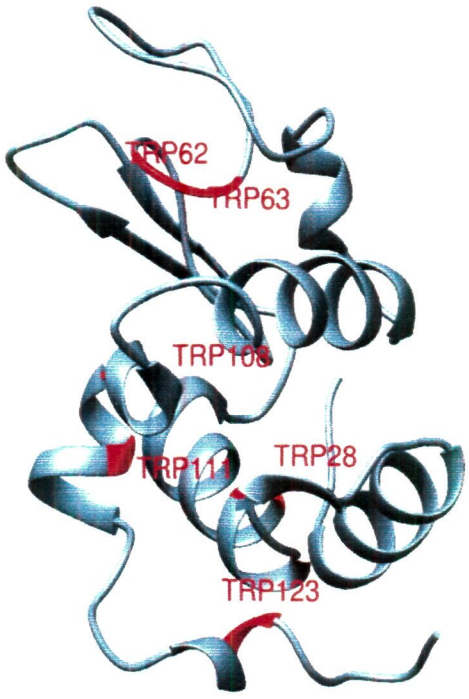

Figure 1.2.3. Crystal structure of hen egg white lysozyme (HEWL) as obtained from PDB having PDB Id 1JPO.

It is a small protein with a molecular weight of 14.3 kD containing 129 amino acids and 4 disulfide bridges. Its tertiary structure consists of two domains, an α-domain

that contains several helices and a ß-domain comprised largely of ß-strands, separated by a cleft that comprises the active site as shown in Figure 1.2.3. The protein has six tryptophan at position 28, 62, 63,108,111 and 123. It has 30% helical and 10% ß-sheet content and has isoelectric point of 11 (Table 1.2.1) [Laurents and Baldwin, 1997].

Table 1.2.1. Physicochemical properties of proteins used in the study as adapted from [Green et al., 1988; Laurents and Baldwin, 1997; Peters, 1996].

Properties	HSA	BSF	HEWL
Type of protein	Non-glycosylated	Glycosylated (24%)	Non glycosylated
Molecular weight (kD)	66.5	48.5	14.3
Number of amino acid	585	341	129
pI	4.7	5.3	11
Number of trptophan	1 (Trp 214)	1 (Trp 51)	6 (Trp 28, 62, 63, 108, 111, 123)
Secondary structure content (X-ray crystallography), *Circular dichroism spectroscopy	64% helix	*10% a-helix, 34% ß-sheet	30% a-helix, 10% ß-sheet

CHAPTER 2

Published in PLoS ONE 8, e71422.

A comprehensive insight into binding of hippuric acid to human serum albumin: a study to uncover its impaired elimination

2.1. Introduction

Uremic toxins are the compounds which retained in the blood during kidney failure and interact negatively with the normal biological functions of the body [Miyamoto et al., 2010]. Hippuric acid (HA) is one of these compounds that accumulates in the blood, and cause stimulation of ammoniagenesis. It may be involved in development of muscular weakness in uremia as it also inhibits glucose utilization in muscles [Duranton et al., 2012; Dzurik et al., 2001; Spustova et al., 1991]. It has also been related to inhibition of organic anion secretion by the kidney [Boumendil-Podevin et al., 1975] and transport at the blood-brain barrier [Ohtsuki et al., 2002]. Thus, HA is consequently a compound of pharmacological interest. It is a glycine conjugate of benzoate, which is formed primarily from aromatic amino acids by gastrointestinal flora or may be directly taken as preservatives from food and beverages [Niwa, 1996]. In a healthy individual, concentration of HA is less than 5 mg/L but increases to values higher than 247±112 mg/L in patients with end-stage renal disease [Vanholder et al., 2003]. Human serum albumin (HSA) is the most abundant plasma protein, single chain, nonglycosylated polypeptide of 66.5 kDa. It is composed of three homologous, predominantly helical domains I- III, each of which contains two subdomains A and B [Sugio et al., 1999]. HSA has one tryptophan residue, Trp214, located in subdomain IIA [He and Carter, 1992; Sudlow et al., 1975]. The principal regions of ligand binding to HSA are located in hydrophobic cavities in subdomains IIA and IIIA, which are consistent with Sudlow sites I and II, respectively [Sudlow et al., 1975]. These binding sites underline the exceptional ability of HSA to interact with many organic and inorganic molecules, thereby making this protein an important regulator of the pharmacokinetic behavior of many drugs as well as intercellular fluxes [Varshney et al., 2011]. In body, it also binds to HA [Duranton et al., 2012] and thus elimination of HA through hemodialysis is only 64% [Hung and Chang, 2001; Vanholder et al., 1992]. However, there is paucity of information on its binding mechanism to HSA. Consequently, it is necessary to investigate its binding energetic,

amino acid involved in binding to explore binding mechanism in the biological system. So, the scope of this work is to investigate the binding affinity, binding enegetics, in details by steady state fluorescence spectroscopy and isothermal titration calorimetry. Location of binding sites is determined by displacement studies and molecular docking studies. Esterase activity of HSA toward *p*-NPA was used to investigate the involvement of Arg410 and Tyr411 of HSA in the binding of HA. Thermal stability in presence of HA was determined using differential scanning calorimetry.

2.2. Materials and methods

2.2.1. Materials and sample preparation. Human serum albumin (A1887; essentially globulin and fatty acid free), warfarin (A2250), phenylbutazone (P8386), and p-nitrophenyl acetate (N8137) were procured from Sigma Aldrich. Hippuric acid (free acid, crystalline; > 99%) was from Himedia. Diazepam was the product of Ranbaxy Laboratories Ltd. All other reagents were of analytical grade. HSA and drug solutions were prepared in 20 mM sodium phosphate buffer (pH 7.4). The protein was dialyzed, and its concentration was estimated spectrophotometerically using $E^{1\%}_{280\ nm}$ = 5.3. All drug solutions were prepared by weight/volume (w/v).

2.2.2. Steady state fluorescence quenching measurements. Fluorescence emission spectra were recorded in range of 300–400 nm on Shimadzu 5301PC fluorescence spectrophotometer equipped with water circulator (Julabo Eyela) with excitation wavelength of 295 nm. Both excitation and emission slits were set at 3 nm. The titration of the HA (0–10 μM) to HSA (5 μM) solutions was carried out at 25, 30, and 37°C. Respective blanks were subtracted for each set of experiment.

2.2.3. Binding displacement measurement using site markers. Different site markers warfarin (WAR) for site I and diazepam (DIA) for site II [Ghuman et al., 2005; Petitpas et al., 2001] were used for performing displacement experiments. The titration of HA were carried out to the solution having protein (5 μM) and site marker in the molar ratio of 1:1. The fluorescence emission spectra were recorded as mentioned in fluorescence measurements and the binding constant values of drug–protein–marker were evaluated using Stern–Volmer equation.

2.2.4. Isothermal titration calorimetric measurements (ITC). The VP-ITC titration microcalorimeter (MicroCal Inc., Northampton, MA) were used to gain insight into the energetics of the binding of HA to HSA at 25, 30, and 37°C. Prior to the titration experiment, all solutions were degassed properly on a thermovac. The 1.44 mL sample and reference cell of the calorimeter were loaded with HSA and 20 mM sodium phosphate buffer (pH 7.4), respectively. The HSA (25 μM) was titrated with HA (1.928 mM) using a 288 μL injection syringe stirring at 307 rpm. Equal volumes of HA solutions (10 μL) were injected into the sample cell containing HSA over 20 s with an interval of 180 s between two consecutive injections. The reference power was set at 16 μcal s^{-1}. The heat associated with each injection was observed as a peak that corresponds to the power required to keep the sample and reference cells at identical temperatures and the data were plotted as integrated quantities. Control experiments were performed by titrating HA into the same buffer to obtain the heats of ligand dilution. Heats of dilution for the ligand and protein were subtracted from the integrated data before curve fitting. The data were fitted and analyzed with a sequential model of two binding sites using Origin 7.0 provided with the MicroCal instrument.

2.2.5. Circular dichroism spectroscopic measurements. To monitor the secondary and tertiary structural change of protein upon interaction with HA, CD spectra of HSA were collected in far (200-250 nm) and near-UV (250-320 nm) at molar ratio of 1:0, 1:5, 1:10 and 1:15 in a JASCO-J815 spectropolarimeter equipped with a Peltier-type temperature controller at 25°C. The CD spectra were collected with 20 nm/min scan speed and a response time of 2 s. The HSA concentration and pathlength of the cell were 5 μM and 0.1 cm, respectively, for far UV CD measurement whereas 15 μM and 1 cm, respectively, for near UV CD measurement. Respective blanks were subtracted.

2.2.6. Differential scanning calorimetric measurements. The differential scanning calorimetric measurements were carried out using VP-DSC microcalorimeter (MicroCal, Northampton, MA). The buffer and protein solutions were degassed under mild vacuum prior to the experiment. Samples were prepared in a 20 mM sodium phosphate buffer, pH 7.4. The DSC measurements of HSA (18 μM) in the presence of different ratios of HA viz. 1:0, 1:5, and 1:10 were performed from 25 to 90°C at a

scan rate of 0.5°C/min. Data were analyzed using Origin software provided with the instrument to obtain the temperature at the midpoint of the unfolding transition (T_m) and calorimetric enthalpy (ΔH°).

2.2.7. Effect of HA binding on esterase-like activity of HSA. Drug site II (Subdomain III A) of HSA possessed esterase-like activity toward p-nitrophenyl acetate (*p*-NPA) [Watanabe et al., 2000]. Thus, reaction of *p*-NPA with HSA in absence and presence of HA (i.e. 0-45 μM) was followed on Perkin-Elmer Lambda 25 double beam UV–vis spectrophotometer attached with Peltier temperature programmer-1 (PTP–1) at 405 nm by monitoring the appearance of yellow product p-nitrophenol for 1 min at 25°C. The molar extinction coefficient of p-nitrophenol was taken as 17800 M^{-1} cm^{-1}. The reaction mixture contained 15 μM HSA whereas *p*-NPA varied from 0 to 600 μM in 20 mM sodium phosphate buffer (pH 7.4). The control (in absence of HSA) was also taken in consideration.

2.2.8. Molecular docking. The SDF format for 3D structure of HA was downloaded from Pubchem database (CID 464) and crystal structure representing HSA was extracted from Protein Data Bank (PDB: 1AO6). Molecular docking simulation of hippuric acid to HSA was performed with Autodock Vina program [Trott and Olson, 2010]. Autodock was used to evaluate ligand binding energies over the conformational search space using Lamarckian genetic algorithm. The residues falling within 5 Å of the two different binding sites of HSA (site I & site II) were extracted and combined to define the binding site residues. Default docking parameters were used. We considered only the minimum energy conformation state of ligand bound protein complex in our study out of ten generated modes. The hydrogen bonding and hydrophobic interactions between ligand and protein were calculated by Accelrys DS Visualizer 2.0 [AccelrysSoftwareInc, 2012] and figure was generated with Chimera 1.7 [Pettersen et al., 2004].

2.2.9. Statistical analysis

All determinations were triplicates, and mean values and standard deviations were calculated, wherever applicable, using SPSS 16.0 programme for windows.

2.3. Results and discussion

2.3.1. Steady state fluorescence quenching measurements. The aromatic fluorophores, tryptophan, tyrosine, and phenylalanine are very sensitive to their microenvironment and thus used for studying conformational changes associated with ligand protein binding. However, tryptophan contributes maximumally to the fluorescence [Ahmad et al., 2011]. The fluorescence intensity of HSA decreases with gradual addition of HA at 25, 30, and 37°C as shown in Figure 2.1.

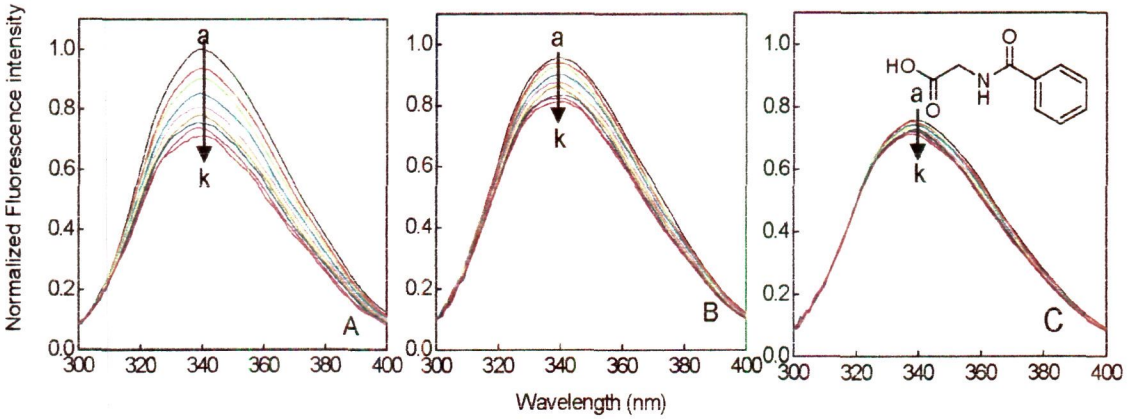

Figure 2.1. Normalized fluorescence emission spectra of HSA in the presence of different concentrations of HA at (A) 25°C (B) 30°C and (C) 37°C. a-k: 0—10 μM of HA at increments of 1 μM. The inset corresponds to the molecular structure of HA.

Thus to investigate the mechanism of quenching, the fluorescence quenching data at 25, 30, and 37°C were analyzed according to the linear Stern–Volmer equation [Lakowicz, 2006]:

$$\frac{F_o}{F} = K_{sv}[Q] + 1 = k_q \tau_o [Q] + 1 \qquad (2.1)$$

where, F_o and F are the fluorescence intensities in the absence and presence of quencher (HA), K_{sv} and k_q are the Stern–Volmer quenching and bimolecular rate constant respectively and τ_o, the average integral fluorescence life time of tryptophan which is ~ 5.71×10^{-9} s [Zaidi et al., 2013a]. The values of K_{sv} and k_q obtained from Stern-Volmer plot (Figure 2.2A) are listed in Table 2.1. It can be seen that, the values of K_{sv} decreases with increasing temperature and k_q was founds to be 10 times greater than the 2×10^{10} M^{-1} s^{-1}, a maximum scatter collision quenching constant of various quenchers with biopolymers. This shows that quenching was not initiated by dynamic

diffusion but from the formation of a strong complex between HSA and HA [Zaidi et al., 2013a].

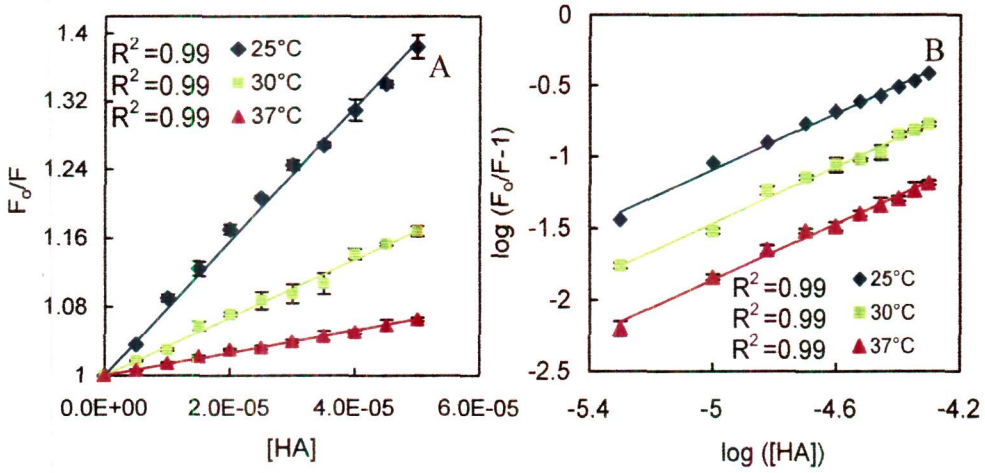

Figure 2.2. Stern–Volmer (A) and log [(F_0-F)/F] versus log[HA] (B) plot at different temperatures.

Table 2.1. Binding and thermodynamic parameters of HA-HSA at different temperatures obtained from fluorescence quenching experiments[a]

Temp (°C)	25	30	37
n	0.98 ± 0.02	0.99 ± 0.01	0.97 ± 0.02
K_{SV} (M^{-1})	(7.80 ± 0.36) ×10^3	(3.30 ± 0.02) ×10^3	(1.31 ± 0.08) ×10^3
K_b (M^{-1})	(6.84 ± 0.19) ×10^3	(3.11 ± 0.22) ×10^3	(1.04 ± 0.01) ×10^3
k_q (M^{-1} s^{-1})	(1.36 ± 0.06)×10^{11}	(5.77 ± 0.03)×10^{11}	(2.29 ± 0.01)×10^{11}
ΔH°(kcal mol^{-1})		-28.68 ± 0.20	
TΔS° (kcal mol^{-1})	-23.48 ± 0.24	-23.88 ± 0.24	-24.43 ± 0.25
ΔG° (kcal mol^{-1})	-5.21 ± 0.02	-4.88 ± 0.06	-4.28 ± 0.01

[a]R^2 for all values ranges from 0.98 to 0.99.

As the quenching mechanism was determined to be static, so the binding constant, K_b, can be calculated from the y-axis intercept of plot of log [(F_0 - F)/F] versus log [HA] (Figure 2.2B) according to equation:

$$\log\left(\frac{F_o}{F}-1\right)=\log K_b+n\log[Q] \qquad (2.2)$$

where, K_b is the binding constant. The values of K_b obtained at different temperature are listed in Table 2.1. It can be seen that, the values of K_{sv} and K_b were almost same that further confirm static quenching mechanism [Lakowicz, 2006]. Furthermore,

change in standard Gibbs free energy ($\Delta G°$) was obtained using Gibbs-Helmholtz equation:

$$\Delta G^{\circ} = -RT \ln K_b \tag{2.3}$$

whereas, change in standard enthalpy (ΔH°) and entropy (ΔS°) were determined from the van't Hoff equation, if ΔH° do not vary significantly over the temperature range studied.

$$\ln K_b = -\frac{\Delta H^{\circ}}{RT} + \frac{\Delta S^{\circ}}{R} \tag{2.4}$$

where R (1.987 cal $mol^{-1}K^{-1}$) is gas constant and T is the absolute temperature (K). For protein-ligand interaction, the signs and magnitude of thermodynamic parameters (ΔH° and ΔS°) can be used to determine the main forces that contribute in complex formation of protein-ligand [Ross and Subramanian, 1981]. Thus, the negative ΔH° indicates the exothermic nature and dominant involvement of electrostatic interactions in the process of HSA-HA complex formation [Thoppil et al., 2008]. However, hydrogen bonding also play role as depicted from the negative signs of ΔH° and ΔS°. Moreover, ΔH° contributes maximally rather than ΔS° to ΔG° that indicates the binding process is enthalpy driven and the decrease in entropy is due to the formation of hydrogen bonds between HA and HSA. In addition, negative sign of ΔG° indicates that the binding of HA with HSA is a spontaneous process. However, the obtained value of thermodynamic parameters may not necessarily the actual values as; such non–calorimetric approach to the thermodynamics has ruthless shortcomings where usually $\Delta H°$ is assumed to be temperature–independent. However, this is the only method to determine an estimate of ΔH° and ΔS° from the fluorescence quenching data at different temperature [Tian et al., 2004]. Furthermore, the binding affinity observed by fluorescence spectroscopy took in consideration the location of quencher, fluorophore and so measures local changes around the fluorophores associated with the optical transition [Nada and Terazima, 2003]. Hence to overcome all these shortcomings, we have done ITC measurements that consider overall global changes in protein ligand interaction [Faergeman et al., 1996].

2.3.2. Binding displacement measurement using site markers. Sudlow et al [Sudlow et al., 1975] proposed that the HSA has two major binding regions namely Sudlow's site I and site II. Site I and II have affinity for WAR and DIA respectively. Thus these drugs were used as site specific markers of HSA. To locate the binding site of HA on HSA, the emitted fluorescence intensity data in the absence and presence of markers were analysed using Stern–Volmer equation. The K_{sv} value of HSA-HA was $(7.80\pm0.36)\times10^3\ M^{-1}$ that decreases to $(2.74\pm0.04)\times10^3\ M^{-1}$ and $(2.03\pm0.03)\times10^3\ M^{-1}$ in presence of WAR and DIA, respectively. These differences in K_{sv} values in absence and presence of site markers are significant enough to deduce the binding sites location as reported earlier [Chi and Liu, 2011; Hu et al., 2009]. As evident from above values, the K_{sv} of HSA-HA decreased markedly in presence of WAR and DIA both, however, relatively more in later. It indicates competition between markers and HA for both site I and site II, however, relatively more for later. Thus, HA binds preferably to site II as compared to site I.

2.3.3. Isothermal titration calorimetric measurements. ITC was used to measure binding affinity and energetics of HA to HSA. Figure 2.3 shows the ITC binding isotherm of HA to HSA at 25, 30, and 37°C in which each peak in top panel represents a single injection of the ligand into protein solution. Bottom panel of this figure shows an integrated plot of the amount of heat liberated per injection as a function of the molar ratio of the ligand to protein. The best fits for the integrated heats was obtained using a two sites sequential binding model with the lowest χ^2. The temperature dependency of the thermodynamic binding parameters of HA to HSA obtained after fitting is summarized in Table 2.2. These results showed that the binding affinity is in the order of 10^4 and 10^3 for high and low affinity binding site respectively which decrease with increase in temperature indicating the formation of complex. Further, the free energy change accompanied the binding of HA to HSA was calculated from equation 2.3, whereas, association constant (K_b) and enthalpy change (ΔH) were used to obtain entropy change according to the equation:

$$\Delta G^\circ = \Delta H^\circ - T\Delta S^\circ \qquad (2.5)$$

The enthalpic and entropic contributions to the Gibbs free energy of binding were used to infer information regarding the mechanism of binding.

Table 2.2.Thermodynamic parameters and association constant of HA-HSA obtained by isothermal titration calorimetry.

	Temp (°C)	K_b (M^{-1})	ΔH° (kcal mol^{-1})	$T\Delta S^\circ$ (kcal mol^{-1})	ΔG° (kcal mol^{-1})
High	25	$(2.75\pm0.51)\times10^4$	-4.41±0.46	-1.90±0.30	-6.05 ± 0.10
affinity	30	$(1.95\pm0.05)\times10^4$	-5.18±0.07	-0.76±0.06	-5.94 ± 0.01
site	37	$(1.54\pm0.06)\times10^4$	-6.14±0.15	-0.20±0.01	-5.93 ± 0.02
Low	25	$(2.80\pm0.49)\times10^3$	-7.58±0.96	-2.88±0.40	-4.69 ± 0.10
affinity	30	$(1.38\pm0.03)\times10^3$	-9.74±0.34	-5.39±0.35	-4.35 ± 0.02
site	37	$(1.29\pm0.07)\times10^3$	-11.11±0.69	-6.69±0.36	-4.41 ± 0.03

It can be seen from Figure 2.3 (insets), that all studied temperature, the enthalpic changes for the binding of HA to both classes of binding site of HSA are all negative, which indicate that the binding process are all exothermic and involves electrostatic interactions [Thoppil et al., 2008]. On contrary, the entropic contributions were favourable for higher affinity binding site while unfavourable for low affinity binding site. It suggests the involvement of hydrogen bonding in binding of HA to low affinity site on HSA [Ross and Subramanian, 1981]. Whereas, negative value of ΔG° suggest that the formation of complex was spontaneous in nature for both set of binding sites at all three temperatures. Further, the slope of plot of ΔH° against $T\Delta S^\circ$ was found to be approximately equal to unity which indicates the enthalpy-entropy compensation effect, a common phenomenon in protein ligand interaction [Zolotnitsky et al., 2004]. Besides, it was also observed that ΔH° varies almost linearly with examined range of temperature and so the change in heat capacity (ΔC_P) was determined according to equation:

$$\Delta C_p^{exp} = \frac{d\Delta H^\circ}{dT} \qquad (2.6)$$

The values of ΔC_P obtained were -0.14±0.11 and -0.28±0.24 kcal $mol^{-1}{}^\circ C^{-1}$ for high and low affinity site respectively. As can be seen from Table 2.1 and 2.2, value of binding affinity obtained by fluorescence spectroscopy differ from ITC that may be due to the consideration of the location of quencher and fluorophore in the later[Faergeman et al., 1996; Nada and Terazima, 2003]. Not only binding affinity, but the values of ΔH° and $T\Delta S^\circ$ also differ whereas the values of ΔG° obtained from

both methods are comparable. It is due to the already discussed limitations of non–calorimetric approach to the thermodynamics that in this approach usually ΔH° is assumed to be temperature–independent as can be seen in literature [Anand et al., 2010; Chi and Liu, 2011; Hu et al., 2009; Thoppil et al., 2008]. Moreover, it cannot be neglected that the evaluation of the thermodynamic parameters obtained from the spectroscopic measurements also based upon the temperature dependence of the binding affinity that may be influence by the location of quencher from the Trp214 as discussed [Faergeman et al., 1996]. This leads to miscalculation of temperature–dependent ΔH° and ΔS°. However, in literature non–calorimetric determination of thermodynamic parameters from fluorescence quenching data at different temperature has been exploited to get an approximate value [Ahmad et al., 2011; Anand et al., 2010; Chi and Liu, 2011; Hu et al., 2009]. Further the van't Hoff enthalpy (ΔH°_{vH}) at each temperature was calculated using equation:

$$\Delta H^{\circ}{}_{vH} = \left[\frac{\left\{ \ln \frac{K(T_2)}{K(T_1)} - \frac{\Delta C_P}{R} \ln \frac{T_2}{T_1} + \frac{\Delta C_P T_1}{R} \left(\frac{1}{T_1} - \frac{1}{T_2} \right) \right\} \times R}{\left(\frac{1}{T_1} - \frac{1}{T_2} \right)} \right] \qquad (2.7)$$

here, $K(T_1)$ and $K(T_2)$ are the values of binding constant at temperatures T_1 and T_2 respectively. The temperature dependency of binding affinity obtained from ITC, is used to calculate the van't Hoff enthalpy values, which do not agree well with the calorimetric enthalpies at all studied temperatures. For example, the value of van't Hoff enthalpy obtained at 25°C obtained by using equation 2.7 was -11.98 and -24.69 kcal $mol^{-1}$for high and low affinity site respectively which differ from calorimetric enthalpies. Such difference is also reported in literature [Keswani et al., 2010] and may indicate that the conformational changes are associated with the binding process which may be induced either by ligand binding or by an increase in temperature. Hence to have better understanding of conformational changes on ligand binding, we have done circular dichroism measurements.

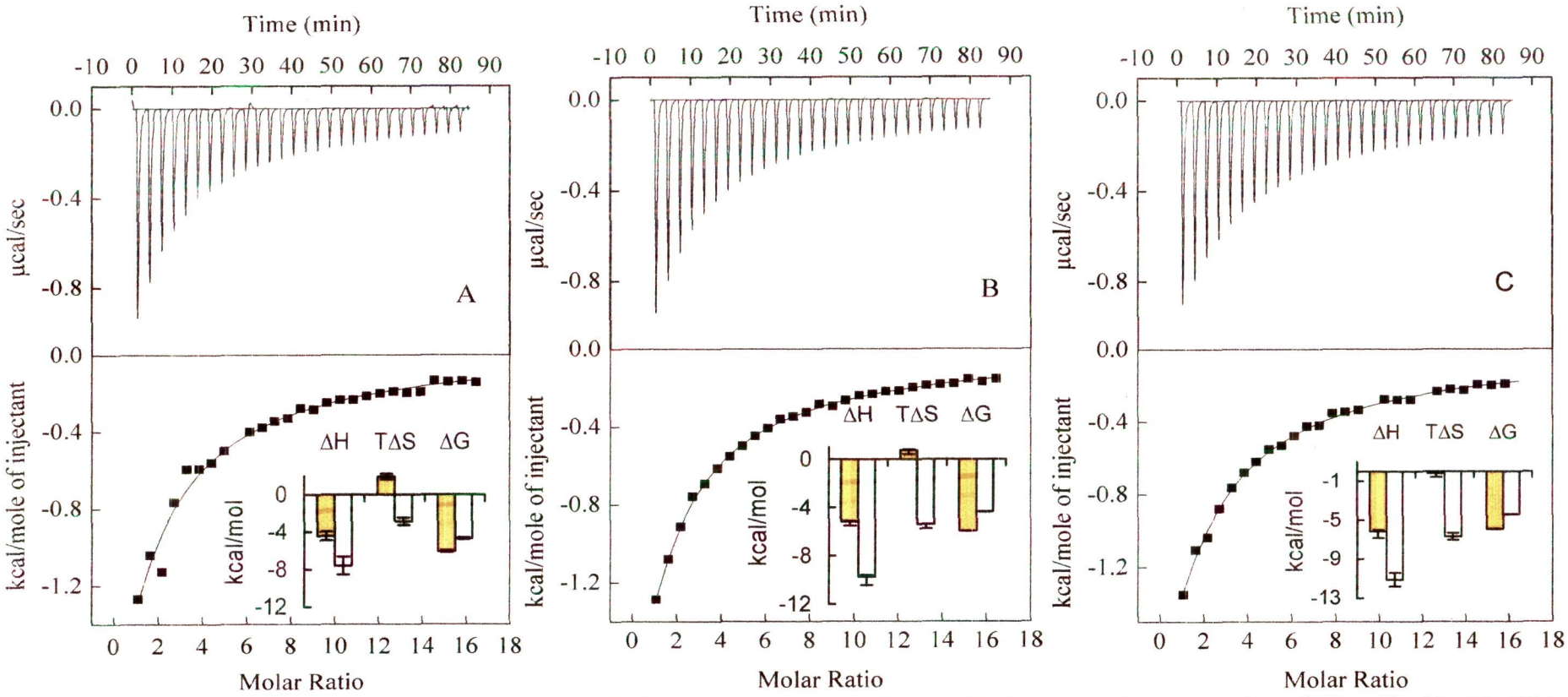

Figure 2.3. Isothermal titration calorimetry of HSA and HA interaction at (A) 25°C, (B) 30°C, and (C) 37°C. Titration of HA with (25 µM) HSA at pH 7.4 shows calorimetric response as successive injections of ligand is added to the sample cell. The solid line represent the best nonlinear least-squares fit of sequential model of two binding site. The inset of A-C represent comparative bar distribution of ΔH°, ΔS° and ΔG° obtained from ITC. Each thermodynamic parameter represented by two bars, open (low affinity site) and filled (high affinity site).

2.3.4. Circular dichroism measurements. The changes in secondary and tertiary structure of the HSA in presence of HA were studied in far-UV CD and near UV CD region at different molar ratio of protein to HA. The results were expressed as MRE (mean residue ellipticity) in deg cm^2 $dmol^{-1}$, which is given by:

$$MRE = \frac{\Theta_{obs}(mdeg)}{10 \times n \times c \times l} \quad (2.8)$$

where Θ_{obs} is the observed ellipticity in millidegrees, c is the concentration of protein in mol/l, l is the length of the light path in centimeters and n is the number of peptide bonds. The far-UV CD and near UV CD spectra of HSA in presence of [HSA]/[HA] ratio of 1:0, 1:5, 1:10 and 1:15 are shown in Figure 2.4 A & B. In the presence of HA, slight increase occur in the secondary structure of HSA as evident from the increase at two minima at 208 and 222 nm that are characterstic of α-helix [Zaidi et al., 2013a]. However, the shape of peaks and the position of peak maximum remained almost unchanged in the presence of HA, indicating that HSA has predominantly α-helix in nature even after binding to the HA.

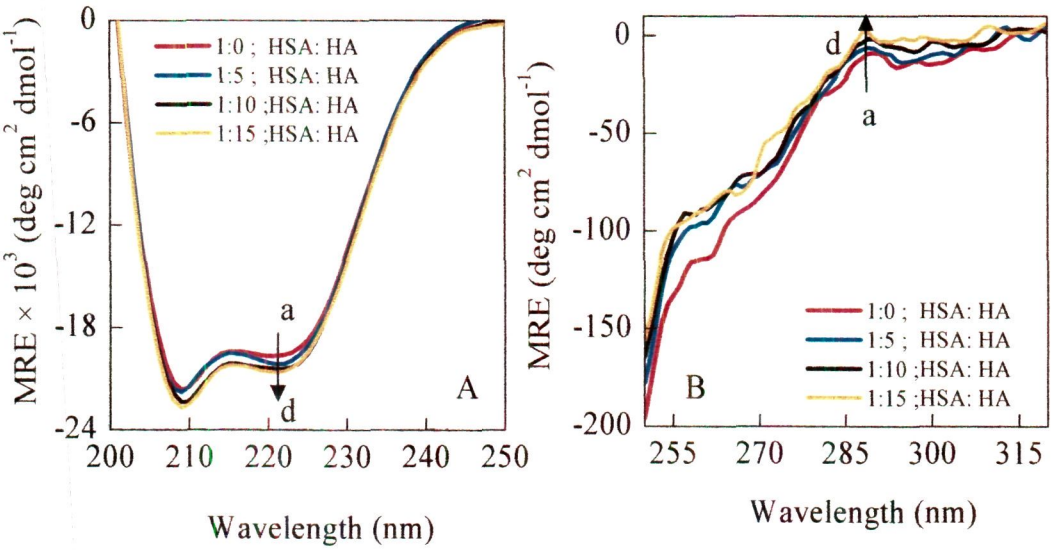

Figure 2.4. Far (A) and near (B) UV CD spectra of HSA in the presence of varying concentration of HA. a-d represent spectra of HSA: HA at molar ratio of 1:0, 1:5, 1:10 and 1:15 respectively in both (A) and (B).

Further as shown in Figure 2.4B, near-UV CD spectra for the HSA showed two minima at 262 and 268 nm and shoulders at 279 and 290 nm, characteristics of disulphide and aromatic chromophores, which is in accordance with literature [Ahmad et al., 2006]. But, change in HSA spectra in presence of HA was observed

that indicates the alteration of tertiary structure at different molar ratio of protein to HA. This confirms that conformational changes occur in the protein upon ligation and thus difference is observed in the values of van't Hoff and calorimetric enthalpies obtained from ITC.

2.3.5. Thermostability measurement by differential scanning calorimetry. Figure 2.5A–C shows the typical excess heat capacity curves for HSA:HA in the molar ratio of 1:0, 1:5, and 1:10 and thermodynamic parameters obtained accompanying thermodynamic denaturation of HSA under these conditions are reported in Table 2.3. It is observed that the thermal unfolding of HSA is irreversible process in absence and presence of HA by reheating the samples after cooling just after the first run. Hence to minimize the kinetic factors, slower scanning rate have been chosen. The changes in the T_m and $\Delta H°$ of the protein in presence of ligand are the most obvious manifestation of ligand binding effects that can be estimated by DSC [Celej et al., 2006]. Thus, to confirm binding of HA to HSA, changes in the T_m and $\Delta H°$ have been monitored by DSC. The denaturation of HSA yielded more than one endothermic peak that reflects the domain denaturation mechanism [Privalov, 1982]. So, it was deconvoluted with the assumption of three sub-transitions and each of which might be related to the links between the three structural domains of HSA.

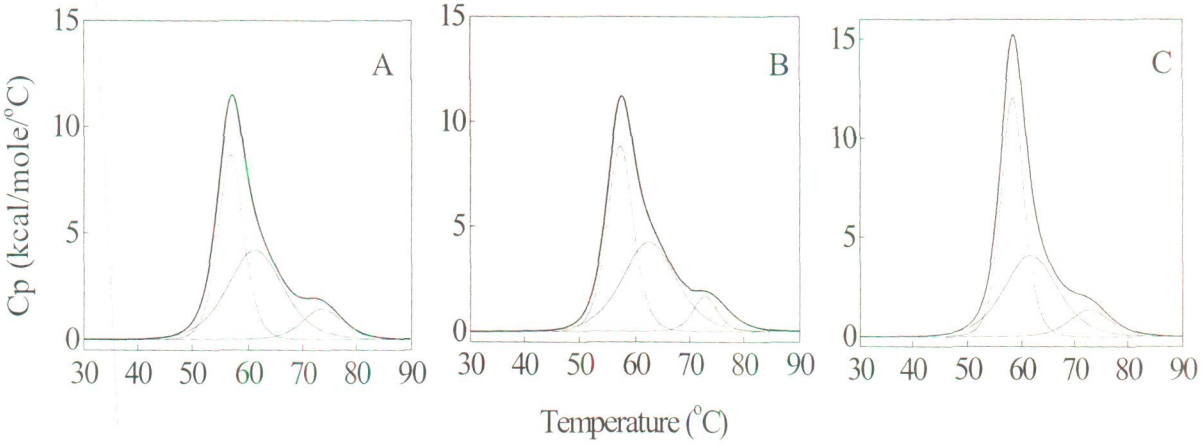

Figure 2.5. Excess heat capacity curves obtained by differential scanning calorimetry for HSA:HA in the molar ratio of (A) 1:0, (B) 1:5, and (C) 1:10.

Further, it is also established that domain III melts prior to domain II, so T_m^1 may corresponds to domain III [Sudlow et al., 1975];[Rezaei Tavirani et al., 2006]. Table 2.3 shows T_m^1, T_m^2 and T_m^3 and respective $\Delta H°$ of native HSA that are in accordance

with the literature [Uversky et al., 1997]. Upon increasing molar ratio to 1:10, the T_m^1 increases appreciably, T_m^2 changes slightly whereas, T_m^3 donot change at all.

Table 2.3. Thermodynamic parameters of HSA in presence of HA obtained by DSC.

	1:0	1:5	1:10
T_m^1 (°C)	56.91±0.09	57.25±0.01	58.36±0.08
T_m^2 (°C)	61.37±0.07	62.51±0.09	63.83±0.02
T_m^3 (°C)	73.65±0.06	73.87±0.04	73.96±0.03
ΔH_1° (kcal mol^{-1})	52.21±0.69	54.41±0.10	68.47±0.80
ΔH_2° (kcal mol^{-1})	55.37±0.71	56.13±0.12	57.37±0.60
ΔH_3° (kcal mol^{-1})	13.96±0.08	13.92±0.07	13.90±0.09

This indicates that, binding of HA to domain III is stronger as compare to domain II whereas, negligible to domain I as higher energy is required to change from the liganded native state into the free unfolded state in case of domain III followed by domain II. Thus, HA preferential binds to the folded or native form of the HSA which causes stabilization of the folded state and hence unfolding of HSA become progressively less favorable as HA concentration increases [Celej et al., 2005; Neelam et al., 2010; Sharma et al., 2012].

2.3.6. Measurement of esterase-like activity of hsa in presence of ha. The Arg410 and Tyr411, crucial amino acid residue present in the centre of drug binding site II of HSA are involved in its esterase-like activity [Watanabe et al., 2000]. Catalytic activity of HSA toward *p*-NPA was investigated to know the involvement of these residues in the binding of HA to HSA. The kinetic constants (K_m and V_{max}) were obtained by fitting the initial rates to Michaelis–Menten equation using Graph-Pad Prism, version 5.0, software as shown in Figure 2.6 by fitting the initial rates tc Michaelis–Menten equation:

$$v = \frac{V_{max}[S]}{K_m + [S]} \qquad (2.9)$$

where ?, V_{max}, K_m, and [S] represent the initial reaction velocity, maximum velocity, Michaelis–Menten constant, and molar concentration of substrate, respectively. Whereas, K_i was calculated from equation:

$$K_m' = \frac{K_m}{K_i} I_o + K_m \qquad (2.10)$$

where, K_m', is the apparent K_m in presence of competitive inhibitor concentration I_o.

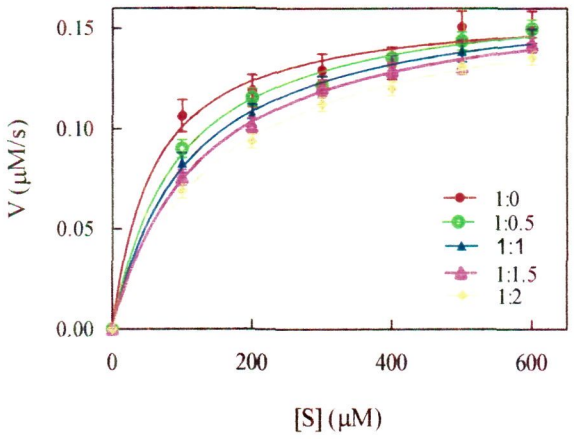

Figure 2.6. Michalies-Menten plot of HSA for *p*-NPA at HSA: HA ratio of 1:0, 1:0.5 1:1, 1:1.5, and 1:2.

Further, the reciprocal of substrate concentration against reciprocal of respective product formation rate are plotted as Lineweaver-Burk plot (Figure 2.7).

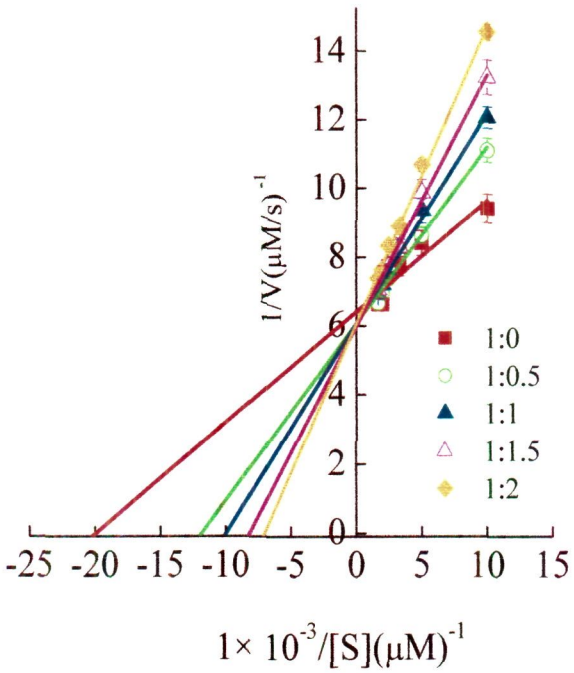

Figure 2.7. Lineweaver-Burk plots of reaction velocity versus substrate concentration for enzyme kinetics of HSA in absence and presence of HA. The molar ratio of HSA:HA examined are 1:0, 1:0.5, 1:1, 1:1:5, and 1:2.

As shown in Table 2.4, the activity of HSA toward *p*-NPA gives K_m and V_{max} equal to 59.36± 05.55 μM and 0.16±0.01 μMs^{-1} respectively whereas in presence of HA, V_{max} remain same while K_m increases. This indicates that the HA inhibits the esterase-like activity of HSA competitively with K_i equals to 21.68 μM and hence Arg410 and Tyr411, of drug binding site II of HSA are involved in binding of HA.

Table 2.4. Kinetic parameters for the hydrolysis of *p*-NPA by HSA in presence of FUR

HSA: FUR	K_m (μM)	V_{max} (μMs^{-1})	$10^5 \times k_{cat}/K_m$ ($\mu M^{-1}s^{-1}$)
1:0	59.36 ± 05.55	0.16 ± 0.01	17.95 ± 1.69
1:0.5	93.50 ± 04.52	0.16 ± 0.02	11.40 ± 0.55
1:1	109.5 ± 07.25	0.16 ± 0.01	09.74 ± 0.64
1:1.5	126.20 ± 10.16	0.16 ± 0.02	08.45 ± 0.68
1:2	153.90 ± 09.50	0.16 ± 0.01	06.93 ± 0.42

2.3.7. Molecular docking. The molecular docking has been employed to further understand the interaction of HA and HSA. The HSA comprises of three homologous domains (I–III): I (residues 1–195), II (196–383), III (384–585), each domain comprises subdomains that posses common structural motifs. The principal regions of ligand binding to HSA are located in hydrophobic cavities in subdomains IIA and IIIA, which are consistent with Sudlow sites I and II, respectively [Sudlow et al., 1975]. In the present study, Autodock Vina program is applied to calculate the possible conformation of the HA that binds to the protein. The best energy ranked results are summarized in Table 2.5 and Figure 2.8, which shows that HA binds to both sites of HSA. Figure 2.8B & D show that HA more favourably fit in the hydrophobic cavity in subdomains IIIA, that corresponds to site II, with ΔG and K_b of -5.9 kcal mol^{-1}, 2.12×10^4 respectively. The Leu387, Ile388, Asn391, Cys392, Leu407, Arg410, Tyr411, Leu430, Val433, Cys438, Ala449 and Leu453 of site II were involved in hydrophobic interaction. However as shown in Figure2.8A & C, HA also fit in cavity of the subdomains IIA, that corresponds to site I, with ΔG and K_b of -5.6 kcal mol^{-1} and 1.28×10^4 respectively. The HA interacts hydrophobically with Lys199, Arg222, Tyr150, Glu153, Ser192, Lys195, Gln196, Trp214, His242, Arg257, Ala291 and Glu292 of site I. Moreover, HA forms two hydrogen bonds with Lys199 having bond length of 2.05Å, 2.16Å and one with Arg222, having bond length of

2.36Å. Thus, HA binds to site II with the high affinity binding site whereas with relatively low affinity to site I.

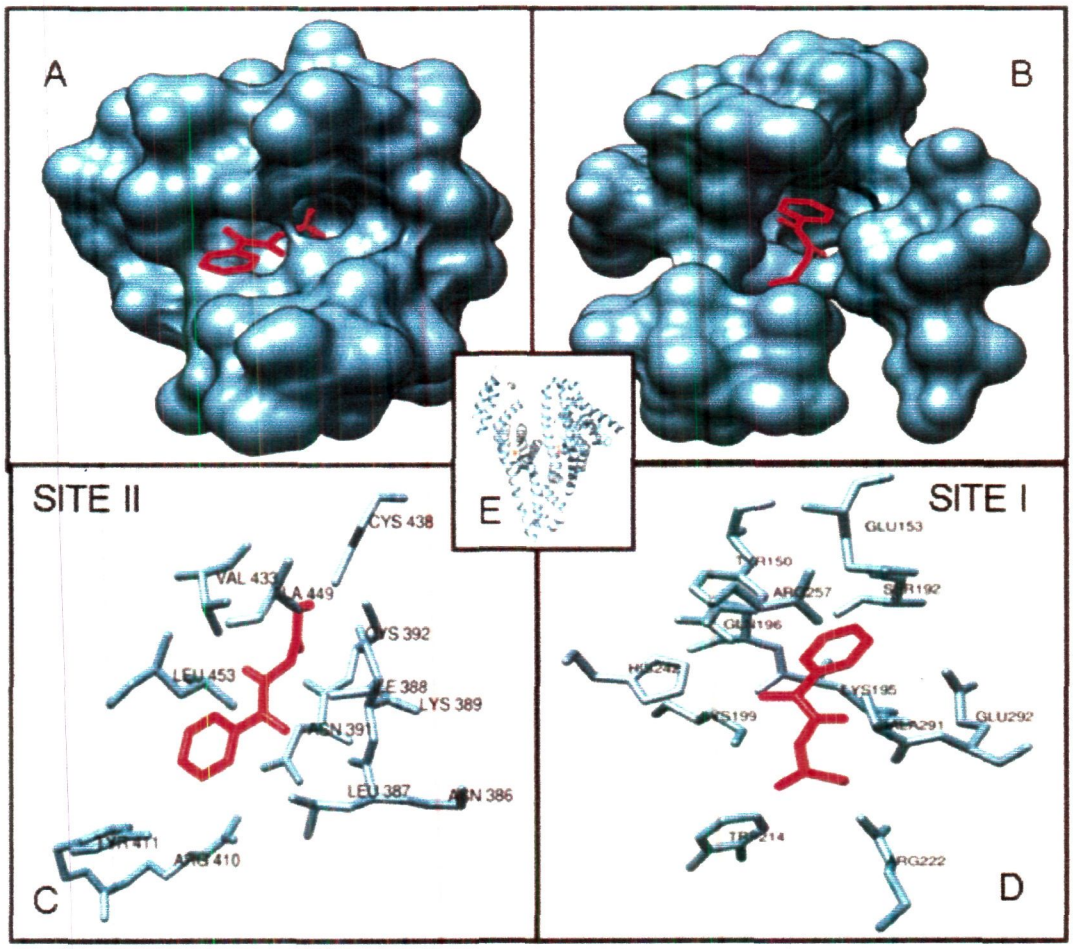

Figure 2.8. Molecular docking of HA and HSA. Molecular surface representation of docked HA in a (A) site II and (B) site I of HSA. Representation of interacting residue of HSA (C) site II and (D) site I interacting with HA.

For site II, values of ΔG obtained by docking are very close to the calorimetrically obtained values whereas, slightly different for site I. The probable explanation for this is that docking was based upon the static and fixed X-ray crystals structure of protein where protein significant structural freedom is not allowed to acquire different conformations upon ligand binding. Unlikely, the calorimetry results are based upon full freedom in the structural flexibility of the protein in aqueous system [Ahmad et al., 2011; Neelam et al., 2010]. Thus, structural rearrangements observed in the HSA that occurred upon HA binding in solution, is a plausible cause of this difference. Further, docking is based on some crucial approximations including the limited number of ligand positions in the trial and omission of protein dynamics. Therefore, molecular docking in this study yields useful information about the specific residues

of HSA involved in the interactions with the HA for better understanding of protein-ligand interaction at the molecular level.

Table 2.5. Molecular docking results of HSA-HA interaction

binding site	amino acid	forces involved	ΔG (kcal mol^{-1})	$K_b(M^{-1})$
	Lys199	H-bonding and Hydrophobic		
Site I	Arg222	H-bonding and Hydrophobic	-5.6	1.28×10^4
	Tyr150	Hydrophobic		
	Glu153	Hydrophobic		
	Ser192	Hydrophobic		
	Lys195	Hydrophobic		
	Gln196	Hydrophobic		
	Trp214	Hydrophobic		
	His242	Hydrophobic		
	Arg257	Hydrophobic		
	Ala291	Hydrophobic		
	Glu292	Hydrophobic		
	Leu387	Hydrophobic		
Site II	Ile388	Hydrophobic	-5.9	2.12×10^4
	Asn391	Hydrophobic		
	Cys392	Hydrophobic		
	Leu407	Hydrophobic		
	Arg410	Hydrophobic		
	Tyr411	Hydrophobic		
	Leu430	Hydrophobic		
	Val433	Hydrophobic		
	Cys438	Hydrophobic		

2.3.8. Binding of HA to HSA affect its elemination. HA is formed primarily from aromatic amino acids by gastrointestinal flora or may be directly taken as preservatives from food and beverages [Niwa, 1996]. In patients with end-stage renal disease, excretion through kidney is hampered and consequently, the concentration of HA increases to values higher than 247±112 mg/L [Vanholder et al., 1992]. So it is believed that it may bind to the HSA and thus its removal may hamper. So to confirm, we examine the binding energetics and amino acid involved in binding of HA to HSA. From above studies, it is found that, HA binds with high affinity to site II while with relatively low affinity to site I of HSA via hydrogen bonding, electrostatic and hydrophobic interaction. Therefore it is confirmed that it bounds to HSA and thus it

elimination may be hampered as shown in Figure 2.9. Moreover, Arg410 and Tyr411 are involved in binding of HA to site II of HSA, that are also crucial for esterase-like activity of HSA. Thus, HA also impinges esterase-like activity of HSA.

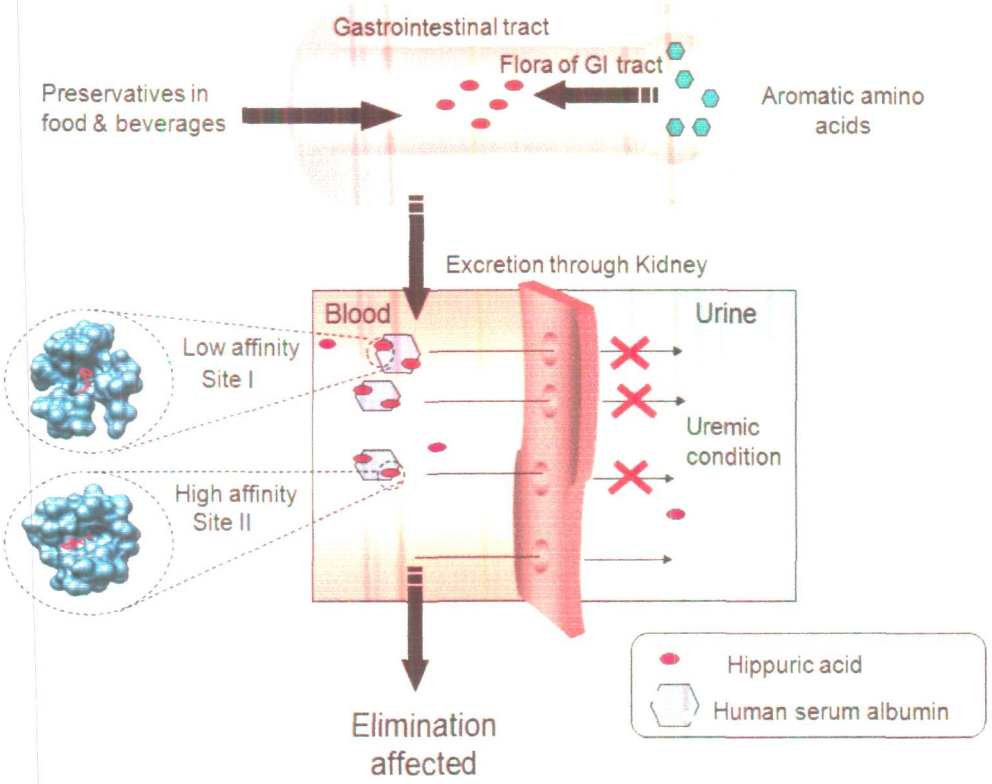

Figure 2.9. Schematic representation of mechanism of HA binding to HSA under uremic condition.

2.4. Conclusions

The present work reports the interaction of HA, a uremic toxin, to HSA. Results indicated that it markedly binds to both drug binding sites of HSA; however binding at site II is relatively more. Further, the quenching mechanism of fluorescence of HSA by HA is a static procedure and their binding is a spontaneous, enthalpically driven, entropically opposed process that involves hydrogen bonding, electrostatic, and hydrophobic interaction. Since it binds to HSA and thus its elimination may hinder. Moreover, it increases the thermostabilty of HSA on binding and inhibits the esterase-like activity of HSA in a competitive manner.

CHAPTER 3

Published in J Phys Chem B, 117:2595-604

Biophysical insight into furosemide binding to human serum albumin: a study to unveil its impaired albumin binding in uremia

3.1. Introduction

Human serum albumin (HSA) is a main carrier for a variety of endogenous and exogenous substances in the body and also plays a key role in maintaining normal osmolarity in plasma and in interstitial fluid [Kragh-Hansen, 1981; Varshney et al., 2010]. It is a single chain nonglycosylated polypeptide of 66.5 kDa. The protein has three homologous domains (I–III), each domain comprises two subdomains (A and B) that possess common structural elements [He and Carter, 1992; Sugio et al., 1999]. As of its transporting role, it binds substances at two major binding regions, namely Sudlow's site I and II, which are located within cavities in subdomains IIA and IIIA, respectively [Sudlow et al., 1975]. Generally, upon absorption exogenous substances like drugs enter into the circulatory system and bind reversibly to serum albumin, which assists in their distribution and deposition [Reed et al., 2001; Seetharamappa and Kamat, 2005]. But, transport of various drugs via albumin in pathological ill condition like uremia, is seriously compromised [Mingrone et al., 1997; Varshney et al., 2011]. Among them, binding of furosemide (FUR), a diuretic drug, is most adversely impaired, which normally binds 99 % to albumin at its total concentration of 10 $\mu g\ mL^{-1}$ [Bojko et al., 2010a; Takamura et al., 2005]. Hence, decrease in the protein bound fraction of FUR may affect the pharmacokinetics of the drug, which includes its tubular secretion and increased metabolic clearance in uremic patients [Wilcox, 2002]. Although the molecular mechanism underlying impaired albumin FUR binding in uremic conditions is poorly understood, two major reasons have been suggested. First, it may be due to some conformational changes in albumin under chronic renal disease but putative structural modifications of pathological HSA have been disputed for decades [Ivanov et al., 2002; Sjoholm et al., 1976; Takamura et al., 1996]. Second, according to the most accepted hypothesis, HSA binding sites might be occupied by uremic toxins, viz. hippuric acid (HA), indoxyl sulfate (IS), and 3-carboxy-4-methyl-5-propyl-2-furanpropionic acid (CMPF), indole 3 acetic acid (IAA), etc [Sarnatskaya et al., 2003]. However, from the available literature, it is found that FUR binds to site I of HSA [Bojko et al., 2010a; Bojko et al., 2010b;

Ivanov et al., 2002] whereas all predominant uremic toxins except CMPF bind mainly to site II of HSA [Bowmer and Lindup, 1982; Ikeda et al., 1984; Sakai et al., 1995]. So, only CMPF is the uremic toxin that directly inhibits the binding of FUR to albumin as they share the same binding site. But, the reason behind inhibition by site II bound uremic toxins of FUR binding to albumin is still unclear. Thus, to elucidate the plausible reason behind impaired albumin binding of FUR, energetic and binding parameters along with the location of FUR binding sites on albumin are determined by fluorescence spectroscopy (steady state and time-resolved), ITC, FRET, esterase activity of HSA, and molecular docking and then the binding site location is correlated with the binding sites of uremic toxins available in the literature. Further, secondary structural changes on the binding of FUR to HSA are monitored by circular dichroism and Fourier transform infrared spectroscopy. This study is the first to utilize ITC, FRET, activity assay, and molecular docking to obtain the binding parameters, energetics, and structural information for binding of FUR to human serum albumin.

3.2. Materials and methods

3.2.1. Materials and sample preparation. Human serum albumin (A1887; essentially globulin and fatty acid free), furosemide (F4381), warfarin (A2250), phenylbutazone (P8386), and p-nitrophenyl acetate (N8130) were procured fom Sigma Aldrich. Diazepam was the product of Ranbaxy Laboratories Ltd. All other reagents were of analytical grade. HSA and drug solutions were prepared in 20 mM sodium phosphate buffer (pH 7.4). The protein was dialyzed and its concentration was estimated spectrophotometerically using $E^{1\%}_{280\ nm}$= 5.3. All drug solutions were prepared by weight/volume (w/v).

3.2.2. Steady state measurements. Steady state absorption measurements were carried out on a Perkin-Elmer Lambda 25 double beam UV–vis spectrophotometer attached with Peltier temperature programmer-1 (PTP-1). All the steady state fluorescence measurements were recorded on Shimadzu 5301PC fluorescence spectrophotometer equipped with water circulator (Julabo Eyela). For fluorescence quenching measurements, HSA (5 μM) was titrated with varying concentrations of FUR (0–11 μM) at 25, 30, and 37°C. These samples were excited at 295 nm, and the

fluorescence emission was collected from 310 to 410 nm. However, for steady state FRET measurements, the fluorescence emission was collected from 300 to 500 nm. The excitation and emission slits were set at 3 nm. Respective blanks were subtracted. The fluorescence intensity was corrected for inner filter effects of protein and ligand using the equation: [Lakowicz, 2006]

$$F_{cor} = F_{obs} D_f 10^{\frac{(A_{295nm} + A_{340nm})}{2}} \quad (3.1)$$

where, F_{cor} and F_{obs} are corrected and observed fluorescence intensities, D_f, is the dilution factor, and $A_{295\ nm}$ and $A_{340\ nm}$ are the sum of the absorbance of protein and ligand at the excitation (295 nm) and emission (340 nm) wavelengths, respectively. The average of $A_{295\ nm}$ and $A_{340\ nm}$ for HSA and FUR lay in the range from 0.02 to 0.07.

3.2.3. Time-resolved fluorescence measurements. Fluorescence lifetime measurements were performed using the time-correlated single photon counting (TCSPC) model 5000 U (Horiba Jobin Yvon). The samples were excited at 295 nm using a NanoLED pulsed laser. The instrument response function (IRF) was obtained using LudoxTM suspension. The full width at half-maxima (fwhm) of the IRF was 750 ps. The emission decay data at 340 nm were analyzed using the software, DAS6, provided with the instrument.

3.2.4. Isothermal titration calorimetric measurements (ITC). The energetics of the binding of FUR to HSA at 25, 30, and 37°C were measured using a VP-ITC titration microcalorimeter (MicroCal Inc., Northampton, MA). Prior to the titration experiment, all samples were degassed properly on a thermovac. The sample and reference cell of the calorimeter were loaded with HSA solution (~8 μM) and 20 mM sodium phosphate buffer (pH 7.4), respectively. Then 10 μL of FUR solution (1.285 mM) were added into the sample cell containing HSA. Each injection was made over 20 s with an interval of 180 s between successive injections. The reference power and stirring speed were set at 16 $\mu cals^{-1}$ and 307 rpm, respectively. Heats of dilution for the ligands were determined in control experiments, and these were subtracted from the integrated data before curve fitting.

3.2.5. Circular dichroism spectroscopic measurements. The far-UV CD spectra of HSA (5 μM) were collected in the presence of FUR at molar ratio of 1:0, 1:1, and 1:2 in a JASCO-J815 spectropolarimeter equipped with a Peltier-type temperature controller at 25, 30, and 37°C. Spectra were collected from 200 to 250 nm with 20 nm/min scan speed and a response time of 2 s. Respective blanks were subtracted.

3.2.6. FT-IR spectroscopic measurements. Spectra of HSA in the presence and absence of drug were collected on a Nicolet 6700 FT-IR spectrophotometer (DTGS detector, Ni-chrome source and KBr beamsplitter) from 1700 to 1600 cm^{-1} using a ZnSe window at room temperature. For each spectrum, 256 scans were averaged with a resolution of 4 cm^{-1}. The drug with HSA was incubated for 1 h prior to scanning. Respective blanks were subtracted. The curve fitting was done by assuming mixed Lorentzian–Gaussian line shape function. The curve fitting, smoothing, baselines correction, and area calculation were carried out using the built-in software (OMNIC version). The resulting fitted curve was analyzed by taking into account the band assignment for the secondary structure previously reported in the literature [Barth, 2007] a-helix (1648–1657 cm^{-1}), ß-sheet (1623–1641 cm^{-1}), turn (1662–1686 cm^{-1}), random coil (1642–1657 cm^{-1}), and ß-antiparallel (1674–1696 cm^{-1}).

3.2.7. Effect of drug binding on esterase activity of HSA. Drug site II of HSA possessed a well-known esterase-like activity toward p-nitrophenyl acetate [Watanabe et al., 2000]. Thus the reaction of *p*-NPA with HSA in the absence and presence of drug (i.e., 0–45 μM) was followed at 405 nm by monitoring the appearance of yellow product p-nitrophenol for 1 min at 25°C. The molar extinction coefficient of p-nitrophenol was taken as 17800 M^{-1} cm^{-1}. The reaction mixture contained 15 μM HSA whereas *p*-NPA varied from 0 to 600 μM in 20 mM sodium phosphate buffer (pH 7.4). The control (in the absence of HSA) was also taken into consideration.

3.2.8. Molecular docking. The crystal structure of HSA (PDB: 1AO6) was retrieved from the Protein Data Bank on which addition of hydrogen atoms was done followed by minimization and optimization using the OPLS 2005 force field in the premin option of Schrödinger GLIDE in Schrödinger protein preparation wizard. The grids were generated and cover all the residues in a 5 Å neighborhood of the phenylbutazone (PBZ) and warfarin (WAR) for site I and DIA for site II. The FUR

molecule was then prepared in the Schrödinger ligprep wizard and predocking preparations were done as that for protein. Docking was then performed using GLIDE and its output G score was calculated as [Friesner et al., 2004]

$$G\ score = H\ bond + eLipo + metal + site + 0.13Coul + 0.065vdW - BuryP - RotB \quad (3.2)$$

where, H bond=hydrogen bonds, Lipo=hydrophobic interactions, metal=metal-binding term, site=polar interactions in the binding site, vdW=van der Waals forces, Coul = Columbic forces, BuryP=penalty for buried polar group, RotB=freezing rotable bonds.

X-Score v1.2.1, was used to calculate negative logarithm of dissociation constant of the ligand to the protein, -log (K_d), and binding energy (kcal mol^{-1}). X-Score was reported to have an accuracy of ±2.2 kcal mol^{-1} to the actual binding energies. The Ligplot program and PyMOL were used for analyzation and visualization of the interaction of docked protein–ligand complex, respectively.

3.2.9. Statistical analysis

All determinations were triplicates, and mean values and standard deviations were calculated, wherever applicable, using SPSS 16.0 programme for windows.

3.3. Results and discussion

3.3.1. Steady state fluorescence results. Tryptophan, tyrosine, and phenylalanine are the three aromatic fluorophores that are used for studying conformational changes on drug binding. However, among them, contribution of tryptophan is maximum [Ahmad et al., 2011]. Fluorescence quenching of aromatic fluorophores in HSA by FUR at three different temperatures viz. 25, 30, and 37°C is evaluated in the presence of varying concentrations of FUR. As shown in Figure 3.1, HSA has the strong emission peak at 340 nm on excitation at 295 nm, which decreases with gradual addition of FUR at all three temperatures [Ahmad et al., 2006; Anand et al., 2011]. However, the quenching of Trp fluorescence emission is maximum at 25°C and minimum at 37°C.

3.3.1.1. Binding affinity. To obtain the Stern–Volmer quenching constant (K_{sv}) and binding constant (K_b), the fluorescence quenching data of HSA-FUR binding at

different temperatures are analyzed by the Stern–Volmer equation and plot of log (F_o/F-1) vs log[Q] respectively: [Lakowicz, 2006]

$$\frac{F_o}{F} = K_{sv}[Q] + 1 = k_q \tau_o [Q] + 1 \tag{3.3}$$

$$\log\left(\frac{F_o}{F} - 1\right) = \log K_b + n\log[Q] \tag{3.4}$$

where F_o and F are the fluorescence intensities in the absence and presence of quencher (FUR), K_{sv} and k_q are the Stern–Volmer quenching and bimolecular rate constants, respectively, and τ_o, is the average integral fluorescence lifetime of tryptophan, which is ~ 5.7×10^{-9} s.

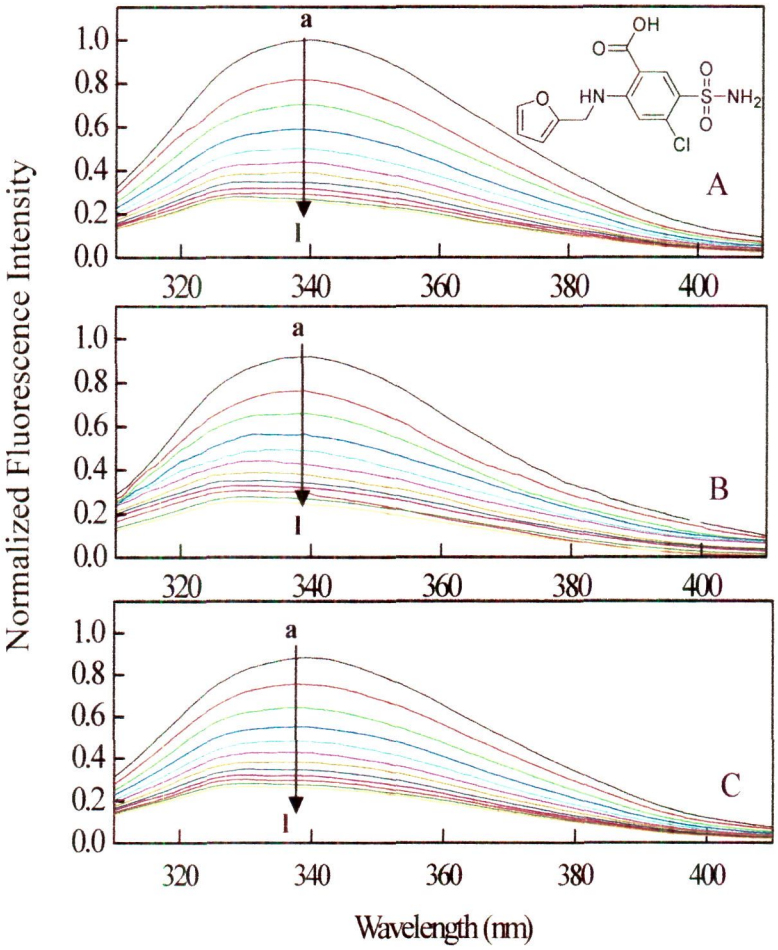

Figure 3.1. Normalized fluorescence emission spectra of HSA in presence of different concentrations of FUR at (A) 25°C B) 30°C, and (C) 37°C. a-l: 0–11 μM of FUR at increments of 1 μM. The inset corresponds to the molecular structure of FUR.

The K_{sv} was calculated from the slope of plot F_o/F vs [Q], whereas the slope and intercept of plot log (F_o/F-1) vs log[Q] give n and K_b, respectively (Figure 3.2A, B).

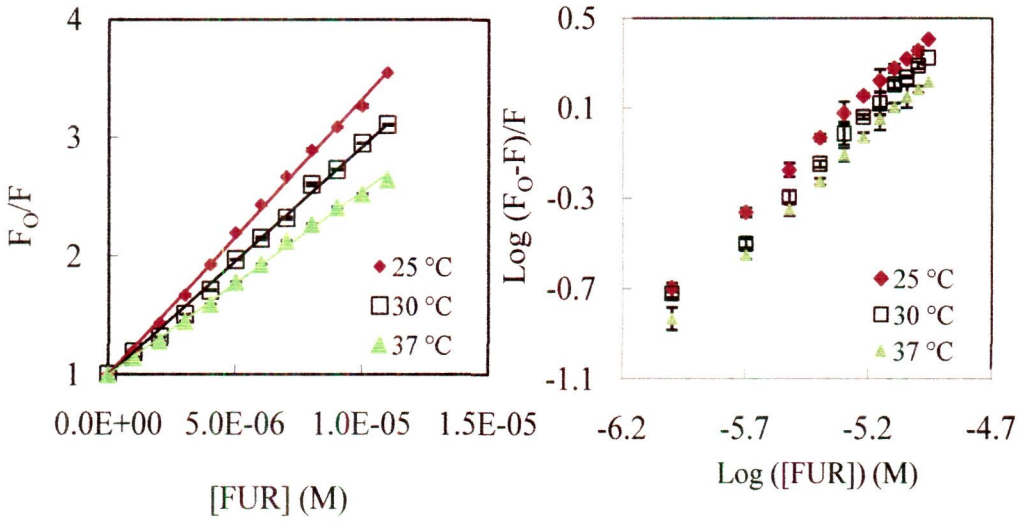

Figure 2. Stern–Volmer (A) and modified Stern–Volmer plots (B) of fluorescence quenching of HSA by FUR at different temperatures.

As shown in Table 3.1, the values for binding constant are on the order of 10^5 and decrease with increasing temperature. This suggests static quenching phenomenon, which is also the reason behind the fall in fluorescence emission of Trp with the rise in FUR concentration [Chi and Liu, 2011; Ibrahim et al., 2010].

3.3.1.2. Mechanism of binding. Fluorescence quenching can be either dynamic or static in nature. In order to know about the quenching mechanism of HSA by FUR, the mechanism assumed to be dynamic. Thus by equation 3.3, k_q was obtained which lies in order of 10^{13} as shown in Table 3.1. However, the k_q for the HSA-FUR system is 1000 times lower than the maximum scatter collision quenching constant of various quenchers with biopolymers (2×10^{10} $M^{-1}s^{-1}$) [Ahmad et al., 2011]. This shows that quenching is not initiated by dynamic diffusion but occurs by formation of a strong complex between HSA and FUR [Anand et al., 2011]. Further, the temperature dependence of K_{sv} is studied as a type of quenching and can be distinguished by the differential response toward temperature and viscosity. In static quenching, K_{sv} decreases with an increase in temperature due to the formation of complex with protein, which undergoes dissociation on increasing temperature. However, for dynamic quenching, K_{sv} increases with temperature as in this case higher temperature results in faster diffusion of quencher and hence larger extent of collisional quenching

[Chi and Liu, 2011]. To further confirm the mechanism, time-resolved fluorescence spectroscopy has been done.

Table 3.1. Binding and thermodynamic parameters of FUR-HSA at different temperatures obtained from fluorescence quenching experiments[a]

Temp (°C)	25	30	37
n	1.05 ± 0.01	1.05 ± 0.02	1.03 ± 0.03
K_{SV} (M^{-1})	(2.29 ± 0.06) ×10^5	(1.90 ± 0.03) ×10^5	(1.52 ± 0.04) ×10^5
K_b (M^{-1})	(4.09 ± 0.07) ×10^5	(3.13 ± 0.08) ×10^5	(1.99 ± 0.03) ×10^5
k_q (M^{-1} s^{-1})	(4.01 ± 0.05)×10^{13}	(3.33 ± 0.04)×10^{13}	(2.66 ± 0.02)×10^{13}
ΔH°(kcal mol^{-1})		-11.07 ± 0.08	
TΔS° (kcal mol^{-1})	-3.41 ± 0.04	-3.47 ± 0.05	-3.55 ± 0.05
ΔG° (kcal mol^{-1})	-7.65 ± 0.03	-7.61 ± 0.02	-7.51 ± 0.01

[a]R^2 for all values ranges from 0.98 to 0.99.

3.3.1.3. Mode of binding. The signs and magnitude of change in enthalpy (ΔH°), entropy (ΔS°), and free energy (ΔG°) for protein–drug interaction can be exploited to evaluate the main forces contributing to formation of a protein–drug complex [Ross and Subramanian, 1981]. According to equation 3.5, ΔH° and ΔS° are obtained from the slope and intercept of a linear van't Hoff plot between ln K_b vs 1/T (not shown).

$$\ln K_b = -\frac{\Delta H^\circ}{RT} + \frac{\Delta S^\circ}{R} \qquad (3.5)$$

and the change in free energy (ΔG) is calculated from Gibbs–Helmholtz equation:

$$\Delta G^\circ = -RT \ln K_b \qquad (3.6)$$

where R (1.987 cal $mol^{-1}K^{-1}$) is the gas constant and T is the absolute temperature (K). The calculated thermodynamic parameter ΔH°, ΔS°, and ΔG° are summarized in Table 3.1. The negative ΔH° and ΔG° signify the exothermic and spontaneous nature of process at all studied temperature. According to [Ross and Subramanian, 1981], negative ΔH° and ΔS° value suggest the involvement of hydrogen bonding in HSA-FUR complex formation and a decrease in entropy is attributed to the formation of hydrogen bonds between FUR and HSA. Furthermore, it is found that the major contribution to ΔG° arises from ΔH° rather than ΔS°, so the binding process is enthalpy driven.

3.3.1.4. Probing binding site using site markers. The determination of binding site location of FUR on HSA is performed by using the simple approach of competitive binding between FUR and site specific markers, viz. warfarin (WAR), phenylbutazone (PBZ) for site I and diazepam (DIA) for site II, [Ghuman et al., 2005; Petitpas et al., 2001] by keeping a constant concentration of protein and marker in the ratio of 1:1 and varying the concentration of FUR (0–11 μM). The ligands bind HSA at two major binding regions, namely Sudlow's site I and site II, which are located within specialized cavities in subdomains IIA and IIIA, respectively [Sudlow et al., 1975]. To probe the binding site of FUR on HSA, K_{sv} values in the absence and presence of markers are calculated by the Stern–Volmer equation and presented in Table 3.2. The values of K_{sv} for FUR decrease in the presence of PBZ and WAR (site I markers). It suggests that FUR binds to site I because in the presence of site markers having the same binding site as that of the test drug, the value of quenching constant should decrease due to competition [Chi and Liu, 2011]. However, a decrease in the values of K_{sv}, for FUR in the presence of DIA (site II marker) is also not negligible, which is suggestive of binding of FUR to site II. But the decrease in K_{sv} of later is small so FUR has a low affinity for site II.

Table 3.2. Effect of site markers on binding of FUR to HSA.

	without the site marker	with PBZ	with WAR	with DIA
K_{sv}	$(2.29\pm0.08)\times10^5$	$(5.01\pm0.02)\times10^4$	$(1.03\pm0.03)\times10^5$	$(1.32\pm0.05)\times10^5$
R^2	0.99	0.99	0.99	0.99

[a]R^2 for all values ranges from 0.98 to 0.99.

3.3.2. Steady state fluorescence resonance energy transfer (FRET). According to Förster nonradiation energy transfer theory, the parameters related to energy transfer can be calculated on the basis of equations as follows [Förster, 1948; Il'ichev et al., 2002]. The efficiency of energy transfer (E) can be calculated as

$$E_{FRET} = \left(1 - \frac{F}{F_o}\right) = \frac{R_o^6}{R_o^6 + r^6} \qquad (3.7)$$

where F_0 and F are the fluorescence intensities of HSA in the absence and presence of drug, respectively, r is the distance between donor and acceptor, and R_0 is the distance at which transfer efficiency equals 50 %, which can be calculated as

$$R_o^6=8.79\times10^{-25}K^2n^{-4}\varphi J \tag{3.8}$$

where K^2 is the factor related to the geometry of the donor and acceptor of dipoles, n is the refractive index of the medium, φ is the fluorescence quantum yield of the donor in the absence of acceptor and J is the overlap integral of donor fluorescence emission and the acceptor absorption, which can be calculated by

$$J=\frac{\int_o^\infty F(\lambda)\varepsilon(\lambda)\lambda^4 d\lambda}{\int_o^\infty F(\lambda)d\lambda} \tag{3.9}$$

where $F(\lambda)$ is the fluorescence intensity of the donor at wavelength range λ which is dimensionless, and $\varepsilon(\lambda)$ is the molar absorptivity (extinction coefficient) of the acceptor at wavelength λ in M^{-1} cm^{-1}. For HSA, K^2, φ and n are taken as 2/3, 0.118, and 1.33, respectively [Cyril et al., 1961]. By using eq 7–9, values of J, E_{FRET}, R_0 and r are calculated and listed in Table 3.3.

Table 3.3. Steady state and time-resolved fluorescence parameters of HSA-FUR.

		Steady state		Time resolved	
J (M^{-1} cm^{-1} nm^4)	R_0 (nm)	r (nm)	E_{FRET}	r (nm)	E_{FRET}
2.45×10^{13}	1.93	2.02	0.43	2.97	0.07

The overlap spectra of normalized fluorescence intensity of donor (Trp214 of HSA) emission and acceptor absorption are shown in Figure 3.3. The binding distance (r) obtained for the system is found to be 2.02 nm. However, it must be mentioned here that if FRET is done by steady state measurements, then the value of E_{FRET} is overestimated as steady state measurements have a contribution from static quenching, which also seems to be the principal reason for lowering the HSA fluorescence emission in the presence of FUR. Hence, to have a better understanding of exclusive FRET, we have characterized HSA-FUR system by time-resolved fluorescence measurements.

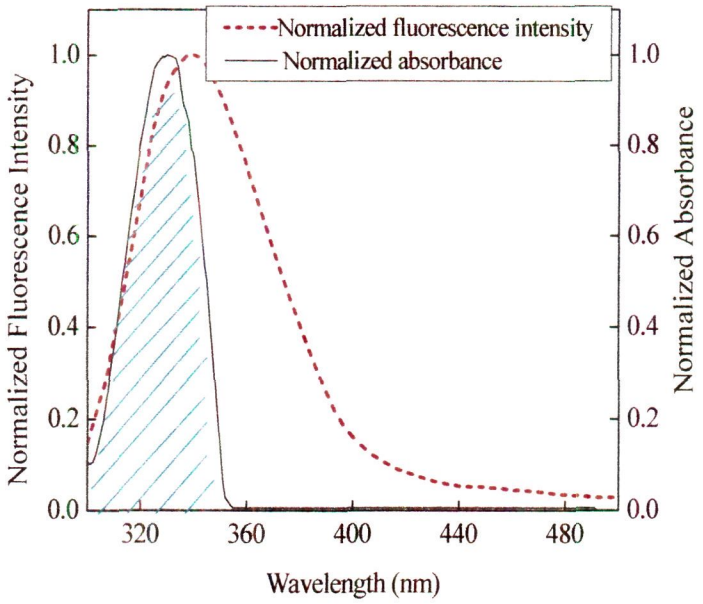

Figure 3.3. Overlap spectra of normalized absorbance of FUR (solid) and normalized fluorescence intensity of HSA (dashed). Equimolar (5 μM) concentration of drug and protein were taken.

3.3.3. Time-resolved fluorescence quenching measurements: Fluorescence lifetime measurement serves as an indicator for exploring the local environment around fluorophores and so can be implicated to understand the interaction between drug and protein [Anand et al., 2010]. At neutral pH in aqueous solution, Trp exhibits multiple exponential decay, which has been attributed to the existence of rotamers (conformational isomers) in determining lifetimes [Anand et al., 2011]. The time-resolved decay profile of HSA in buffer and in the presence of FUR are displayed in Figure 3.4. All the experimental decay curves are well reproduced with biexponential decay function as evidenced by the statistical parameters like χ^2 which is close to 1 and distribution of weighted residuals. When the biexponential decay law is used, it is often useful to determine intensity-averaged lifetime (τ_{avg}) from the deacy times (τ) and pre-exponential factors (α_1 and α_2) using [Lakowicz, 2006]

$$\tau_{avg} = \frac{\alpha_1\tau_1^2 + \alpha_2\tau_2^2}{\alpha_1\tau_1 + \alpha_2\tau_2} \qquad (3.10)$$

The intensity-averaged lifetimes (τ_{avg}) obtained were compared with those calculated by amplitude-averaged lifetime method (data not shown) using [Kelkar et al., 2005]

$$\langle \tau_{avg} \rangle = \alpha_1 \tau_1 + \alpha_2 \tau_2 \qquad (3.11)$$

Although differences are observed in values of τ_{avg} and $\langle \tau_{avg} \rangle$ but, they are acceptable as reported in literature [Haldar et al., 2008; Haldar et al., 2012; Kelkar et al., 2005].

Table 3.4. Time-resolved fluorescence decay parameters of HSA in presence of FUR

HSA:FUR	α_1	τ_1(ns)	α_2	τ_2(ns)	τ_{avg}
1:0	0.39	2.17	0.61	6.45	5.70
1:1	0.40	1.80	0.60	6.13	5.41
1:2	0.46	1.86	0.54	6.18	5.29

The τ_{avg} of HSA is found to be 5.7 ns, which decreases marginally even in the presence of a saturating concentration of FUR, as shown in Figure 3.4 and Table 3.4.

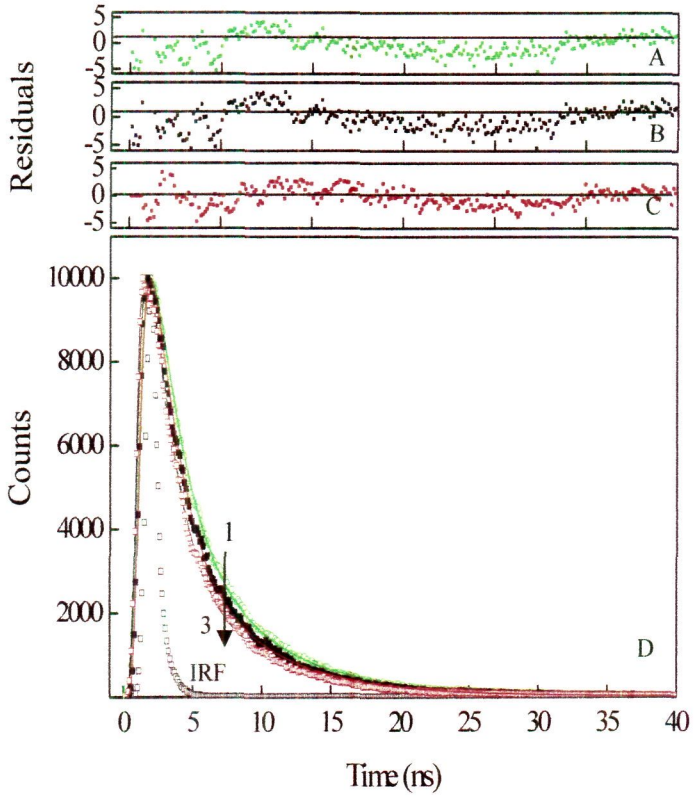

Figure 3.4. Time-resolved fluorescence decay profile of HSA in absence and presence of FUR. Panels A–C show the distribution of weighted residuals for biexponential fitting for 1:0, 1:1, and 1:2 HSA:FUR.. IRF indicates the instrument response function. The panel D shows the fluorescence lifetime decay of HSA: FUR at ratio of (1)1:0, (2)1:1, and (3)1:2.

This is due to the charge transfer process from the indole ring of Trp214 to the nearby substituent which slightly enhances on binding with FUR and thus causes a slight decrease in the fluorescence lifetime. It is indicative of a small contribution of

dynamic quenching as only those molecules that suffer dynamic quenching have an exclusive contribution in decrease of the fluorescence lifetime [Beechem and Brand, 1985]. Thus, the time-resolved transfer efficiency (E) calculated from fluorescence lifetime measurements exclusively reports the energy transfer during the process of dynamic quenching and is obtained by using the following equation:

$$E=1-\frac{\tau}{\tau_o} \tag{3.12}$$

where τ and τ_0 are the lifetime of Trp in the presence and absence of FUR, respectively. Table 3.3 represents the FRET parameters obtained from steady state and time-resolved measurements. The magnitudes of E_{FRET} estimated from time-resolved lifetime measurements are found to be much lower than the value obtained by steady state measurements because of the exclusive contribution of dynamic quenching in the former. Thus it can be said that the mechanism of FRET is indeed operational but the magnitude of transfer efficiency is small.

3.3.4. Isothermal titration calorimetric measurements. ITC allows the measurement of the magnitude of binding affinity, and the two contributing thermodynamic terms: enthalpy (ΔH^o) and entropy (ΔS^o) changes. A representative calorimetric titration profile of the binding of FUR to HSA at 25, 30 and 37°C is shown in Figure 3.5(A–C). In the top panel, each peak represents a single injection of the drug into protein solution. The bottom panel shows an integrated plot of the amount of heat liberated per injection as a function of the molar ratio of the drug to protein. Association constant (K_b) and enthalpy change (ΔH^o) were directly obtained after fitting whereas free energy change is calculated from equation 3.6. The entropy change is calculated by

$$\Delta G^\circ = \Delta H^\circ - T\Delta S^\circ \tag{3.13}$$

and change in specific heat capacity can be calculated from [Ladbury and Williams, 2004].

$$\Delta C_p^{exp} = \frac{d\Delta H^\circ}{dT} \tag{3.14}$$

Further the van't Hoff enthalpy (ΔH_{vH}) at each temperature is calculated with

$$\Delta H^{\circ}_{vH} = \left[\frac{\left\{ \ln \frac{K(T_2)}{K(T_1)} - \frac{\Delta C_P}{R} \ln \frac{T_2}{T_1} + \frac{\Delta C_P T_1}{R} \left(\frac{1}{T_1} - \frac{1}{T_2} \right) \right\} \times R}{\left(\frac{1}{T_1} - \frac{1}{T_2} \right)} \right] \quad (3.15)$$

Here, $K(T_1)$ and $K(T_2)$ are the values of binding constant at temperatures T_1 and T_2, respectively. The temperature dependency of the thermodynamic binding parameters of FUR to HSA is summarized in Table 3.5. The titration of FUR to HSA results in negative heat deflection at all studied temperatures, indicating that the binding is an exothermic process (Figure 3.5). Because albumin can bind ligand at multiple binding sites, we fit the data for two sites by the sequential binding model. The values of binding constant obtained are of the order of 10^4 and 10^3 and thus can be referred as high and low affinity sites, respectively, at each studied temperature. However, the binding constants for both types of binding sites decrease with an increase in temperature, indicating the formation of FUR-HSA complex. Besides, it is observed that at both sites of HSA, a strong dependence of ΔH° and $T\Delta S^{\circ}$ exists with temperature whereas ΔG° was insensitive to it (Table 3.5). As evident from the value of ΔH° and ΔS°, the binding become more exothermic with a rise in temperature, though it is entropically opposed. The negative ΔH° and ΔS° values at all studied temperatures suggest the involvement of hydrogen bonding in HSA-FUR complex formation [Chi and Liu, 2011]. Furthermore, the plot between ΔH° vs $T\Delta S^{\circ}$ at high and low affinity sites shows the slope of 1.02 and 0.99, respectively, which indicates the enthalpy–entropy compensation effect in which enthalpy gain due to the formation of H-bond is counterbalanced by entropic penalty due to the burial of involved groups. This effect is common in protein–ligand interaction [Zolotnitsky et al., 2004]. Almost linear dependency of the ΔH with the temperature was observed in an examined range of temperature, whose slope was used to determine the change in heat capacity (ΔC_p). The values of ΔC_p were -0.18±0.11 and -0.94±0.24 kcal $mol^{-1}{}^{\circ}C^{-1}$ for high and low affinity sites, respectively. The negative value of ΔC_p is suggestive of specific binding accompanied by the burial of nonpolar residues [Kumaran and Jez, 2007]. The results of ITC were in agreement with that of fluorescence spectroscopy. However, variation in magnitude of binding affinity and thermodynamic parameters was observed, which may be due to the fact that the calorimetric analysis measures a global change in property of the system whereas spectroscopic analysis measures

local changes around the fluorophores/chromophores associated with the optical transition [Faergeman et al., 1996; Nada and Terazima, 2003].

Table 3.5. Thermodynamic parameters and association constant of FUR-HSA obtained by ITC.

	Temp (°C)	K_b (M^{-1})	$\Delta H°$ (kcal mol^{-1})	$T\Delta S°$ (kcal mol^{-1})	$\Delta G°$ (kcal mol^{-1})
High	25	$(8.24\pm0.45)\times10^4$	-12.61±0.29	-5.91±0.02	-6.70 ± 0.01
affinity	30	$(7.03\pm0.25)\times10^4$	-14.74±0.24	-8.03±0.04	-6.71 ± 0.02
site	37	$(5.58\pm0.12)\times10^4$	-14.91±0.15	-8.18±0.07	-6.73 ± 0.01
Low	25	$(6.47\pm0.41)\times10^3$	-12.37±0.55	-7.18±0.05	-5.19 ± 0.02
affinity	30	$(6.21\pm0.24)\times10^3$	-14.34±0.42	-9.09±0.04	-5.25 ± 0.03
site	37	$(2.76\pm0.11)\times10^3$	-23.40±0.72	-18.52±0.03	-4.88 ± 0.01

The binding stoichiometry obtained from spectroscopy and calorimetry was also different, which may be due to photophysical problem because of the presence of single Trp214 in HSA [Ahmad et al., 2011]. Further, using equation 3.15 and data presented in Table 3.5, it is observed that the values of calorimetric enthalpies do not agree well with the van't Hoff enthalpy calculated at all studied temperatures. It indicates linkage of contribution of displacement of solvent ions and conformational changes with the binding process, which may be induced either by ligand binding or by an increase in temperature [Faegerman et al., 1996]. This observation is further supported by non linear van't Hoff plot between temperature and lnK, which is also an important indication of conformational alterations linked to the binding process. So, FTIR and far-UV CD measurements are performed to monitor the secondary structure alteration on FUR binding.

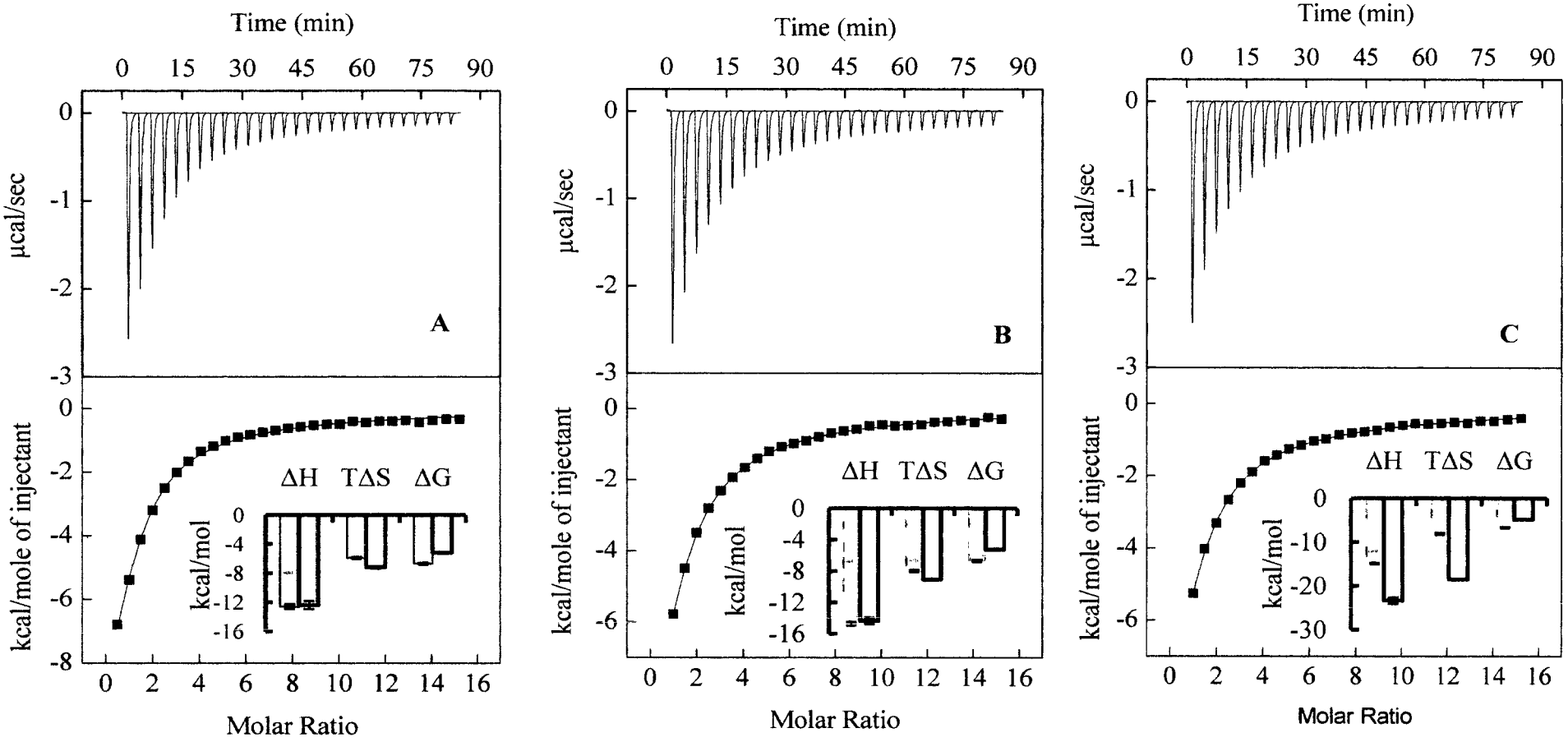

Figure 3.5. Isothermal titration calorimetry of HSA and FUR interaction at (A) 25°C, (B) 30°C, and (C) 37°C. Titration of FUR with (18 µM) HSA at pH 7.4 shows calorimetric response as successive injections of ligand are added to the sample cell. The solid line represents the best nonlinear least squares fit of sequential model of two binding site.The insets of A–C represent comparative bar distribution of ΔH, ΔS and ΔG at high (filled bar) and low (open bar) affinity binding site.

3.3.5. Circular dichroism measurements. To monitor the secondary structural change of protein upon interaction with FUR, we perform far UV circular dichroism. The results are expressed as MRE (mean residue ellipticity) in deg cm^2 $dmol^{-1}$, which is given by

$$\text{MRE} = \frac{\Theta_{obs}(\text{mdeg})}{10 \times n \times c \times l} \tag{3.16}$$

where θ_{obs} is the observed ellipticity in millidegrees, c is the concentration of protein in mol/L, l is the length of the light path in centimeters, and n is the number of peptide bonds.

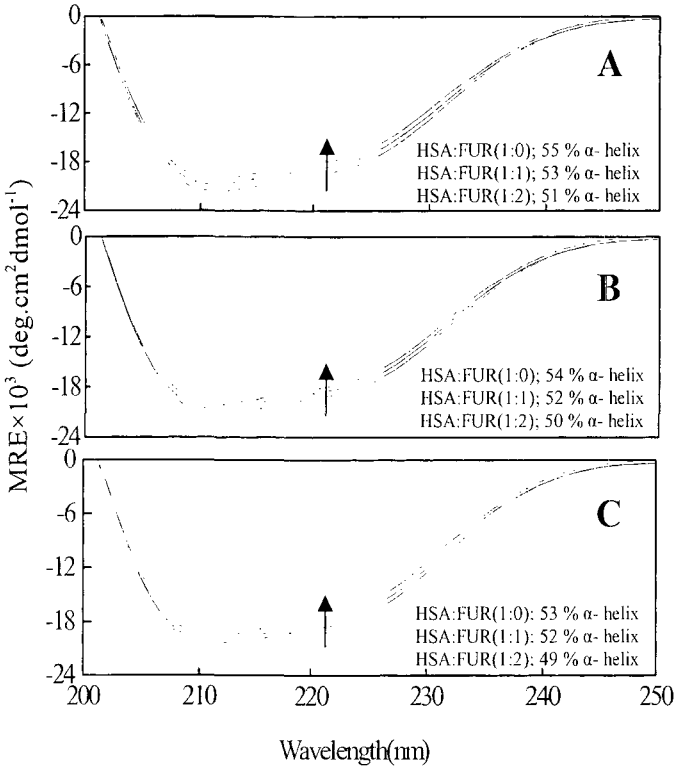

Figure 3.6. Circular dichroism spectra of HSA (5 μM) in the presence of FUR at ratios of (1)1:0, (2)1:1, and (3)1:2 at (A) 25°C, (B) 30°C, and (C) 37°C.

Panels A–C of Figure 3.6 shows the far-UV CD spectra of HSA in the absence and presence of FUR at 25, 30, and 37°C, respectively. The far-UV CD spectra of HSA exhibit two negative bands at 208 and 222 nm, which is characteristic of the typical α-helix structure of protein [Ahmad et al., 2006; Ahmad et al., 2011]. Furthermore, to investigate the change in percent α helical structure of HSA on addition of FUR, we analyze CD data by the method of [Chen et al., 1972]:

$$\%a\text{-helix} = \left(\frac{MRE_{222nm} - 2{,}340}{30{,}300} \right) \times 100 \qquad (3.17)$$

The estimated percent a-helical content in free HSA is 55, 54, and 53 % at 25, 30, and 37°C respectively, which is in reasonable accord with the available literature [Ahmad et al., 2006; Ahmad et al., 2011; Beauchemin et al., 2007]. The data compiled in the inset of Figure 3.6A–C indicate the slight decrease in a-helical content on addition of FUR in ratios of 1:1 and 1:2 (HSA:FUR) at all studied temperatures. The observed decrease in percent a-helical content might be induced by the formation of the FUR–HSA complex. However, the shape of peaks and the position of peak maximum remain almost unchanged in the presence and absence of FUR, indicating that HSA is predominantly a-helix in nature even after binding to the drug.

3.3.6. FTIR spectroscopic measurements. Band frequencies due to amide I, II, and III vibrations in the IR region are sensitive to the secondary structure of protein.

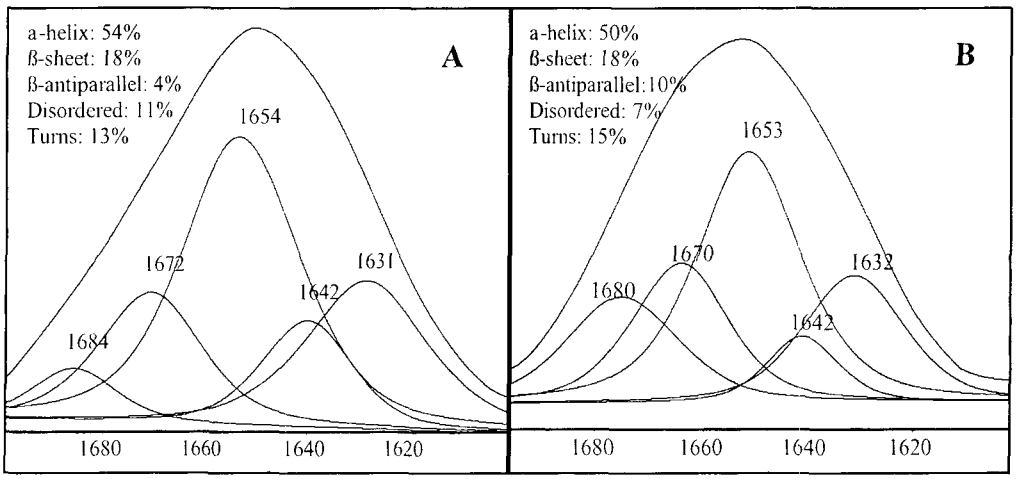

Figure 3.7. The fitted amide I band of HSA-FUR complex at (A) 1:0, (B) 1:1 HSA to FUR ratio in 20 mM sodium phosphate, pH 7.4 in the region of 1700-1600 cm^{-1}.

But, generally, amide I (1700–1600 cm^{-1}) is analyzed to investigate the change in secondary structure of protein as it reflects C=O stretching vibration of the amide group weakly coupled with in plane NH bending and CN stretching [Tian et al., 2004]Figure 3.7A, B shows the fitted curve of HSA and HSA-FUR complex in a molar ratio of 1:1. The free HSA has 54% a-helix, 18% ß-sheet, 4% ß-antiparallel, 11% disordered, and 13% turn, which is reasonable accord with the literature [Froehlich et al., 2009]. From Figure 3.7, it can be seen that there is not much

difference in the position of amide I components, but their intensities differ. So, from quantitative analysis of the amide I band, it was observed that amount of α-helix decreases on HSA-FUR complex formation, which agrees with far-UV CD results.

3.3.7. Effect of drug binding on esterase-like activity of HSA. The Arg410 and Tyr411 present in the center of drug binding site II of HSA are the two crucial amino acid residues involved in esterase-like activity [Watanabe et al., 2000]. Thus, esterase-like activity of HSA using p-nitrophenyl acetate as the substrate is investigated in the presence and absence of FUR to know the involvement of Arg410 and Tyr411 in FUR binding. Kinetic constants are obtained using Graph-Pad Prism, version 5.0, software by fitting the initial rates to Michaelis–Menten equation:

$$v = \frac{V_{max}[S]}{K_m + [S]} \tag{3.18}$$

where v, V_{max}, K_m, and [S] represent the initial reaction velocity, maximum velocity, Michaelis–Menten constant, and molar concentration of substrate, respectively. Further, K_i was calculated from equation.

$$K_m^{'} = \frac{K_m}{K_i} I_o + K_m \tag{3.19}$$

where $K_m^{'}$, is the apparent K_m in the presence of competitive inhibitor concentration I_o. Figure 3.7 shows the Michaelis–Menten and double reciprocal plot in the absence and presence of different drug to HSA molar ratios. HSA acts as esterase toward *p*-NPA and shows K_m and V_{max} equals 59.36 μM and 0.16 μM s^{-1} respectively (Table 3.6), which remain similar even in the presence of a FUR to HSA ratio of 0.5. However, on a further increase in the ratio of FUR to HSA, there occurs inhibition of activity in a competitive manner with K_i equal to 28.72 μM; i.e., K_m changes while V_{max} remain nearly unaltered, as shown in Figure 3.8 and Table 3.6. Because FUR has drug site I as a high affinity site up to a FUR to HSA ratio of 0.5, the drug binds mainly to site I on HSA and thus no changes occur in K_m,V_{max} and k_{cat}/K_m ratio. But on a further increase in FUR concentration over HSA, the drug starts binding to its low affinity site, which has Arg410 and Tyr411 amino acid residues, and thus competitively inhibits esterase-like activity of HSA and hence a decrease in catalytic efficiency is observed. This confirms the involvement of these amino acids in FUR binding to HSA.

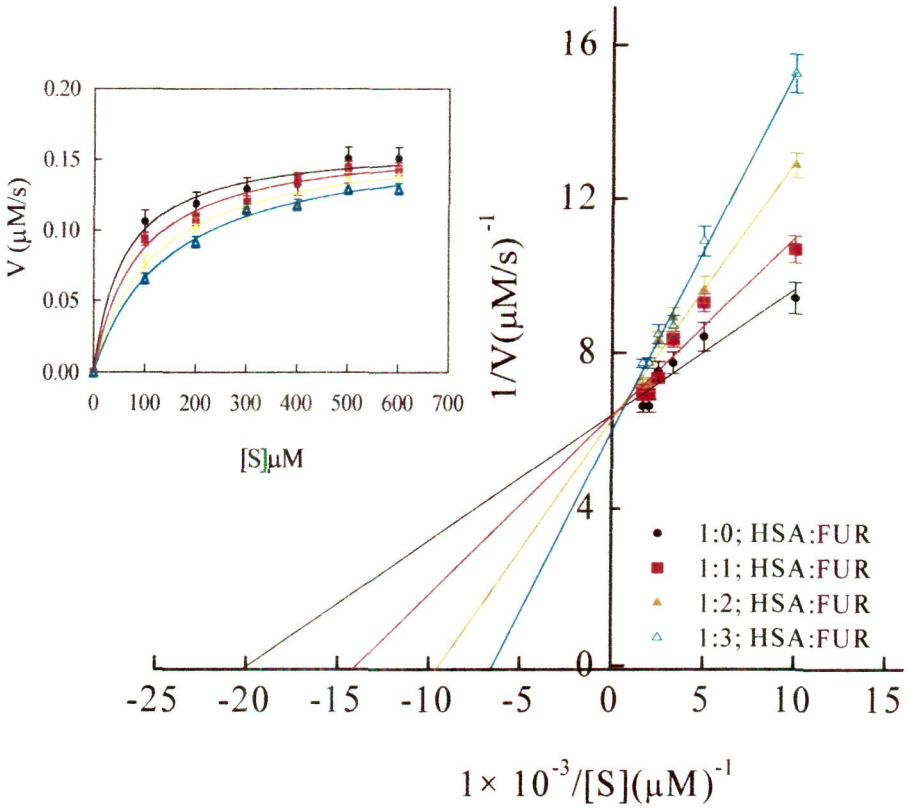

Figure 3.8. Plot between 1/V and 1/[S] for esterase-like activity of HSA at varying molar ratio of HSA:FUR (inhibitor). The inset shows the Michalies–Menten plot of HSA for *p*-NPA under same condition. The effect of varying concentration of FUR on the apparent K_m for *p*-NPA(S) was examined in 20 mM sodium phosphate, pH 7.4 at 25°C. HSA (15 μM) and HSA:FUR ratios of 1:0, 1:1, 1:2, and 1:3 were used.

Table 3.6. Kinetic parameters for the hydrolysis of *p*-NPA by HSA in presence of FUR

HSA: FUR	K_m (μM)	V_{max} (μMs^{-1})	$10^5 \times k_{cat}/K_m$ (μM^{-1}s^{-1})
1:0	59.36 ± 05.55	0.16 ± 0.01	17.95 ± 1.23
1:0.5	60.12 ± 05.52	0.16 ± 0.01	17.73 ± 0.55
1:1	86.60 ± 06.47	0.16 ± 0.02	12.30 ± 0.65
1:2	120.40 ± 09.42	0.16 ± 0.01	08.85 ± 1.11
1:3	149.60 ± 10.67	0.16 ± 0.02	07.12 ± 2.41

3.3.8. Molecular docking studies of FUR-HSA interaction. The binding sites of FUR on HSA were located by using docking software GLIDE [Friesner et al., 2004]. Figure 3.9A, B and Table 3.7 represent the involvement of crucial amino acid residues in the binding of FUR to the two different sites on HSA. The residues that overlap with specific site markers of site I (i.e., PBZ, WAR) and site II (DIA) are also shown. According to the GLIDE score, the FUR fit most favorably in site I of HSA with GLIDE and X-score of -7.32 and -7.99 kcal mol^{-1}, respectively.

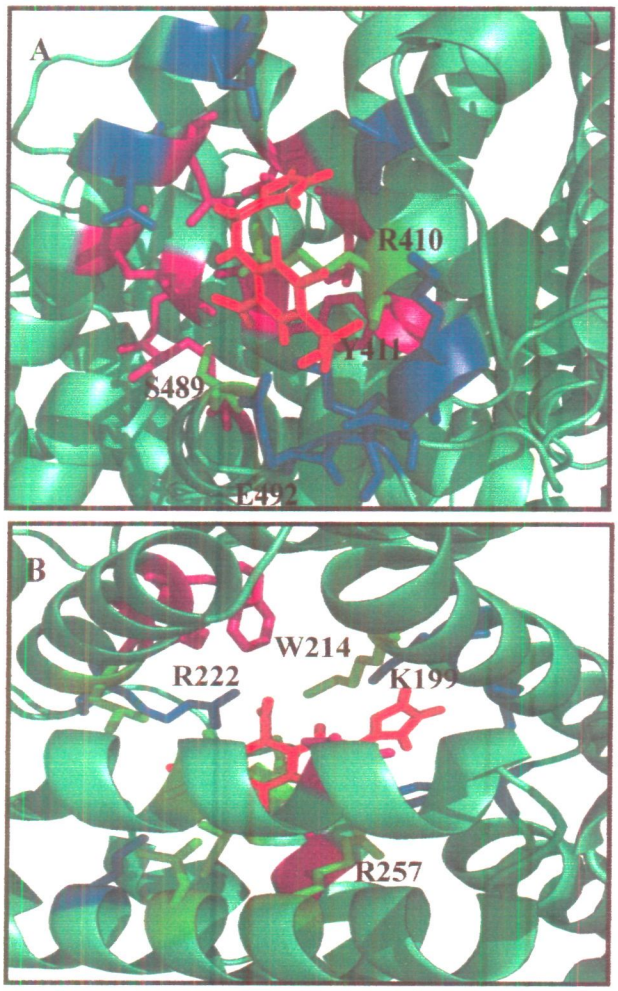

Figure 3.9. Cartoon representation of docked FUR (red) in site I (A) of HSA and new site near site II (B). Residue interacting with FUR only (blue), PBZ and DIA only (purple), and common to FUR, PBZ, or DIA (green)

Figure 3.10B and Table 3.7 show that at site I, FUR hydrophobically interacts with Ala291, Leu238, Lys195, Tyr150, and Trp214 whereas O1, O4, and N1 groups involved in hydrogen bonding with the NH_2 group of Lys199 of HSA with bond length of 3.10, 2.69, and 2.98 Å, respectively. The two side chain NH_2 groups of Arg222 also interact with O5 of FUR having hydrogen bond length of 2.85 and 2.66 Å. However, FUR also binds to a site that is in the vicinity of site II of HSA with GLIDE and X-score of -5.53 and -6.89 kcal mol^{-1}, respectively. This site shares some of the amino acid residues of site II like Arg410, Lys414, Ser489, and Glu492. The NH_2 group of the side chain of Arg410 and Lys414 and OH of carboxylate group of Glu492 of HSA interact with O1, O5, and O2 of FUR with hydrogen bond lengths of 3.24, 2.62, and 2.66 Å, respectively. Moreover, FUR interacts hydrophobically with Lys413, Gln390, Leu394, Ala406, Val493, and others (Figure 3.10A).

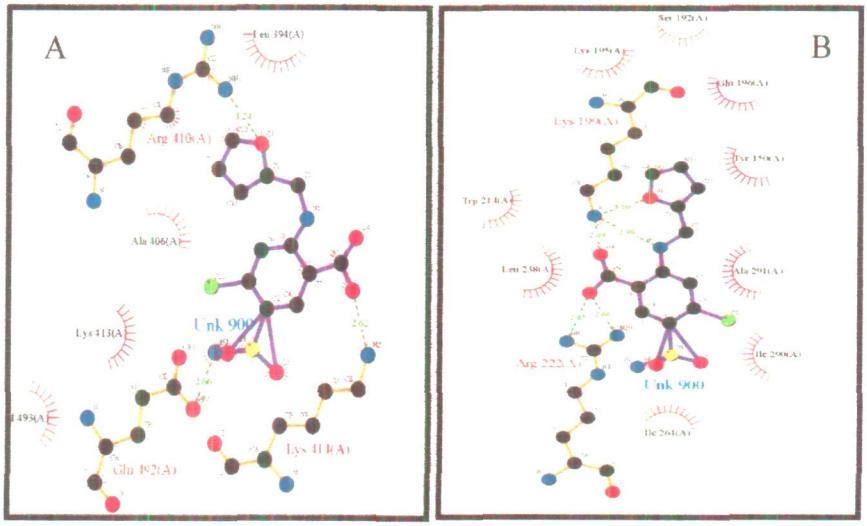

Figure 3.10. Lig plots of FUR with HSA at (C) new site and (D) site I.

Figure 3.11A &B show the molecular surface representation of FUR in the binding pockets of HSA. Thus FUR has drug binding site I as the high affinity binding site whereas a new site that shares Arg410 and some other amino acid residues like Lys414 and Ser489 has site II as the low affinity binding site. Further, it is also established that FUR-HSA binding involves hydrogen bonding and hydrophobic interaction as the main binding forces.

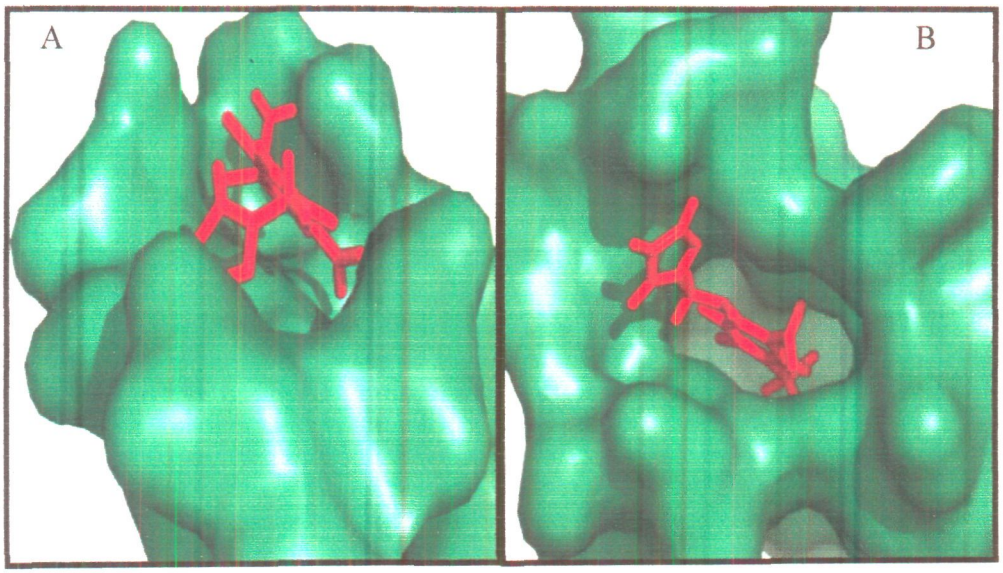

Figure 3.11.Molecular surface structure of HSA with FUR (red) at (A) new site (B) and site I.

Table 3.7. Results of docking of HSA with FUR as obtained from GLIDE docking software

binding site	amino acid	ΔASA (Å^2)	forces involved	GLIDE Score (kcal mol^{-1})	X-Score (kcal mol^{-1})	-log (K_d)	Number of other residues (5 Å)
Site I	Ala291	36.67	Hydrophobic interaction	-7.32	-7.99	5.86	5
	Leu238	30.27	Hydrophobic interaction				
	Lys199	21.96	Hydrogen bonding [*Lys199-NH_2---O=C FUR(2.69 Å) *Lys199-NH_2----NH FUR(2.98 Å) *Lys199-NH_2---O=C FUR(3.10 Å)]				
	Arg222	19.00	Hydrogen bonding [*Arg222-NH_2---O=C FUR(2.85 Å *Arg222-NH_2---O=C FUR(2.66 Å)]				
	Lys195	16.10	Hydrophobic interaction				
	Tyr150	15.80	Hydrophobic interaction				
	Arg257	14.13	Hydrophobic interaction				
	Ile290	13.03	Hydrophobic interaction				
	Leu260	12.65	Hydrophobic interaction				
	Leu219	12.53	Hydrophobic interaction				
	Ile264	10.89	Hydrophobic interaction				
	Ser192	10.35	Hydrophobic interaction				
New site (Near site II)	Arg410	64.43	Hydrogen bonding [*Arg-410-NH_2---O=C FUR(3.24 Å)	-5.53	-6.89	5.05	-
	Glu492	30.83	*Glu-492 -C=O---NH_2 FUR(2.66 Å)]				
	Lys413	24.55	Hydrophobic interaction				
	Gln390	19.31	Hydrophobic interaction				
	Leu394	15.17	Hydrophobic interaction				
	Ala406	14.80	Hydrophobic interaction				
	Lys414	13.38	Hydrogen bonding [*Lys-414-NH_2---O=C FUR(2.62 Å)]				
	Val493	11.66	Hydrophobic interaction				
	Ser489	10.12	Hydrophobic interaction				

3.3.9. Correlation between binding sites of FUR and uremic toxins. To account for the mechanisms that govern inhibition of FUR binding to HSA in uremia, we carefully examined the relationship between the FUR and the uremic toxin binding sites. From the above studies, it is found that the FUR primarily binds to site I of HSA while with relatively low affinity to a site having some crucial residues (Arg410, Lys414 and Ser489) of site II. However, available literature [Bowmer and Lindup, 1982; Ikeda et al., 1984; Sakai et al., 1995] suggests that uremic toxins like IS, IAA, HA bind mainly to site II while CMPF binds to site I of HSA. Thus, these findings suggest that FUR competes directly with site I bound uremic toxins (CMPF) while indirectly competes with site II bound uremic toxins (IA, IS, HA) for some residue as shown in Figure 3.12.

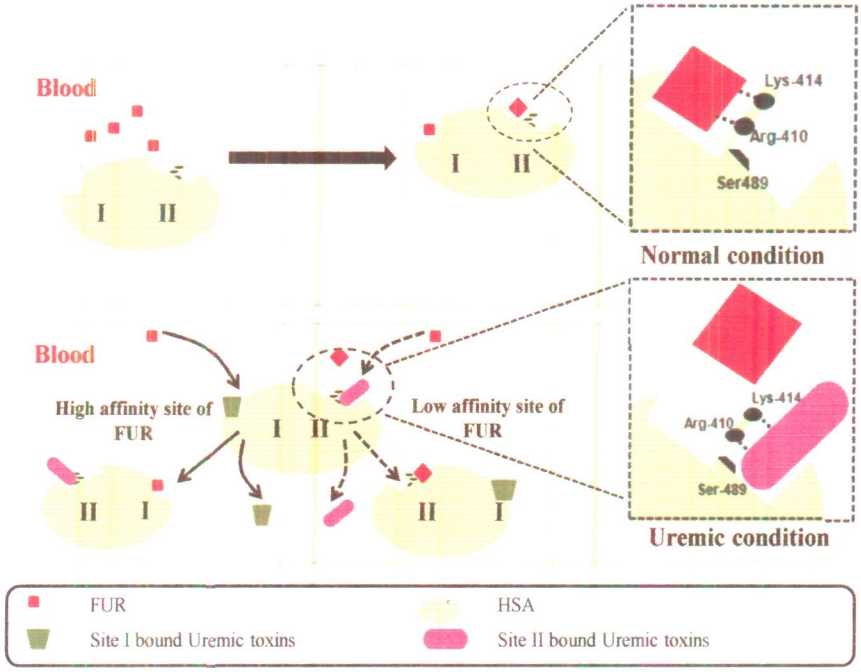

Figure 3.12. Schematic representation of mechanism of FUR binding to HSA under normal and uremic condition.

3.4. Conclusions

In this study, the mechanism of impaired binding of FUR to HSA in uremia is uncovered by determining binding energetic and binding sites of FUR on HSA. Results indicated that the quenching mechanism of fluorescence of HSA by FUR is static procedure and their binding is spontaneous, enthalpically driven, entropically opposed process which involves both hydrogen bonding and hydrophobic interaction.

Moreover, FUR strongly binds to site I of HSA and with relatively low affinity to a site having some crucial amino acid residue like Arg410 and Lys414 and Ser489 of site II. Thus it directly competes with the site I bound uremic toxins (CMPF) and indirectly competes with site II bound uremic toxins (IA, IS, HA). Furthermore, our study could also be helpful to explicate the reason behind impaired albumin binding of all those drugs which possess similar binding site.

CHAPTER 4

Different modes of interaction of sodium dodecyl sulphate (SDS) to bovine serum fetuin at acidic and neutral pH: a mechanistic study

4.1. Introduction

Surfactants are amphiphilic molecules that preferentially absorbed at interfaces [Tanford, 1973]. They have wide range of applications from food industry to cosmetics and the drug industry [Moore et al., 2003; Rangel-Yagui et al., 2005]. They are regularly used in biochemical laboratories for membrane protein solubilization and crystallization [Keller et al., 2006; Prive, 2007]. Therefore, their effects on biological macromolecules, particularly on proteins are always the topic of utmost investigation. Among surfactants, sodium dodecyl sulphate (SDS) occupies a special place in regular laboratory due to its extensive use in protein purification and characterization [Tulumello et al., 2012; Wieprecht et al., 2001]. It is an anionic surfactant with a 12-carbon hydrophobic tail and a negatively charged sulfate hydrophilic head group. It is known to interact with globular proteins, and in general, causes denaturation almost 1000 times lower concentration that is generally needed for other chemical denaturants such as urea [Chamani et al., 2006; Lee et al., 2011; Moosavi-Movahedi et al., 2005; Nielsen et al., 2007]. Moreover, it also help in renaturation of proteins [Lanckriet and Middelberg, 2004; Moriyama et al., 2003]. The mode of SDS binding to proteins distinguished according to the concentration. At the sub-critical micellar concentratios (sub-CMC), SDS monomers bind to proteins by predominantly hydrophobic interactions causing unfolding of the tertiary structure, and at concentrations higher than CMC, the micelles nucleate on the hydrophobic patches of the protein chain driving it to expand [Bhuyan, 2010]. SDS also alter the activities of many proteins [Bhattachary: and Bhattacharyya, 2009]. Even though the classical binding characteristics of SDS–protein complexes [Chakraborty and Basak, 2008; La Mesa, 2005; Moriyama et al., 2012; Naidu and Prabhu, 2011; Otzen, 2002; Tanford, 1968] and the binding phenomenon used in the commonly employed procedure of SDS-polyacrylamide gel electrophoresis (PAGE) have been established [Reynolds and Tanford, 1970], the mode of interaction of SDS with glycoproteins especially more negatively charged (sialic acid) is still not understood well. Furthermore, SDS mimics the native hydrophobic milieu of the phospholipids bilayer

in vivo and thus study of protein surfactant interaction serves as model for membrane proteins and lipids interaction [Gangabadage et al., 2008; Ulmer and Bax, 2005]. Increased knowledge in this area may play a role in understanding the membrane protein-lipid interaction and analysis of glycoprotein in SDS gel electrophoresis. Bovine serum fetuin (BSF) has frequently been used as model glycoprotein [Hermentin et al., 1996; Kennedy et al., 1993; Wang et al., 1998a; Wang et al., 1996] and so taken as model protein in present study. It contains six carbohydrate chains, three N-linked glycosylation sites and three O-linked glycosylation sites, which comprise 24% of its total molecular weight (48,585) along with 8% sialic acid [Green et al., 1988]. It contains 341 amino acids and their sequence shows over 70% similarities to human a_2-HS glycoprotein [Dziegielewska et al., 1990]. It is a member of the cystatin superfamily of cysteine protease inhibitors [Binkert et al., 1999; Galembeck and Cann, 1974].

Interaction of surfactants with proteins depends on the charge on the head group, length of the hydrophobic tail [Moriyama and Takeda, 2005]. Thus keeping in mind these criteria, the mode of interaction of SDS with a glycoprotein, bovine serum fetuin (BSF) is studied in sub- critical micellar concentration at pH above (pH 7.4) and below (pH 2) pI to know the effect of solution condition on mode of interaction of SDS to glycoprotein. The binding of SDS with BSF was studied by steady state, time resolved fluorescence spectroscopy and isothermal titration calorimetry (ITC) at sub-micellar concentration (sub-CMC), as proteins interact differently with the monomeric and the micellar forms of surfactants [Otzen, 2002]. The changes in secondary structures were elucidated by far-UV circular dichroism. The Thioflavin-T (ThT) binding, turbidity measurements and transmission electron microscopy was used to analyze the nature of aggregates formed. To the best of our knowledge, such study on glycoprotein has been seldom reported in the literature.

4.2. Materials and Methods

4.2.1. Materials and sample preparation. Fetuin from fetal bovine serum (BSF) (F3004), sodium dodecyl sulphate (SDS) (L-3125), were procured from Sigma Aldrich. All other reagents and buffer components used were of analytical grade. The protein was dialyzed and its concentration was estimated spectrophotometerically

using $E^{1\%}_{278\ nm} = 4.5$ [Murray et al., 1969]. SDS solutions were prepared by weight/volume (w/v) in 20 mM buffer of pH 2 (glycine-HCl buffer) and 7.4 (sodium phosphate buffer). The pH measurements were carried out on Mettler Toledo pH meter (Seven Easy S20-K) model using a Expert ''Pro3 in 1'' type electrode.

4.2.2. Critical micellar concentration measurements (CMC). The CMC of SDS was determined at pH 2 and 7.4 by isothermal titration calorimetry (ITC). For CMC determination by ITC, concentrated surfactant solution of SDS micelle systems (40 mM) were titrated into 20 mM buffer of pH 2 and 7.4 in a VP-ITC titration microcalorimeter (MicroCal Inc., Northampton, MA) at 25 °C.

4.2.3. Molecular modeling and solvent accessible surface analysis. The protein molecule was modeled by Protein Homology/analogY Recognition Engine (Phyre2) [Kelley and Sternberg, 2009]. Phyre2 takes a sequence, builds a profile using PSI-BLASTs, and automatically compares it to templates deposited in the structural classification of proteins database and PDB. The amino acid sequence of BSF was directly taken from the protein database having accession number CAA34596.1. The solvent accessible surface area was calculated by InterProSurf [Negi et al., 2007] and structure was visualized with Chimera 1.7 [Pettersen et al., 2004].

4.2.4. Turbidity measurements. Turbidity measurements of BSF (5 μM) in presence of SDS at sub-micellar concentrations in 20 mM buffer of pH 2 and 7.4 after the overnight incubation were taken. The measurements were carried out at 350 nm on Perkin Elmer Lambda 25 double beam spectrometer using sample cell of pathlength 10 mm at 25°C.

4.2.5. Steady state fluorescence spectroscopic measurements. The fluorescence measurements of BSF (5 μM) in presence of SDS at sub-micellar concentrations in 20 mM buffer of pH 2 and 7.4 were taken after overnight incubation. All fluorescence measurements were done using Shimadzu 5301PC fluorescence spectrophotometer equipped with water circulator (Julabo Eyela) at 25°C. The excitation and emission slits were set at 5 nm for ThT and intrinsic fluorescence measurements. Samples were excited at 295 and 440 nm for intrinsic fluorescence and ThT measurements respectively. The emission spectra were recorded in the range of 300-500 nm for

intrinsic fluorescence and 450-600 nm for ThT measurements. A stock solution of ThT was prepared in distilled water and its concentration was determined using molar extinction coefficient of $\varepsilon_M = 36{,}000\ M^{-1}cm^{-1}$ at 412 nm[Biancalana and Koide, 2010]. ThT was added to protein samples in the molar ratio of 1:2. The intrinsic fluorescence was of BSF in presence of SDS (1mM) at different ionic strength (0-3.5 mM NaCl) at pH 7.4.

4.2.6. Isothermal titration calorimetric measurements (ITC). The energetics of the binding of SDS to BSF at 25°C was measured using a VP-ITC titration microcalorimeter (MicroCal Inc., Northampton, MA). Prior to the titration experiment, all samples were degassed properly on a thermovac. The sample and reference cell of the calorimeter were loaded with protein solution (20 μM) and 20 mM sodium phosphate buffer (pH 7.4), respectively. Then multiple injections of 10 μL of SDS solution (17 mM) were made into the sample cell containing protein in absence and presence of 1, 2 mM NaCl. Each injection was made over 20 s with an interval of 180 s between successive injections. The reference power and stirring speed were set at 16 μcal^{-1} and 307 rpm, respectively. Heats of dilution for protein and heat of micellization of SDS were subtracted from the integrated data before curve fitting. The titration of SDS with BSF was also done with same methodology in presence of 1 and 2 mM NaCl.

4.2.7. Circular dichroism spectroscopic measurements. To monitor the secondary structural changes of BSF (5 μM) in presence of SDS at sub-micellar concentrations in 20 mM buffer of pH 2 and 7.4 after the overnight incubation, CD spectra were collected in far (200-250 nm) in JASCO-J815 spectropolarimeter equipped with a Peltier-type temperature controller at 25°C with a cuvette 0.1 cm pathlength. The scan speed and a response time were set as 20 nm/min and 2 s respectively. The secondary structural changes of BSF in presence of SDS (1mM) at different ionic strength (0-3.5 mM NaCl) at pH 7.4 were also observed.

4.2.8.Time-resolved fluorescence measurements. Fluorescence lifetime measurements were performed using the time-correlated single photon counting (TCSPC) model 5000 U (Horiba Jobin Yvon) equipped with water circulator at 25°C. The BSF in presence of varying concentration of SDS (0-3.5 mM) after overnight

incubation were excited at 295 nm using a NanoLED pulsed laser. The instrument response function (IRF) was obtained using LudoxTM suspension. The full width at half-maxima (fwhm) of the IRF was 750 ps. The emission decay data at 340 nm were analyzed using the software, DAS6, provided with the instrument.

4.2.9. Transmission electron microscopic measurements (TEM). Transmission electron micrographs of BSF in presence 0.75 mM SDS in 20 mM buffer of pH 2 and 7.4 were on transmission electron microscope operating at an accelerating voltage of 120kV.The samples were diluted appropriately and applied to Formavar/carboncoated grids (300-mesh), blotted and air dried. The samples were then negatively stained with 2% (w/v) uranyl acetate prior to imaging.

4.2.10. Statistical analysis

All determinations were triplicates, and mean values and standard deviations were calculated, wherever applicable, using SPSS 16.0 programme for windows.

4.3. Results and Discussion

4.3.1. Critical micelle concentration determination (CMC). To understand the mode of interaction of monomeric SDS to BSF, it is necessary to determine CMC value as proteins interact differently with the monomeric and the micellar forms of SDS [Otzen, 2002]. The CMC can be determined in a single titration experiment by ITC. To illustrate this, concentrated surfactant solution of SDS micelle systems were titrated into 20 mM buffer of pH 2 and 7.4. At concentrations below the CMC the reaction is

$$\text{micelles} \rightarrow \text{monomers}, \tag{4.1}$$

and at concentrations above the CMC, the reaction is

$$\text{concentrated micelles} \rightarrow \text{dilute micelles} \tag{4.2}$$

At 25°C, titration of concentrated SDS into water elicits a titration profile with endothermic peaks (Figure 4.1A & B). The endothermic peaks represent the dispersion of the concentrated micelle solution (demicellization) upon titration into buffer [Liu and Guo, 2007].

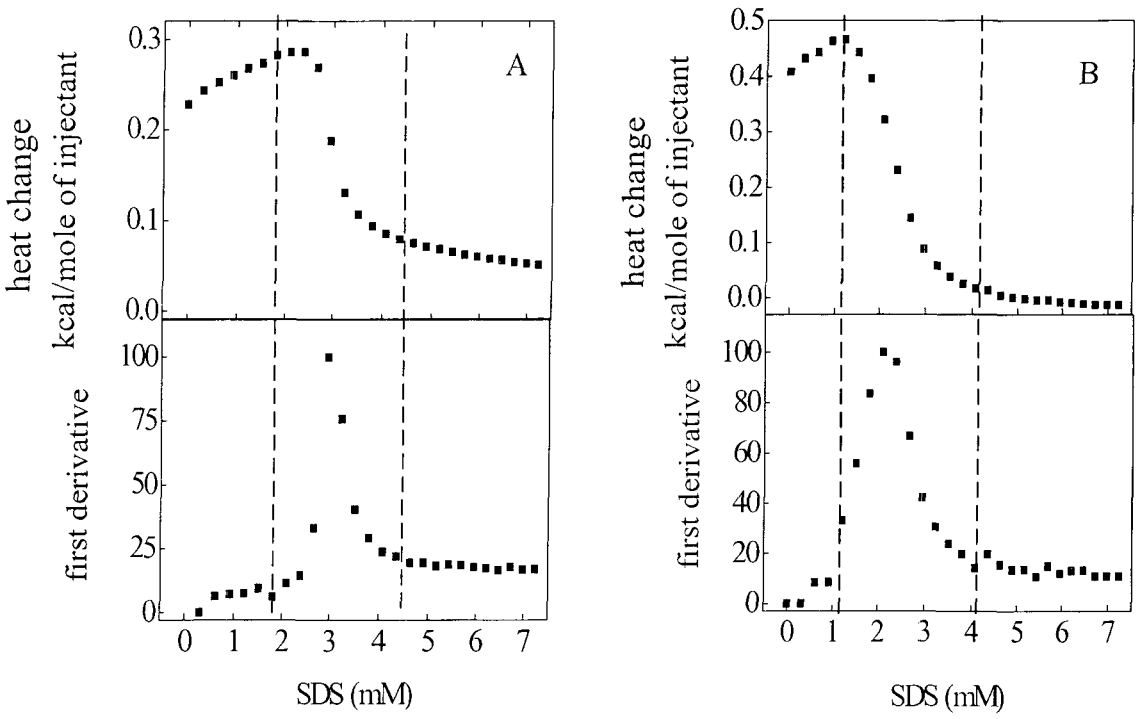

Figure 4.1. Determination of critical micellar concentration (CMC) of SDS by isothermal titration calorimetry (A) at pH 7.4 (B) 2. Upper panel in each figure represents integrated heat per injection, normalized with respect to the injected number of moles of SDS (0-7 mM). Bottom panel represents first derivative of the above transition curve.

As the surfactant concentration increases, the process of demicellization comes to a halt and the reaction enthalpy approaches zero. Since CMC is not seen as a sharp 'phase boundary' but is defined as the midpoint of a rather broad transition range [Garavito and Ferguson-Miller, 2001]. Therefore, a more precise quantitation of the midpoint and the width of the micellization process, it is advantageous to plot the first derivative of the ΔH vs [SDS] curve [Heerklotz and Seelig, 2000] as shown in bottom panel of Figure 4.1A & B. Thus, the CMC value of SDS in pH 2 and 7.4 corresponding to the midpoint of inflection was found to be 2.16 and 3.10 mM that agrees well as reported earlier [Liu and Guo, 2007; Naidu and Prabhu, 2011].

4.3.2. Molecular Modeling. Although BSF has frequently been used as model glycoprotein [Hermentin et al., 1996; Kennedy et al., 1993; Wang et al., 1998a; Wang et al., 1996] but its crystal structure is not yet explored. However, it is well established that it contains 341 amino acid residues and has a single tryptophan at position 51 [Wang et al., 1998a]. Furthermore, it shows high sequence homology to the members of cystatin family [Dziegielewska et al., 1990]. Thus, to get an idea about the molecular structure and location of tryptophan (Trp), BSF is modeled by the Protein Homology/analogY Recognition Engine (Phyre2) and visualized by

Chimera1.7 as shown in Figure 4.2A & B. Figure 4.2A, clearly shows that the tryptophan (Trp 51) is located on outer region as for the monellin, another member of cystatin family and thus it may show similar characterstic features in solution. Figure 4.2B shows the molecular surface of BSF colored by amino acid hydrophobicity according to Kyte and Doolittle scale [Kyte and Doolittle, 1982]. The most hydrophilic amino acid represented by blue then white and the most hydrophobic by orange red. Furthermore to get an idea of surface occupied by nonpolar amino acid residues, solvent accessible surface area was calculated from InterProSurf [Negi et al., 2007]. It was found that out of total solvent accessible surface area of 19649 $Å^2$, non-polar amino acid residues occupy maximal area (12895 $Å^2$). Thus it can be said that hydrophobic regions were distributed all over the protein molecule.

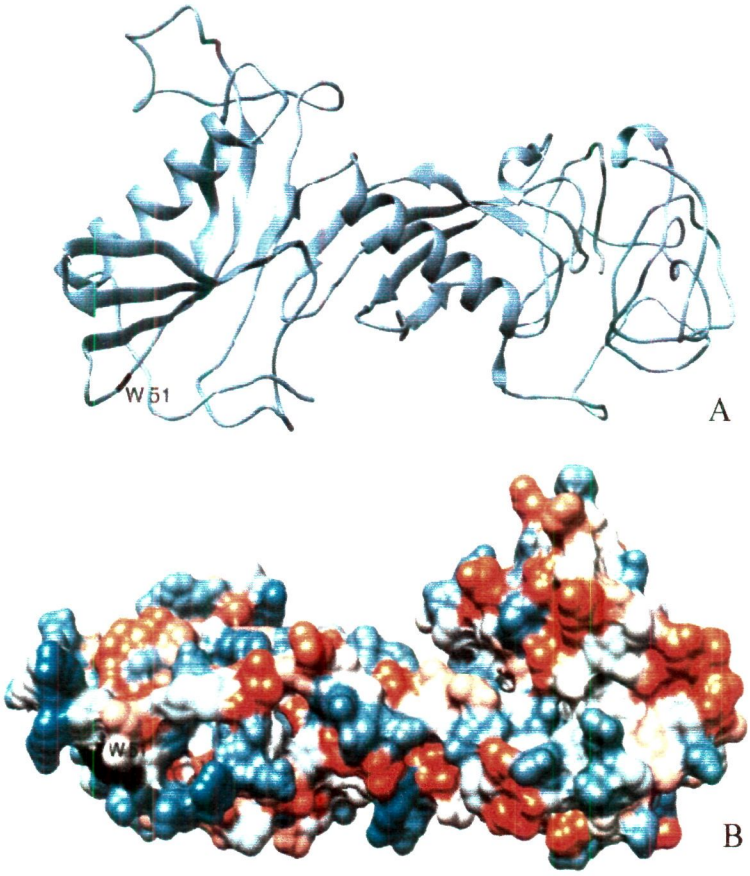

Figure 4.2. Molecular structure of BSF as obtained from molecular modeling by Phyre2. (A) The molecular structure of BSF showing its secondary structure. (B) molecular surface of BSF colored by amino acid hydrophobicity according to Kyte and Doolittle scale [Kyte and Doolittle, 1982]. The most hydrophobic by orange red, most hydrophilic by blue.

Sub-micellar concentrations of SDS induce aggregation in BSF at pH 2.

4.3.3. Turbidity measurements. Turbidity of samples at a non-absorbing wavelength can be used to rapidly detect insoluble protein aggregates [Pellaud et al., 1999]. Thus optical density at 350 nm (OD_{350}) of BSF in presence of sub-micellar concentrations of SDS in buffer of pH 2 (pH below pI) and 7.4 (pH above pI) was taken and summarized in Figure 4.3. It was observed that the solution of BSF in presence of sub-micellar SDS concentrations have significant values of OD_{350} for pH 2 whereas it was insignificant for pH 7.4.

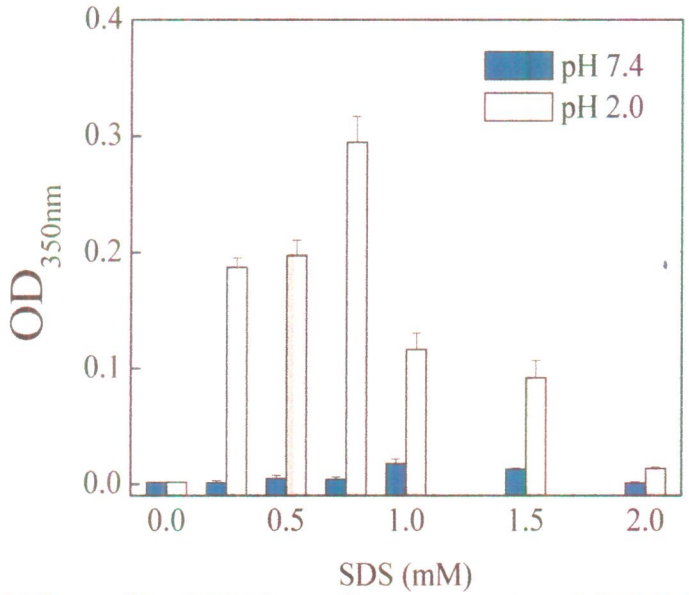

Figure 4.3. Turbidity profile of BSF in varying concentration of SDS (0-2 mM) at pH 2 and 7.4.

Furthermore it was observed that at pH 2, the turbidity increases in presence of SDS < 0.75 mM. It may be due to aggregation of BSF on interaction with SDS. However, there are two possible scenario of SDS interaction to BSF at pH 2. Firstly, at pH below isoelectric point, protein carries a net positive charge, so when anionic SDS interacts with protein, charge neutralization occurs and a point is reached where the net charge on protein in presence of SDS becomes zero and that leads to aggregation of protein. However, the net charge becomes zero only in presence of a specific concentration of SDS, below and above of that, protein-SDS complex has either net positive or negative charge. Therefore, SDS causes aggregation of BSF only at specific concentration of SDS which is not the case in present study. Secondly, when SDS interacts with BSF through its negatively charged head groups then the hydrophobic tails of SDS on protein-SDS complex become free, that increases surface hydrophobicity of protein-SDS complex. As a result, the protein-SDS complex

interacts with each other, not the water, and cause protein to undergo aggregation. The formation of aggregates, however, decreases in presence of SDS above 0.75 mM due to repulsion between the protein-SDS complexes having excess net negative charge acquired as a result of interaction with more SDS. However, since the turbidity of BSF at pH 2 in presence of SDS was observed for a range of of 0-2 mM SDS, thus the second scenario is most fitted for the studied condition. Aggregation of the protein-SDS complex at pH values below the isoelectric point at low surfactant concentration is common and has been reported for the lysozyme-SDS system [Hung et al., 2010] as well as for the bovine serum albumin-SDS system [Santos et al., 2003]. However, to detect the nature of aggregates formed in presence of sub-micellar concentration of SDS at pH 2, ThT and CD measurements were performed.

4.3.4. Circular dichroism measurements. Circular dichroism spectroscopy was used to analyze the protein secondary structures in solution. Figure 4.4A shows the far-UV CD spectra of BSF in sub-micellar concentrations of SDS at pH 2. The spectra of BSF at pH 2 in absence of SDS, has a minimum at 208 nm and a small shoulder at 220 nm. The essentially small minimum at 222 nm suggests that the protein has low α-helical content.

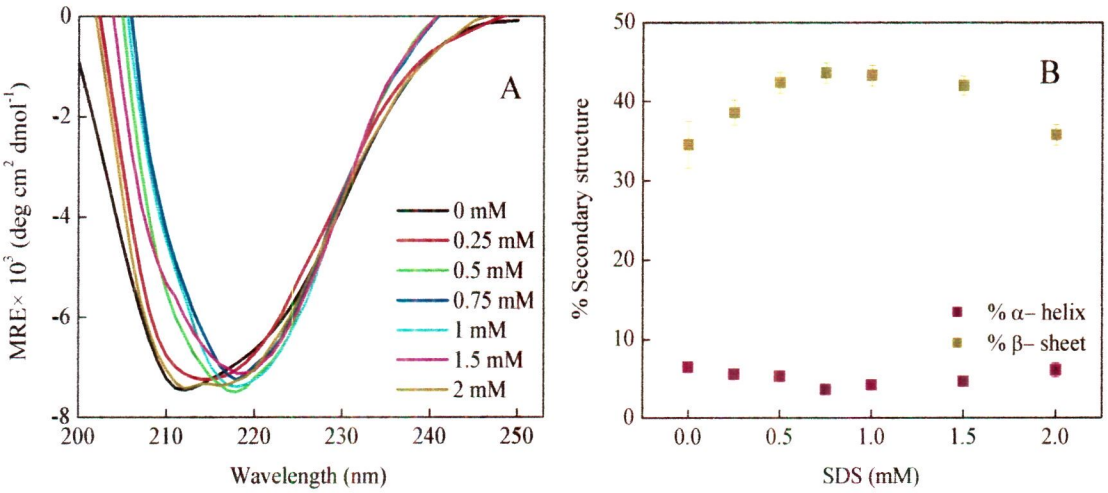

Figure 4.4.Secondary structural changes in presence of SDS by far-UV CD at pH 2. (A) far-UV CD spectra of BSF in presence of SDS (0-2mM) (B) percent secondary structure content of BSF in presence of SDS (0-2mM).

The secondary structural contents of BSF in presence of varying concentration of SDS at pH 2 were obtained by K2D3 software [Louis-Jeune et al., 2012] and summarized in Table 4.1 and shown in Figure 4.4B. It was observed that on increasing concentration of SDS, transition from α-helix to β-sheet occurs with peak at 218 nm

which may be attributed to the formation of amyloid fibrils. Furthermore, the pattern of increment of β-sheet content as mentioned in Table 4.1 was same as observed for turbidity measurements. However, to confirm the formation of amyloid fibrils in presence of SDS at pH 2, ThT measurements were performed.

Table 4.1. The percent secondary structure content of BSF in presence of SDS (0-2mM) at pH 2 as obtained by K2D3 software of secondary structure analysis.

SDS (mM)	% α-helix	% β-sheet
0	6.45	34.51
0.25	5.53	38.58
0.5	5.28	42.35
0.75	3.61	43.59
1	4.18	43.26
1.5	4.63	41.99
2	6.08	35.78

4.3.5. Thioflavin-T binding measurements. A standard fluorescent dye, ThT, which experiences a marked enhancement in its fluorescence intensity upon binding to amyloid structures, was introduced as a regular characteristic molecular probe to detect the formation of amyloid fibrils [Biancalana and Koide, 2010].

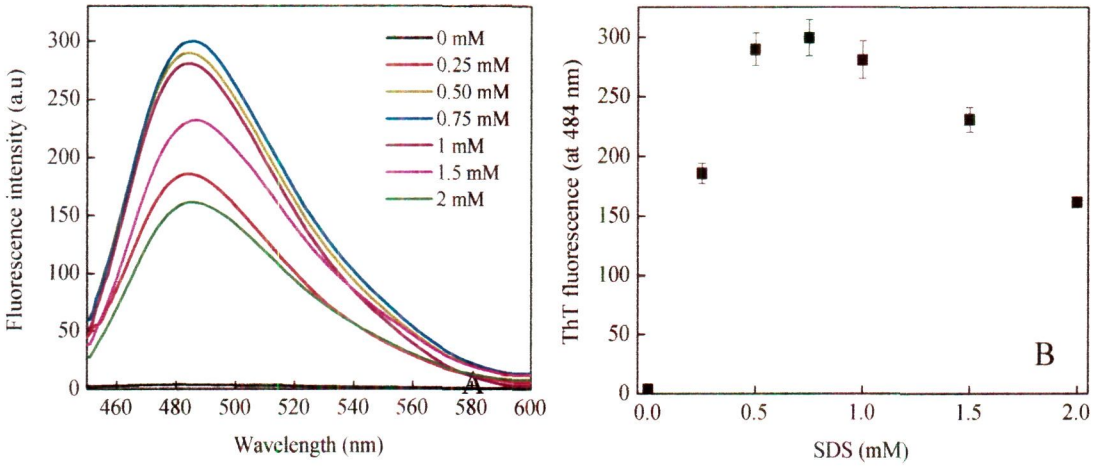

Figure 4.5. Effect of SDS (0-2 mM) on ThT fluorescence. (A) ThT fluorescence spectra of BSF and (B) ThT fluorescence intensity profile (at 484 nm) of BSF in presence of 0-2 mM SDS at pH 2.

ThT has a low fluorescence quantum yield in solution which increases considerably when bound to amyloid fibrils, displaying its high propensity to interact with amyloid fibrils [Morshedi et al., 2007]. Figure 4.5A & B show ThT fluorescence spectra of BSF and the change in ThT fluorescence intensity at 484 nm in presence of SDS (0-2 mM) at pH 2. As shown in figure, BSF has negligible ThT fluorescence intensity in

absence of SDS (Figure 4.5A). But, on addition of SDS, an increase in ThT fluorescence intensity occurs till 0.75 mM. It may be due to the fact that at pH 2, protein exists in partial unfolded form with exposed hydrophobic patches and positively charge residues [Naseem et al., 2003]. These charged residues exert the electrostatic repulsion between protein molecules and so prevents aggregation. But when SDS interacts with BSF through its negatively charged head groups then the hydrophobic tails of SDS on protein-SDS complex become free, that increases surface hydrophobicity of protein-SDS complex. As a result, the protein-SDS complex interacts with each other, not the water, and cause protein to undergo aggregation as indicated by increase in ThT fluorescence intensity. The formation of aggregates, however, decreases in presence of SDS above 0.75 mM due to repulsion between the protein-SDS complexes having excess net negative charge acquired as a result of interaction with more SDS and thus decreases in ThT fluorescence intensity at higher sub-micellar SDS concentration.

4.3.6. Transmission electron microscopic measurements (TEM). In parallel to spectroscopic measurements, aggregates of BSF in presence of SDS at pH 2 were clearly visible in transmission electron microscopic images however, no such structure were observed at pH 7.4 as shown in Figure 4.6A & B. The similar aggregates were also reported in lysozyme [Hung et al., 2010], bovine serum albumin [Santos et al., 2003] in presence of SDS at low pH.

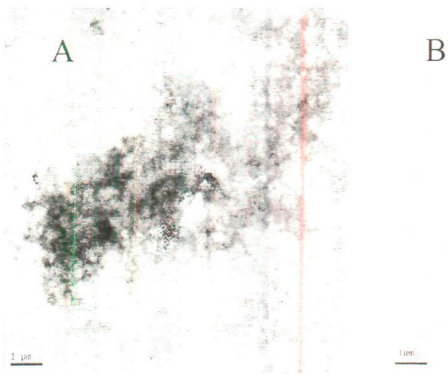

Figure 4.6.TEM images of BSF in presence of 0.75 mM SDS (A) at pH 2 and (B) at pH 7.4.

In sub-micellar concentration, SDS binds to BSF at pH 7.4.

4.3.7. Isothermal titration calorimetric measurements (ITC). The binding affinity and binding energetics of SDS to BSF were measured using ITC. Figure 4.7 shows the ITC binding isotherms of SDS to BSF in different ionic strength at 25°C in which each peak in top panel represents a single injection of the SDS into protein solution. Bottom panel of each figure shows an integrated plot of the amount of heat liberated per injection as a function of the molar ratio of the SDS to protein. As shown in Figure 4.7A, the complete titration profile can be divided into three characteristic regions: (A) at low SDS concentrations starting nearly at 0.22 mM, a small endothermic heat flow is observed with a inclination toward exothermic effects, followed by (B) a significant shift in heat flow from the endothermic to exothermic, (C) the exothermic heat flow then levels out at an intermediate concentration range of molar ratio 93 (approximately 1.86 mM SDS), and this ends with an upward bend. At still higher concentrations of SDS, the endothermic contribution increases, and the inflection point signifies that there is a reduction in the protein-surfactant interactions. These profiles are best fitted for the integrated heats having lowest χ^2 using a two independent binding site model with each site binding to more than one molecule of SDS. The binding parameters of SDS with BSF at different ionic strength obtained after fitting are summarized in Table 4.2. Results shows that the SDS binds to BSF at two sites, one with high affinity (K_1~ 10^5) whereas to other with low affinity (K_1~ 10^3). More SDS molecules interacts with lower affinity binding sites whereas lesser with higher affinity sites of BSF. Furthermore, from the thermodynamic parameters, enthalpy changes (ΔH°) and entropy changes (ΔS°), the forces involved in binding of SDS to proteins can be predicted [Ross and Subramanian, 1981]. It can be seen from Table 4.2, values of ΔH° and ΔS° were zero/slight negative and positive respectively at both sites. The positive ΔS° indicates disruption of the hydrogen bonding network between water molecules. The hydrogen bonds are reoriented tangentially to non polar surface to minimize disruption of the hydrogen bonded 3D network of water molecules and thus leads to a structured water "cage" around the nonpolar surface. Thus, a positive entropic effect originating from the hydrophobic interaction that results in disruption of highly dynamic hydrogen bonds between molecules of water by the non polar solute [Singh and Kishore, 2006].

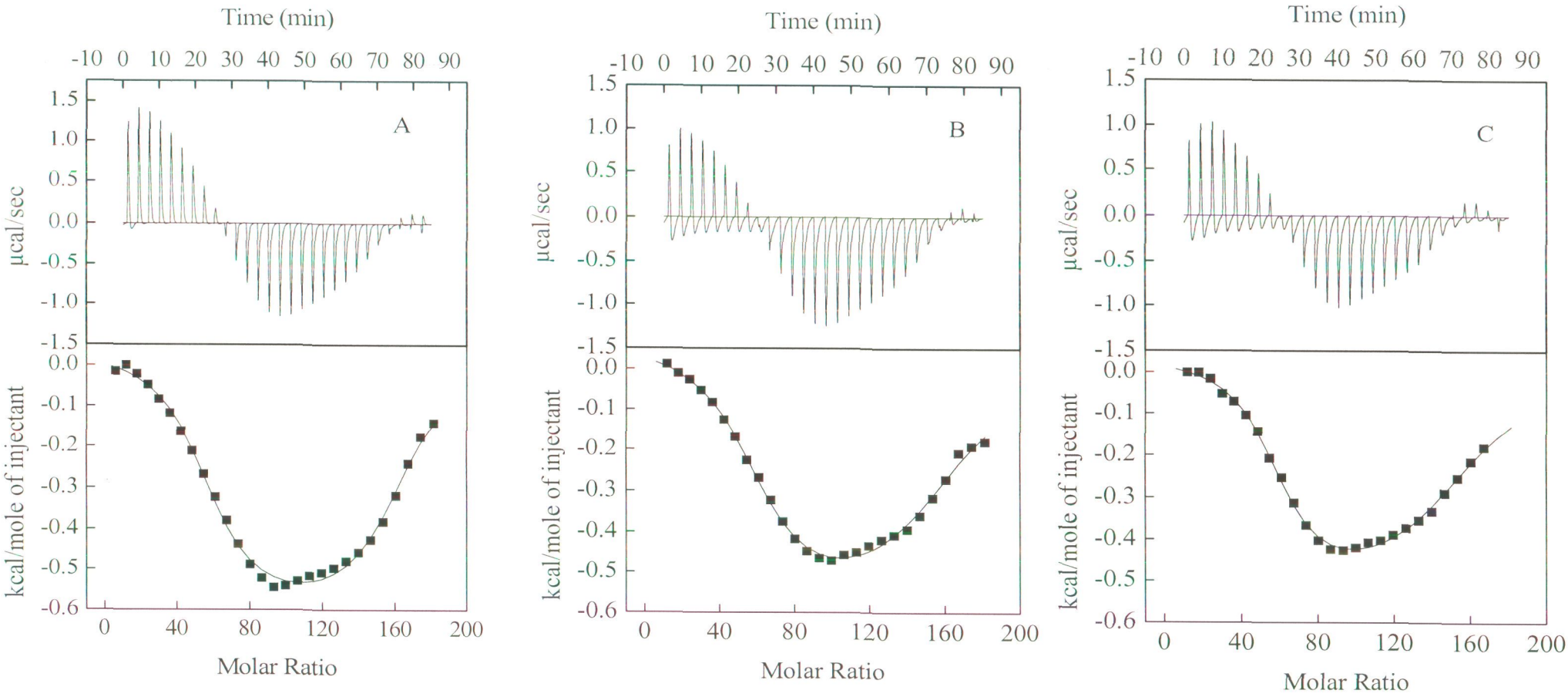

Figure 4.7. Isothermal titration calorimetric profiles of BSF with SDS in presence at different ionic strength (A) 0 mM (B) 1 mM and (C) 2 mM NaCl.

Table 4.2. Thermodynamic parameters obtained by isothermal titration calorimetric measurements of BSF with SDS.

	BSF	**BSF (1 mM NaCl)**	**BSF (2 mM NaCl)**
N_1	55.0 ± 1.01	56.8 ± 1.21	56.50± 0.89
K_1 (M^{-1})	(2.01 ± 1.65) × 10^5	(2.02 ± 0.63) × 10^5	(2.93 ± 0.82) × 10^5
ΔH_1^o (kcal mol^{-1})	0.04 ± 0.01	0.07 ± 0.01	0.03 ± 0.01
$T\Delta S_1^o$ (kcal mol^{-1})	7.20	7.30	7.47
ΔG_1^o (kcal mol^{-1})	-7.16	-7.23	-7.44
N_2	103 ± 1.72	103 ± 2.84	104 ± 2.07
K_2	(9.13 ± 0.36) × 10^3	(9.20 ± 1.07) × 10^3	(9.83 ± 1.65) × 10^4
ΔH_2^o (kcal mol^{-1})	-0.63 ± 0.01	-0.62 ± 0.03	-0.64 ± 0.01
$T\Delta S_2^o$ (kcal mol^{-1})	5.30	5.56	5.82
ΔG_2^o (kcal mol^{-1})	-5.93	-6.18	-6.46

Thus it can be said that, at the sub-CMC concentrations, SDS monomers bind to proteins predominantly by hydrophobic interactions via hydrophobic tails. Further, the values of ΔG^o were negative and mainly obtained by the entropic components, so the interactions of SDS to BSF were spontaneous. Further, to rule out the role of electrostatic interaction, the effect of ionic strength on binding of SDS to BSF was studied by performing titration of SDS to BSF in presence of 1, 2 mM NaCl at pH 7.4 and 25°C. The binding profiles are shown in Figure 4.7(A- C) and data summarized in Table 4.2. As shown, the value of the binding constants for low and high affinity sites increases with the rise in the ionic strength which indicates the affinity sites increases with increase in ionic strength. This behavior indicates SDS binding to BSF donot involves electrostatic interaction in which case the binding affinity is expected to decrease with an increase in the ionic strength since the ions of NaCl also competes for binding to protein. The results that SDS interaction with BSF are hydrophobic in nature draws further support from the fact that at neutral pH, BSF are negatively charged (pI~5) and thus have lesser chances of interaction with negatively charged head group of SDS via electrostatic interaction. These types of findings were also observed by [Bhuyan, 2010].

4.3.8. Intrinsic fluorescence spectroscopic measurements. Fluorescence spectroscopy is widely employed to study proteins and peptides conformation [Zaidi et al., 2013b]. Among three aromatic amino acids Trp, Tyr and Phe, Trp has highest

fluorescence yield which is influenced by the microenvironment due to presence of indole group [Liu and Guo, 2007]. Thus to get the information on the effect of SDS on BSF, Trp was excited and fluorescence intensities were taken at 340 nm. Furthermore, the changes in the wavelength of the emission maximum (λ_{max}), a parameter sensitive to protein conformation, were also taken in consideration for analysis since the λ_{max} depends on the environment of the tryptophanyl residues [Naeem and Khan, 2004]. BSF has a single Trp at position 51 [Wang et al., 1998a], located on outer region as evident from molecular modeling results.

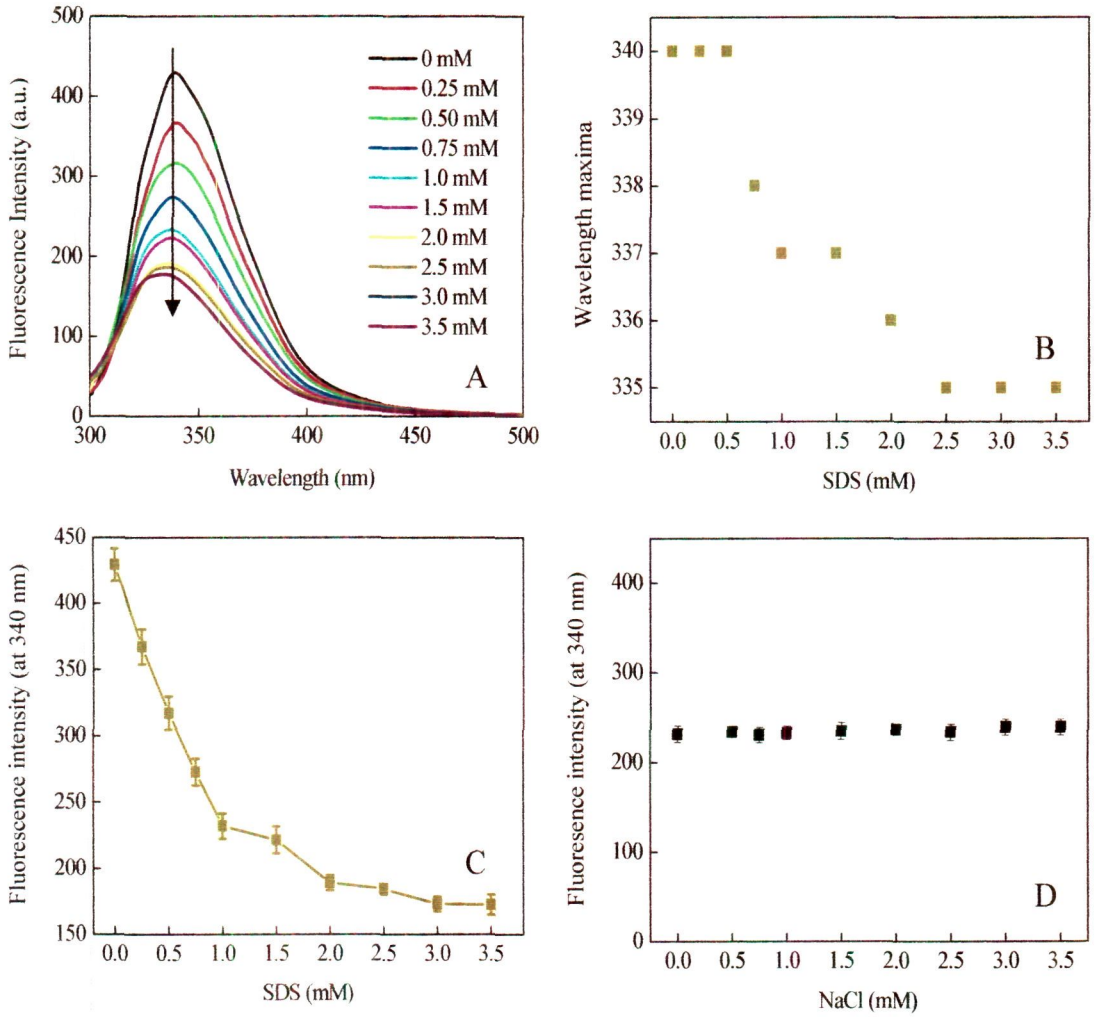

Figure 4.8. Steady state fluorescence results of BSF in presence of SDS (0-3.5 mM). (A) fluorescence spectra of BSF in presence of SDS (0-3.5 mM) (B) changes in emission maximum of BSF in presence of SDS (0-3.5 mM) (C) fluorescence intensity profile of BSF in presence of SDS (0-3.5 mM) (D) fluorescence intensity profile of BSF in presence of SDS 1mM at different ionic strength (0-3.5 mM).

The fluorescence emission spectra, changes in the wavelength of the emission maximum and fluorescence intensity at 340 nm of BSF in presence of SDS (0-3.5 mM) were shown in Figure 4.8 A, B & C respectively. As shown, on increasing SDS

concentration, there occurs sharp decrease in fluorescence intensity up to 1mM, followed by gradual decrease till 2 mM and beyond which almost no change was observed. Furthermore, decrease in fluorescence intensities was accompanied by concomitant blue shifts of 5 in $\lambda_{max.}$ It is noticeable that the changes in λ_{max} also show same pattern as that of fluorescence intensities upon increasing SDS concentration. The observed decrease in fluorescence intensities might be due to the interaction of SDS to Trp51 whereas blue shift in λ_{max} occurs as a result of the non-polar environment around Trp that may be generated due to alkyl chain of SDS molecules as suggested by ITC results also. However to confirm that the SDS molecules at pH 7.4 in sub-micellar concentration interact via alkyl chain and not by charged head group, the effect of ionic strength on binding of SDS (1 mM) to BSF was studied at 0-3.5 mM NaCl at pH 7.4 and results are shown in Figure 4.8D. On increasing ionic strength, fluorescence intensity donot show any demarcated changes and thus it confirms that the SDS donot interact via electrostatic interaction and thus hydrophobic interaction are the leading forces. The hydrophobic environment generated around Trp 51 may induce secondary structural changes in BSF as reported earlier for other protein system [Blondelle et al., 1995; Chakraborty and Basak, 2008; Hugonin et al., 2008; Roman et al., 2010; Wieprecht et al., 2001]. Thus far-UV circular dichroism measurements were performed to know the secondary structural changes of BSF in presence of SDS (0-3.5 mM).

4.3.9. Far-UV circular dichroism measurements. The SDS-induced secondary structural changes of BSF were illustrated by far-UV CD. Figure 4.9A shows the CD spectra of BSF in presence of different concentration of SDS (0-3.5 mM). To monitor the secondary structural change of protein upon interaction with SDS, results are expressed as MRE (mean residue ellipticity) in deg cm^2 $dmol^{-1}$, which is given by

$$\text{MRE} = \frac{\Theta_{obs}(\text{mdeg})}{10 \times \text{n} \times c \times l} \qquad (4.3)$$

where θ_{obs} is the observed ellipticity in millidegrees, c is the concentration of protein in mol/L, l is the length of the light path in centimeters, and n is the number of peptide bonds. Further, percent secondary structural content in presence of varying concentration of SDS were calculated by K2D3. As shown in Figure 4.9A, on increasing the SDS concentration, the minima at 208 and 222 nm of BSF deepens.

Further from Figure 4.9B, percent helical content increases with increasing SDS concentration. The α-helix and β-sheet contents of BSF were found to be 10 and 34% respectively.

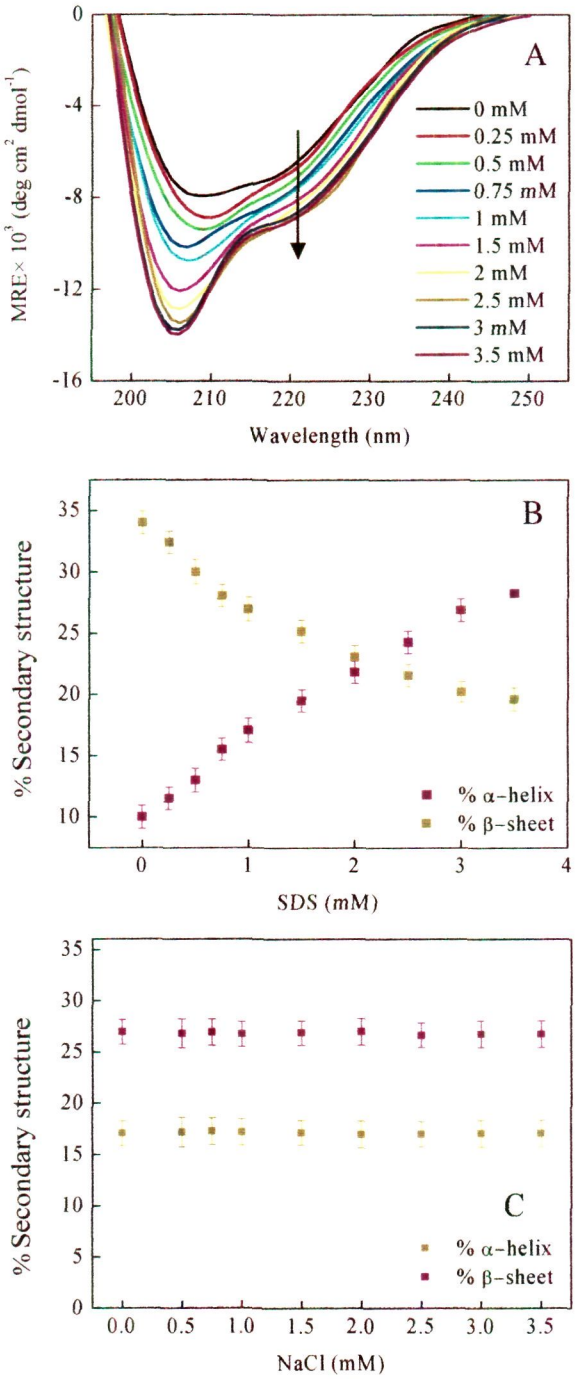

Figure 4.9. Secondary structural changes in presence of SDS by far-UV CD. (A) far-UV CD spectra of BSF (B) percent helical content of BSF in presence of SDS (0-3.5 mM) (C) percent helical content of BSF in presence of 1mM SDS at varying ionic strength (0-3.5 mM NaCl).

When SDS was added, there occurs sharp increase in percent α-helical content with concomitant loss in β-sheet contents up to 1mM, followed by gradual increase till 2 mM and beyond which almost no change was observed. The pattern observed in

increment of percent helical content has direct correlation with the steady state fluorescence results. Thus it can be said that the interaction of alkyl chain of SDS around Trp51 generates hydrophobic environment that may cause induction of secondary structural changes as reported earlier for other protein system [Blondelle et al., 1995; Chakraborty and Basak, 2008; Hugonin et al., 2008; Roman et al., 2010; Wieprecht et al., 2001]. Further from Figure 4.9C, it is clear that the α-helical content of BSF in presence of 1 mM SDS donot vary at different ionic strength. It indicates that NaCl (0-0.35 mM) donot perturb the secondary structure of protein under studied condition, which is necessary prerequisite for determining the type of interaction by studying the effect of ionic strength.

4.3.10. Time-resolved fluorescence spectroscopic measurements. To understand the interaction between SDS and protein, the local environment around fluorophore (Trp) can be explored by measurement of fluorescence lifetime [Anand et al., 2010]. It is observed that at neutral pH in aqueous solution, Trp exhibits multiple exponential decay which has been attributed to the existence of conformers (conformational isomers) in determining lifetimes [Lakowicz, 2006]. The time-resolved decay profiles of BSF at submicellar concentrations of SDS with bi-exponential fitting are shown in Figure 4.10A & B. All the experimental decay curves are well fitted as evidenced by the statistical parameters like chi-square (χ^2) which was close to 1 and distribution of weighted residuals. When using the bi-exponential decay law it is often useful to determine the average lifetime (τ_{avg}) which is given by [Kelkar et al., 2005; Zaidi et al., 2013a]

$$\tau = \alpha_1 \tau_1 + \alpha_2 \tau_2 \qquad (4.5)$$

The decay parameters obtained are summarized in Table 4.3. BSF has Trp51 in polar and non-constrained environment in absence of SDS as evident from the low α-helical content and molecular modeling results, so fluorescence lifetime value is 3.97 ns. This value is near to the fluorescence lifetime of a member from the same cystatin family, monellin, that also possess Trp exposed to the solvent environment [Peon et al., 2002]. As can be seen from Figure 4.10B and Table 4.3, the average fluorescence lifetime first decrease till 2.5 mM and beyond which almost no change is observed. The decrease in fluorescence lifetime may be due to the transition among Trp conformers as well as charge transfer process from indole ring of Trp51 to nearby

substituent which enhanced on binding with SDS. Thus to understand contribution of individual lifetime in multiexponential decay, an effort has been made by observing the relative amplitudes of lifetime. It is believed that Trp has three conformers, A, B and C [Lakowicz, 2006].

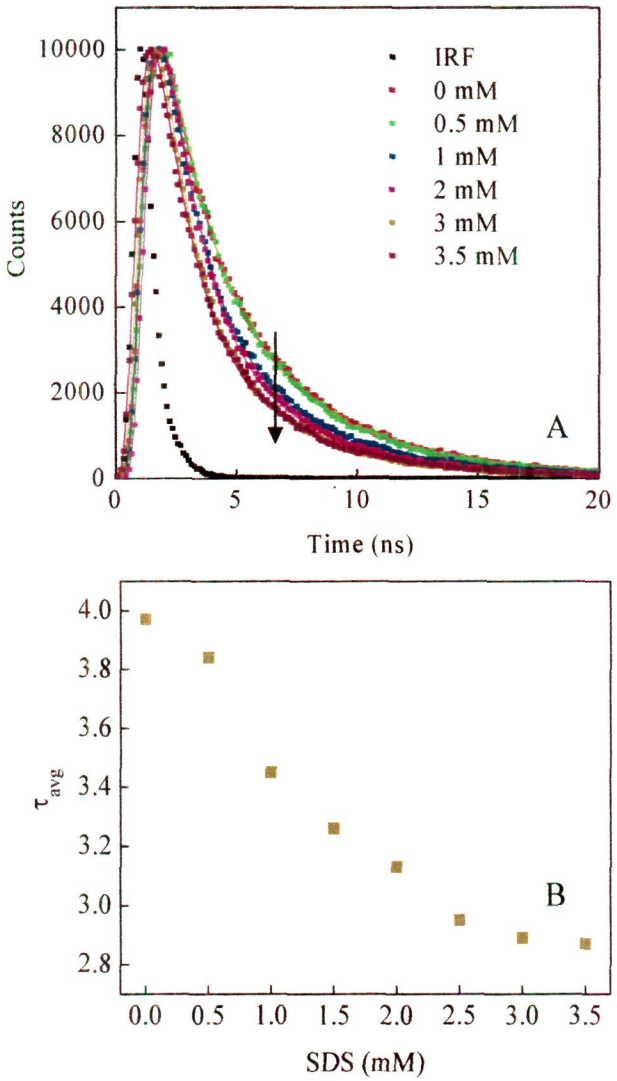

Figure 4.10. Time-resolved fluorescence decay profile of (A) BSF and (B) average fluorescence lifetime as a function of SDS. IRF indicates the instrument response function. Out of these, conformer C is rather stable and conversion from C to either A or B is difficult on a nanosecond time scale. Because Trp exhibits multiexponential decays in aqueous solutions, the faster component can be attributed to conversion of rapidly interconverting A and B conformers into conformer C whereas the longer lifetime mainly arises due to the conversion of conformer C into rapidly interconverting A and B conformers [Alcala et al., 1987]. As evident from the relative amplitude values from Table 4.3, the contribution from relatively stable conformer C, (shorter lifetime) and rapidly interconverting conformer A and B, (longer lifetime) of BSF are 27.16,

72.84% respectively. But due to increase in secondary structural content on increasing SDS concentrations to 2.5 mM, Trp51 experiences non polar constrained environment. As a consequence, the conversion from conformers C to A/B decreases that increase the relative amplitude of the shorter lifetime. Furthermore, beyond 2.5 mM, not much change in secondary structure was observed, thus no change is seen in relative amplitude. Thus the change in secondary structure may be associated with the transition among Trp conformers. Furthermore, a small contribution of dynamic quenching cannot be neglected in decrement of fluorescence lifetime in presence of SDS.

Table 4.3. Time resolved fluorescence decay parameters of BSF in presence of SDS.

SDS (mM)	α_1	τ_1 (ns)	α_2	τ_2 (ns)	τ_{avg} (ns)
0	27.16	1.48	72.84	4.91	3.97
0.5	30.21	1.46	69.79	4.88	3.84
1	40.10	1.36	59.90	4.86	3.45
1.5	40.72	1.26	59.28	4.64	3.26
2	43.18	1.20	56.82	4.61	3.13
2.5	43.91	1.14	56.09	4.38	2.95
3	43.97	1.14	56.03	4.27	2.89
3.5	45.22	1.14	54.78	4.31	2.87

4.4. Conclusions

The mode of interaction of anionic detergent, SDS with BSF in sub- critical micellar concentration is different at pH above (pH 7.4) and below (pH 2) pI and is shown in Figure 4.11. At pH 2, SDS interacts with BSF through its negatively charged head groups and thus the hydrophobic tails of SDS on protein-SDS complex become free, that increases surface hydrophobicity of protein-SDS complex. As a result, the protein-SDS complex interacts with each other, not the water, and cause protein to undergo aggregation. The nature of aggregates is amyloid due to enhance ThT binding and ß-sheet formation. The formation of amyloid fibrils, however, decreases in presence of SDS above certain concentration (0.75 mM) due to repulsion between the protein-SDS complexes having excess net negative charge acquired as a result of interaction with more SDS. However, at pH 7.4, SDS interacts with BSF at two sites, high affinity ($K_1 \sim 10^5$) and low affinity ($K_1 \sim 10^3$). Binding of SDS to BSF occurs

with the positive ΔS° that indicates disruption of the hydrogen bonding network between water molecules. The hydrogen bonds are reoriented tangentially to non polar surface to minimize disruption of the hydrogen bonded 3D network of water molecules and thus leads to a structured water "cage" around the nonpolar surface. Thus, a positive entropic effect is originating from the hydrophobic interaction that results in disruption of highly dynamic hydrogen bonds between molecules of water by the SDS molecules. Moreover, due to hydrophobic environment generated by alkyl chain of SDS molecules around tryptophan, induction of α-helical structure in BSF occurs. This increase in α-helical content on increasing SDS concentrations constrain environment around tryptophan. As a consequence, the interconversion of conformers decreases and resulted in decrement of fluorescence lifetime for BSF. These findings demonstrate that the mode of interaction of SDS to protein is different under different solution condition.

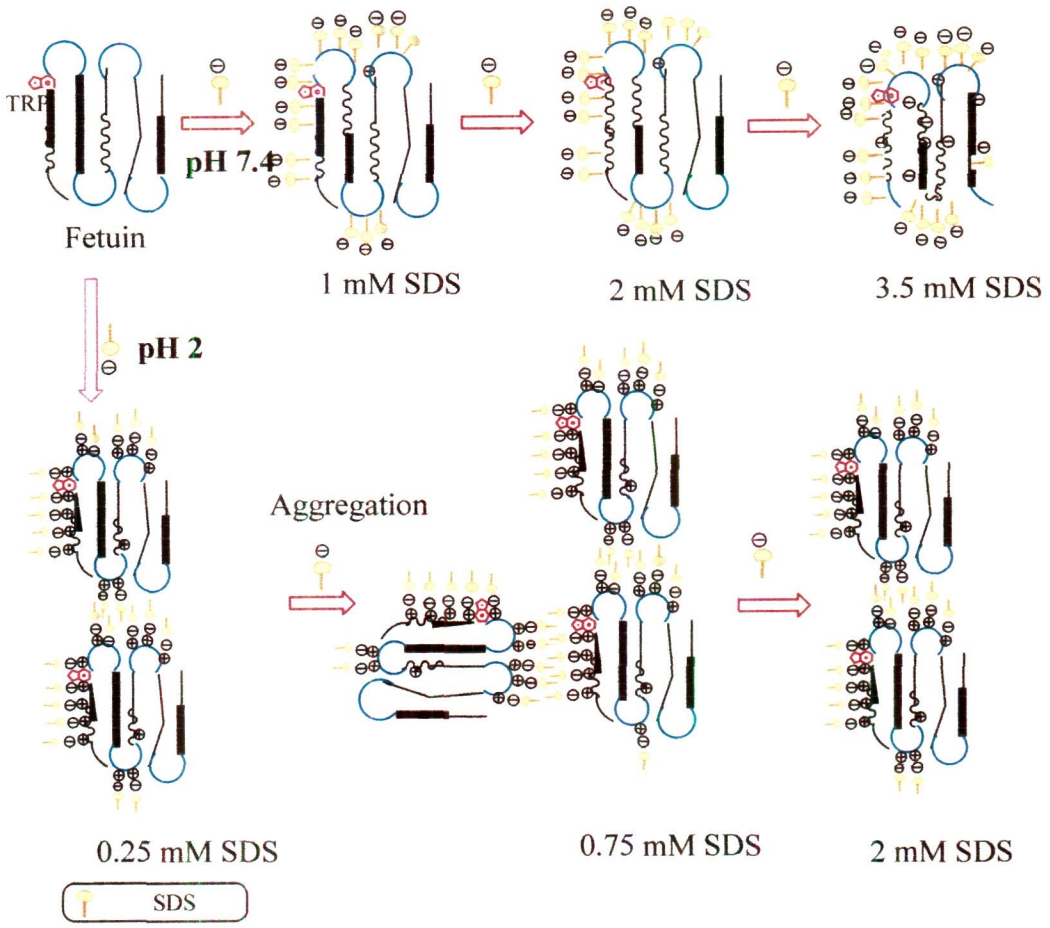

Figure 4.11.Mode of interaction of SDS with BSF at pH 2 and 7.4.

CHAPTER 5

N-Acetylneuraminic acid inhibits heat-induced amyloid fibrillization of hen egg white lysozyme: a plausible rescue from amyloid based neurodegenerative disorders

5.1. Introduction

A number of neurodegenerative disorders, including Parkinson's, Alzheimer's, and prion diseases are linked to protein misfolding and aggregation [Safar and Prusiner, 1998; Sipe, 1992]. There is a range of globular proteins [Chiti and Dobson, 2009] and in particular amyloid ß (Aß) peptide, microtubule-associated protein tau and a-synuclein (aS), that underwent structural transformations from native functional form into fibrillar assemblies [Uversky and Fink, 2004]. The emergent class of protein misfolding diseases paves a way for development of therapeutic molecules. Though a large number of small molecules including polyphenols [Porat et al., 2006], glycol-acridines [Vuong et al., 2013], osmolytes [Kar and Kishore, 2007] have been shown to inhibit fibril formation but presently, there is no approved therapeutic agent exists that blocks the formation of amyloid structures. There are many reasons that affect the development of protein aggregation inhibitors including the specificity of inhibitor that limits its use for specific type of protein misfolding disease [Lendel et al., 2009], inability to cross blood brain barrier, elevation of immunological response and unstability in biological fluids and tissues. Thus a potential inhibitor should overcome all these problems and affect one or more of the steps involved in the course of amyloid formation that includes destabilization of the native state, nucleation, elongation and lateral accumulation of fibrils [Morshedi et al., 2007]. Thus keeping in mind all these criteria, extensive research is going on the determination of sugars effect on the amyloid formation in biologically safe concentrations. Generally sugars are believed to stabilize the native state of proteins [James and McManus, 2012] and are part of our biological system. It has also been reported that glucose utilization declines in the brain of Alzheimer's patients. Thus impairment of brain glucose metabolism might be a cause of Alzheimer's disease [Chen and Zhong, 2013]. Another sugar molecule, trehalose also receives special interest because of its effectiveness in the treatment of neurodegenerative diseases associated with peptide

or protein aggregation [Liu et al., 2009; Perucho et al., 2012]. These studies direct our attention towards a sugar molecule which is associated to brain i.e. n-acetylneuraminic acid (Neu5Ac). It is a nine-carbon, non reducing, acidic, monosaccharide that occur naturally at the end of sugar chains attached to the surfaces of cells and soluble proteins and is found in human body. In the human body, the highest concentration of Neu5Ac occurs in the brain where it participates as an integral part of ganglioside structure in synaptogenesis and neural transmission. The majority is present in gangliosides (65%), glycoproteins (32%) whereas only 3% is free. It is also find in body fluids like cerebrospinal fluid, saliva, urine, tears and human milk. Moreover, Neu5Ac has potential to act as antimicrobial agent and is also associated with brain development and memory [Wang and Brand-Miller, 2003]. The fact that emphasizes the association of Neu5Ac to brain and memory development is the benefit of human milk in the brain development. In human milk, 70% Neu5Ac is found attached to the terminal end of free oligosaccharides which get hydrolysed in the intestine by sialidase and free Neu5Ac is released. The concentration of Neu5Ac in human milk was found to be around 3.56 mM; however it may vary with various lactational intervals [Carlson 1985]. In recent studies it is observed that in Alzheimer's patients, ganglioside Neu5Ac content in cerebral cortex was decreased and thus may be associated with the neurodegenerative disorders. Since it is a part of physiological system, so it is able to cross blood brain barrier, immunologically non-responsive and remain stabile in biological fluids and tissues. Thus Neu5Ac is consequently compound of pharmacological interest and hence its inhibition potency against amyloid fibril formation of model protein, hen egg-white lysozyme (HEWL) is examined in present study. HEWL is an excellent experimental system to study the protein amyloid fibrillization because of high homology to human lysozyme in structure which is one of the proteins that cause an amyloid disease upon mutation [Booth et al., 1997; Uversky, 2007]. Thus in this study, the kinetics of heat induced amyloid formation in HEWL and then its attenuation by Neu5Ac by using various spectroscopic, microscopic and calorimetric techniques was investigated. The mechanism of inhibition of heat induced amyloid formation in HEWL by Neu5Ac was also determined.

5.2. Materials and methods

5.2.1. Materials. Hen egg-white lysozyme, HEWL (L6876), N-acetyl neuraminic acid, Neu5Ac (A0812), thioflavin-T, and 1-anilino-8-naphthalene sulfonic acids, ANS, were obtained fom Sigma Aldrich. All other reagents were of analytical grade. HEWL was dialyzed and its concentration was estimated spectrophotometerically using $E^{1\%}_{280\ nm}$= 26.4 [Williams et al., 1965]. Neu5Ac solution was prepared in 20 mM sodium phosphate buffer (pH 7.4) by weight/volume (w/v). ThT and ANS solutions were prepared using $E^{1\%}_{412\ nm}$= 36,000 $M^{-1}cm^{-1}$ [Groenning, 2010] and using $E^{1\%}_{350\ nm}$= 5000 $M^{-1}cm^{-1}$ [Qadeer et al., 2012] respectively.

5.2.2. Samples preparation. HEWL was dissolved to a final concentration of 10 μM in 20 mM sodium phosphate buffer (pH 7.4) in absence and presence of different concentrations of Neu5Ac (0-8 mM) for 7 days at 65°C under constant stirring. Aliquots were taken from each set after regular intervals for analysis. It should be noted that the Neu5Ac is a non reducing sugar and thus it remain stable in solution over extended time periods and no "browning" of the solution was observed even after heating over 168 hours at studied concentration.

5.2.3. Turbidity measurements. Turbidity measurements of samples were carried out at 350 nm on Perkin Elmer Lambda 25 double beam spectrometer. The pathlength of sample cell used was 1 cm.

5.2.4. ThT fluorescence measurements. ThT fluorescence measurements were recorded on Shimadzu 5301PC fluorescence spectrophotometer equipped with water circulator (Julabo Eyela) from 460 to 600 nm. The excitation was set at 440 nm and emission was recorded at 485 nm. The excitation and emission slits were set at 3 and 5 nm respectively. The samples were incubated for 30 min after adding ThT in the ratio of 1:2 (protein: ThT).

5.2.5. ANS fluorescence measurements. ANS was added to the samples in the ratio of 1:20 and fluorescence was recorded from 400 to 600 nm on Shimadzu 5301PC fluorescence spectrophotometer. The excitation and emission slits were set at 3 and 5

nm respectively. The samples were incubated for 30 min after adding ANS in the ratio of 1:20 (protein: ANS).

5.2.6. Circular dichroism spectroscopic measurements. The far-UV CD spectra of samples were collected in a JASCO-J815 spectropolarimeter equipped with a Peltier-type temperature controller at 25°C. Spectra were collected from 190 to 250 nm with 20 nm/min scan speed and a response time of 2 s. Respective blanks were subtracted.

5.2.7. FTIR spectroscopic measurements. Spectra of HEWL in the presence and absence of Neu5Ac were collected on a FTIR (Interspec 2020) spectrophotometer from 1700 to 1600 cm^{-1} using a KBr window at room temperature. For each spectrum, 256 scans were averaged with a resolution of 4 cm^{-1}. Respective blanks were subtracted. The curve was analyzed by taking into account the band assignment for the secondary structure previously reported in the literature [Barth, 2007] a-helix (1647–1657 cm^{-1}), ß-sheet (1623–1641 cm^{-1}), turn (1662–1686 cm^{-1}), random coil (1642–1657 cm^{-1}), and ß-antiparallel (1674–1696 cm^{-1}).

5.2.8. Transmission electron microscopic measurements (TEM). Transmission electron micrographs were collected on transmission electron microscope operating at an accelerating voltage of 120 kV. The samples were diluted appropriately and applied to Formavar/carboncoated grids (300-mesh), blotted and air dried. The samples were then negatively stained with 2% (w/v) uranyl acetate prior to imaging.

5.2.9. Cell viability assay (MTT). The U-87MG (human neuronal glioblastoma) cells were cultured in DMEM medium supplemented with fetal bovine seum in a 5% CO_2 humified atmosphere. Cells were plated at a 5×10^3 of cells/ well in 96-well plates for cell viability assay, incubated for 24 h, and then the medium was changed before incubation with samples. Samples were initially diluted in culture medium and then added to the cells to achieve the required final concentration. In order to evaluate cell viability, 10 µL of 3-(4,5-dimethylthiazol-2-yl)-2,5 diphenyltetrazolium Bromide (MTT) dye (5 mg/ml) in PBS) was added to each well (150 µL) and incubated for 2 h. Extraction buffer was added and then absorbance was measured at 570 nm after overnight incubation on Elisa plate reader (96-well multiscanner autoreader) (Bio Rad model 680). The untreated cells were used as controls. It should be noted that the

cytotoxicities of HEWL and Neu5Ac in working concentration were also assessed but no significant changes with respect to control was observed.

5.2.10. Differential scanning calorimetric measurements. The differential scanning calorimetric measurements were carried out using VP-DSC microcalorimeter (MicroCal, Northampton, MA). The buffer and protein solutions were degassed under mild vacuum prior to the experiment. Samples were prepared in a 20 mM sodium phosphate buffer, pH 7.4. The DSC measurements of HEWL (40 μM) in the absence and presence of 4 and 8 mM Neu5Ac were performed from 25 to 90°C at a scan rate of 1°C/min. Data were analyzed using Origin software provided with the instrument to obtain the temperature at the midpoint of the unfolding transition (T_m) and calorimetric enthalpy (? H°).

5.2.11. Isothermal titration calorimetric measurements (ITC). The binding energetic of Neu5Ac to HEWL at 25°C was measured using a VP-ITC titration microcalorimeter (MicroCal Inc., Northampton, MA). Prior to the titration experiment, all samples were degassed properly on a thermovac. The sample and reference cell of the calorimeter were loaded with HEWL solution (20 μM) and 20 mM sodium phosphate buffer (pH 7.4), respectively. Then 10 μL of Neu5Ac solution (43 mM) were added into the sample cell containing HEWL. Each injection was made over 20 s with an interval of 180 s between successive injections. The reference power and stirring speed were set at 16 $\mu cals^{-1}$ and 307 rpm, respectively. Heats of dilution for the ligand were determined in control experiment, and were subtracted from the integrated data before curve fitting.

5.2.12. Statistical analysis

All experminents were done in triplicates, and mean values and standard deviations were calculated, wherever applicable, using SPSS 16.0 programme for windows.

5.3. Results and discussion

The formation of HEWL amyloid aggregates was achieved by incubating the protein at 65 °C for 168 hours (7 days). Under these conditions the partially folded state of HEWL is most likely to be highly populated [Arnaudov and de Vries, 2005]. When

the populations of the intermediate states become very high, the formation of amyloid fibrils is highly favored. Thus the presence and kinetics of aggregates formed was confirmed by several independent methods viz turbidity measurements, ThT binding, ANS binding, CD spectroscopy, FTIR and TEM. Furthermore, the effect of Neu5Ac was also observed on the heat-induced fibrillization of HEWL.

5.3.1. Turbidity measurements. Turbidity at a non-absorbing wavelength can be used to rapidly detect insoluble protein aggregates [Cascella et al., 2013; Pellaud et al., 1999]. Thus, absorbance at 350 nm was taken over a course of 168 hours (7days) and presented in Figure 5.1A. As shown in Figure 5.1A, there occurs an increase in absorbance values at 350 nm till 96 hours, beyond which no further increment was observed. It indicates the scattering of light by sample that may be due to the formation of aggregates in HEWL.

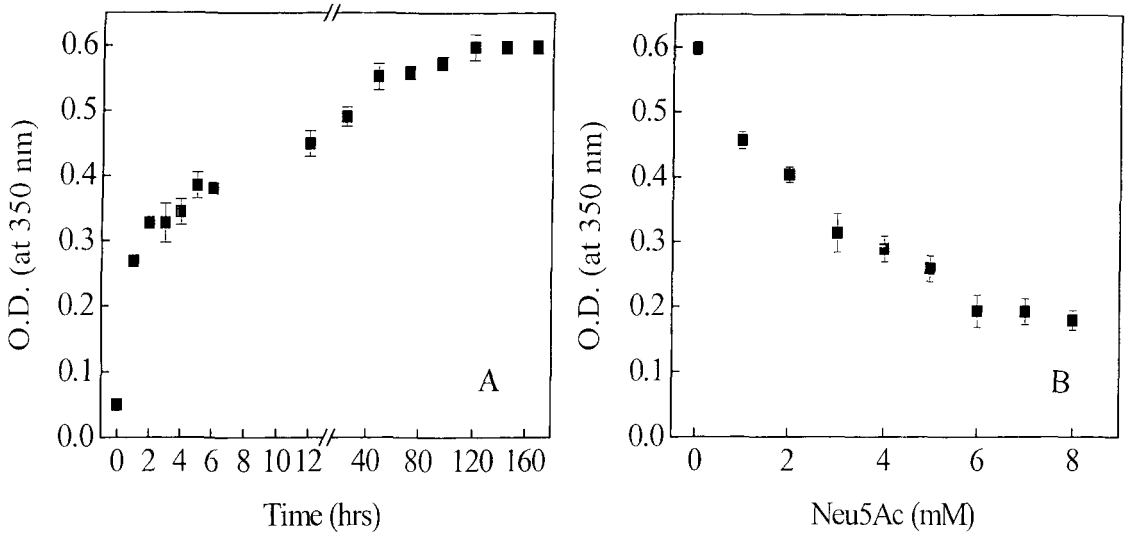

Figure 5.1. Turbidity measurements. (A) Turbidity of HEWL incubated at 65 °C over a period of 168 hours (7 days) at different time interval and (B) turbidity after 168 hours incubation of HEWL in presence of varying concentration (0-8 mM) of Neu5Ac.

However in presence of Neu5Ac, there occurs a decrease in turbidity after 168 hours incubation of HEWL in presence of varying concentration (0-8 mM) of Neu5Ac as shown in Figure 5.1B. This indicates that the Neu5Ac inhibits the formation of aggregates in HEWL.

5.3.2. ThT fluorescence measurements. For probing the kinetics of amyloid formation of HEWL and its inhibition by Neu5Ac under studied condition, ThT fluorescence was monitored as it binds to cross ß sheet-structure, which cause increase in fluorescence intensity [Groenning, 2010]. Figure 5.2A & B shows the ThT

fluorescence emission spectra and ThT fluorescence intensity at 484 nm of HEWL at different time intervals over a time course of 168 hours (7 days) respectively.

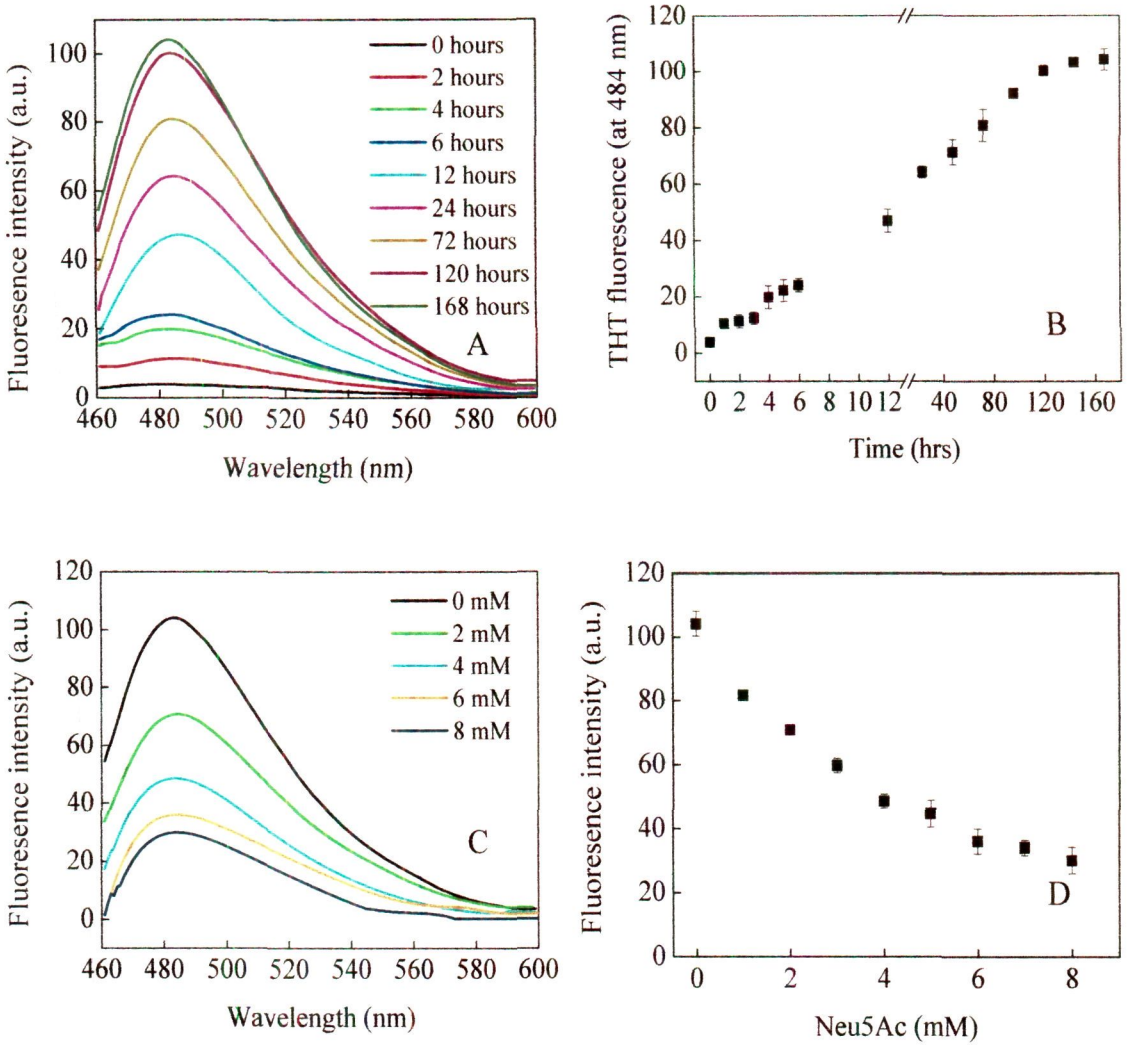

Figure 5.2. ThT fluorescence intensity measurements. A) ThT fluorescence spectra of HEWL incubated at 65°C over a period of 168 hours (7 days) at different time interval and (B) ThT fluorescence intensity profile (at 484 nm) of HEWL incubated at 65°C over a period of 168 hours (7 days) at different time interval (C) ThT fluorescence spectra of HEWL incubated at 65°C after 168 hours incubation in presence of varying concentration (0-8 mM) of Neu5Ac. (D) ThT fluorescence intensity of HEWL incubated at 65°C after 168 hours incubation in presence of varying concentration (0-8 mM) of Neu5Ac.

As shown in Figure 5.2B, increase in ThT fluorescence intensity was observed after a lag phase (nucleation) of 1hr, followed by the log phase (elongation) of 95 hours and the system reached its saturation (equilibration) after 96 hours. It indicates that the formation of amyloid fibrils. However, in presence of Neu5Ac, there occurs a decrease in ThT fluorescence intensity after 168 hours incubation of HEWL in presence of varying concentration (0-8 mM) of Neu5Ac as shown in Figure 5.2C &

D. This indicates that formation of amyloid fibrils of HEWL were inhibited by the Neu5Ac. Furthermore from the nature of curve presented in Figure 5.3, all of the known stages nucleation, elongation and equilibration seem to be affected by Neu5Ac.

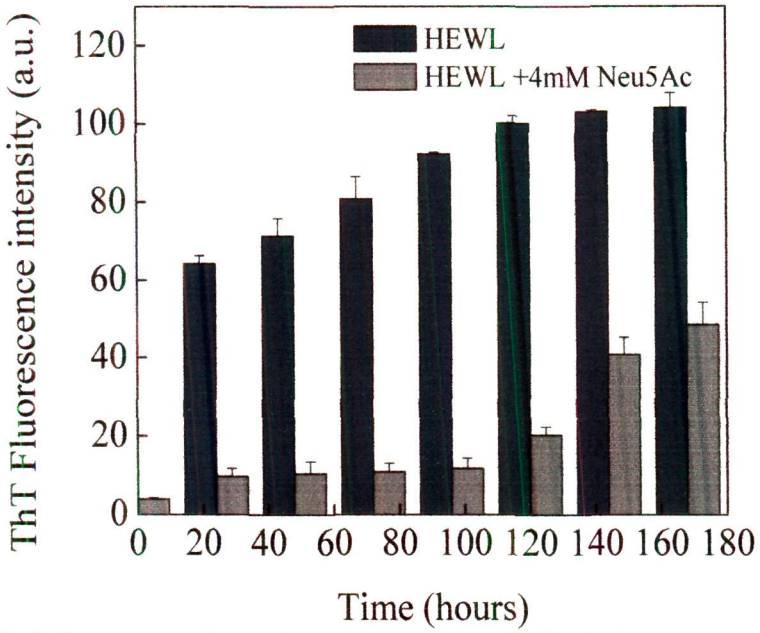

Figure 5.3. ThT fluorescence intensity measurements of HEWL in presence of 4mM Neu5Ac at different time intervals over a period of 168 hours (7 days).

5.3.3. ANS binding measurements. On amyloid formation, hydrophobicity of solvent-exposed surfaces increases [Cheon et al., 2007]. Thus, change in surface hydrophobicity of HEWL under studied condition was monitored by ANS fluorescence intensity. Figure 5.4A & B shows the fluorescence emission spectra of ANS over a time course of 168 hours (7 days) and the profile of ANS fluorescence intensity at 480 nm respectively. As shown in Figure 5.4B, HEWL at zero hour have negligible ANS fluorescence with wavelength maximum (λmax) equal to 500 nm. However, as time increases, there occurs an increase in ANS fluorescence with concomitant blue shift till 96 hours, beyond which no increment was observed. It indicates increased hydrophobicity of solvent-exposed surfaces that indirectly demonstrates the formation of amyloid fibrils. However, in presence of Neu5Ac, there occurs a decrease in ANS fluorescence intensity after 168 hours incubation of HEWL at varying concentrations (0-8 mM) of Neu5Ac as shown in Figure 5.4C & D. This indicates that in presence of Neu5Ac, the hydrophobicity of solvent-exposed surfaces

decreases. It may be due to the inhibition of amyloid fibrils formation of HEWL by the Neu5Ac.

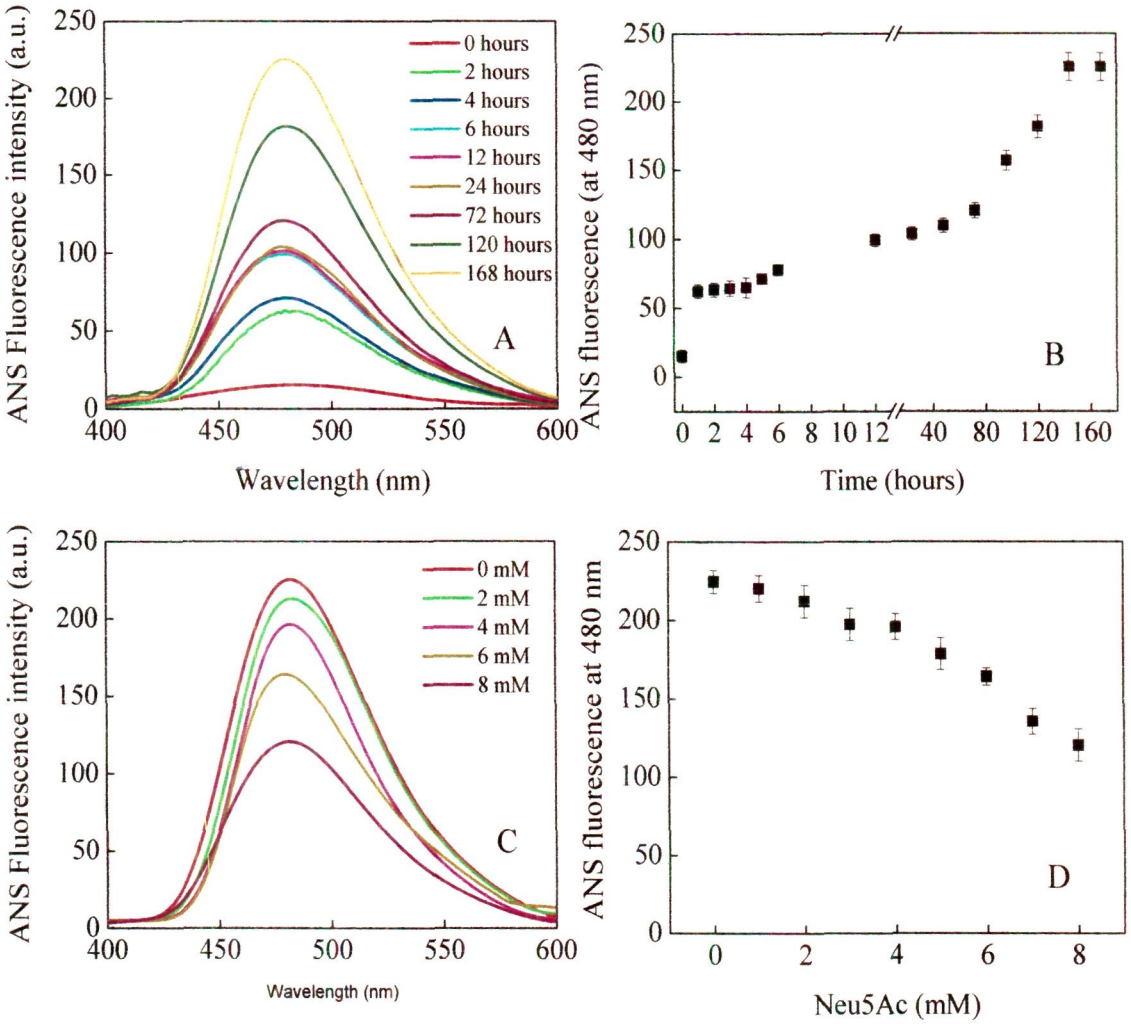

Figure 5.4. ANS fluorescence measurements. A) ANS fluorescence spectra of HEWL incubated at 65 °C over a period of 168 hours (7 days) at different time interval and (B) ANS fluorescence intensity profile (at 480 nm) of HEWL incubated at 65°C over a period of 168 hours (7 days) at different time interval (C) ANS fluorescence spectra of HEWL incubated at 65°C after 168 hours incubation at varying concentration (0-8 mM) of Neu5Ac. (D) ANS fluorescence intensity of HEWL incubated at 65°C after 168 hours incubation in presence of varying concentration (0-8 mM) of Neu5Ac.

5.3.4. Circular dichroism measurements. The change in secondary structures of HEWL samples incubated at 65 °C for different time over a period of 168 hours was observed by far-UV CD and shown in Figure 5.5A. The spectra of HEWL at pH 7.4 at zero hour have a minimum at 208 and 222 nm, a characterstic of α-helix. To monitor the secondary structural change of protein, results are expressed as MRE (mean residue ellipticity) in deg cm^2 $dmol^{-1}$, which is given by

$$MRE=\frac{\Theta_{obs}(mdeg)}{10\times n\times c\times l} \quad (5.1)$$

where $?_{obs}$ is the observed ellipticity in millidegrees, c is the concentration of protein in mol/L, l is the length of the light path in centimeters, and n is the number of peptide bonds. As shown in Figure 5.5A, with increase in time of incubation, the negative MRE values decreases at both minimum that indicates the decrement in a-helical content. However to calculate the percent secondary structure content, K2D3 [Louis-Jeune et al., 2012] was used and results are shown in Figure 5.5B and Table 5.1.

Table 5.1. The percent secondary structure content of HEWL incubated at pH 7.4, 65 °C as measured by CD spectroscopy and estimated by K2D3 software of secondary structure analysis.

Incubation time (at 65 °C)(hours)	% a-sheet	% ß-sheet
0	36.37	12.25
1	35.92	15.42
2	29.48	18.07
3	23.49	21.30
4	13.98	26.62
5	12.32	28.55
6	10.92	30.71
24	4.36	36.60
48	4.26	36.76
72	3.58	37.91
96	3.41	38.13
120	3.31	38.57
144	3.30	38.66
168	3.21	38.80

The HEWL at zero hour contain a-helix and ß-sheet content equals to 36.37 and 12.25% respectively that agrees well with the literature [Morshedi et al., 2007]. However, with increase in incubation time, a-helical content decreases with concomitant increase in ß-sheet content till 96 hours beyond which no significant changes was observed. This transition from a-helix to ß-sheet is attributed to the formation of amyloid fibrils. Furthermore, the changes in secondary structural changes of HEWL incubated at 65°C after 168 hours incubation in presence of Neu5Ac cannot be monitored by far-UV CD spectroscopic measurements because it

give noise in the far-UV region. Thus to determine the effect of Neu5Ac on secondary structure of HEWL incubated at 65°C after 168 hours, FTIR spectroscopic measurements were performed.

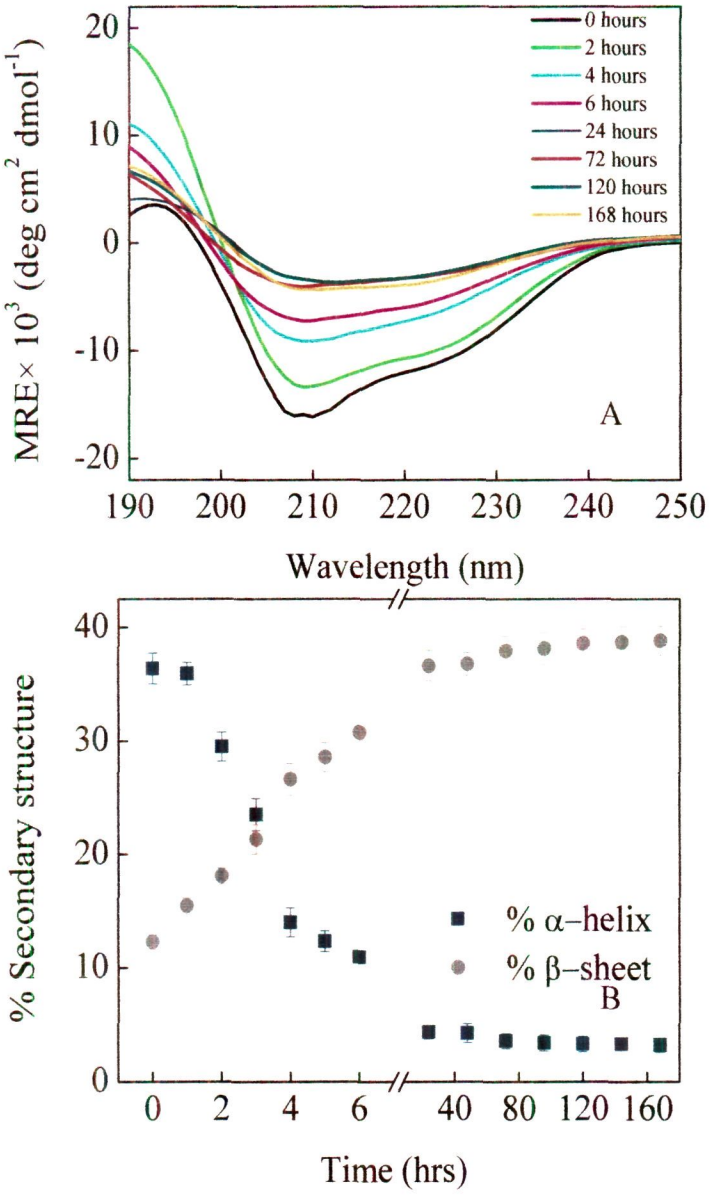

Figure 5.5. Far-UV circular dichroism measurements. (A) Far-UV CD spectra of HEWL incubated at 65°C over a period of 168 hours (7 days) at different time interval (B) Percent secondary structural changes as obtained by K2D3.

5.3.5. FTIR spectroscopic measurements. Band frequencies due to amide I, II, and III vibrations in the IR region are sensitive to the secondary structure of protein. But, generally, amide I (1700–1600 cm^{-1}) is analyzed to investigate the change in secondary structure of protein as it reflects C=O stretching vibration of the amide group weakly coupled with in plane NH bending and CN stretching [Tian et al., 2004]. Figure 5.6A & B shows the amide I band of HEWL incubated at 65°C for zero

and 168 hours and Figure 5.6B shows the amide I band of HEWL incubated at 65°C after 168 hours in presence of 4, 8 mM Neu5Ac. As summarized in Table 5.2, the HEWL at zero hour has peak at 1652 cm^{-1} that attribute to the presence of α-helix as the major secondary structure which is reasonable accord with the literature [Sassi et al., 2011].

Table 5.2. Amide I band peak of HEWL in absence and presence of Neu5Ac as obtained by FTIR measurements.

Samples	Amide I band peak	Predominant secondary structure
HEWL (at zero hour)	1652	α-helix
HEWL (at 168 hours)	1637	β-sheet
HEWL (at 168 hours) in presence of 4 mM Neu5Ac	1648	α-helix
HEWL (at 168 hours) in presence of 8 mM Neu5Ac	1650	α-helix

However, as time of incubation increases to 168 hours, the peak in amide I region shifts to 1637 cm^{-1} that attribute to the presence of β-sheet. These observations agree well with far-UV CD results. The transition from α-helix to β-sheet is due to the formation of amyloid fibrils as formation of β-sheet is prerequisite for amyloid fibrils formation.

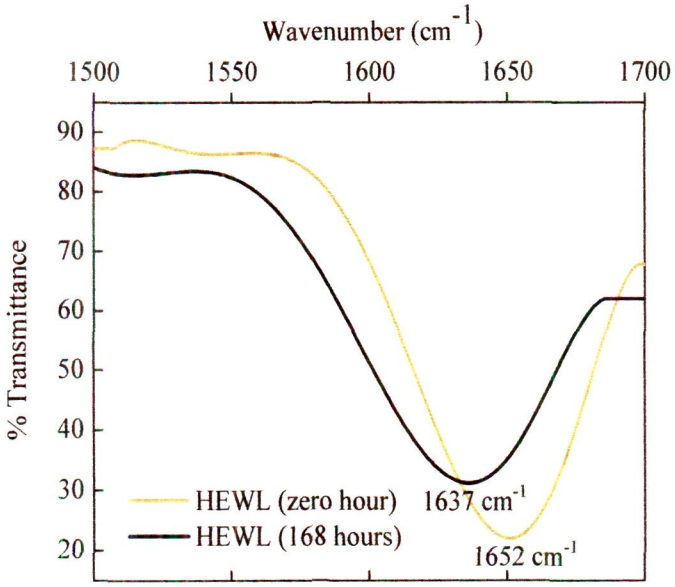

Figure 5.6. FTIR measurements of HEWL incubated for (A) zero hours and (B) 168 hours.

However, peak in amide I band shifts back to 1650 cm^{-1} after 168 hours incubation of HEWL in presence of 8 mM Neu5Ac. It indicates that Neu5Ac resists the transition from α-helix to β-sheet and consequently inhibits the amyloid formation in HEWL.

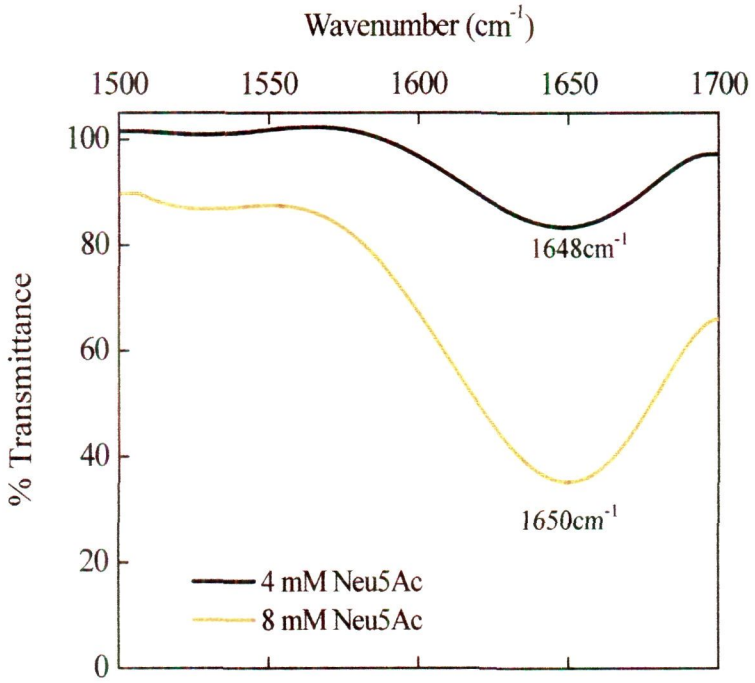

Figure 5.7. FTIR measurements of HEWL incubated at 65 °C after 168 hours incubation in presence of (A) 4 mM and (B) 8 mM of Neu5Ac.

5.3.6. Transmission electron microscopy (TEM). Figure 5.8A & B represents the TEM images of HEWL incubated at 65°C for zero hours and 168 hours. The HEWL at zero hour was taken as control. In parallel to spectroscopic measurements, aggregation was clearly visible in HEWL incubated at 65°C for 168 hours, as compare to control. In presence of Neu5Ac, aggregation of HEWL decreases as shown by lower density of aggregates on increasing concentration of Neu5Ac to 4 and 8 mM. (Figure 5.8C & D). Thus it indicates that Neu5Ac inhibits the formation of heat induced aggregates in HEWL

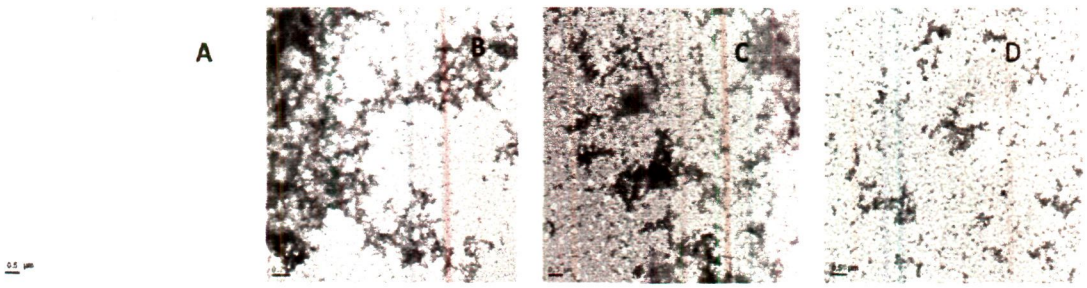

Figure 5.8. TEM images of (A) HEWL incubated at 65°C for zero hour (B) HEWL incubated at 65°C for 168 hours (C) HEWL incubated at 65°C after 168 hours in presence of Neu5Ac 4mM and (C) HEWL incubated at 65 °C after 168 hours in presence of 8mM Neu5Ac

5.3.7. Cell Viability Assay (MTT). The aggregated/amyloid fibrils are believed to be toxic to neurons [Brorsson et al., 2010; Gharibyan et al., 2007]. Thus the cytotoxicity of different aged HEWL fibrils was examined on U-87MG (human neuronal glioblastoma) cells by MTT reduction assay at 48 and 72 hours as shown in Figure 5.9.

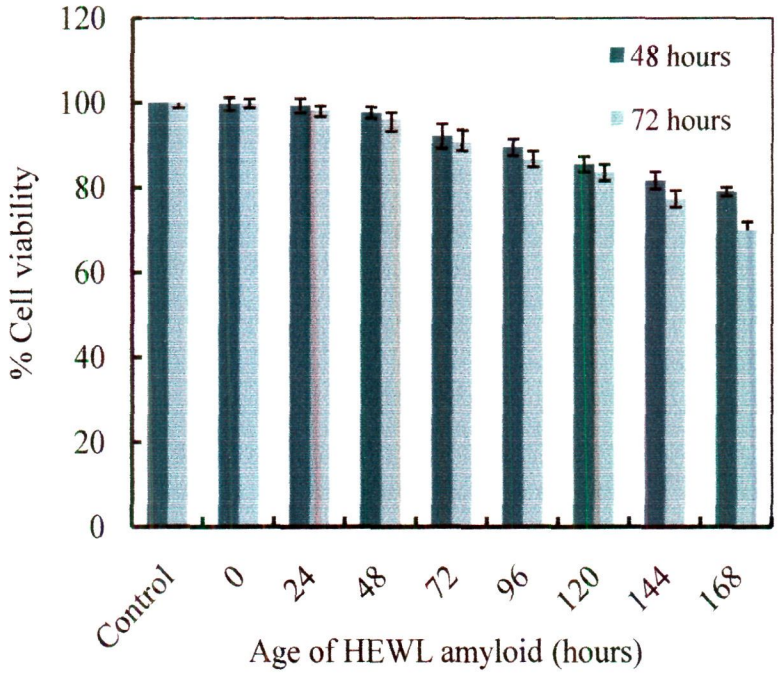

Figure 5.9. Time-dependent cytotoxic effect of different age HEWL fibrils by MTT reduction assay.

MTT undergoes reduction by mitochondrial dehydrogenses to soluble formazan that serves as the indicator of metabolically active cells and inhibition of this reaction is indicative of cytotoxicity. The percentage of cell viability (or the percentage of MTT reduction) was observed to decreases with the age of amyloid fibrils and with time as shown in Figure 5.9. It indicates that the 168 hours old fibrillar species of HEWL have most pronounced cytotoxic effect after 72 hours. Thus, the effect of different aged HEWL amyloid fibrils formed in presence of Neu5Ac on U-87MG cells, was observed after 72 hours and presented in Figure 5.10. As shown in Figure 5.10, HEWL amyloid fibrils formed in presence of Neu5Ac shows an increase in percentage of cell viability and thus it can be said that the cytotoxic effect of HEWL amyloid fibrils is significantly attenuated in presence of Neu5Ac.

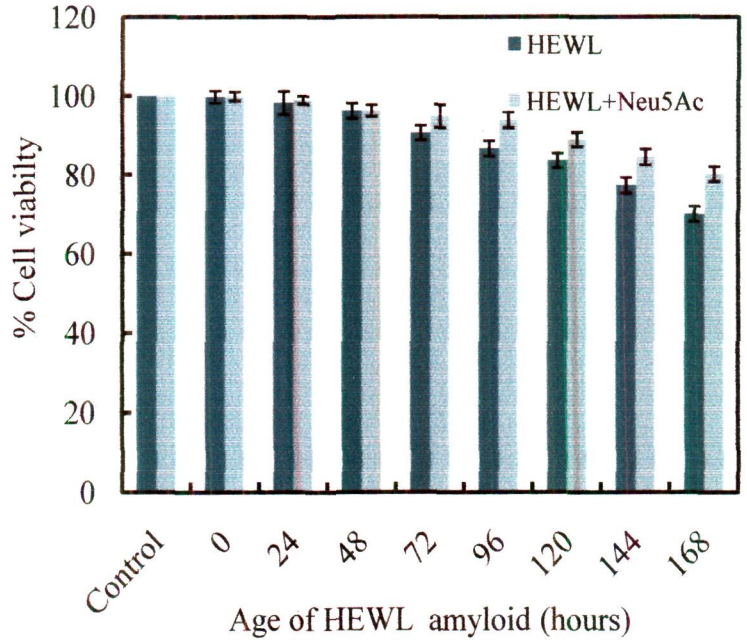

Figure 5.10. Time-dependent cytotoxic effect of different age HEWL fibrils in absence and presence of 4 mM Neu5Ac after 72 hours by MTT reduction assay.

Mechanism of inhibition of heat-induced fibrillization of HEWL by Neu5Ac.

In the present study, it is observed that Neu5Ac inhibits the heat-induced fibrillization of HEWL. The various events occurring in the course of amyloid formation of HEWL includes destabilization of the native state, nucleation, elongation and lateral accumulation of fibrils and thus it is expected that the potential inhibitor may affect one or more of the steps involved. Thus DSC measurements have been done to know the effect of Neu5Ac on stabilization of native state of HEWL.

5.3.8. Thermostability measurement by differential scanning calorimetric measurements.

The thermal denaturation of a protein occurs at the thermal transition temperature (T_m) which is calculated as the midpoint of the thermogram peak, and integration of the area under the peak gives the calorimetric enthalpy ($\Delta H_{cal}°$). Figure 5.11(A—C) shows the typical excess heat capacity curves for HEWL in presence of varying concentration (0-10mM) of Neu5Ac. The excess heat capacity curves were deconvoluted with the assumption of single-transition and obtained thermodynamic

parameters are reported in Table 5.3. The concentration of HEWL selected for this study was chosen such that it remains in solution. As summarized in Table 5.3, the ΔT_m and $\Delta H_c°$ of HEWL were 73.47 °C and 61.85 kcal mol^{-1} that agrees well with the values earlier reported [Bruzdziak et al., 2013]. The value of change in thermal transition temperature (ΔT_m) increases to 74.41 and 76.32 in presence of 4 and 8 mM Neu5Ac respectively. Furthermore the value of calorimetric enthalpy ($\Delta H_{cal}°$) also increases with increase in concentration of Neu5Ac. It indicates that the Neu5Ac cause stabilization of HEWL and hence thermal unfolding of HEWL become progressively less favorable as evident from the increase in value of $\Delta H_{cal}°$ with increase in concentration of Neu5Ac [Celej et al., 2005; Neelam et al., 2010; Sharma et al., 2012]. These results suggest that the Neu5Ac protects HEWL against thermal unfolding and thus prevent its conversion to aggregated prone species. However, this stabilization may results from the binding of Neu5Ac to HEWL as the changes in the T_m and ΔHcal° of the protein in presence of ligand are the most obvious manifestation of ligand binding [Zaidi et al., 2013b]. Thus to know whether these changes in T_m and ΔHcal° are manifestation of binding of Neu5Ac to HEWL, ITC measurements were performed.

Table 5.3.Thermodynamic parameters of HEWL in presence Neu5Ac as obtained by differential scanning calorimetry

Neu5Ac (mM)	T_m^1 (°C)	ΔH_{cal}° (kcal mol^{-1})	$\Delta H_{cal}^{\circ}/\Delta H_{vant}^{\circ}$
0	73.47 ± 0.012	61.85 ± 0.02	0.99
4	74.41 ± 0.020	62.55 ± 0.01	0.98
8	76.32 ± 0.010	68.72 ± 0.01	0.99

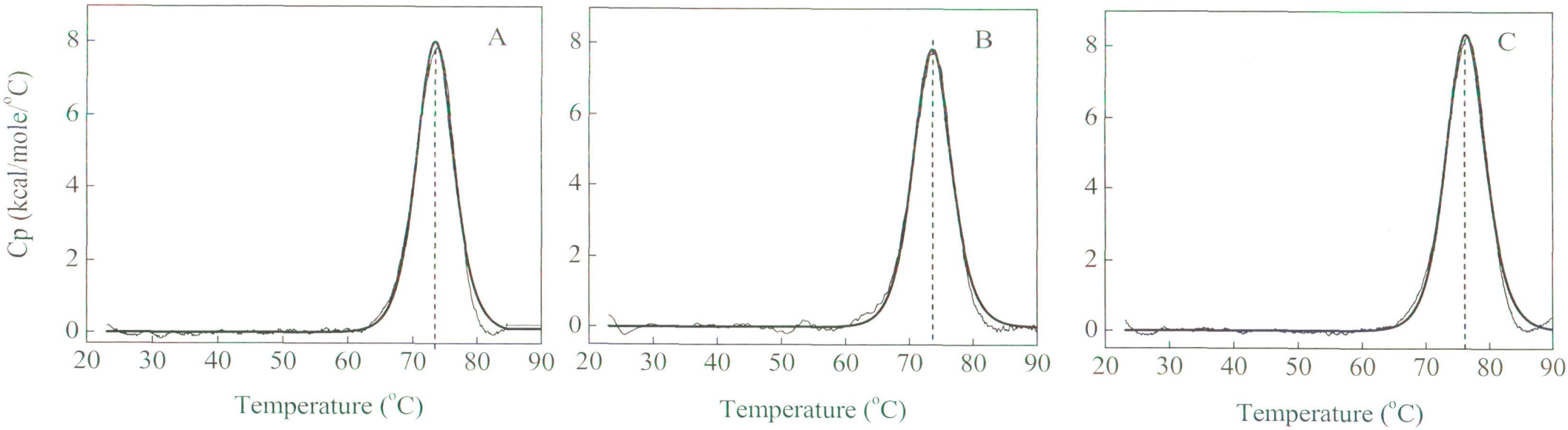

Figure 5.11. Excess heat capacity curves obtained by differential scanning calorimetry of HEWL in presence (A) 0 (B) 4 mM and (C) 8 mM Neu5Ac at pH 7.4

5.3.9. Isothermal titration calorimetric measurements. ITC was used to measure binding affinity and energetics of Neu5Ac to HEWL at 25 °C. Figure 5.12 shows the ITC binding isotherm of Neu5Ac to HEWL at 25°C in which each peak in top panel represents a single injection of the Neu5Ac into 20 mM sodium phosphate buffer, 7.4 (red) and in protein solution (black). Bottom panel of this figure shows an integrated plot of the amount of heat liberated per injection as a function of the molar ratio of the Neu5Ac to protein. As shown in Figure 5.12, there were no significant changes observed in heat on Neu5Ac mixing into buffer and protein.

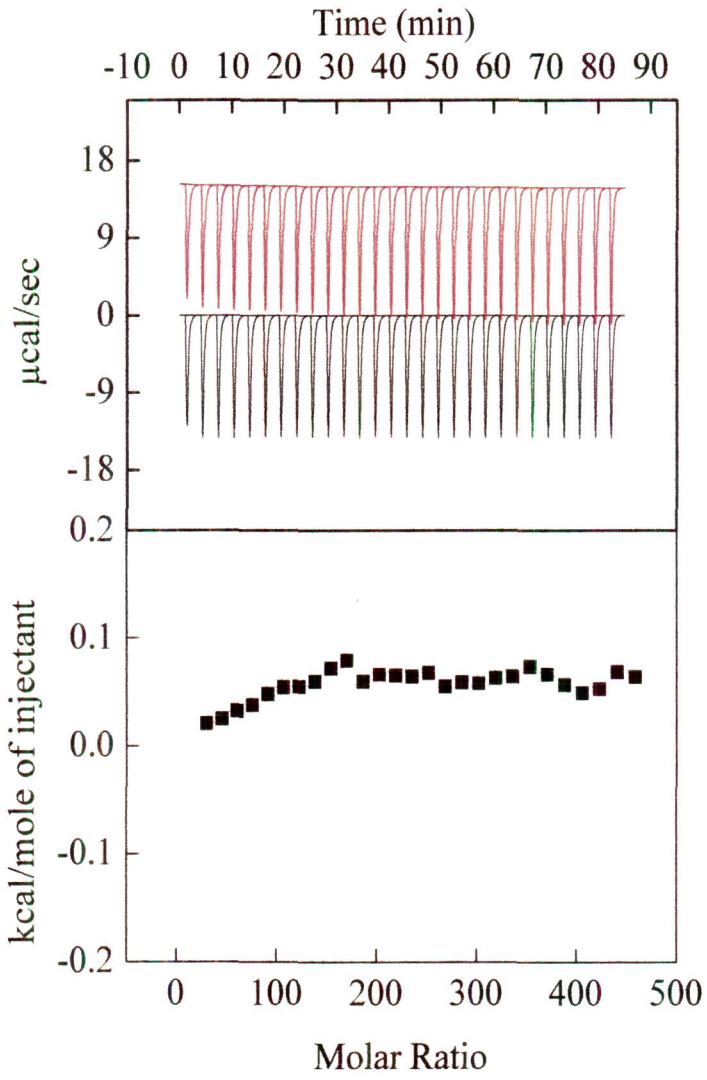

Figure 5.12. Isothermal titration calorimetric profile of Neu5Ac to HEWL.

It leads to absence of the binding profile in the titration of Neu5Ac to HEWL. Thus results clearly indictes that Neu5Ac donot bind to HEWL and remain excluded and thus increase in stability of HEWL as observed by DSC measurements is not the consequence of Neu5Ac binding. However increase in stability of HEWL without

binding Neu5Ac may be due to the mechanism of preferential hydration like other sugar molecules [Abe et al., 2013; Liu et al., 2009]. According to which, the sugar molecules get excluded from the environment around the protein and are replaced by water.

5.4. Conclusions

In the present study, the kinetics of heat induced amyloid formation in HEWL and its attenuation by Neu5Ac have been studied. When HEWL incubated at 65°C for 168 hours then the amyloid formation occurs as evident from the increase in ThT binding, increased hydrophobicity of solvent-exposed surfaces, transition of a-helix to ß-sheet. Furthermore the amyloid fibrils of HEWL generated under studied condition are cytotoxic to the human neuronal glioblastoma. However this fibrillization process is inhibited by Neu5Ac as it decreases ThT binding, hydrophobicity of solvent-exposed surfaces, and transition of a-helical structure to ß-sheet. Furthermore, Neu5Ac also protect cells against cytotoxic nature of HEWL amyloid fibrils. The mechanism by which Neu5Ac attenuates the heat induced amyloid formation in HEWL was also determined. It is observed that the Neu5Ac donot bind to protein and stabilizes the native state of HEWL according to the effect of preferential hydration rather than direct interaction with protein. In preferential hydration mechanism, Neu5Ac molecules gets excluded from the environment around the protein and are replaced by water that stabilizes the protein against thermal stress and consequently donot permit HEWL to undergo fibrillization. Thus Neu5Ac may be a potential therapeutic candidate for inhibition of amyloid fibril formation.

BIBLIOGRAPHY

Abe, M., Abe, Y., Ohkuri, T., Mishima, T., Monji, A., Kanba, S., Ueda, T., 2013. Mechanism for retardation of amyloid fibril formation by sugars in Vlambda6 protein. Protein Sci 22, 467-474.

AccelrysSoftwareInc. 2012. Discovery Studio Modeling Environment Release 3.5. Accelrys Software Inc, San Diego.

Ahmad, B., Parveen, S., Khan, R.H., 2006. Effect of albumin conformation on the binding of ciprofloxacin to human serum albumin: a novel approach directly assigning binding site. Biomacromolecules 7, 1350-1356.

Ahmad, E., Rabbani, G., Zaidi, N., Khan, M.A., Qadeer, A., Ishtikhar, M., Singh, S., Khan, R.H., 2012. Revisiting ligand-induced conformational changes in proteins: essence, advancements, implications and future challenges. J Biomol Struct Dyn 31, 630-648.

Ahmad, E., Rabbani, G., Zaidi, N., Singh, S., Rehan, M., Khan, M.M., Rahman, S.K., Quadri, Z., Shadab, M., Ashraf, M.T., Subbarao, N., Bhat, R., Khan, R.H., 2011. Stereo-selectivity of human serum albumin to enantiomeric and isoelectronic pollutants dissected by spectroscopy, calorimetry and bioinformatics. PLoS One 6:e26186.

Alcala, J.R., Gratton, E., Prendergast, F.G., 1987. Fluorescence lifetime distributions in proteins. Biophys J 51, 597-604.

Amzel, L.M., 2000. Calculation of entropy changes in biological processes: folding, binding, and oligomerization. Methods Enzymol 323, 167-177.

Anand, U., Jash, C., Mukherjee, S., 2010. Spectroscopic probing of the microenvironment in a protein-surfactant assembly. J Phys Chem B 114, 15839-15845.

Anand, U., Jash, C., Boddepalli, R.K., Shrivastava, A., Mukherjee, S., 2011. Exploring the mechanism of fluorescence quenching in proteins induced by tetracycline. J Phys Chem B 115, 6312-6320.

Arnaudov, L.N., de Vries, R., 2005. Thermally induced fibrillar aggregation of hen egg white lysozyme. Biophys J 88, 515-526.

Barratt, E., Bingham, R.J., Warner, D.J., Laughton, C.A., Phillips, S.E., Homans, S.W., 2005. Van der Waals interactions dominate ligand-protein association in a protein binding site occluded from solvent water. J Am Chem Soc 127, 11827-11834.

Barth, A., 2007. Infrared spectroscopy of proteins. Biochim Biophys Acta 1767, 1073-1101.

Beauchemin, R., N'Soukpoe-Kossi, C.N., Thomas, T.J., Thomas, T., Carpentier, R., Tajmir-Riahi, H.A., 2007. Polyamine analogues bind human serum albumin. Biomacromolecules 8, 3177-3183.

Beechem, J.M., Brand, L., 1985. Time-resolved fluorescence of proteins. Annu Rev Biochem 54, 43-71.

Bhattacharya, R., Bhattacharyya, D., 2009. Resistance of bromelain to SDS binding. Biochim Biophys Acta 1794, 698-708.

Bhattacharya, S., Hall, S.E., Li, H., Vaidehi, N., 2008. Ligand-stabilized conformational states of human beta(2) adrenergic receptor: insight into G-protein-coupled receptor activation. Biophys J 94, 2027-2042.

Bhuyan, A.K., 2010. On the mechanism of SDS-induced protein denaturation. Biopolymers 93, 186-199.

Biancalana, M., Koide, S., 2010. Molecular mechanism of Thioflavin-T binding to amyloid fibrils. Biochim Biophys Acta 1804, 1405-1412.

Binkert, C., Demetriou, M., Sukhu, B., Szweras, M., Tenenbaum, H.C., Dennis, J.W., 1999. Regulation of osteogenesis by fetuin. J Biol Chem 274, 28514-28520.

Bissantz, C., Kuhn, B., Stahl, M., 2010. A medicinal chemist's guide to molecular interactions. J Med Chem 53, 5061-5084.

Blondelle, S.E., Ostresh, J.M., Houghten, R.A., Perez-Paya, E., 1995. Induced conformational states of amphipathic peptides in aqueous/lipid environments. Biophys J 68, 351-359.

Bojko, B., Sulkowska, A., Maciazek-Jurczyk, M., Rownicka, J., Pentak, D., Sulkowski, W.W., 2010a. Alterations of furosemide binding to serum albumin induced by increased level of fatty acid. J Pharm Biomed Anal 51, 273-277.

Bojko, B., Sulkowska, A., Maciazek-Jurczyk, M., Rownicka, J., Sulkowski, W.W. 2010b. Influence of myristic acid on furosemide binding to bovine serum albumin. Comparison with furosemide-human serum albumin complex. Spectrochim Acta A Mol Biomol Spectrosc 76, 6-11.

Booth, D.R., Sunde, M., Bellotti, V., Robinson, C.V., Hutchinson, W.L., Fraser, P.E., Hawkins, P.N., Dobson, C.M., Radford, S.E., Blake, C.C., Pepys, M.B., 1997.

Instability, unfolding and aggregation of human lysozyme variants underlying amyloid fibrillogenesis. Nature 385, 787-793.

Bosshard, H.R., 2001. Molecular recognition by induced fit: how fit is the concept? News Physiol Sci 16, 171-173.

Boumendil-Podevin, E.F., Podevin, R.A., Richet, G., 1975. Uricosuric agents in uremic sera. Identification of indoxyl sulfata and hippuric acid. J Clin Invest 55, 1142-1152.

Bourassa, P., Dubeau, S., Maharvi, G.M., Fauq, A.H., Thomas, T.J., Tajmir-Riahi, H.A., 2011. Binding of antitumor tamoxifen and its metabolites 4-hydroxytamoxifen and endoxifen to human serum albumin. Biochimie 93, 1089-1101.

Bowmer, C.J., Lindup, W.E., 1982. Decreased drug binding in uraemia: effect of indoxyl sulphate and other endogenous substances on the binding of drugs and dyes to human albumin. Biochem Pharmacol 31, 319-323.

Brorsson, A.C., Bolognesi, B., Tartaglia, G.G., Shammas, S.L., Favrin, G., Watson, I., Lomas, D.A., Chiti, F., Vendruscolo, M., Dobson, C.M., Crowther, D.C., Luheshi, L.M., 2010. Intrinsic determinants of neurotoxic aggregate formation by the amyloid beta peptide. Biophys J 98, 1677-1684.

Bruzdziak, P., Panuszko, A., Stangret, J., 2013. Influence of Osmolytes on Protein and Water Structure: A Step To Understanding the Mechanism of Protein Stabilization. J Phys Chem B [Epub ahead of print].

Brylinski, M., Skolnick, J., 2008. What is the relationship between the global structures of apo and holo proteins? Proteins 70, 363-377.

Carlson, S.E., 1985. N-acetylneuraminic acid concentrations in human milk oligosaccharides and glycoproteins during lactation. Am J Clin Nutr 41, 720–726.

Cascella, R., Conti, S., Mannini, B., Li, X., Buxbaum, J.N., Tiribilli, B., Chiti, F., Cecchi, C., 2013. Transthyretin suppresses the toxicity of oligomers formed by misfolded proteins in vitro. Biochim Biophys Acta 1832, 2302-2314.

Celej, M.S., Dassie, S.A., Freire, E., Bianconi, M.L., Fidelio, G.D., 2005. Ligand-induced thermostability in proteins: thermodynamic analysis of ANS-albumin interaction. Biochim Biophys Acta 1750, 122-133.

Celej, M.S., Dassie, S.A., Gonzalez, M., Bianconi, M.L., Fidelio, G.D., 2006. Differential scanning calorimetry as a tool to estimate binding parameters in multiligand binding proteins. Anal Biochem 350, 277-284.

Chakraborty, A., Basak, S., 2008. Effect of surfactants on casein structure: a spectroscopic study. Colloids Surf B Biointerfaces 63, 83-90.

Chamani, J., Vahedian-Movahed, H., Saberi, M.R., 2011. Lomefloxacin promotes the interaction between human serum albumin and transferrin: a mechanistic insight into the emergence of antibiotic's side effects. J Pharm Biomed Anal 55, 114-124.

Chamani, J., Moosavi-Movahedi, A.A., Rajabi, O., Gharanfoli, M., Momen-Heravi, M., Hakimelahi, G.H., Neamati-Baghsiah, A., Varasteh, A.R., 2006. Cooperative alpha-helix formation of beta-lactoglobulin induced by sodium n-alkyl sulfates. J Colloid Interface Sci 293, 52-60.

Chatterjee, T., Pal, A., Dey, S., Chatterjee, B.K., Chakrabarti, P., 2012. Interaction of virstatin with human serum albumin: spectroscopic analysis and molecular modeling. PLoS One 7, e37468.

Chen, Y.H., Yang, J.T., Martinez, H.M., 1972. Determination of the secondary structures of proteins by circular dichroism and optical rotatory dispersion. Biochemistry 11, 4120-4131.

Chen, Z., Zhong, C., 2013. Decoding Alzheimer's disease from perturbed cerebral glucose metabolism: implications for diagnostic and therapeutic strategies. Prog Neurobiol 108, 21-43.

Cheon, M., Chang, I., Mohanty, S., Luheshi, L.M., Dobson, C.M., Vendruscolo, M., Favrin, G., 2007. Structural reorganisation and potential toxicity of oligomeric species formed during the assembly of amyloid fibrils. PLoS Comput Biol 3, 1727-1738.

Chi, Z., Liu, R., 2011. Phenotypic characterization of the binding of tetracycline to human serum albumin. Biomacromolecules 12, 203-209.

Chiti, F., Dobson, C.M., 2009. Amyloid formation by globular proteins under native conditions. Nat Chem Biol 5, 15-22.

Chodera, J.D., Mobley, D.L., 2013. Entropy-enthalpy compensation: role and ramifications in biomolecular ligand recognition and design. Annu Rev Biophys 42, 121-142.

Conte, A., Pellegrini, S., Tagliazucchi, D., 2003. Synergistic protection of PC12 cells from beta-amyloid toxicity by resveratrol and catechin. Brain Res Bull 62, 29-38.

Cooper, A., Johnson, C.M., 1994. Introduction to microcalorimetry and biomolecular energetics. Methods Mol Biol 22, 109-124.

Corlin, D.B., Johnsen, C.K., Nissen, M.H., Heegaard, N.H., 2010. Glycosaminoglycans enhance the fibrillation propensity of the beta2-microglobulin cleavage variant--DeltaK58-beta2m. Biochem Biophys Res Commun 402, 247-251.

Cyril, L., Earl, J.K., Sperry, W.M., . 1961. E & F. N. Spon,, London.

Duranton, F., Cohen, G., De Smet, R., Rodriguez, M., Jankowski, J., Vanholder, R., Argiles, A., 2012. Normal and pathologic concentrations of uremic toxins. J Am Soc Nephrol 23, 1258-1270.

Dziegielewska, K.M., Brown, W.M., Casey, S.J., Christie, D.L., Foreman, R.C., Hill, R.M., Saunders, N.R., 1990. The complete cDNA and amino acid sequence of bovine fetuin. Its homology with alpha 2HS glycoprotein and relation to other members of the cystatin superfamily. J Biol Chem 265, 4354-4357.

Dzurik, R., Spustova, V., Krivosikova, Z., Gazdikova, K., 2001. Hippurate participates in the correction of metabolic acidosis. Kidney Int Suppl 78, S278-281.

Edelstein, S.J., 2013. Allosteric interactions after 50 years. J Mol Biol 425, 1391-1395.

Eftink, M.R., Anusiem, A.C., Biltonen, R.L., 1983. Enthalpy-entropy compensation and heat capacity changes for protein-ligand interactions: general thermodynamic models and data for the binding of nucleotides to ribonuclease A. Biochemistry 22, 3884-3896.

Emsley, J., 1980. Very strong hydrogen bonds. Chem Soc Rev 9, 91-124.

Faergeman, N.J., Sigurskjold, B.W., Kragelund, B.B., Andersen, K.V., Knudsen, J., 1996. Thermodynamics of ligand binding to acyl-coenzyme A binding protein studied by titration calorimetry. Biochemistry 35, 14118-14126.

Falconer, R.J., Collins, B.M., 2011. Survey of the year 2009: applications of isothermal titration calorimetry. J Mol Recognit 24, 1-16.

Ferrer, M.L., Duchowicz, R., Carrasco, B., de la Torre, J.G., Acuna, A.U., 2001. The conformation of serum albumin in solution: a combined phosphorescence depolarization-hydrodynamic modeling study. Biophys J 80, 2422-2430.

Fischer, E., 1894. Einfluss der configuration auf die wirkung der enzyme. . Ber Dtsch Chem Ges 27, 2984-2993.

Förster, T., 1948. Intermolecular Energy Migration and Fluorescence. Ann. Phys 2, 55-75.

Frauenfelder, H., Sligar, S.G., Wolynes, P.G., 1991. The energy landscapes and motions of proteins. Science 254, 1598-1603.

Friesner, R.A., Banks, J.L., Murphy, R.B., Halgren, T.A., Klicic, J.J., Mainz, D.T., Repasky, M.P., Knoll, E.H., Shelley, M., Perry, J.K., Shaw, D.E., Francis, P., Shenkin, P.S., 2004. Glide: a new approach for rapid, accurate docking and scoring. 1. Method and assessment of docking accuracy. J Med Chem 47, 1739-1749.

Froehlich, E., Mandeville, J.S., Jennings, C.J., Sedaghat-Herati, R., Tajmir-Riahi, H.A., 2009. Dendrimers bind human serum albumin. J Phys Chem B 113, 6986-6993.

Galembeck, F., Cann, J.R., 1974. Fetuin as a trypsin inhibitor. Arch Biochem Biophys 164, 326-331.

Gallivan, J.P., Dougherty, D.A., 1999. Cation-pi interactions in structural biology. Proc Natl Acad Sci U S A 96, 9459-9464.

Gangabadage, C.S., Najda, A., Bogdan, D., Wijmenga, S.S., Tessari, M., 2008. Dependence of the size of a protein-SDS complex on detergent and Na+ concentrations. J Phys Chem B 112, 4242-4245.

Garavito, R.M., Ferguson-Miller, S., 2001. Detergents as tools in membrane biochemistry. J Biol Chem 276, 32403-32406.

Gasymov, O.K., Glasgow, B.J., 2007. ANS fluorescence: potential to augment the identification of the external binding sites of proteins. Biochim Biophys Acta 1774, 403-411.

Gerstein, M., Lesk, A.M., Chothia, C., 1994. Structural mechanisms for domain movements in proteins. Biochemistry 33, 6739-6749.

Gharibyan, A.L., Zamotin, V., Yanamandra, K., Moskaleva, O.S., Margulis, B.A., Kostanyan, I.A., Morozova-Roche, L.A., 2007. Lysozyme amyloid oligomers

and fibrils induce cellular death via different apoptotic/necrotic pathways. J Mol Biol 365, 1337-1349.

Ghuman, J., Zunszain, P.A., Petitpas, I., Bhattacharya, A.A., Otagiri, M., Curry, S., 2005. Structural basis of the drug-binding specificity of human serum albumin. J Mol Biol 353, 38-52.

Gonzalez-Iglesias, R., Pajares, M.A., Ocal, C., Espinosa, J.C., Oesch, B., Gasset, M., 2002. Prion protein interaction with glycosaminoglycan occurs with the formation of oligomeric complexes stabilized by Cu(II) bridges. J Mol Biol 319, 527-540.

Green, E.D., Adelt, G., Baenziger, J.U., Wilson, S., Van Halbeek, H., 1988. The asparagine-linked oligosaccharides on bovine fetuin. Structural analysis of N-glycanase-released oligosaccharides by 500-megahertz 1H NMR spectroscopy. J Biol Chem 263, 18253-18268.

Groenning, M., 2010. Binding mode of Thioflavin T and other molecular probes in the context of amyloid fibrils-current status. J Chem Biol 3, 1-18.

Haldar, S., Raghuraman, H., Chattopadhyay, A., 2008. Monitoring orientation and dynamics of membrane-bound melittin utilizing dansyl fluorescence. J Phys Chem B 112, 14075-14082.

Haldar, S., Chaudhuri, A., Gu, H., Koeppe, R.E., 2nd, Kombrabail, M., Krishnamoorthy, G., Chattopadhyay, A., 2012. Membrane organization and dynamics of "inner pair" and "outer pair" tryptophan residues in gramicidin channels. J Phys Chem B 116, 11056-11064.

Harding, S.E., Chowdhry, B.Z., 2001. Protein-ligand interactions: hydrodynamics and calorimetry. Chapter 1, Oxford university press, New York, USA.

He, X.M., Carter, D.C., 1992. Atomic structure and chemistry of human serum albumin. Nature 358, 209-215.

Heerklotz, H., Seelig, J., 2000. Titration calorimetry of surfactant-membrane partitioning and membrane solubilization. Biochim Biophys Acta 1508, 69-85.

Hermentin, P., Witzel, R., Kanzy, E.J., Diderrich, G., Hoffmann, D., Metzner, H., Vorlop, J., Haupt, H., 1996. The hypothetical N-glycan charge: a number that characterizes protein glycosylation. Glycobiology 6, 217-230.

Hu, Y.J., Liu, Y., Xiao, X.H., 2009. Investigation of the interaction between Berberine and human serum albumin. Biomacromolecules 10, 517-521.

Hudson, S.A., Ecroyd, H., Dehle, F.C., Musgrave, I.F., Carver, J.A., 2009. (-)-epigallocatechin-3-gallate (EGCG) maintains kappa-casein in its pre-fibrillar state without redirecting its aggregation pathway. J Mol Biol 392, 689-700.

Hugonin, L., Barth, A., Graslund, A., Peralvarez-Marin, A., 2008. Secondary structure transitions and aggregation induced in dynorphin neuropeptides by the detergent sodium dodecyl sulfate. Biochim Biophys Acta 1778, 2580-2587.

Hung, H.C., Chang, G.G., 2001. Multiple unfolding intermediates of human placental alkaline phosphatase in equilibrium urea denaturation. Biophys J 81, 3456-3471.

Hung, Y.T., Lin, M.S., Chen, W.Y., Wang, S.S., 2010. Investigating the effects of sodium dodecyl sulfate on the aggregative behavior of hen egg-white lysozyme at acidic pH. Colloids Surf B Biointerfaces 81, 141-151.

Ibrahim, N., Ibrahim, H., Kim, S., Nallet, J.P., Nepveu, F., 2010. Interactions between antimalarial indolone-N-oxide derivatives and human serum albumin. Biomacromolecules 11, 3341-3351.

Ikeda, K., Yoshitomi, H., Nakayama, T., Goto, S., Kimura, T., 1984. Plasma protein binding of frusemide in renal failure rabbits: investigation of endogenous protein binding inhibitors. J Pharm Pharmacol 36, 663-667.

Il'ichev , Y.V., Perry , J.L., Simon, J., 2002. Interaction of Ochratoxin A with Human Serum Albumin. A Common Binding Site of Ochratoxin A and Warfarin in Subdomain IIA. J. Phys. Chem. B 106, 460–465.

Ivanov, A.I., Korolenko, E.A., Korolik, E.V., Firsov, S.P., Zhbankov, R.G., Marchewka, M.K., Ratajczak, H., 2002. Chronic liver and renal diseases differently affect structure of human serum albumin. Arch Biochem Biophys 408, 69-77.

James, S., McManus, J.J., 2012. Thermal and solution stability of ysozyme in the presence of sucrose, glucose, and trehalose. J Phys Chem B [Epub ahead of print].

Johnson, C.M., 2013. Differential scanning calorimetry as a tool for protein folding and stability. Arch Biochem Biophys 531, 100-109.

Kar, K., Kishore, N., 2007. Enhancement of thermal stability and inhibition of protein aggregation by osmolytic effect of hydroxyproline. Biopolymers 87, 339-351.

Katayama, N., Orita, M., Yamaguchi, T., Hisamichi, H., Kuromitsu, S., Kurihara, H., Sakashita, H., Matsumoto, Y., Fujita, S., Niimi, T., 2008. Identification of a key element for hydrogen-bonding patterns between protein kinases and their inhibitors. Proteins 73, 795-801.

Kelkar, D.A., Chattopadhyay, A., Chakrabarti, A., Bhattacharyya, M., 2005. Effect of ionic strength on the organization and dynamics of tryptophan residues in erythroid spectrin: a fluorescence approach. Biopolymers 77, 325-334.

Keller, S., Heerklotz, H., Jahnke, N., Blume, A., 2006. Thermodynamics of lipid membrane solubilization by sodium dodecyl sulfate. Biophys J 90, 4509-4521.

Kelley, L.A., Sternberg, M.J., 2009. Protein structure prediction on the Web: a case study using the Phyre server. Nat Protoc 4, 363-371.

Kelly, S.M., Price, N.C., 2000. The use of circular dichroism in the investigation of protein structure and function. Curr Protein Pept Sci 1, 349-384.

Kennedy, D.M., Skillen, A.W., Self, C.H., 1993. Colorimetric assay of glycoprotein glycation free of interference from glycosylation residues. Clin Chem 39, 2309-2311.

Keswani, N., Choudhary, S., Kishore, N., 2010. Interaction of weakly bound antibiotics neomycin and lincomycin with bovine and human serum albumin: biophysical approach. J Biochem 148, 71-84.

Koshland, D.E., 1958. Application of a theory of enzyme specificity to protein synthesis. Proc Natl Acad Sci U S A 44, 98-104.

Kragh-Hansen, U., 1981. Molecular aspects of ligand binding to serum albumin. Pharmacol Rev 33, 17-53.

Kragh-Hansen, U., 2013. Molecular and practical aspects of the enzymatic properties of human serum albumin and of albumin-ligand complexes. Biochim Biophys Acta. 1830, 5535-5544.

Kukic, P., Nielsen, J.E., 2010. Electrostatics in proteins and protein-ligand complexes. Future Med Chem 2, 647-666.

Kumaran, S., Jez, J.M., 2007. Thermodynamics of the interaction between O-acetylserine sulfhydrylase and the C-terminus of serine acetyltransferase. Biochemistry 46, 5586-5594.

Kyte, J., Doolittle, R.F., 1982. A simple method for displaying the hydropathic character of a protein. J Mol Biol 157, 105-132.

La Mesa, C., 2005. Polymer-surfactant and protein-surfactant interactions. J Colloid Interface Sci 286, 148-157.

Ladbury, J.E., Williams, M.A., 2004. The extended interface: measuring non-local effects in biomolecular interactions. Curr Opin Struct Biol 14, 562-569.

Lakowicz, J.R., 2006. Principles of Fluorescence. Plenum press. New York, USA.

Lanckriet, H., Middelberg, A.P., 2004. Operational regimes for a simplified one-step artificial chaperone refolding method. Biotechnol Prog 20, 1861-1867.

Landschulz, W.H., Johnson, P.F., McKnight, S.L., 1988. The leucine zipper: a hypothetical structure common to a new class of DNA binding proteins. Science 240, 1759-1764.

Laurents, D.V., Baldwin, R.L., 1997. Characterization of the unfolding pathway of hen egg white lysozyme. Biochemistry 36, 1496-1504.

Lee, A., Tang, S.K., Mace, C.R., Whitesides, G.M., 2011. Denaturation of proteins by SDS and tetraalkylammonium dodecyl sulfates. Langmuir 27, 11560-11574.

Lendel, C., Bertoncini, C.W., Cremades, N., Waudby, C.A., Vendruscolo, M., Dobson, C.M., Schenk, D., Christodoulou, J., Toth, G., 2009. On the mechanism of nonspecific inhibitors of protein aggregation: dissecting the interactions of alpha-synuclein with Congo red and lacmoid. Biochemistry 48, 8322-8334.

Leveugle, B., Scanameo, A., Ding, W., Fillit, H., 1994. Binding of heparan sulfate glycosaminoglycan to beta-amyloid peptide: inhibition by potentially therapeutic polysulfated compounds. Neuroreport 5, 1389-1392.

Li, S., Schoneich, C., Borchardt, R.T., 1995. Chemical instability of protein pharmaceuticals: Mechanisms of oxidation and strategies for stabilization. Biotechnol Bioeng 48, 490-500.

Lin, J.H., Lu, A.Y., 1997. Role of pharmacokinetics and metabolism in drug discovery and development. Pharmacol Rev 49, 403-449.

Lina, F.Y., Chen, W.Y., Ruaan, R.C., Huang, H.M., 2000. Microcalorimetric studies of interactions between proteins and hydrophobic ligands in hydrophobic interaction chromatography: effects of ligand chain length, density and the amount of bound protein. J Chromatogr A 872, 37-47.

Liu, F.F., Ji, L., Dong, X.Y., Sun, Y., 2009. Molecular insight into the inhibition effect of trehalose on the nucleation and elongation of amyloid beta-peptide oligomers. J Phys Chem B 113, 11320-11329.

Liu, Y., Guo, R., 2007. Interaction between casein and sodium dodecyl sulfate. J Colloid Interface Sci 315, 685-692.

Louis-Jeune, C., Andrade-Navarro, M.A., Perez-Iratxeta, C., 2012. Prediction of protein secondary structure from circular dichroism using theoretically derived spectra. Proteins.

Ma, B., Kumar, S., Tsai, C.J., Nussinov, R., 1999. Folding funnels and binding mechanisms. Protein Eng 12, 713-720.

Ma, S.F., Anraku, M., Iwao, Y., Yamasaki, K., Kragh-Hansen, U., Yamaotsu, N., Hirono, S., Ikeda, T., Otagiri, M., 2005. Hydrolysis of angiotensin II receptor blocker prodrug olmesartan medoxomil by human serum albumin and identification of its catalytic active sites. Drug Metab Dispos 33, 1911-1919.

Mingrone, G., De Smet, R., Greco, A.V., Bertuzzi, A., Gandolfi, A., Ringoir, S., Vanholder, R., 1997. Serum uremic toxins from patients with chronic renal failure displace the binding of L-tryptophan to human serum albumin. Clin Chim Acta 260, 27-34.

Miyamoto, Y., Iwao, Y., Tasaki, Y., Sato, K., Ishima, Y., Watanabe, H., Kadowaki, D., Maruyama, T., Otagiri, M., 2010. The uremic solute indoxyl sulfate acts as an antioxidant against superoxide anion radicals under normal-physiological conditions. FEBS Lett 584, 2816-2820.

Moore, P.N., Puvvada, S., Blankschtein, D., 2003. Challenging the surfactant monomer skin penetration model: penetration of sodium dodecyl sulfate micelles into the epidermis. J Cosmet Sci 54, 29-46.

Moosavi-Movahedi, A.A., Gharanfoli, M., Nazari, K., Shamsipur, M., Chamani, J., Hemmateenejad, B., Alavi, M., Shokrollahi, A., Habibi-Rezaei, M., Sorenson, C., Sheibani, N., 2005. A distinct intermediate of RNase A is induced by sodium dodecyl sulfate at its pK(a). Colloids Surf B Biointerfaces 43, 150-157.

Moriyama, Y., Takeda, K., 2005. Protective effects of small amounts of bis(2-ethylhexyl)sulfosuccinate on the helical structures of human and bovine serum albumins in their thermal denaturations. Langmuir 21, 5524-5528.

Moriyama, Y., Kawasaka, Y., Takeda, K., 2003. Protective effect of small amounts of sodium dodecyl sulfate on the helical structure of bovine serum albumin in thermal denaturation. J Colloid Interface Sci 257, 41-46.

Moriyama, Y., Kondo, N., Takeda, K., 2012. Secondary structural changes of homologous proteins, lysozyme and alpha-lactalbumin, in thermal denaturation up to 130 degrees C and sodium dodecyl sulfate (SDS) effects on these changes: comparison of thermal stabilities of SDS-induced helical structures in these proteins. Langmuir 28, 16268-16273.

Morshedi, D., Rezaei-Ghaleh, N., Ebrahim-Habibi, A., Ahmadian, S., Nemat-Gorgani, M., 2007. Inhibition of amyloid fibrillation of lysozyme by indole derivatives-possible mechanism of action. FEBS J 274, 6415-6425.

Motamedi-Shad, N., Garfagnini, T., Penco, A., Relini, A., Fogolari, F., Corazza, A., Esposito, G., Bemporad, F., Chiti, F., 2012. Rapid oligomer formation of human muscle acylphosphatase induced by heparan sulfate. Nat Struct Mol Biol 19, 547-554, S541-542.

Murray, A.C., Oikawa, K., Kay, C.M., 1969. Circular dichroism studies on native fetuin and some of its derivatives. Biochim Biophys Acta 175, 331-338.

Nada, T., Terazima, M., 2003. A novel method for study of protein folding kinetics by monitoring diffusion coefficient in time domain. Biophys J 85, 1876-1881.

Naeem, A., Khan, R.H., 2004. Characterization of molten globule state of cytochrome c at alkaline, native and acidic pH induced by butanol and SDS. Int J Biochem Cell Biol 36, 2281-2292.

Naidu, K.T., Prabhu, N.P., 2011. Protein-surfactant interaction: sodium dodecyl sulfate-induced unfolding of ribonuclease A. J Phys Chem B 115, 14760-14767.

Naseem, F., Khan, R.H., Haq, S.K., Naeem, A., 2003. Characterization of molten globule state of fetuin at low pH. Biochim Biophys Acta 1649, 164-170.

Neelam, S., Gokara, M., Sudhamalla, B., Amooru, D.G., Subramanyam, R., 2010. Interaction studies of coumaroyltyramine with human serum albumin and its biological importance. J Phys Chem B 114, 3005-3012.

Negi, S.S., Schein, C.H., Oezguen, N., Power, T.D., Braun, W., 2007. InterProSurf: a web server for predicting interacting sites on protein surfaces. Bioinformatics 23, 3397-3399.

Nielsen, M.M., Andersen, K.K., Westh, P., Otzen, D.E., 2007. Unfolding of beta-sheet proteins in SDS. Biophys J 92, 3674-3685.

Ninham, B.W., Parsegian, V.A., 1970. Van der Waals forces. Special characteristics in lipid-water systems and a general method of calculation based on the Lifshitz theory. Biophys J 10, 646-663.

Niwa, T., 1996. Organic acids and the uremic syndrome: protein metabolite hypothesis in the progression of chronic renal failure. Semin Nephrol 16, 167-182.

Nys, M., Kesters, D., Ulens, C., 2013. Structural insights into Cys-loop receptor function and ligand recognition. Biochem Pharmacol. 86, 1042-1053.

Ohtsuki, S., Asaba, H., Takanaga, H., Deguchi, T., Hosoya, K., Otagiri, M., Terasaki, T., 2002. Role of blood-brain barrier organic anion transporter 3 (OAT3) in the efflux of indoxyl sulfate, a uremic toxin: its involvement in neurotransmitter metabolite clearance from the brain. J Neurochem 83, 57-66.

Olivieri, J.R., Craievich, A.F., 1995. The subdomain structure of human serum albumin in solution under different pH conditions studied by small angle X-ray scattering. Eur Biophys J 24, 77-84.

Otzen, D.E., 2002. Protein unfolding in detergents: effect of micelle structure, ionic strength, pH, and temperature. Biophys J 83, 2219-2230.

Patching, S.G., 2013. Surface plasmon resonance spectroscopy for characterisation of membrane protein-ligand interactions and its potential for drug discovery. Biochim Biophys Acta.

Pellaud, J., Schote, U., Arvinte, T., Seelig, J., 1999. Conformation and self-association of human recombinant transforming growth factor-beta3 in aqueous solutions. J Biol Chem 274, 7699-7704.

Peon, J., Pal, S.K., Zewail, A.H., 2002. Hydration at the surface of the protein Monellin: dynamics with femtosecond resolution. Proc Natl Acad Sci U S A 99, 10964-10969.

Perozzo, R., Folkers, G., Scapozza, L., 2004. Thermodynamics of protein-ligand interactions: history, presence, and future aspects. J Recept Signal Transduct Res 24, 1-52.

Pertinhez, T.A., Bouchard, M., Smith, R.A., Dobson, C.M., Smith, L.J., 2002. Stimulation and inhibition of fibril formation by a peptide in the presence of different concentrations of SDS. FEBS Lett 529, 193-197.

Perucho, J., Casarejos, M.J., Gomez, A., Solano, R.M., de Yebenes, J.G., Mena, M.A., 2012. Trehalose protects from aggravation of amyloid pathology induced by isoflurane anesthesia in APP(swe) mutant mice. Curr Alzheimer Res 9, 334-343.

Peters, J.T., 1996. All About Albumin: Biochemistry, Genetics and Medical Applications, Academic Press, San Diego, CA,.

Petitpas, I., Bhattacharya, A.A., Twine, S., East, M., Curry, S., 2001. Crystal structure analysis of warfarin binding to human serum albumin: anatomy of drug site I. J Biol Chem 276, 22804-22809.

Pettersen, E.F., Goddard, T.D., Huang, C.C., Couch, G.S., Greenblatt, D.M., Meng, E.C., Ferrin, T.E., 2004. UCSF Chimera--a visualization system for exploratory research and analysis. J Comput Chem 25, 1605-1612.

Porat, Y., Abramowitz, A., Gazit, E., 2006. Inhibition of amyloid fibril formation by polyphenols: structural similarity and aromatic interactions as a common inhibition mechanism. Chem Biol Drug Des 67, 27-37.

Privalov, P.L., 1982. Stability of proteins. Proteins which do not present a single cooperative system. Adv Protein Chem 35, 1-104.

Prive, G.G., 2007. Detergents for the stabilization and crystallization of membrane proteins. Methods 41, 388-397.

Qadeer, A., Rabbani, G., Zaidi, N., Ahmad, E., Khan, J.M., Khan, R.H., 2012. 1-Anilino-8-naphthalene sulfonate (ANS) is not a desirable probe for determining the molten globule state of chymopapain. PLoS One 7, e50633.

Rajarathnam, K., Rosgen, J., 2013. Isothermal titration calorimetry of membrane proteins - Progress and challenges. Biochim Biophys Acta. [Epub ahead of print].

Rangel-Yagui, C.O., Pessoa, A., Jr., Tavares, L.C., 2005. Micellar solubilization of drugs. J Pharm Pharm Sci 8, 147-165.

Reed, M.D., Myers, C.M., Blumer, J.L., 2001. Influence of midazolam on the protein binding of ketorolac. Current Therapeutic Research 62, 558–565.

Reynolds, J.A., Tanford, C., 1970. The gross conformation of protein-sodium dodecyl sulfate complexes. J Biol Chem 245, 5161-5165.

Rezaei Tavirani, M., Moghaddamnia, S.H., Ranjbar, B., Amani, M., Marashi, S.A., 2006. Conformational study of human serum albumin in pre-denaturation temperatures by differential scanning calorimetry, circular dichroism and UV spectroscopy. J Biochem Mol Biol 39, 530-536.

Roman, E.A., Rosi, P., Gonzalez Lebrero, M.C., Wuilloud, R., Gonzalez Flecha, F.L., Delfino, J.M., Santos, J., 2010. Gain of local structure in an amphipathic peptide does not require a specific tertiary framework. Proteins 78, 2757-2768.

Ross, P.D., Subramanian, S., 1981. Thermodynamics of protein association reactions: forces contributing to stability. Biochemistry 20, 3096-3102.

Safar, J., Prusiner, S.B., 1998. Molecular studies of prion diseases. Prog Brain Res 117, 421-434.

Sakai, T., Takadate, A., Otagiri, M., 1995. Characterization of binding site of uremic toxins on human serum albumin. Biol Pharm Bull 18, 1755-1761.

Salonen, L.M., Ellermann, M., Diederich, F., 2011. Aromatic rings in chemical and biological recognition: energetics and structures. Angew Chem Int Ed Engl 50, 4808-4842.

Santarelli, V.P., Eastwood, A.L., Dougherty, D.A., Horn, R., Ahern, C.A., 2007. A cation-pi interaction discriminates among sodium channels that are either sensitive or resistant to tetrodotoxin block. J Biol Chem 282, 8044-8051.

Santos, S.F., Zanette, D., Fischer, H., Itri, R., 2003. A systematic study of bovine serum albumin (BSA) and sodium dodecyl sulfate (SDS) interactions by surface tension and small angle X-ray scattering. J Colloid Interface Sci 262, 400-408.

Sarnatskaya, V.V., Lindup, W.E., Ivanov, A.I., Yushko, L.A., Tjia, J., Maslenny, V.N., Gurina, N.M., Nikolaev, V.G., 2003. Extraction of uraemic toxins with activated carbon restores the functional properties of albumin. Nephron Physiol 95, p10-18.

Sarroukh, R., Goormaghtigh, E., Ruysschaert, J.M., Raussens, V., 2013. ATR-FTIR: a "rejuvenated" tool to investigate amyloid proteins. Biochim Biophys Acta 1828, 2328-2338.

Sasahara, K., Yagi, H., Naiki, H., Goto, Y., 2007. Heat-induced conversion of beta(2)-microglobulin and hen egg-white lysozyme into amyloid fibrils. J Mol Biol 372, 981-991.

Sassi, P., Giugliarelli, A., Paolantoni, M., Morresi, A., Onori, G., 2011. Unfolding and aggregation of lysozyme: a thermodynamic and kinetic study by FTIR spectroscopy. Biophys Chem 158, 46-53.

Scatena, L.F., Brown, M.G., Richmond, G.L., 2001. Water at hydrophobic surfaces: weak hydrogen bonding and strong orientation effects. Science 292, 908-912.

Seedher, N., Bhatia, S., 2006. Interaction of non-steroidal anti-inflammatory drugs, etoricoxib and parecoxib sodium, with human serum albumin studied by fluorescence spectroscopy. Drug Metabol Drug Interact 22, 25-45.

Seetharamappa, J., Kamat, B.P., 2005. Study of the interaction between fluoroquinolones and bovine serum albumin. J Pharm Biomed Anal 39, 1046-1050.

Shahabadi, N., Khorshidi, A., Moghadam, N.H., 2013. Study on the interaction of the epilepsy drug, zonisamide with human serum albumin (HSA) by spectroscopic and molecular docking techniques. Spectrochim Acta A Mol Biomol Spectrosc 114, 627-632.

Sharma, R., Choudhary, S., Kishore, N., 2012. Insights into the binding of the drugs diclofenac sodium and cefotaxime sodium to serum albumin: calorimetry and spectroscopy. Eur J Pharm Sci 46, 435-445.

Sharp, K.A., Honig, B., 1990. Electrostatic interactions in macromolecules: theory and applications. Annu Rev Biophys Biophys Chem 19, 301-332.

Singh, S.K., Kishore, N., 2006. Thermodynamic insights into the binding of Triton X-100 to globular proteins: a calorimetric and spectroscopic investigation. J Phys Chem B 110, 9728-9737.

Sipe, J.D., 1992. Amyloidosis. Annu Rev Biochem 61, 947-975.

Sjoholm, I., Kober, A., Odar-Cederlof, I., Borgaa, O., 1976. Protein binding of drugs in uremic and normal serum: the role of endogenous binding inhibitors. Biochem Pharmacol 25, 1205-1213.

Soldi, G., Plakoutsi, G., Taddei, N., Chiti, F., 2006. Stabilization of a native protein mediated by ligand binding inhibits amyloid formation independently of the aggregation pathway. J Med Chem 49, 6057-6064.

Spustova, V., Gajdos, M., Opatrny, K., Jr., Stefikova, K., Dzurik, R., 1991. Serum hippurate and its excretion in conservatively treated and dialysed patients with chronic renal failure. Physiol Res 40, 599-606.

Stark, J.L., Powers, R., 2012. Application of NMR and molecular docking in structure-based drug discovery. Top Curr Chem 326, 1-34.

Straub, F.B., Szabolcsi, G., 1964. On the dynamic aspects of protein structure) In: Molecular Biology, Problems and Perspectives Izdat, Nauka.

Sudlow, G., Birkett, D.J., Wade, D.N., 1975. The characterization of two specific drug binding sites on human serum albumin. Mol Pharmacol 11, 824-832.

Sugio, S., Kashima, A., Mochizuki, S., Noda, M., Kobayashi, K., 1999. Crystal structure of human serum albumin at 2.5 A resolution. Protein Eng 12, 439-446.

Takamura, N., Maruyama, T., Otagiri, M., 1997. Effects of uremic toxins and fatty acids on serum protein binding of furosemide: possible mechanism of the binding defect in uremia. Clin Chem 43, 2274-2280.

Takamura, N., Haruta, A., Kodama, H., Tsuruoka, M., Yamasaki, K., Suenaga, A., Otagiri, M., 1996. Mode of interaction of loop diuretics with human serum albumin and characterization of binding site. Pharm Res 13, 1015-1019.

Takamura, N., Maruyama, T., Chosa, E., Kawai, K., Tsutsumi, Y., Uryu, Y., Yamasaki, K., Deguchi, T., Otagiri, M., 2005. Bucolome, a potent binding inhibitor for furosemide, alters the pharmacokinetics and diuretic effect of furosemide: potential for use of bucolome to restore diuretic response in nephrotic syndrome. Drug Metab Dispos 33, 596-602.

Tanford, C., 1968. Protein denaturation. Adv Protein Chem 23, 121-282.

Tanford, C., 1973. The Hydrophobic Effect: Formation of Micelles and Biological Membranes. John Wiley & Sons Inc, New York.

Thoppil, A.A., Sharma, R., Kishore, N., 2008. Complexation of beta-lactam antibiotic drug carbenicillin to bovine serum albumin: energetics and conformational studies. Biopolymers 89, 831-840.

Tian, J., Liu, J., He, W., Hu, Z., Yao, X., Chen, X., 2004. Probing the binding of scutellarin to human serum albumin by circular dichroism, fluorescence spectroscopy, FTIR, and molecular modeling method. Biomacromolecules 5, 1956-1961.

Tobi, D., Bahar, I., 2005. Structural changes involved in protein binding correlate with intrinsic motions of proteins in the unbound state. Proc Natl Acad Sci U S A 102, 18908-18913.

Torrice, M.M., Bower, K.S., Lester, H.A., Dougherty, D.A., 2009. Probing the role of the cation-pi interaction in the binding sites of GPCRs using unnatural amino acids. Proc Natl Acad Sci U S A 106, 11919-11924.

Trott, O., Olson, A.J., 2010. AutoDock Vina: improving the speed and accuracy of docking with a new scoring function, efficient optimization, and multithreading. J Comput Chem 31, 455-461.

Tsai, C.J., Ma, B., Nussinov, R., 1999. Folding and binding cascades: shifts in energy landscapes. Proc Natl Acad Sci U S A 96, 9970-9972.

Tuckerman, M.E., Marx, D., Parrinello, M., 2002. The nature and transport mechanism of hydrated hydroxide ions in aqueous solution. Nature 417, 925-929.

Tulumello, D.V., Johnson, R.M., Isupov, I., Deber, C.M., 2012. Design, expression, and purification of de novo transmembrane "hairpin" peptides. Biopolymers 98, 546-556.

Ulmer, T.S., Bax, A., 2005. Comparison of structure and dynamics of micelle-bound human alpha-synuclein and Parkinson disease variants. J Biol Chem 280, 43179-43187.

Uversky, V.N., Fink, A.L., 2004. Conformational constraints for amyloid fibrillation: the importance of being unfolded. Biochim Biophys Acta 1698, 131-153.

Uversky, V.N., Fink, A.L., 2007. Protein Misfolding, Aggregation and Conformational Diseases: Part B: Molecular Mechanisms of Conformational Diseases . Protein reviews 6, Springer, New York, U.S.A.

Uversky, V.N., Narizhneva, N.V., Ivanova, T.V., Tomashevski, A.Y., 1997. Rigidity of human alpha-fetoprotein tertiary structure is under ligand control. Biochemistry 36, 13638-13645.

Vanholder, R., De Smet, R., Glorieux, G., Argiles, A., Baurmeister, U., Brunet, P., Clark, W., Cohen, G., De Deyn, P.P., Deppisch, R., Descamps-Latscha, B., Henle, T., Jorres, A., Lemke, H.D., Massy, Z.A., Passlick-Deetjen, J., Rodriguez, M., Stegmayr, B., Stenvinkel, P., Tetta, C., Wanner, C., Zidek, W.,

2003. Review on uremic toxins: classification, concentration, and interindividual variability. Kidney Int 63, 1934-1943.

Vanholder, R.C., De Smet, R.V., Ringoir, S.M., 1992. Assessment of urea and other uremic markers for quantification of dialysis efficacy. Clin Chem 38, 1429-1436.

Varshney, A., Rehan, M., Subbarao, N., Rabbani, G., Khan, R.H., 2011. Elimination of endogenous toxin, creatinine from blood plasma depends on albumin conformation: site specific uremic toxicity & impaired drug binding. PLoS One 6, e17230.

Varshney, A., Sen, P., Ahmad, E., Rehan, M., Subbarao, N., Khan, R.H., 2010. Ligand binding strategies of human serum albumin: how can the cargo be utilized? Chirality 22, 77-87.

Vuong, Q.V., Siposova, K., Nguyen, T.T., Antosova, A., Balogova, L., Drajna, L., Imrich, J., Li, M.S., Gazova, Z., 2013. Binding of glyco-acridine derivatives to lysozyme leads to inhibition of amyloid fibrillization. Biomacromolecules 14, 1035-1043.

Wang, B., Brand-Miller, J., 2003. The role and potential of sialic acid in human nutrition. Eur J Clin Nutr 57, 1351-1369.

Wang, C., Lascu, I., Giartosio, A., 1998a. Bovine serum fetuin is unfolded through a molten globule state. Biochemistry 37, 8457-8464.

Wang, C., Eufemi, M., Turano, C., Giartosio, A., 1996. Influence of the carbohydrate moiety on the stability of glycoproteins. Biochemistry 35, 7299-7307.

Wang, C.I., Lewis, R.J., 2013. Emerging opportunities for allosteric modulation of G-protein coupled receptors. Biochem Pharmacol 85, 153-162.

Wang, H., Zhang, M., Bianchi, M., Sherry, B., Sama, A., Tracey, K.J., 1998b. Fetuin (alpha2-HS-glycoprotein) opsonizes cationic macrophagedeactivating molecules. Proc Natl Acad Sci U S A 95, 14429-14434.

Wang, W., 1999. Instability, stabilization, and formulation of liquid protein pharmaceuticals. Int J Pharm 185, 129-188.

Ward, W.H., Holdgate, G.A., 2001. Isothermal titration calorimetry in drug discovery. Prog Med Chem 38, 309-376.

Wasik, R., Lebska, M., Felczak, K., Poznanski, J., Shugar, D., 2010. Relative role of halogen bonds and hydrophobic interactions in inhibition of human protein

kinase CK2alpha by tetrabromobenzotriazole and some C5-substituted analogues. J Phys Chem B 114, 10601-10611.

Watanabe, H., Tanase, S., Nakajou, K., Maruyama, T., Kragh-Hansen, U., Otagiri, M., 2000. Role of arg-410 and tyr-411 in human serum albumin for ligand binding and esterase-like activity. Biochem J 349 Pt 3, 813-819.

Wieprecht, T., Rothemund, S., Bienert, M., Krause, E., 2001. Role of helix formation for the retention of peptides in reversed-phase high-performance liquid chromatography. J Chromatogr A 912, 1-12.

Wilcox, C.S., 2002. New insights into diuretic use in patients with chronic renal disease. J Am Soc Nephrol 13, 798-805.

Williams, E.J., Herskovits, T.T., Laskowski, M., Jr., 1965. Location of chromophoric residues in proteins by solvent perturbation. 3. Tryptophyls in lysozyme and in alpha-chymotrypsinogen and its derivatives. J Biol Chem 240, 3574-3579.

Zaidi, N., Ahmad, E., Rehan, M., Rabbani, G., Ajmal, M.R., Zaidi, Y., Subbarao, N., Khan, R.H., 2013a. Biophysical insight into furosemide binding to human serum albumin: a study to unveil its impaired albumin binding in uremia. J Phys Chem B 117, 2595-2604.

Zaidi, N., Ajmal, M.R., Rabbani, G., Ahmad, E., Khan, R.H., 2013b. A Comprehensive Insight into Binding of Hippuric Acid to Human Serum Albumin: À Study to Uncover Its Impaired Elimination through Hemodialysis. PLoS One 8, e71422.

Závodszky, P., Abaturov, L.B., Varsavszkij, J.M., 1966. Structure of glyceraldehyde-3-phosphate dehydrogenase and its alteration by coenzyme binding. Acta Biochim Biophys Acad Sci Hung 1, 389-402.

Zhang, W., Dai, X., Zhao, Y., Lu, X., Gao, P., 2009. Comparison of the different types of surfactants for the effect on activity and structure of soybean peroxidase. Langmuir 25, 2363-2368.

Zolotnitsky, G., Cogan, U., Adir, N., Solomon, V., Shoham, G., Shoham, Y., 2004. Mapping glycoside hydrolase substrate subsites by isothermal titration calorimetry. Proc Natl Acad Sci U S A 101, 11275-11280.

LIST OF PUBLICATIONS

1. **Zaidi, N.**, Ahmad, E., Rehan, M., Rabbani, G., Ajmal, M.R., Zaidi, Y., Subbarao, N., Khan, R.H., 2013. Biophysical insight into furosemide binding to human serum albumin: a study to unveil its impaired albumin binding in uremia. J Phys Chem B 117, 2595-2604.

2. **Zaidi, N.**, Ajmal, M.R., Rabbani, G., Ahmad, E., Khan, R.H., 2013. A comprehensive insight into binding of hippuric acid to human serum albumin: A Study to Uncover Its Impaired Elimination through Hemodialysis. PLoS One 8, e71422.

3.Ahmad, E., Rabbani, G., **Zaidi, N.**, Khan, M.A., Qadeer, A., Ishtikhar, M., Singh, S., Khan, R.H., 2013. Revisiting ligand-induced conformational changes in proteins: essence, advancements, implications and future challenges. J Biomol Struct Dyn 31, 630-648.

4.Qadeer, A., Rabbani, G., **Zaidi, N.**, Ahmad, E., Khan, J.M., Khan, R.H., 2012. 1-anilino-8-naphthalene sulfonate (ANS) is not a desirable probe for determining the molten globule state of chymopapain. PLoS One. e50633.

5.Ahmad, E., Rabbani, G., **Zaidi, N.**, Singh, S., Rehan, M., Khan, M.M., Rahman, S.K., Quadri, Z., Shadab, M., Ashraf, M.T., Subbarao, N., Bhat, R., Khan, R.H., 2011. Stereo-selectivity of human serum albumin to enantiomeric and isoelectronic pollutants dissected by spectroscopy, calorimetry and bioinformatics. PLoS One 6:e26186.

6. Rabbani, G., Ahmad, E., **Zaidi, N.**, Khan, R.H., 2011. pH-dependent conformational transitions in coalbumin (ovotransferrin), a metalloproteinase from hen egg white. Cell Biochem Biophys 62, 487-499.

7. Rabbani, G., Ahmad, E., **Zaidi, N.**, Khan, R.H., 2011. pH-induced molten globule state of Rhizopus niveus lipase is more resistant against thermal and chemical denaturation than its native state. Cell Biochem Biophys 61,551-560.

8. Ahmad, E., Rabbani, G., **Zaidi, N.**, Khan, R.H., 2012. Pollutant-induced modulation in conformation and β-lactamase activity of human serum albumin PLoS One 7:e38372.

9. **Zaidi, N.**, Khan, R.H., (2013). Protein ligand interaction and associated conformational changes- a complete tale. (Manuscript submitted)

10. **Zaidi, N.**, Khan, R.H., 2013. Different modes of interaction of sodium dodecyl sulphate (SDS) to bovine serum fetuin at acidic and neutral pH: a mechanistic study. (Manuscript submitted)

11. **Zaidi, N.**, Ajmal, M.R., Zaidi, Y., Khan, R.H., 2013. N-Acetylneuraminic acid inhibits heat-induced amyloid fibrillization of lysozyme by enhancing its thermal stability. (Manuscript submitted)

12. **Zaidi, N.**, Khan, R.H. SDS interacts differently with asialofetuin at acidic and neutral pH. (Manuscript submitted)

13. **Zaidi, N.**, Khan, R.H. Insight into structural, thermodynamic and functional alteration of albumin under uremia. (manuscript in prepararion)

14. Zaidi, Y., Arjumand, F., **Zaidi, N.**, Usmani T.A.., Zubair H, Akhtar, K., Husain M, Shadab G.G.H.A., 2013. A comprehensive insight into anticancer property and toxicity induced by chiral copper based drug candidate. (Manuscript submitted)

THE JOURNAL OF
PHYSICAL CHEMISTRY

Article

pubs.acs.org/JPCB

Biophysical Insight into Furosemide Binding to Human Serum Albumin: A Study To Unveil Its Impaired Albumin Binding in Uremia

Nida Zaidi,[†] Ejaz Ahmad,[†] Mohd Rehan,[‡] Gulam Rabbani,[†] Mohammad R. Ajmal,[†] Yusra Zaidi,[§] Naidu Subbarao,[‡] and Rizwan H. Khan*[,†]

[†]Interdisciplinary Biotechnology Unit, Aligarh Muslim University, Aligarh 202002, India

[‡]School of Computational and Integrative Sciences, Jawaharlal Nehru University, New Delhi 110062, India

[§]Department of Zoology, Aligarh Muslim University, Aligarh 202002, India

Supporting Information

ABSTRACT: Exogenous substances like drugs, when absorbed, enter into the circulatory system and bind reversibly and extensively to human serum albumin (HSA). But transport of various drugs like a diuretic, furosemide (FUR), via albumin in uremia is seriously compromised due to accumulation of uremic toxins. The reason behind it is explored by investigating the binding mechanism of FUR to HSA. Isothermal titration calorimetry results show that FUR binds with HSA at high ($K_b \sim 10^4$) and low affinity ($K_b \sim 10^3$) sites whereas spectroscopic results predict binding at a single site ($K_b \sim 10^5$). Thermodynamic analysis shows that the HSA-FUR complex formation occurs via hydrogen bonds and hydrophobic interactions and undergoes slight structural changes, as evident by FTIR and far-UV CD. Further, the lifetime of HSA decreases only marginally and thus the magnitude of energy transfer efficiency is small, as obtained by time-resolved measurements. A displacement experiment predicts that the FUR binds mainly to site I but a new site having lower affinity is also observed, which shares some residues with site II as supported by molecular docking results. Results revealed that in uremia, FUR indirectly competes for Arg410, Lys414, and Ser489 with site II bound uremic toxins and directly competes for site I with site I bound uremic toxins.

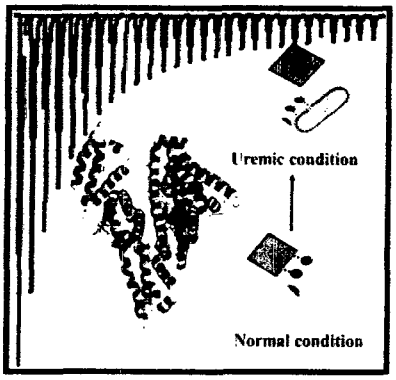

1. INTRODUCTION

Human serum albumin (HSA) is a main carrier for a variety of endogenous and exogenous substances in the body and also plays a key role in maintaining normal osmolarity in plasma and in interstitial fluid.[1−3] It is a single chain nonglycosylated polypeptide of 66.5 kDa. The protein has three homologous domains (I−III), each domain comprises two subdomains (A and B) that possess common structural elements.[4,5] As of its transporting role, it binds substances at two major binding regions, namely Sudlow's site I and II, which are located within cavities in subdomains IIA and IIIA, respectively.[6] Generally, upon absorption exogenous substances like drugs enter into the circulatory system and bind reversibly to serum albumin, which assists in their distribution and deposition.[7,8] But, transport of various drugs via albumin in a pathological ill condition like uremia, is seriously compromised.[9,10] Among them, binding of furosemide (FUR), a diuretic drug, is most adversely impaired, which normally binds 99% to albumin at its total concentration of 10 μg mL^{-1}.[11,12] Hence, a decrease in the protein bound fraction of FUR may affect the pharmacokinetics of the drug, which includes its tubular secretion and increased metabolic clearance in uremic patients.[13] Although the molecular mechanism underlying impaired albumin FUR binding in uremic conditions is poorly understood, two major reasons have been suggested. First, it may be due to some conformational changes in albumin under chronic renal disease but putative structural modifications of pathological HSA have been disputed for decades.[14−16] Second, according to the most accepted hypothesis, HSA binding sites might be occupied by uremic toxins, viz. hippuric acid (HA), indoxyl sulfate (IS), 3-carboxy-4-methyl-5-propyl-2-furanpropionic acid (CMPF), indole-3 acetic acid (IAA), etc.[17] However, from the available literature, it is found that FUR binds to site I of HSA[11,16,18] whereas all predominant uremic toxins except CMPF bind mainly to site II of HSA.[19−21] So, only CMPF is the uremic toxin that directly inhibits the binding of FUR to albumin as they share the same binding site. But, the reason behind inhibition by site II bound uremic toxins of FUR binding to albumin is still unclear. Thus, to elucidate the plausible reason behind impaired albumin binding of FUR, energetic and binding parameters along with the location of FUR binding sites on albumin are determined by fluorescence spectroscopy (steady state and time-resolved), ITC, FRET, esterase activity of HSA, and molecular docking and then the binding site location is correlated with the binding sites of uremic toxins available in the literature. Further, secondary structural changes

Received: July 14, 2012
Revised: January 28, 2013

dx.doi.org/10.1021/jp3069877 | J. Phys. Chem. B XXXX, XXX, XXX−XXX

PLOS | ONE

A Comprehensive Insight into Binding of Hippuric Acid to Human Serum Albumin: A Study to Uncover Its Impaired Elimination through Hemodialysis

Nida Zaidi, Mohammad Rehan Ajmal, Gulam Rabbani, Ejaz Ahmad, Rizwan Hasan Khan*

Interdisciplinary Biotechnology Unit, Aligarh Muslim University, Aligarh, Uttar Pradesh, India

Abstract

Binding of hippuric acid (HA), a uremic toxin, with human serum albumin (HSA) has been examined by isothermal titration calorimetry (ITC), differential scanning calorimetry (DSC), molecular docking, circular dichroism (CD) and fluorescence spectroscopy to understand the reason that govern its impaired elimination through hemodialysis. ITC results shows that the HA binds with HSA at high ($K_b \sim 10^4$) and low affinity ($K_b \sim 10^3$) sites whereas spectroscopic results predict binding at a single site ($K_b \sim 10^3$). The HA form complex with HSA that involves electrostatic, hydrogen and hydrophobic binding forces as illustrated by calculated thermodynamic parameters. Molecular docking and displacement studies collectively revealed that HA bound to both site I and site II; however, relatively strongly to the later. Esterase-like activity of HSA confirms the involvement of Arg410 and Tyr411 of Sudlow site II in binding of HA. CD results show slight conformational changes occurs in the protein upon ligation that may be responsible for the discrepancy in van't Hoff and calorimetric enthalpy change. Furthermore, an increase in T_m^1 and T_m^2 is observed from DSC results that indicate increase in stability of HSA upon binding to HA. The combined results provide that HA binds to HSA and thus its elimination is hindered.

Citation: Zaidi N, Ajmal MR, Rabbani G, Ahmad E, Khan RH (2013) A Comprehensive Insight into Binding of Hippuric Acid to Human Serum Albumin: A Study to Uncover Its Impaired Elimination through Hemodialysis. PLoS ONE 8(8): e71422. doi:10.1371/journal.pone.0071422

Editor: Rajagopal Subramanyam, University of Hyderabad, India

Received March 30, 2013; **Accepted** July 1, 2013; **Published** August 9, 2013

Funding: Financial assistance to NZ in the form of a Senior Research Fellowship was supported by the Council of Scientific and Industrial Research (CSIR), New Delhi, India. The funders had no role in study design, data collection and analysis, decision to publish, or preparation of the manuscript.

Competing Interests: RK is a PLOS ONE Editorial Board member. This does not alter the authors' adherence to all the PLOS ONE policies on sharing data and materials.

* E-mail: rizwanhkhan@hotmail.com

Introduction

Uremic toxins are the compounds which retained in the blood during kidney failure and interact negatively with the normal biological functions of the body [1]. Hippuric acid (HA) is one of these compounds that accumulates in the blood, and cause stimulation of ammoniagenesis. It is involved in development of muscular weakness in uremia as it also inhibits glucose utilization in muscles [2–4]. It has also been related to inhibition of organic anion secretion by the kidney [5] and transport at the blood-brain barrier [6]. Consequently, HA is a compound of pharmacological interest. It is a glycine conjugate of benzoate, which is formed primarily from aromatic amino acids by gastrointestinal flora or may be directly taken as preservatives from food and beverages [7]. In a healthy individual, concentration of HA is less than 5 mg/L but increases to values higher than 247±112 mg/L in patients with end-stage renal disease [8].

Human serum albumin (HSA) is the most abundant plasma protein, single chain, nonglycosylated polypeptide of 66.5 kDa. It is composed of three homologous, predominantly helical domains I–III, each of which contains two subdomains A and B [9]. HSA has one tryptophan residue, Trp214, located in subdomain IIA [10,11]. The principal regions of ligand binding to HSA are located in hydrophobic cavities in subdomains IIA and IIIA, which are consistent with Sudlow sites I and II, respectively [12]. These binding sites underline the exceptional ability of HSA to interact with many organic and inorganic molecules, thereby making this protein an important regulator of the pharmacokinetic behavior of many drugs as well as intercellular fluxes [13]. In body, it also binds to HA [2] and thus elimination of HA through hemodialysis is only 64% [14,15]. However, there is paucity of information on its binding mechanism to HSA. Consequently, it is necessary to investigate the binding energetic, amino acid involved in binding of HA to HSA to explore its binding mechanism in the body. So, the scope of this work is to evaluate these in details by studying the binding energetic using steady state fluorescence spectroscopy and isothermal titration calorimetry. Binding sites is determined by displacement studies whereas estimation of amino acid involved in binding, by molecular docking and esterase-like activity of HSA toward *p*-NPA. Thermal stability in presence of HA is determined using differential scanning calorimetry.

Materials and Methods

Materials and Sample Preparation

Human serum albumin (A1887; >96%), warfarin (A2250; >98%), phenylbutazone (P8386; >99%), and *p*-nitrophenyl acetate (N8137; >99%) were procured from Sigma Aldrich. Hippuric acid (free acid, crystalline; >99%) was from Himedia. The number in the parenthesis corresponds to the purity of the compounds. All other reagents were of analytical grade. HSA and drug solutions were prepared in 20 mM sodium phosphate buffer (pH 7.4). HSA was passed through Sephacryl-S200 gel filtration column, dialyzed, and its concentration was estimated spectro-

Journal of Biomolecular Structure and Dynamics
iFirst, 2012, 1–19

Taylor & Francis
Taylor & Francis Group

REVIEW ARTICLE

Revisiting ligand-induced conformational changes in proteins: essence, advancements, implications and future challenges

Ejaz Ahmad[a], Gulam Rabbani[a], Nida Zaidi[a], Mohammad Azam Khan[a], Atiyatul Qadeer[a], Mohd Ishtikhar[a], Saurabh Singh[b] and Rizwan Hasan Khan[a]*

[a]*Interdisciplinary Biotechnology Unit, Aligarh Muslim University, Aligarh 202 002, India;* [b]*Plant Sciences Department, Weizmann Institute of Science, Rehovot 76100, Israel*

Communicated by Ramaswamy H. Sarma

(*Received 23 March 2012; final version received 5 June 2012*)

Ligand-induced conformational changes are of immense importance for the biological activity of a protein. An in-depth understanding of salutary and deleterious effects of ligand-induced conformational alterations in single- and multi-chain proteins would lend a hand in human welfare. Unlike single-chain proteins, the function of multichain proteins depends upon the inherent properties of the subunit interfaces. The interfaces of temporary oligomeric proteins and the active sites of enzymes are of similar characteristics but the interfaces are more conservative than the active sites. Therefore, these interfaces may possibly be represented as drug targets by inhibition or induction of the oligomerization process. Thus without detailed structural understanding of ligand-induced conformational changes in a protein, structure-based rational drug designing is a great challenging task. So the purpose of this review is to clarify or enlighten the reader at the degree of internal motions related to protein backbone and side-chain flexibility which occur on binding of small molecule to a protein target. This can prove helpful to improve the conformational prediction for a protein–ligand complex. Besides a detailed description of protein–ligand interaction, this review also focuses on structure–activity relationships of protein which will surely help in the rational drug designing.

Keywords: aggregation; conformational alteration; drug designing; protein-ligand interactions; protein stability; structure-function relationship

Introduction

Most of the physiological processes are associated with complex formation between protein and ligand. The proteins associated with the physiological process are either directly or indirectly affected by ligands (Alberts et al., 2002). These ligands may be protein, peptide, small chemical compound, metal or ions. For instance an enzyme adenylyl cyclase, which involves in the breakdown of glycogen and fats, is stimulated by epinephrine and glucagon (Tornheimm & Ruderman, 2011). It is also stimulated by luteinizing hormone and antidiuretic hormone in the synthesis of estrogen/progesterone and in conservation of water respectively. Furthermore, phospholipase C is affected by Angiotensin during contraction of smooth muscles in blood vessels while in myocardial contraction, acetylcholine affect K^+ channel. Moreover, enkephalins, endorphins and opioids cause stimulation of Ca^{++}, K^+ channels which bring change in neuro-electrical activity (Lodish et al., 2000). Thus most of the endogenous and exogenous ligands are associated with enzymes, receptors and channels and bring changes in protein structure. The small changes are acquired from the rearrangement of side-chains flexibility and/or backbone flexibility of loops in the vicinity of the active site ultimately changes in the radius of gyration. However, large-scale motions like partial unfolding/refolding of the protein structure, domain reorientations, domain closure (closed state) accompanied by loop motions (hinge-bending motions) were also observed. So, to understand how universal factors such as extent of hydrophobicity, degree of polarity, hydrogen bonding, solvation characteristics, electrostatic potential, conformational dynamics and conformational flexibility of a protein are altered upon ligand binding is of enormous significance.

Besides the detailed mode of protein–ligand interactions, the purpose of the present review is to enlighten the various ligand-induced conformations adopted by the protein molecules as the protein molecule adopts different

*Corresponding author. Email: rizwanhkhan@hotmail.com

ISSN 0739-1102 print/ISSN 1538-0254 online

http://dx.doi.org/10.1080/07391102.2012.706081
http://www.tandfonline.com

1-Anilino-8-Naphthalene Sulfonate (ANS) Is Not a Desirable Probe for Determining the Molten Globule State of Chymopapain

Atiyatul Qadeer, Gulam Rabbani, Nida Zaidi, Ejaz Ahmad, Javed M. Khan, Rizwan H. Khan*

Interdisciplinary Biotechnology Unit, Aligarh Muslim University, Aligarh, India

Abstract

The molten globule (MG) state of proteins is widely detected through binding with 1-anilino-8-naphthalene sulphonate (ANS), a fluorescent dye. This strategy is based upon the assumption that when in molten globule state, the exposed hydrophobic clusters of protein are readily bound by the nonpolar anilino-naphthalene moiety of ANS molecules which then produce brilliant fluorescence. In this work, we explored the acid-induced unfolding pathway of chymopapain, a cysteine proteases from *Carica papaya*, by monitoring the conformational changes over a pH range 1.0–7.4 by circular dichroism, intrinsic fluorescence, ANS binding, acrylamide quenching, isothermal titration calorimetry (ITC) and dynamic light scattering (DLS). The spectroscopic measurements showed that although maximum ANS fluorescence intensity was observed at pH 1.0, however protein exhibited ~80% loss of secondary structure which does not comply with the characteristics of a typical MG-state. In contrast at pH 1.5, chymopapain retains substantial amount of secondary structure, disrupted side chain interactions, increased hydrodynamic radii and nearly 30-fold increase in ANS fluorescence with respect to the native state, indicating that MG-state exists at pH 1.5 and not at pH 1.0. ITC measurements revealed that ANS molecules bound to chymopapain *via* hydrophobic interaction were more at pH 1.5 than at pH 1.0. However, a large number of ANS molecules were also involved in electrostatic interaction with protein at pH 1.0 which, together with hydrophobically interacted molecules, may be responsible for maximum ANS fluorescence. We conclude that maximum ANS-fluorescence alone may not be the criteria for determining the MG of chymopapain. Hence a comprehensive structural analysis of the intermediate is essentially required.

Citation: Qadeer A, Rabbani G, Zaidi N, Ahmad E, Khan JM, et al. (2012) 1-Anilino-8-Naphthalene Sulfonate (ANS) Is Not a Desirable Probe for Determining the Molten Globule State of Chymopapain. PLoS ONE 7(11): e50633. doi:10.1371/journal.pone.0050633

Editor: Eugene A. Permyakov, Russian Academy of Sciences, Institute for Biological Instrumentation, Russian Federation

Received September 6, 2012; **Accepted** October 23, 2012; **Published** November 29, 2012

Funding: Financial assistance to A. Qadeer, G. Rabbani, N. Zaidi, J.M. Khan and E. Ahmad in the form of a Senior Research Fellowship was supported by the Council of Scientific and Industrial Research (CSIR), New Delhi, India. R.H. Khan is an Associate Professor in A.M.U., Aligarh. No additional external funding was received for this study. The funders had no role in study design, data collection and analysis, decision to publish, or preparation of the manuscript.

Competing Interests: The authors have declared that no competing interests exist.

* E-mail: rizwanhkhan@hotmail.com

Introduction

The process of protein folding, despite being one of the most intensely investigated areas, remains obscure in terms of its detailed molecular mechanism. The spontaneity and extreme cooperativity of this process makes it a challenging task to unravel the entire mechanism mainly because of the inability to populate the distinct intermediate states that encompass the folding pathway of a nascent polypeptide [1–3]. Characterization of these intermediates is the key to unlock the step by step mechanism and to extend our knowledge on the principles governing protein folding [4,5].

In past, a lot of attention has been paid to molten globule (MG), an intermediate with feasible occurrence as a general physical state in the folding pathway of globular proteins [6–8]. The MG state generally corresponds to late folding intermediate and has been obtained for many proteins under different solvent conditions [9–12]. In order to be defined as a typical molten globule, an intermediate requires being a compact collapsed state with substantial amount of secondary structure, loose tertiary contacts without tight side chain packing and a solvent accessible hydrophobic core [13]. Conventionally, the exposed hydrophobic clusters of folding intermediates are detected through 1-anilino-8-naphthalene sulfonate (ANS) binding, a much utilized fluorescence probe for detecting the non-polar character of proteins and membranes [14]. In fact, the available literature reveals that molten globule state is mostly pinpointed from its maximum ANS binding ability under the conditions studied since the other typical features *viz* pronounced secondary structure and disrupted tertiary contacts often seem to merge with intermediates lying in the vicinity of MG-state [12,15–20]. Such utilization of ANS which is based upon the principle that ANS is practically non fluorescent in water but produces brilliant fluorescence upon binding to hydrophobic sites of protein [21] generally ignores the contribution of sulfonate group that was earlier considered as a mere solublizing agent for otherwise almost water-insoluble anilino-naphthalene moiety. However, the role of electrostatic interactions in ANS-protein interaction was highlighted later in the findings that ANS binding to proteins depends upon protein cationic charge and pH of the solution and occurs precisely through ion-pair formation between sulfonate group of ANS and side chains of Arg/Lys/His residues of polypeptide chain [22,23]. A more recent study has revealed that interaction of sulfonate group of ANS with charged centers of Arg and Lys residues resulted in enhanced

Stereo-Selectivity of Human Serum Albumin to Enantiomeric and Isoelectronic Pollutants Dissected by Spectroscopy, Calorimetry and Bioinformatics

Ejaz Ahmad[1], Gulam Rabbani[1], Nida Zaidi[1], Saurabh Singh[2], Mohd Rehan[3], Mohd Moin Khan[1], Shah Kamranur Rahman[1], Zainuddin Quadri[1], Mohd. Shadab[1], Mohd Tashfeen Ashraf[4], Naidu Subbarao[3], Rajiv Bhat[2], Rizwan Hasan Khan[1]*

1 Interdisciplinary Biotechnology Unit, Aligarh Muslim University, Aligarh, India, 2 School of Biotechnology, Jawaharlal Nehru University, New Delhi, India, 3 School of Computational and Integrative Sciences, Jawaharlal Nehru University, New Delhi, India, 4 School of Biotechnology, Gautam Buddha University, Greater Noida, India

Abstract

1-naphthol (1N), 2-naphthol (2N) and 8-quinolinol (8H) are general water pollutants. 1N and 2N are the configurational enantiomers and 8H is isoelectronic to 1N and 2N. These pollutants when ingested are transported in the blood by proteins like human serum albumin (HSA). Binding of these pollutants to HSA has been explored to elucidate the specific selectivity of molecular recognition by this multiligand binding protein. The association constants (K_b) of these pollutants to HSA were moderate (10^4–10^5 M^{-1}). The proximity of the ligands to HSA is also revealed by their average binding distance, r, which is estimated to be in the range of 4.39–5.37 nm. The binding free energy (ΔG) in each case remains effectively the same for each site because of enthalpy–entropy compensation (EEC). The difference observed between ΔC_p^{exp} and ΔC_p^{calc} are suggested to be caused by binding-induced flexibility changes in the HSA. Efforts are also made to elaborate the differences observed in binding isotherms obtained through multiple approaches of calorimetry, spectroscopy and bioinformatics. We suggest that difference in dissociation constants of pollutants by calorimetry, spectroscopic and computational approaches could correspond to occurrence of different set of populations of pollutants having different molecular characteristics in ground state and excited state. Furthermore, our observation of enhanced binding of pollutants (2N and 8H) in the presence of hemin signifies that ligands like hemin may enhance the storage period of these pollutants in blood that may even facilitate the ill effects of these pollutants.

Citation: Ahmad E, Rabbani G, Zaidi N, Singh S, Rehan M, et al. (2011) Stereo-Selectivity of Human Serum Albumin to Enantiomeric and Isoelectronic Pollutants Dissected by Spectroscopy, Calorimetry and Bioinformatics. PLoS ONE 6(11): e26186. doi:10.1371/journal.pone.0026186

Editor: Jörg Langowski, German Cancer Research Center, Germany

Received May 12, 2011; **Accepted** September 22, 2011; **Published** November 2, 2011

Funding: Financial assistance to E. Ahmad in the form of a Senior Research Fellowship was supported by the Council of Scientific and Industrial Research (CSIR), New Delhi, India. The funders had no role in study design, data collection and analysis, decision to publish, or preparation of the manuscript.

Competing Interests: The authors have declared that no competing interests exist.

* E-mail: rizwanhkhan@hotmail.com

Introduction

α-naphthol [1-naphthol (1N)], β-naphthol [2-naphthol (2N)] and 8-quinolinol [8-hydoxy quinoline (8H)] are non-persistent organic water pollutants. They have similar properties. They are sparingly soluble in water and exhibit antiseptic properties. One way in which naphthols differ from each other is the form of their crystals. 1N crystallizes in prisms and 2N in plates. Cellular presence of 1N causes depolymerization of spindle microtubules and apparent uncoupling of karyokinesis and cytokinesis in mitotic cells. Although at a much lower frequency, presence of 2N also causes similar configurations. 1N has been investigated as a mutagen and reproductive effector and has also been associated with reduced testosterone levels [1]. Naphthols are used in the synthesis of certain azo-dyes and antioxidants for rubbers and as indicators in chemical analyses. 8H is used as a metal chelating agent, in preparing antiseptics, deodorants, fungicides etc. Their accumulation in body causes cyanosis, liver damage, nephritis, circulatory collapse and even death.

All these three pollutants are transported in blood by plasma proteins like human serum albumin (HSA). HSA is a 585 amino acid long heart-shape monomer comprising three structurally homologous domains each of which displays specific and functional characteristics. Each of these three domains is composed of sub-domains A and B providing flexibility to the protein molecule so that the protein can bind to a variety of ligands. HSA is responsible for the transport, storage and metabolism of many therapeutic drugs in the blood thereby restricting their free, active concentrations and therefore can significantly affect their pharmacokinetics and metabolism. Two distinct binding sites, commonly referred to as Sudlow site 1 and site 2, have been identified in HSA for various drugs [2]. Site 1 binds to bulky hydrophobic and heterocyclic molecules with a centrally located negative charge (e.g. warfarin, phenylbutazone). Site 2 binds to aromatic carboxylic acids with a negative charge at one end distal from the remaining hydrophobic structure (e.g. diazepam, ibuprofen). Binding of ligands to albumin alters the pattern and volume of distribution, lowers the rate of clearance, and increases the plasma half-life of the ligand. A detailed characterization of the protein's binding property to different ligands is therefore necessary not only to understand its key physiological functions but also to understand its impact on ligand transport and delivery.

Cell Biochem Biophys
DOI 10.1007/s12013-011-9237-x

ORIGINAL PAPER

pH-Dependent Conformational Transitions in Conalbumin (Ovotransferrin), a Metalloproteinase from Hen Egg White

Gulam Rabbani · Ejaz Ahmad · Nida Zaidi · Rizwan Hasan Khan

Abstract Acid unfolding pathway of conalbumin (CA), a monomeric glycoprotein from hen egg white, has been investigated using far- and near-UV CD spectroscopy, intrinsic fluorescence emission, extrinsic fluorescence probe 1-anilino-8-napthalene sulfonate (ANS) and dynamic light scattering (DLS). We observe pH-dependent changes in secondary and tertiary structure of CA. It has native-like α-helical secondary structure at pH 4.0 but loss structure at pH 3.0. The CA existed exclusively as a pre-molten globule state and molten globule state in solution at pH 4.0 and pH 3.0, respectively. The effect of pH on the conformation and thermostability of CA points toward its heat resistance at neutral pH. DLS results show that MG state existed as compact form in aqueous solutions with hydrodynamic radii of 4.7 nm. Quenching of tryptophan fluorescence by acrylamide further confirmed the accumulation of an intermediate state, partly unfolded, in-between native and unfolded states.

Keywords Conalbumin · DLS · Hydrodynamic radii · Molten globule · pH denaturation · Translational diffusion coefficients

Abbreviations

ANS	1-anilino-8-napthalene sulfonate
CA	Conalbumin
DLS	Dynamic light scattering
GnHCl	Guanidine hydrochloride
MG	Molten globule
MRE	Mean residue ellipticity
P_d	Polydispersity
T_m	Mid-point temperature

G. Rabbani · E. Ahmad · N. Zaidi · R. H. Khan (✉)
Interdisciplinary Biotechnology Unit, Aligarh Muslim University, Aligarh 202 002, India
e-mail: rizwanhkhan@hotmail.com

Published online: 21 July 2011

Introduction

Equilibrium and kinetic intermediates have been identified in the unfolding/refolding reactions of several proteins [1–3]. Several globular proteins when exposed to extreme pH conditions undergo significant conformational changes resulting in formation of intermediate states, with varying stability, such as molten globule (MG) state. Structural characterization of intermediates or MG state that populate in the folding/unfolding process is essential to understand the protein folding mechanism [4]. At MG state, the protein retains most of the secondary structures, but has a tendency to lose some of the tertiary structures [5–7]. The MG states are believed to be general folding intermediates because they populate both in the equilibrium and kinetic folding/unfolding pathways [8].

Egg white proteins are considered model of choice for studying proteins because of their high nutritional and biological value [9]. Conalbumin (CA), one of the main iron-binding monomeric glycoproteins containing D-mannose and D-galactose sugar moiety, is present in egg white. It transports and scavenges Fe(III) in poultry eggs. It belongs to transferrin family and exhibits features typical for α-helical proteins. The function of CA is generally accepted as that of iron transport. It binds two atoms of Fe(III), one in each domain. The order of iron binding is pH dependent; at pH 6.0, it binds first to the C-domain, but at pH 8.5, it first binds to the N-domain. It is a major contributor to the natural defense system in egg white, which provides protective barrier against infection by microbial flora [10]. An important

Cell Biochem Biophys
DOI 10.1007/s12013-011-9335-9

ORIGINAL PAPER

pH-Induced Molten Globule State of *Rhizopus niveus* Lipase is More Resistant Against Thermal and Chemical Denaturation Than Its Native State

Gulam Rabbani · Ejaz Ahmad · Nida Zaidi · Sadaf Fatima · Rizwan Hasan Khan

Abstract Here, we have characterized four pH-dependent states: alkaline state, "B" (pH 9.0), native state, "N" (pH 7.4), acid-induced state, "A" (pH 2.2) and molten globule state, "MG" (pH 1.8) of *Rhizopus niveus* lipase (RNL) by CD, tryptophanyl fluorescence, ANS binding, DLS, and enzyme activity assay. This "MG" state lacks catalytic activity and tertiary structure but it has native-like significant secondary structure. The "R_h" of all the four states of RNL obtained from DLS study suggests that the molecular compactness of the protein increases as the pH of solution decreases. Kinetic analysis of RNL shows that it has maximum catalytic efficiency at state "B" which is 15-fold higher than state "N." The CD and tryptophanyl fluorescence studies of RNL on GuHCl and temperature-induced unfolding reveal that the "MG" state is more stable than the other states. The DSC endotherms of RNL obtained at pH 9.0, 7.4, and 2.2 were with two transitions, while at pH 1.8 it showed only a single transition.

Keywords Lipase · pH denaturation · Molten globule · *Rhizopus niveus* lipase · Thermal stability · GuHCl denaturation

Abbreviations

ANS	1-Anilino-8-napthalene sulfonate
C_m	Midpoint concentration
DSC	Differential scanning calorimetry
GuHCl	Guanidine hydrochloride
ΔH	Enthalpy
MG	Molten globule
T_m	Midpoint temperature
RNL	*Rhizopus niveus* lipase
DLS	Dynamic light scattering

Introduction

Understanding of the molecular basis of protein stability draws attention of investigators both for perspective comprehension of the principles of the protein structure and for the possible biotechnological applications through development of solvent-protein engineering. Maintenance of a proper structure is an essential prerequisite for a functional activity of a protein. Hence, one of the primary requirements for a protein to be of industrial importance is its functional stability, which is guided by both thermodynamic and kinetic parameters [1]. Enzymatic activity and conformational stability of proteins can be measured by pH denaturation [2], thermal denaturation [3] and by chemical unfolding such as guanidine hydrochloride (GuHCl) and urea as these two chaotropic agents are commonly used as protein denaturants [4].

The characterization of unfolded and partially folded state of protein is essential to understand the protein folding and its stability. It is well known that the protein folding is a highly cooperative and spontaneous process, which does not need the presence of any additional factors. The folded conformation adapted by a protein is generally governed by its amino acid sequence suggesting the underlying stereo chemical code for protein folding [5].

Electronic supplementary material The online version of this article (doi:10.1007/s12013-011-9335-9) contains supplementary material, which is available to authorized users.

G. Rabbani · E. Ahmad · N. Zaidi · S. Fatima · R. H. Khan (✉)
Interdisciplinary Biotechnology Unit, Aligarh Muslim University, Aligarh 202 002, India
e-mail: rizwanhkhan@hotmail.com

Published online: 04 January 2012

Pollutant-Induced Modulation in Conformation and β-Lactamase Activity of Human Serum Albumin

Ejaz Ahmad, Gulam Rabbani, Nida Zaidi, Basir Ahmad, Rizwan Hasan Khan*

Interdisciplinary Biotechnology Unit, Aligarh Muslim University, Aligarh, India

Abstract

Structural changes in human serum albumin (HSA) induced by the pollutants 1-naphthol, 2-naphthol and 8-quinolinol were analyzed by circular dichroism, fluorescence spectroscopy and dynamic light scattering. The alteration in protein conformational stability was determined by helical content induction (from 55 to 75%) upon protein-pollutant interactions. Domain plasticity is responsible for the temperature-mediated unfolding of HSA. These findings were compared to HSA-hydrolase activity. We found that though HSA is a monomeric protein, it shows heterotropic allostericity for β-lactamase activity in the presence of pollutants, which act as K- and V-type non-essential activators. Pollutants cause conformational changes and catalytic modifications of the protein (increase in β-lactamase activity from 100 to 200%). HSA-pollutant interactions mediate other protein-ligand interactions, such as HSA-nitrocefin. Therefore, this protein can exist in different conformations with different catalytic properties depending on activator binding. This is the first report to demonstrate the catalytic allostericity of HSA through a mechanistic approach. We also show a correlation with non-microbial drug resistance as HSA is capable of self-hydrolysis of β-lactam drugs, which is further potentiated by pollutants due to conformational changes in HSA.

Citation: Ahmad E, Rabbani G, Zaidi N, Ahmad B, Khan RH (2012) Pollutant-Induced Modulation in Conformation and β-Lactamase Activity of Human Serum Albumin. PLoS ONE 7(6): e38372. doi:10.1371/journal.pone.0038372

Editor: Rajagopal Subramanyam, University of Hyderabad, India

Received December 14, 2011; **Accepted** May 4, 2012; **Published** June 7, 2012

Funding: Financial assistance to E. Ahmad, G. Rabbani and N. Zaidi in the form of a Senior Research Fellowship was supported by the Council of Scientific and Industrial Research (CSIR), New Delhi, India. R.H. Khan is an Associate Professor in A.M.U., Aligarh. No additional external funding received for this study. The funders had no role in study design, data collection and analysis, decision to publish, or preparation of the manuscript.

Competing Interests: Rizwan Hasan Khan is a PLoS ONE Editorial Board member. This does not alter the authors' adherence to all the PLoS ONE policies on sharing data and materials.

* E-mail: rizwanhkhan@hotmail.com

Introduction

Human serum albumin (HSA) is the most abundant multifunctional single chain protein in blood plasma. HSA plays important physiological and pharmacokinetical roles by binding and transporting exo- and endo-genous compounds [1,2]. It also possesses some enolase, esterase and hydrolase activities [3]. Thus, this protein contains both binding and catalytic sites [4]. This is heart-shaped and 80×80×30 Å in size [5] and the molecular topology can be easily changed because of its flexible nature as demonstrated in physicochemical studies [6]. Transportation of solute is one of the best characterized roles of this protein which solublizes ligands and targets them to cells through binding to specific cell receptors. HSA bound to specific ligands are recognized by specific cellular receptors through the ligand-dependent conformations of this protein [7]. Additionally, upon ligand binding, albumin undergoes physiologically relevant structural changes as in case of HSA-oleate interaction. As a consequence of the alteration in the nature of the local environment surrounding Cys-34, the long chain of fatty acid regulates the radical-trapping antioxidant activity [8]. These ligand-dependent changes in protein conformations are specific to the type of ligands and more precisely to their capacity to accumulate in the binding pockets. The ligand-induced structural changes in HSA are suggested to mediate its role in receptor-mediated cellular interaction as well as solute transport in physiological conditions.

We have studied the effect of pollutants on the structure and function of HSA. 1-naphthol (1N), 2-naphthol (2N) and 8-quinolinol (8H) shown in Figure 1 are direct or indirect (metabolite) organic pollutants and their accumulation in body can cause cyanosis, liver damage, nephritis, circulatory collapse and even death. A detailed study on the mode of interaction between HSA and these pollutants has been already performed and reported by our group [9] and the amino acid residues to which the pollutants bind are shown in Figure 2. In the present study, the effects of pollutant binding to HSA have been analyzed by a number of techniques. UV-visible, fluorescence spectroscopy, circular dichroism and dynamic light scattering are used to investigate the structural changes in protein associated with ligand binding. Here, our study offers not only direct proof for ligand-induced conformational alterations in protein, but also a clear understanding of the nature and after effects of these changes.

Materials and Methods

Materials

Fatty acid free human serum albumin (A1887), 1N (N2780) and 2N (185507) were from Sigma-Aldrich, USA, 8-quinolinol (8H), tris and hydrochloric acid were from Qualigens, India, whereas nitrocefin (484400) was a product of Calbiochem.

BIOGRAPHY

Nida Zaidi was born at Uttar Pradesh, India on March 8, 1985. She passed secondary school examination from Zakir Husain model senior secondary school in 2000 and senior secondary school examination from Aligarh muslim university in 2002. She obtained B.Sc. (Hons) in biochemistry (2006) and M.Sc. in biotechnology (2008) from the same university. She joined interdisciplinary biotechnology unit as a Ph.D student in November, 2008. She qualified CSIR-JRF and GATE in 2008. Presently, she is senior research fellow of CSIR, India.

Permanent address: 4/253, Tayyab colony, New sir syed nagar, Aligarh, U.P.

Email: nida.zaidi08@gmail.com, nida_zaidi08@yahoo.co.in